MASSEY
UNIVERSITY

Browning and Blistering of Mozzarella During High Temperature Pizza Baking

A thesis presented in partial fulfilment of the requirements for the degree of

Doctor of Philosophy

in

Chemical and Bioprocess Engineering

At Massey University, Manawatū

New Zealand

Daniel Joseph Thornton

2021

Abstract

Mozzarella and pizza baking are large and growing industries, and manufacturers and commercial operators need to know how their cheese will function during baking. The aim of this research was to develop a kinetic model describing the Maillard browning reaction occurring at the surface of Mozzarella during high temperature cooking, and to develop a conceptual model for how blister formation and growth is influenced by baking conditions.

Image analysis using lightness, L*, from the CIELAB colour space (L*a*b*) colour scale was used to measure the development of brown colour during baking. An experimental method was developed using a DSLR camera to record colour data and an Infrared (IR) camera to study the Maillard browning reaction. A first order kinetic model was fitted to the lightness data using non-linear regression, with the temperature dependence found to follow the Arrhenius Law. The activation energy (E_a) and the kinetic rate constant at 120°C (k_{120}), were fitted to two data sets. One based on an average region of interest (Average ROI kinetics, E_a = 124 kJ.mol^{-1} & k_{120} = 5.0x10^{-4} s^{-1}); and the other based on a discrete localised region where blistering occurred (P1 kinetics, E_a = 101.3 kJ.mol^{-1} and k_{120} = 3 .65x10^{-4} s^{-1}). Predicted L* was used to create a visual representation of predicted browning for the whole cheese surface which matched well with the shape and the outlines of the browned regions of the experimental data. The goodness of fit was better based on the Average ROI kinetics with an R^2 of 0.88, compared to 0.66 for the P1 kinetics.

A modified commercial pizza oven (Lincoln Impinger II 1100 Series) was characterised to provide information and data for the development of experimental techniques and analysis of baked pizzas. The modifications to the oven allowed for accurate temperature measurement, bake time, mass logging, and variable air flow. Air flow measurements showed that most of the air comes from below, based on the impinger layout, and there was minimal change to air flow within the control limits. The heat transfer coefficient (HTC) within the oven was measured using two methods; heating an aluminium block (29.1 to 37.1 Wm^{-2}K^{-1}), and water evaporation (43.4 to 45.7 Wm^{-2}K^{-1}).

To analyse pizzas baked in the modified oven, an image analysis method was developed to process post baking images. MATLAB was used to process images of pizzas baked under a range of conditions, which involved colour conversion and correction, thresholding and determining characteristics. A dynamic thresholding method was developed to account for the variation in overall surface colour and provided consistent and accurate identification of blistering and browning of baked pizzas. The blister analysis process was applied to the experimental and predicted data from the kinetics experiment to determine blister characteristics. A general trend was identified, where blister numbers increased to a maximum and then reduced over time. Blister size was found to increase with time, which can be attributed to blister growth and also the joining of adjacent blisters as they continue to grow. Overall, the P1 kinetics gave a better fit across all of the experimental trials with R^2 values ranging from 0.94 to 0.99, compared to the fit for the average kinetics at 0.90 to 0.98.

The overall process of cheese baking can be categorised into several stages; melt and flow, steam formation, bubbling, drying and blistering and browning. The conceptual model developed, proposed that low heat flux conditions trend towards fewer but larger blisters and high heat flux conditions trend towards a greater number of small blisters. Blister nucleation was found to be likely be more affected by bake time and temperature, than from initial conditions. It was found that the initial form factor (shreds vs slices) of Mozzarella did not affect the nucleation of blisters. The effect of baking conditions on blister characteristics was studied by baking pizza at a range of time and temperature combinations, with temperatures from 220 to 288°C and bake times from 6 to 15 minutes. Baking repeatability was found to be reliable and reproducible, with the % mass loss

consistent with a standard error of 0.2% and the level of browning with a standard error of less than 3% for each set of operating conditions assessed.

Blister characteristics were assessed from binary images based on the dynamic thresholding process. Observations from the images showed that the size of blisters decreased as oven temperature increased and baking time decreased. It was found that a higher oven temperature, and hence higher heat flux, resulted in greater blister numbers where blister coverage was less than 50%. Above 50%, it was found that further blister growth and characteristics were not sensitive to oven temperature.

Analysis of the time for the onset of moisture loss and blistering relative to oven temperature found that as oven temperature increased, the time difference between the initiation of moisture loss and blister formation reduced from approximately 5 minutes at 220°C down to approximately 2 minutes at 280°C. This indicated that heat flux has a greater effect on blister initiation than overall moisture loss which suggested that heat flux has a greater effect on surface moisture loss in comparison to bulk moisture loss. This connection suggested that the pizza surface dried out faster relative to the overall moisture loss as oven temperature increased, and as moisture is lost, the viscosity of the cheese increases. At high heat flux, there is limited time for bubbles to form before a stable skin forms and the surface dries out. In addition, an increased viscosity means that there would be more resistance to growth. The resulting blisters would be smaller than for low heat flux conditions. If the cheese surface dries slower, there is more time for bubble growth before viscosity increases and a stable skin and hence larger blisters are formed. This suggested that there is a critical moisture content where the cheese surface forms a stable skin where temperature can rise above 100°C.

To further study the effects of baking conditions on blister formation and growth, a benchtop oven was modified to measure and record surface colour, surface temperature and mass loss in real time during baking. A series of trials were carried out to bake cheese within the modified oven at temperatures of 168°C, 175°C, and 185°C for a minimum of 25 minutes each. The 10^{th} percentile, 90^{th} percentile, minimum and maximum values showed a pattern where initially the overall range is wide but reduces as the average temperature approaches 100°C, and then variation increases beyond 110°C. This pattern was similar for the L* data. Across all oven temperatures the 90^{th} percentile and maximum L* values were similar, which agreed with the observations of lower surface temperatures in the 10^{th} percentile and minimums across all oven temperatures. In contrast, there was a significant decrease in 10^{th} percentile and minimum L* values as oven temperature increases, due to the increased surface temperatures relative to oven temperature.

It was found that the original dynamic threshold was not suitable for analysis of the benchtop oven data as a result of different lighting conditions, so a new dynamic threshold equation was developed based on sensory evaluation. The analysis of binary images created using the new equation showed that blisters formed in less time at higher temperatures and blister coverage increased linearly relative to bake time, which agreed with the earlier analysis. Heat flux was found to be significantly lower for the benchtop oven, with the time to achieve 10% blister coverage at the highest oven temperature taking approximately 6 minutes longer compared to the lowest oven temperature from the commercial oven trials. The heat flux to the cheese layer for the commercial oven experiments was estimated to compare the effect of heat flux on the average blister size between the two experiments. It was found that there was a linear correlation between heat flux and average blisters size for the combined results, which suggested that this correlation may hold true irrespective of differences in oven setup and operating conditions. For blister initiation, a similar trend was observed from the benchtop data analysis as for the commercial oven data. Combining the blister initiation data suggested that the onset of browning is highly correlated to oven temperature, which is consistent with the temperature dependence of the Maillard reaction.

The developed kinetic parameters were applied to the integrated kinetic equation to assess the performance of the model in a different application. It was found that the predicted images and subsequent blister characteristics matched well with the experimental data, especially for blister coverage, with and R^2 of 0.99.

The findings from these experiments and analysis indicate that surface drying dynamics are fundamental to browning and blister development. Blister growth and size is governed by the moisture content and therefore viscosity, at the cheese surface. Oven temperature (and therefore heat flux) dictates how fast the surface will dry and therefore the general blister characteristics. Bake time determines the desired level of baking based on blister/browning coverage. Hence heat flux and cheese surface dynamics, in regard to the rate of moisture loss and viscosity, are the critical factors in determining browning and blistering and characteristics.

The experiments and methods developed, and the understanding of cheese behaviour and influential factors during baking have potential benefits for the high temperature food processing industry, especially cheese manufacture and applications. Benefits include improved accuracy and consistency of product assessment, control over baking characteristics and reduced production costs. The image analysis process developed provides an objective measure of blister characteristics, which are otherwise subject to individual interpretation. This process could be applied in a commercial setting give a robust, repeatable and consistent means of product quality and performance assessment. Given the developed understanding of the fundamentals that drive blister formation and browning it is possible to manipulate parameters that affect surface drying dynamics. This could be through external baking conditions, such as a multi-stage baking process, or adjusting the cheese composition itself to achieve a desired result.

The findings from this study resulted in a kinetic model describing Maillard browning of Mozzarella during baking as well as a good insight into the fundamentals that affect blister formation and growth to better understand the Maillard reaction and its application in high temperature food processing.

Acknowledgements

Like a good cheese, some things take time to mature until the time is right for it to hit the shelves. This work would not have been possible without the help and support from my supervisors, colleagues, friends and family. I would like to thank Professor John Bronlund, Dr. Colin Brown, Dr. Michael Parker and Dr. Peter Wiles for the opportunity to do this project and the ongoing support and guidance throughout the process.

Thank you to the Primary Growth Partnership (PGP) and Fonterra for funding this project and the School of Engineering and Advanced Technology at Massey University for accommodating me. It was a privilege to play a part in the PGP program alongside other researchers working at the forefront of research in the dairy industry. Furthermore, the support and inspiration from the academic, technical and administrative staff was greatly appreciated. In particular I would like to thank John Edwards, Anne-Marie Jackson, Warwick Johnson, Nick Look, Gary Radford, Glenda Rosoman, and Anthony Wade.

Thanks to my family, friends, colleagues, and all those that shared part of the journey and experience with me. Although not always on topic, many a great conversation was had to either help the process or provide necessary distraction. In no particular order thank you Mum and Dad, Amy, Hamish, Geoff, Aroha, Colin, Felicity, Nik, Eli, Grace, Jacky, Sureewan, Hammertron, Gonzalo, Tony and Mario.

A special thanks to Allen Yeung for his help in the lab with hours of pizza baking and analysis, and Colin Brown for the great banter, discussions, laughter, and all round support. Also, the home cooked pizza was a refreshing change from the mountains of plain cheese pizza.

When searching the literature for this project I came across a number of correlations, some that were relevant and some that were more of a…stretch. One in particular comes to mind which found that the USA per capita cheese consumption of Mozzarella correlated with the number civil engineering doctorates awarded between 2000 and 2009. So, anyone looking to get a doctorate in civil engineering should consider including cheese pizza into their regular diet.

Two gold fish are in a tank when one turns to the other and says “do you know how to drive this thing?” (FYI I still laugh at this)

Table of Contents

Page

List of Tables

List of Figures

Chapter 1
Introduction

Mozzarella cheese is part of the essential product mix produced by the global dairy industry and is highly sought after in the world market. The Mozzarella and pizza cheese industry is ever growing and different markets have different demands in regard to quality characteristics such as blistering and browning.

One of the most important characteristics considered in the pizza baking industry is the visual appearance of a baked pizza, which is normally used to evaluate quality. The overall appearance is generally attributed to the browning and blistering of cheese. Mozzarella is the most common cheese utilised in commercial pizza baking, exhibiting desirable functional attributes such as stretching, melting and browning. The consumption of Mozzarella has increased significantly in the past 30 years, driven largely by the rise in popularity of pizza, growing nearly 10-fold in the USA to 5.25kg per capita and totalling 1.89 billion kilograms in 2017 (Kindstedt, 2019).

Mozzarella manufacturers need to know how their cheese will function during baking. Industrial cooking systems such as fast-cooking forced air or microwave ovens have different effects on the performance of the cheese. As Mozzarella consumption grows in different markets and food systems, it has been become more important to understand and control the properties of a cheese to have specific melt, stretch, cooked colour and textural properties (Rankin *et al.*, 2005).

Several researchers have studied Mozzarella and other cheeses in relation to high temperature baking to quantify their baking properties under various conditions. Image analysis techniques have been commonly employed for such studies (Wang & Sun, 2003; Ma *et* al., 2013a and Ma *et* al., 2014), but these studies have not investigated the kinetics of browning based on the dynamic temperature and time relationship and the subsequent effect on cheese properties.

1.1 Research Aim

This research aimed to study the kinetics of Maillard browning of Mozzarella during high temperature baking, including the effect temperature and time of the cooking process have on the reaction and the subsequent formation of blisters. This understanding would lead to insights into how baking conditions and cheese properties influence pizza appearance in commercial food processes. In addition, an understanding of the blister formation and propagation process would allow development of a conceptual model that could predict pizza baking characteristics based on baking conditions.

1.2 Research Objectives

The specific objectives to achieve this research aim were to:

- Develop a heating/cooking system for Mozzarella and a method for measuring and assessing browning (an image analysis method), applicable for the study of the non-enzymatic browning reaction. This system and process would provide reliable experimental data to develop a kinetic model (Chapter 3)
- Develop an applicable kinetic model for the non-enzymatic browning of Mozzarella to predict browning rates as a function of temperature and time (Chapter 3)
- Characterise a modified commercial pizza oven to quantify the magnitude and distribution of temperature, air flow, and heat transfer rates within the oven (Chapter 4).

- Develop a method to assess blister formation consistently on pizzas baked under controlled conditions (Chapter 5).
- Develop and test a conceptual model that links baking conditions to the cooked outcome with respect to blister formation and growth (Chapter 6).
- Develop an experiment and method to measure surface temperature, colour and mass loss to assess their impact on browning and blister formation and growth (Chapter 7)

Chapter 2
Literature Review

One of the most important characteristics of a baked pizza is the visual appearance and is normally used to evaluate quality. The overall appearance is generally attributed to the browning and blistering of cheese. Mozzarella is the most common cheese utilised in commercial pizza baking, exhibiting desirable functional attributes such as stretching, melting and browning. In the USA, more than 70% of the Mozzarella produced is used in the manufacture of pizza (Matzdorf et al. 1994).

This chapter reviews the literature on cheese properties and functionality in relation to melt and flow, Maillard browning and blister formation to summarise the understanding based on current research. Methods for measuring and analysing the Maillard reaction for food systems are discussed, as well the kinetic models for prediction of the reaction. This review has a particular focus on Mozzarella and its application in pizza baking.

2.1 Cheese melting and baking

The melting of cheese consists of a complex set of factors that define how and when cheese melts and flows during pizza baking. The changes that cheese undergoes during pizza baking can be broken down into three basic stages (illustrated in Figure 2.1), which are differentiated by the temperatures at which they occur. Initial fat melting occurs below 38°C, flow and shred fusion occurs between 55 to 80°C and blister formation and browning occurs at 100°C and above (Rudan & Burbano, 1998 and Brown & Bronlund, 2015).

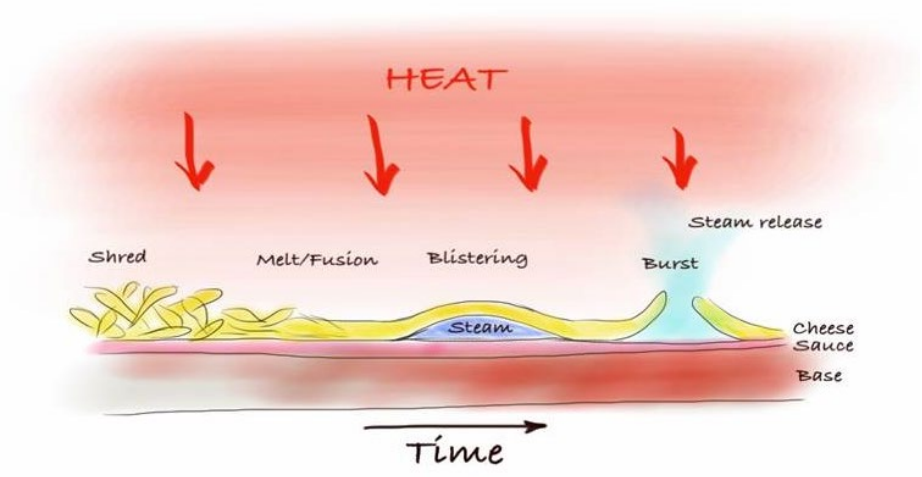

Figure 2.1 – Conceptualising cheese melting through to blister formation and browning (Brown & Bronlund, 2015)

Fat melting occurs during the initial stages of pizza baking, becoming fully liquid by about 38°C. As the temperature raises, the protein-protein, protein water and protein calcium interactions are altered, causing a reduction in the cheese viscosity (Rankin *et al.*, 2005). As the cheese shreds begin to collapse under the force of gravity, the shreds fuse together to eventually form a continuous layer of cheese. During this phase the protein matrix collapses, and free oil is released which impedes

moisture loss. As the temperature continues to increase to 100°C and above, moisture converts to steam, forming bubbles and provides the force to overcome the internal elastic and stretch resistance of cheese (Ma, *et al.*, 2013b). Water vapour and air trapped within the cheese layer creates pockets to form bubbles or blisters. Depending on the viscosity and the elasticity of the cheese, the blisters may burst or form a stable skin. As further heat is applied, moisture evaporates from the surface and temperature continues to increase to allow Maillard browning reactions to occur (McSweeny, 2007).

2.2 Cheese properties and functionality

Cheese is a complex matrix comprised mainly of lipids, proteins, water, and minerals (Fennema, 1996). The behaviour of cheese is influenced by baking conditions, properties of the cheese and complex interactions between components and reactions, which affect melting, flow, browning and blistering (Johnson & Olson 1985 and McSweeny, 2007). Cheese is considered a viscoelastic material, where texture and rheological properties play critical roles in melting and flow (Lucey *et al.*, 2003).

2.2.1 Meltability, flowability and strechability

Cheese is heated for a range of food applications including pizza, pasta, and burgers. To create the desired functionality, it is essential to understand the properties of cheese and how they are affected by heat. To understand and describe the behaviour of cheese, several parameters have been defined to describe and express functional properties. There are several key parameters considered relevant to cheese melt and flow, including meltability, flowability, and stretchability, which are all important functions of Mozzarella (Wadhwani *et al.*, 2011). Table 2.1 describes these functional properties (Fox *et al.*, 2000).

Table 2.1 – Functional properties of cheese and their definition (Fox *et al.*, 2000)

Property	Definition
Meltability	The capacity of cheese to soften to a molten cohesive mass on heating
Flowability	The capacity of melted cheese to flow
Stretchability	The capacity of melted cheese to create strings, cohesive fibres, or sheets during extension

The melting characteristics of Mozzarella are prime factors in determining quality and functionality for particular applications (Kuo *et al.*, 2000). Mozzarella is popular in many prepared and ready-to-eat foods, particularly for pizza production. Consumer acceptance of such a product can largely depend on the melting quality and characteristics of the cheese, in terms of both the resulting visual appearance and eating quality (Kuo *et al.*, 2001). Additional functional properties considered in research related to cheese baking include free-oil formation, blistering and browning (Gunasekaran and Ak, 2003).

2.2.2 Free oil formation

Fat in cheese occurs as globules contained within the protein network. Free oil formation is where fat melts and separates from the melted cheese forming oil pockets, particularly at the cheese surface (Lucey, 2008). Variation and changes in free oil occur due to the ingredients, composition and the baking conditions the cheese is subjected to and have been linked to the meltability,

flowability and strechability of cheese (Gunasekaran & Ak, 2003, Hong, *et al.*, 1998, Ma *et al.*, 2013a). In addition, Rudan and Barbano (1998) suggest that free oil may be useful in the control of blister formation and browning.

2.2.3 Blistering and browning

Browning and blistering of Mozzarella are considered to be essential quality attributes for pizza baking performance (Jana & Tagalpallewar, 2017). Blistering refers to visual bubbles on the surface of a pizza. Blisters form when water vapour produced under a layer of melted cheese creates bubbles. Cheese with high tensile stress (higher viscosity) will tend to form stable bubbles, which have more surfaces exposed to dehydration and thus form a skin or blister during baking (McSweeny, 2007). Research has indicated that blistering is affected by cheese functionality and melt properties (Hong *et al.*, 1998). Blister size, shape, and other characteristics are dependent on bubble size and factors that affect the apparent viscosity of the cheese such as proteolysis, moisture to protein ratio, and pH (Rudan & Barbano, 1998).

The browning of cheese is related to the formation of blisters. The colour changes of cheese during baking mainly relate to non-enzymatic browning, predominantly the Maillard reaction, (Rankin *et al.*, 2005). Maillard browning is complex set of reactions between amino acids and sugars, involving several steps and pathways that result in changes to the appearance and taste of foods (Demir *et al.*, 2002). These reactions are important in the production of foods due to their contribution to the flavour, colour and aroma and may or may not be desirable depending on the application (Eskin *et al.*, 2005; Nursten, 2005).

Several factors have been suggested to affect cheese browning and blistering including both baking conditions and cheese melt properties (Johnson & Olson, 1985 and Hong *et al.*, 1998). A study by Wang and Sun (2003) found that the extent of browning is significantly affected by baking time, temperature and their interaction.

2.3 Factors affecting cheese properties and functionality

The properties of cheese are associated with its complex network, structure, and interactions within the network. Cheese melting is related to changes within the protein matrix. During pizza baking, compositional factors have been shown to affect Mozzarella cheese melting, flow and browning, including protein, moisture content, fat content, and salt content (Rudan & Burbano, 1998 and Gunasekaran & Ak, 2003). The functional properties of cheese can be affected by cheese production conditions and baking conditions in addition to compositional factors (Kosikowski & Mistry, 1997). This review focusses on the compositional factors and baking conditions of cheese as a raw material.

Describing the effect of specific factors is difficult as it is the complex interactions occurring that cause a change in the functional properties.

2.3.1 Protein

Flowability is primarily governed by the strength of protein-to-protein interactions that bind fibres together. A study by Rankin *et al.* (2005) found that the relationship between milk proteins and milk fat has a significant impact on cheese stretching. A higher protein (casein) content results in hard curd with limited stretchability, and higher fat results in soft curd that stretches at lower temperatures (Rankin *et al.*, 2005). This agrees with research by McSweeny (2007), who identified that strong protein-to-protein interactions limit and restrict flow, in comparison to weak interactions which can result in excessive flow. This research also considered proteolysis, which weakens protein-to-protein interactions, thus leading to increased flow.

2.3.2 Moisture

With regard to cheese flow during baking, it is thought that the fat and water content play a significant role. The water component of cheese exists in three states; free, bound and entrapped. Free water is easily extracted and is distributed in the serum channels, whereas bound water is structurally bound with the casein matrix. Entrapped water is unbound but not in a continuous serum channel (Everett & Auty, 2008).

In general, the greater the moisture content of cheese, the softer it is and the better its meltability (Gunasekaran & Ak, 2003). A high moisture content, specifically a high moisture-to-protein ratio, results in lower protein density and thus weaker protein -to-protein interactions (McSweeny, 2007). This research suggests that higher moisture content increases the viscoelastic properties of cheese. This can be achieved through having higher initial moisture, or by restricting moisture loss during baking. Zhu *et al* (2015) investigated Mozzarella cheese flow relative to moisture content and found that the influence of moisture content could be described using an exponential relationship. As moisture content decreased, the viscosity of the cheese increased exponentially. They found that a decrease in moisture content of 15%, increases the molten cheese viscosity by a factor of 10.

Rudan and Barbano (1998) proposed that surface moisture affects browning, where during bubble growth the cheese surface rises and thins out. This causes free oil to flow away from the rising blister and results in moisture loss at the surface. They go on to state that the variation in browning appearance is relative to the degree of surface moisture loss.

Rankin *et al.* (2005) identified that for an increase in cheese moisture, the level of browning decreased. It was presumed that the increased moisture minimised the heat-induced browning reaction by flashing off, protecting the cheese proteins during cooking. Ma *et al.* (2013b) studied the blistering and browning properties of Mozzarella and found that cheese with the highest moisture content had the biggest blisters, and the cheese with the lowest moisture contents had the smallest blisters. They suggest that Mozzarella with a higher moisture content may result in the production of more steam during heating, and hence cause larger blisters.

Surface moisture has a been identified as a key parameter in relation to the onset and extent of browning. A cheese that dehydrates extensively at the surface during heating will exhibit more intense browning than a comparable cheese that resists dehydration (McSweeny, 2007). A study by Ma *et al.* (2014) determined that the prevention of moisture evaporation from cheese results in less intensive browning. Their work also identified that the steam force is related to cheese moisture content, where Mozzarella generated the most steam (in comparison to other common cheeses) and thus is a driving force for bubble formation.

2.3.3 Fat

Fox *et al*. (2000) stated that the form of fat globules may affect the properties of cheese such as; meltability, flowability or firmness. These properties are influenced by fat globule distribution and size or more complex interactions, which depend on the cheese production process and conditions such as temperature, ingredients, and aging (Everett & Olson, 2003; Półtorak *et al.*, 2015). Desai and Nolting (1994) suggested that fat globules contained within the protein network can be considered as “fillers” that affect the rheological functional properties of cheese. Pizza baking performance significantly decreased as the fat percentage decreases, affecting meltability, flow, and free oil (Rudan *et al.*, 1999). Free oil influences cheese blistering properties where more blisters form on Mozzarella with less free oil (Ma *et al.*, 2013a).

Gunasekaran and Ak (2003) found that higher fat improves the meltability of cheese and produces more free-oil. They presumed that changes in the reduction of meltability at lower fat contents is due to the loss of the plasticising action of the protein matrix and increased cross-linking. High fat content and therefore lower protein density and weaker protein -to-protein interactions, coincides with higher moisture to protein ratio; higher fat also provides lubrication for layers of fibres to slide past one another during melting (McSweeny, 2007). Conversely, a lower number of fat globules results in a denser structural network leading to a firm and dry cheese that melts poorly (Emmons *et al*., 1980).

2.3.4 Baking Conditions

There are several parameters that can be controlled during pizza baking including, baking time, temperature and air flow. Temperature and airflow relate to the rate that heat is applied (i.e. heat flux) and baking time dictates the duration a pizza is exposed to heat for rate processes such as flow and Maillard browning to occur.

As temperature increases, the protein-protein bonds relax and cheese behaviour becomes more fluid like and can flow (Lucey *et al.*, 2003). Wang and Sun (2002a) investigated the meltability of cheese relative to temperature and found that meltability increased with temperature from 70 to 130°C. At higher temperatures, meltability reduced due to the loss of fat and moisture from the cheese matrix.

Baking temperature also affects the colour change of cheese. It has been shown that during the initial stages of heating, Mozzarella increases in whiteness up to temperatures as high as 100°C (Wang & Sun, 2003). For browning colour change, it has been found that it is more a function of heating temperature than heating duration (Gunasekaran & Ak, 2003), suggesting the reactions have relatively high activation energies. Research has been conducted on products during high temperature cooking, such as biscuits, crackers, and bread, which indicate that the initiation of the darkening stage of surface colour changes during browning occurs between 105-120°C, depending on the application (Shibukawa et al., 1989; Broyart *et al.*, 1998; Purlis & Salvadori, 2009 and Purlis, 2010).

Wang and Sun (2003) assessed the browning of cheese at various baking temperatures and found that for Mozzarella, browning rate increased almost proportionally to cooking temperature from 70 to 200°C. At a low temperature for extended durations (70°C for 20 min) the cheese did not brown, but substantial browning occurred at a high temperature for even a brief time (1 to 3 min at 200°C). The influence of temperature on the Maillard reaction has been well observed, where several researchers have confirmed that the rate of reaction increases with temperature (Labuza *et al.*, 1994; Martins *et al.*, 2001).

Forced air convection ovens are commonly used for pizza baking, which give more rapid and even heating than conventional ovens. A review by Lucey (2003) identified that for pizza baking, forced hot air flow dries out the cheese surface and is more likely to lead to blistering and browning. Blisters are prone to additional drying and as a result, browning rate is greater with the use of forced-air ovens. This agrees with Rankin *et al.* (2005) who determined that Mozzarella is more susceptible to dehydration and skinning in a forced-convection oven. Excessive drying at the surface may be attributed to inadequate release of free oil, or poor water-holding capacity (McSweeny, 2007).

2.3.5 Modelling Cheese Flow

Rudan and Barbano (1998) describe a model of mozzarella cheese melting and browning during baking and a comparison of the process between full fat and lower fat mozzarella. When full fat cheese is heated (Figure 2.2A) the fat melts and becomes liquid and some of the fat is forced to the cheese surface. The melted fat coats the exposed shreds and as temperature increases, changes occur in the interactions between proteins, water and calcium resulting in a decrease in the apparent viscosity. This causes the cheese shreds to collapse and flow. In contrast, for fat-free and lower fat cheese (Figure 2.2B) the absence or lack of fat at the surface means there is inadequate fat transport to the surface during heating. As a result, at higher temperatures the cheese shred surface rapidly dehydrates and skin formation occurs, which limits the ability to melt and flow.

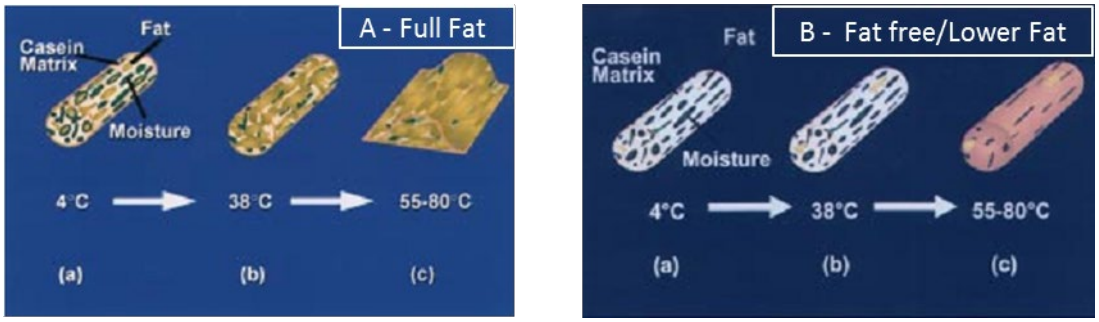

Figure 2.2A & B – Schematic diagram of cheese shred melting for full fat and fat free/low fat cheese (Rudan & Burbano, 1998)

Reducing the fat content of Mozzarella results in poor functionality during pizza baking, limiting shred melt and fusion, and consequently affects browning and blister formation. Dehydration of the cheese shred surface and skin formation are critical events that occur during baking.

"Prevention of dehydration and skin formation at the surface of the cheese shred appear to be the key that unlocked the mystery of Mozzarella cheese melting and browning during pizza baking" (Rudan & Burbano 1998).

2.4 Measuring and Modelling Browning

Browning occurs due to non-enzymatic chemical reactions which form coloured compounds during the baking process (Eskin *et al.*, 2005). Methods for determining the Maillard browning reaction can be separated into two general categories; direct and indirect. The direct method aims to measure the chemical components that contribute to the brown pigment formation or the consumption of the reactants. The indirect method involves measuring the physical colour change as a result of the Maillard reaction.

Direct methods are generally destructive, laborious and time consuming and not conducive to measuring colour development in the process (Purlis & Salvadori, 2007). This review focusses on the indirect method for browning measurement and how colour can be analysed. Indirect methods are currently preferred for food engineering applications (Purlis, 2010).

2.4.1 Indirect methods of colour measurement

Colour is an inherently subjective attribute. How colour is perceived differs between individuals and is dependent on several factors such as lighting conditions (Gonzalez & Woods, 2007). Due to this difference, many industries use a combination of human vision and instrumental systems for colour measurement. The aim of these instrumental systems is to simulate the way that the human eye

perceives the colour of an object. Using specified and consistent lighting conditions, it is possible to obtain an objective, quantitative and comparable measure of colour (Dufossé & Galaup, 2010).

The appearance of baked foods can be evaluated using several methods including sensory, colourimetry, and image analysis. Sensory analysis is subjective and qualitative (Rudan & Barbano, 1998), where colourimetry and image analysis are objective and quantitative (León *et al.*, 2006). Traditionally, colorimeters have been used extensively for colour measurement in the food industry (Cho *et al.*, 2016). However, this method is limited in that only a small section or small surface area of a food is analysed at any one time. Hence measurements can be unrepresentative (particularly when applied to heterogenous surfaces) and global analysis of a food's surface is difficult (León *et al.*, 2006). The development of image analysis or computer vision methods for colour measurement, overcome many of these inherent disadvantages.

2.4.2 Image analysis method

Image analysis is a computational technique that uses digital image capture and image processing software to provide a cheaper and more versatile method of colour measurement for foods compared to traditional colour measuring instruments (Yam & Papadakis, 2004; Fan *et al.,* 2020). Figure 2.3 illustrates an image analysis setup with the relevant components (Brosnan & Sun, 2004).

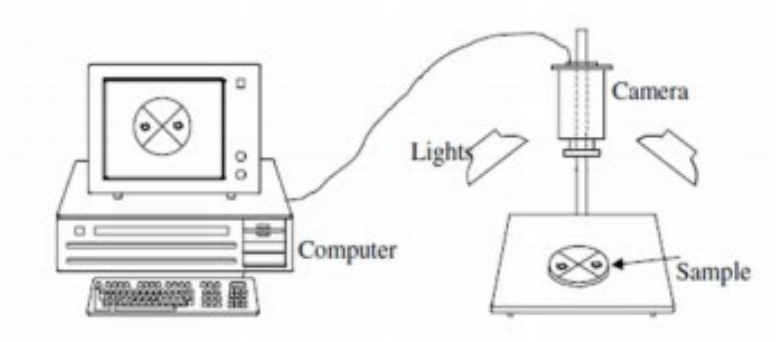

Figure 2.3 – Components of an image capture system (Brosnan & Sun, 2004)

Image analysis is favourable as it is more efficient and objective, allowing for a greater depth of information on colour change and variation of the subject. It can also be used to investigate the shape and spread of surface features (Ma *et al.*, 2013a). Image analysis provides a non-destructive, rapid, accurate and consistent method which has attracted extensive research aimed at aiding or replacing human inspection (Brosnan & Sun, 2004; Mendoza *et al.*, 2007). In addition, the computer vision method provides a means of making continuous measurements (Wang & Sun, 2003).

In terms of cheese baking, browning and blisters formed during the process result in a nonhomogeneous pattern of colour distribution. Uneven colour distribution occurs when baking Mozzarella, which makes measuring colour difficult for conventional colorimeters and hence the use of machine vision and image analysis has been applied for cheese baking evaluation (Wang & Sun, 2002b; Ma *et al.*, 2014. In addition, non-uniformity in the surface characteristics suggests that there is variation in surface temperature that causes the variation in colour formation. Hence it is important to be able to measure an entire surface, which image analysis provides.

2.4.3 Image analysis process

The process of image analysis involves three main steps; image acquisition, image processing and image understanding (Gunasekaran, 2001; Sonka *et al.*, 2008; Ma *et al.*, 2016). Image acquisition is the capturing of a digital image under controlled conditions. The lighting setup is critical and must be well controlled as the quality of illumination affects the images captured (Fan *et al.*, 2020). The appearance of an object can change severely by adjusting the lighting, which can either clarify or blur the object of interest (Brosnan & Sun, 2004). Often an image of a colour standard is used to ensure the accuracy and consistency of colour assessment during image processing (Gunasekaran, 2001; Brosnan & Sun, 2004; Gonzalez & Woods, 2007).

Image processing can be broken down into image pre-processing (image enhancement and calibration), segmentation (partitioning the image), and feature extraction (obtaining qualitative information) (Brosnan & Sun, 2004; Gonzalez & Woods, 2007). The key part of image processing is segmentation, the purpose of which is to divide an image into parts based on the regions of interest. A region of interest can be divided based on a particular property such as brightness, colour, reflectivity, or texture (Sonka *et al.*, 2008). There are several techniques used for segmentation, including; thresholding, edge-based segmentation and region based segmentation (Sun, 2000; Gonzalez & Woods, 2007; and Sonka *et al.*, 2008). Thresholding is a simple and fast technique that is commonly used for simple food systems (Brosnan & Sun, 2004).

Colour representation is important for the image analysis process. The RGB model is most often used for camera sensors, which is a device dependent model. To overcome the issues with this, alternative colour spaces are commonly used, such as the L*a*b* colour space (León *et al.*, 2006 and Wu & Sun, 2013).

2.4.3.1 Colour space

The measurement of physical colour change quantifies the amount of light reflected by the food surface relative to a given colour space. Several different colour space models exist for digital image colourimetry, including; RGB, CMYK, HSV/HSL, CIE XYZ, L*a*b*, and YUV (Fan *et al.* 2020). For food research applications using image analysis, colour is generally represented by the CIE L*a*b* colour space. This is an internationally recognised standard for colour measurement developed by the Commission Internationale de l'Eclairage (CIE) in 1976 (León *et al.*, 2006). The three parameters of this model represent lightness (L*), redness (a*) and yellowness (b*) respectively. L* values range between 0 and 100 (0 indicates black, 100 indicates white); a* indicates position between magenta (red) and green (negative [-] values indicate green, and positive [+] values indicate magenta); *b** indicates position between yellow and blue (negative [-] values indicate blue, and positive [+] values indicate yellow) (Gilchrist *et al.*, 1999). The L*a*b* colour is not dependent on the measuring device and provides a consistent colour regardless of the input or output device (Yam & Papadakis, 2004).

Image analysis has been used for the study of cheese browning. Wang and Sun (2003) analysed the baking of cheese based on a defined Browning Factor (BF), which is the ratio of Grey Value (GV) before and after cooking. Ma *et al.* (2013a) applied the L*a*b* colour model to images and calculated the average values for browning and blisters on pizzas using computer software. Based on the advantages, and its popular use for food applications, the CIE L*a*b* colour system will be used for image analysis in this study.

2.4.4 Kinetic modelling of high temperature browning

The Maillard browning reaction is well known with respect to its effect on food quality and attributes such as colour, flavour, taste and aroma. To predict and control Maillard browning during food processing applications it has been necessary to develop mathematical models. Kinetic modelling

can be applied to chemical changes in food or changes in physical parameters (including colour) as a function of time and temperature (Liu *et al,* 2008; Boekel, 2009). If the rate and temperature dependence of a kinetic reaction is identified, the occurrence of the change can be predicted and therefore controlled (Martins *et al.*, 2001; Viollota & Hawkes, 2007). Such modelling approaches have been applied to food systems to understand and describe the Maillard reaction as a function of time and temperature.

The reaction kinetics of foods during thermal processing consider the generation of products and degradation of reactant component concentrations. A kinetic model can capture chemical and physical changes in the mathematical model by including characteristic kinetic parameters such as activation energies and rate constants (Van Boekel, 2008). Giannakourou and Taoukis (2007) have given a detailed description on the use of kinetics for food applications. Based on the general rate law for closed systems with only one compound reacting, the disappearance of a compound (A) can be written as shown in Equation 2.1.

$$-\frac{d[A]}{dt} = k[A]^n \qquad \text{Eqn. 2.1}$$

$[A]$ is the concentration of the relevant component in the food (concentration units), k is the reaction rate constant (concentration units$^{-(n-1)}$.min^{-1}) and *n* is the reaction order (usually $0 \le n \le 2$). The decrease in concentration of A over time t is proportional to the concentration of that component. The order of reaction accounts for the sensitivity of the reaction rate to the substrate concentration (Giannakourou & Taoukis, 2007). Given a constant temperature, Equation 2.1 can be integrated based on a chosen reaction order with respect to time.

After integration (at a constant temperature), a zero order (n=0) reaction is described by:

$$[A] = [A]_0 - kt \qquad \text{Eqn. 2.2}$$

a first-order (n=1) is described reaction by:

$$[A] = [A]_0 \exp(-kt)\text{、} \qquad \text{Eqn. 2.3}$$

and a second-order (n=2) is described reaction by:

$$\frac{1}{[A]} = \frac{1}{[A]_0} + kt \qquad \text{Eqn. 2.4}$$

Kinetic reactions rates are known to be influenced by temperature. The temperature dependence of a reaction rate constant (k) is commonly described by the Arrhenius equation (Cunha & Oliveira, 2000; Martins *et al.*, 2001), Equation 2.5:

$$k = k_0 \exp\left(-\frac{E_a}{RT}\right) \qquad \text{Eqn. 2.5}$$

Where k_0 is the Arrhenius constant (s^{-1}); E_a is the activation energy; R is the universal gas constant (8.3145 J.mol^{-1}.K^{-1}) and T is the absolute temperature (K).

The Maillard reaction is complex and the use of simple kinetics means that observed parameters such as rate constant account for a combination of several elementary rate constants (Martins *et al.*,

2001). Most works in literature consider first order kinetics for Maillard browning, although zero and second are also common. According to Heldman and Lund (1992), colour changes can be modelled by using a first-order reaction rate and the effect of temperature on non-enzymatic browning reaction rate is usually expressed using an Arrhenius-type relationship. When applying kinetic modelling of this type to describe colour change, it is implicitly assumed that the change in colour is proportional to the depletion of key substrates in the chemical reaction. Once these substrates are gone, no further colour change occurs (Rajchasom, 2014).

First order kinetics have frequently been used to describe the browning reaction based on colour change indicated by CIE L*a*b* colour system. L* and a* have been identified as the most relevant indicators of browning (Matzdorf *et al.*, 1994). L* has been used for the measurement of kinetics of colour change in a number of high temperature food applications, including cracker baking (Broyart *et al*., 1998), tofu (Baik & Mittal, 2003), potato baking and frying potato cooking and frying (Nourian & Ramswamy, 2003), Pastry baking (Rajchasom, 2014) and nut roasting (Lukac *et al*., 2007).

To express browning reaction kinetics for this case, the rate equation (Eqn 2.1) is generally converted to be in terms of extent of reaction (X) (Rajchasom, 2014);

$$\frac{d[X]}{dt} = k[1-X]^n \qquad \text{Eqn. 2.6}$$

Where the extent of reaction (X) is given by:

$$X = \frac{L^* - L^*_\infty}{L^*_0 - L^*_\infty} \qquad \text{Eqn. 2.7}$$

Where L^*, L^*_0 and L^*_∞ are the measured colour at time t, 0 and at steady state respectively. The colour at steady state (L^*_∞) is taken to infer the point where reactant concentrations for the browning have been reduced to zero.

The Maillard reaction rate is highly affected by temperature, where an increase in temperature leads to an increase of the reactivity of components (Ames, 1990 and Martins *et al.*, 2001). This temperature difference is generally explained by the Arrhenius equation (Equation 2.5). The activation energy of the Maillard browning reported in research has a wide range for various applications. Walstra (2003) reported that the typical activation energy for Maillard reactions is 100-180 kJ.mol^{-1}. Additional reported activation energy values were between 67.9 and 70.8 kJ.mol^{-1} for cracker baking (Broyart *et al*., 1998), 34.8 and 89.9 kJ.mol^{-1} for a frying process (Nourian & Ramswamy, 2003), 28 and 140 kJ.mol^{-1} for drying processes (Rapusas & Driscoll, 1995 and Lopez *et al*., 1997) and 31.5 and 50.7 kJ.mol^{-1} for a grilling process (Matsuda *et al*., 2013).

2.5 Conclusions

The browning of cheese during baking is generally attributed to the Maillard reaction, a complex reaction that influences food appearance and qualities. The properties and functionality of cheese vary due to a range of factors including both compositional and baking conditions. The effect of these parameters on surface drying and flow can influence the formation and growth of blister and the subsequent colour change. Due to this potential variation it makes sense to use a single origin cheese for investigation throughout the thesis.

Most studies use image analysis to investigate colour change during thermal processing. Those studies assessed the average colour to represent the formation of brown colour relative to time and temperature history. Often the brown colour that occurs in foods is not uniform due to surface variation, which is likely to be due to variations in temperature. For cheese, this is evident due to the formation of blisters which heat and brown preferentially. For this reason, it is important to be able to measure and assess changes across an entire surface. Therefore, in the next chapter, a cooking system will be developed with the use of image analysis to measure colour and temperature change across a surface of a sample of cheese and determine the browning kinetics.

Once data for colour changes at different temperature time histories are available, a dynamic kinetic model, initially assuming 1^{st} order kinetics and the Arrhenius law can be developed to link processing conditions to the extent of colour change.

Chapter 3
Browning Kinetics

In terms of cheese baking, the characteristics of browning and blistering are linked, where browning is broadly the onset of brown colouration due to the application of heat, and blistering can be considered the formation of discrete regions of browned material. The browning reaction itself is attributed to Maillard browning and is dependent on reactant concentration and temperature. Blistering is the occurrence of localised regions of more intense browning due to differences in surface temperature history. To simplify the investigation the characteristics of browning and blistering were decoupled to focus initially on browning. This allowed for the formation and kinetics of browning to be investigated independently.

Literature has shown that compositional variation can influence the characteristics of cheese, including the degree of browning. Hence, one type of cheese was used for all experimentation throughout the thesis to control for this. Both the shred and slab format of the cheese were the same composition and from the same origin, a commercially produced Mozzarella obtained from Fonterra (Palmerston North New Zealand). The composition of this Mozzarella is shown in Table 3.1 below, as provided by Fonterra.

Table 3.1 – Experimental conditions for cheese slab browning trials

Moisture (g/100g)	Protein (g/100g)	Fat (g/100g)	Salt (g/100g)
48.7	25.6	21.4	1.3

3.1 Formation of Hypotheses

The Maillard reaction is a very complex process with various pathways, a network of reactions, and several influencing factors as discussed in the literature review. For the purposes of this study, the visual impact of the reaction, the appearance of brown colour during heating, is the most important characteristic to consider, as opposed to the formation of certain chemical compounds at different stages of the reaction. Therefore, a simplified approach was taken whereby the complex chemistry was not considered and instead there was direct focus on the physical colour change of a sample when heated.

In order to quantify changes in colour, a method of measuring colour was required. For a wide range of studies, the CIE L*a*b* scale has been used to assess colour changes and has been used to describe browning kinetics (Broyart *et al.*, 1998; Baik & Mittal, 2003; Nourian & Ramswamy, 2003; Rajchasom, 2014; and (Lukac *et al.*, 2007). The three parameters, L*a*b* represent lightness, redness, and yellowness respectively. In many cases, L* has been used for the measurement of the kinetics of colour change and modelling of the browning process (Broyart *et al.*, 1998; Baik & Mittal, 2003; Ilo & Berfhofer 1999; and Nourian & Ramswamy, 2003).

In terms of a visual colour change during browning, many researchers have found that first order kinetics apply, however zero and second order reactions have also been used (Martins *et al.*, 2001). It is assumed that the colour change is proportional to a reduction in the reactant concentration and at some point, the reactants will run out, at which point no further colour change would occur. Research regarding the high temperature browning of foods mostly found that browning follows first order kinetics, so it was expected that Mozzarella would follow the same kinetics. Therefore, a

first order model was developed, where the rate of reaction is dependent on the concentration of brown colour and temperature.

3.2 Development of Experimental Method to Characterise Browning Kinetics

The adopted approach for investigating the browning kinetics of mozzarella during baking was to measure colour change in relation to time and temperature. There are three main considerations in order to experimentally measure this process; colour, temperature, and the application of heat. Isothermal conditions are difficult to produce and control during a cheese baking process and therefore a method to measure colour and temperature dynamically during processing was required. Temperature is likely to vary across a cheese surface during heating, due to localised variation in heat flow, steam pocket formation (lifting the cheese surface) and other surface characteristics. If local measurements for temperature and colour could be obtained at the same position and time, then non-isothermal kinetic modelling could be applied.

3.2.1 Measuring Colour

Methods of measuring colour change were explored as part of the literature research. The chosen method to assess colour change was the use of machine vision. There are other methods for measuring colour change, such as colourimetry, however these methods are limited to a small assessment area and cannot be carried out in-process.

The machine vision process involves taking a digital image (or video) and converting still images (or frames) into the L*a*b* colour space, where both L* and a* are considered valuable in assessing the progression of browning (Martin *et al*, 2001). This method was non-destructive and allowed for a large sample area to be recorded and assessed. To capture the colour data for the experiment a Nikon D3100 DSLR camera (Nikon Corporation) was used, recorded in the sRGB colour format.

3.2.2 Measuring Temperature

Thermocouples measure temperature accurately with good resolution and accuracy, however are largely limited to measuring a point source. Infrared thermometers measure the thermal energy radiating from an object to calculate, display and record temperatures across the surface. They provide a non-contact method of recording the surface temperature of a material of known emissivity. Taking it one step further, infrared cameras capture and display a relatively large area and convert radiated thermal energy into a recordable array of temperatures. An infrared camera can be used to capture and record temperature of a relatively large region without compromising the sample or collection of a corresponding colour image at the same time.

A FLIR E60 Infrared Camera (FLIR System, Inc.) was used to measure and record surface temperature. This particular camera had a range of useful specifications and features including:

- The ability to record infrared video as well as still IR images and visible light images simultaneously utilising a built in 3.1MP camera
- A resolution of 320x240 resulting in a matrix of temperatures that can be converted into .csv files for analysis
- A USB port to connect to PC for control using FLIR software

3.2.3 Application of Heat

Options for heating a sample are limited due to space and operational constraints brought using two cameras in the process. For these reasons the use of an enclosed oven is difficult. Heat guns (manufactured for removing paint and wallpaper) deliver both heat and air flow and were found to be suitable for heating samples while taking up minimal space. They also simulate commercial

baking conditions that use focussed forced air convection. Two heat guns (Bosch, 2000W PHG 630 DCE) were used as the heating source for the experimental setup. These heat guns had two fan speed settings and could be controlled from 50-630°C, giving a good level of control in order to setup a feasible experimental process.

3.3 Experimental Setup

This section describes the development of a process to apply heat and light under controlled conditions, and measure both surface temperature and colour data over a wide area.

3.3.1 Temperature and Colour Data Collection

The most important considerations in the setup of this experiment were to maximise both the quantity, but also quality of information. The IR camera had a low resolution compared to the DSLR cameras with 320x240 pixels, compared to 4608x3072 pixels for the DSLR. In addition, the IR camera had a short focal length which would cause distortion and blurring of an IR image if the IR camera was at an angle to the sample. To optimise the quality and quantity of the data from the IR camera, it was placed directly above the sample (0.22m above the sample) to give the best focus and therefore accuracy of measurement. The DSLR camera was then placed as close as possible to the IR camera (0.30m above the sample) to minimise the angle compared to the sample, as illustrated in Figure 3.1. This allowed for the most data to be captured and minimised any optical distortion due to the angle. To capture images during the experimental trials, both the IR camera and DSLR camera were linked to a computer, which allowed for camera settings to be controlled and for the shutter to be triggered remotely. As a result, the cameras did not need to be handled and they remained in the same positions throughout the experiments.

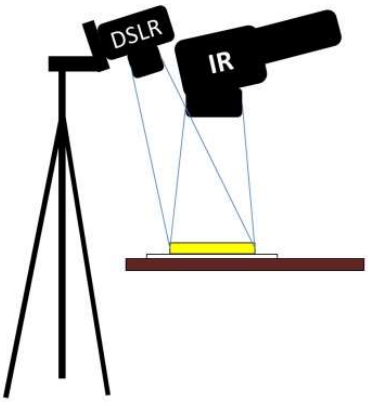

Figure 3.1 – Illustration of the position of the DSLR camera in relation to the IR camera above the sample position to minimise optical distortion

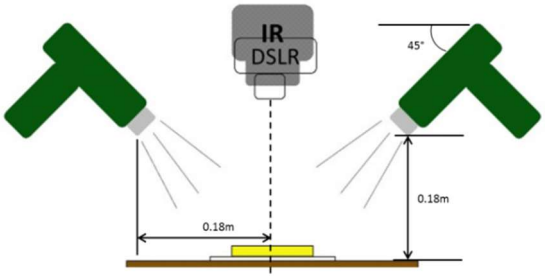

Figure 3.2 – Experimental setup showing the position and angle of the two heat guns and the IR and DLSR cameras centred above the sample position

To apply heat to the surface, two heat guns were used; one on either side of the sample, at a 45°C angle to the centre. The heat guns were held in place using clamp stands and positioned so the outlet nozzle was 0.18m from the table surface and 0.18m from the centre of the sample, as illustrated in Figure 3.2. This provided even heat distribution within the target region on a sample. Note that heat and airflow were not required to be perfectly even as long as conditions were consistent to minimise variation during and between trials. The change in surface colour and temperature was recorded over the entire sample surface and therefore time/temperature and time/colour histories could be captured over the sample surface.

3.3.2 Lighting

When cheese is heated, oil and liquid forms on the surface that creates reflections from the light source. Reflections result in an incorrect representation of the surface colour of the cheese for images taken with a digital camera. Therefore, the data for positions on the sample surface where reflection occurred was inadequate for analysis. It was important to minimise this effect in order to maximise the quality and quantity of useable data.

Various methods were tested to assess the quality of lighting for this application. The main goal was to light the subject while minimising the amount of light reflecting directly from the source to the camera. This involved adjusting the number and position of light sources as well as reflecting off and shining through different materials to create diffuse light. All methods using reflection and refraction resulted in various scattering of light, however reflection on the cheese surface remained. Some setups resulted in minimal surface reflection, however the subject was too dimly lit for adequate image capture. All experiments were carried out in a darkroom to eliminate any variation due to outside light sources.

A common technique in photography and machine vision is to use polarising filters to help control lighting conditions and manage reflections. Cross polarisation can avoid unwanted specular reflections, which can be achieved by illuminating the object with polarised light and using a polarizing filter on the camera lens capturing the image (Zude, 2009). This works by adjusting the filter on the camera so that light is polarised perpendicular to the light source, thereby isolating a single plane of light. Figure 3.3 shows an example of the effect of cross polarisation on the surface of baked cheese. For these images the camera was fitted with a polarising filter and a second polarising filter was used to show the comparison between the application of non-polarised and polarised light. This technique was found to be successful and was therefore adopted in the experimental setup in order to minimise reflection.

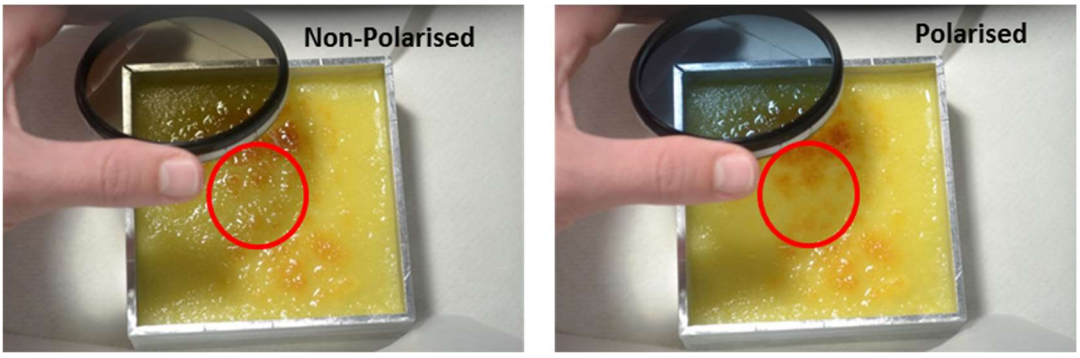

Figure 3.3 – Images of the surface of baked cheese showing the effects of non-polarised light compared to polarised light

To create polarised light a polarising filter had to be placed in front of the both the light source and the camera. This was achieved by using polarised film recovered from a LCD computer screen, which was cut and fitted to the end of hollow tubes made from aluminium foil. A circular polarised filter was fitted to the DSLR camera. The tubes of foil were fitted to the lamps to maximise and direct the polarised light produced. To align the polarising films, a small piece of the same sourced film was placed where the sample would be, and the foil tubes were rotated while looking at the live view through the camera. Optimum polarisation was achieved when the piece of polarising film appeared darkest as viewed through the camera filters and lens. Each lamp was aligned individually to ensure that light of the same angle of polarisation was exiting each lamp and matched the angle of polarisation of the filter on the camera. The result was a series of lamps emitting light with the same angle of polarisation to minimise bright spots of reflection. Two lamps were required to achieve

even lighting and adequate camera shutter speeds as the polarising filters cut out a significant amount of light. Figure 3.4 illustrates the position and setup of the polarising filters and figure 3.5 shows the actual experimental setup.

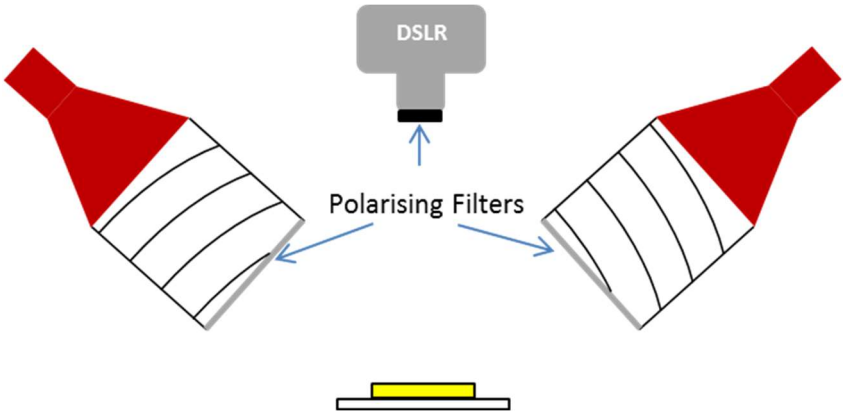

Figure 3.4 – Schematic of the lighting setup and positions of the polarising filters on the light sources and the DSLR camera

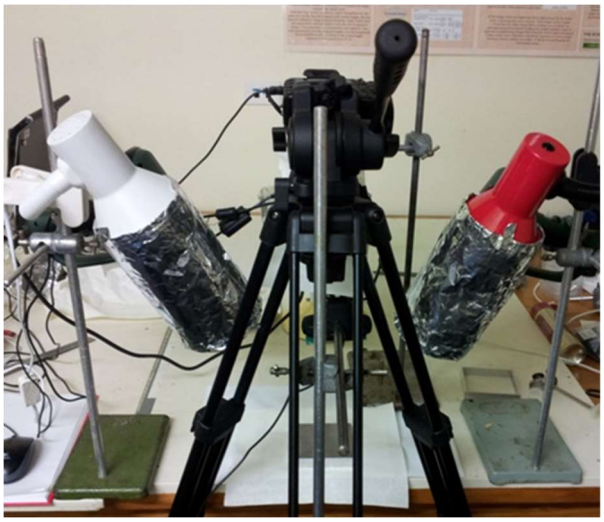

Figure 3.5 – The experimental setup for lighting, heating and image capture during cheese browning trials

3.3.3 Calibrated Colour Measurement

The representation of colour in images can vary significantly depending on lighting conditions. A light box was used to capture accurate representation of samples if adjustments based on 'actual' colour were required at a later stage. A light box provides a standard, calibrated, set of lighting conditions that allows for reproducible and comparable results. The light source within the light box was a panel of LEDs, which provided diffuse light of known colour temperature. The LED panel was controlled to be at a consistent known colour temperature (D65), and polarising filters, both on the light source and camera, were used to control and adjust reflections as necessary. Light from the LED panels passes through a polarising filter, which is reflected off the subject through a circular polarisation filter on a DLSR camera where the image is captured.

For each image taken, a colour chart (Xrite ColorChecker Classic) was placed next to the sample to allow for post processing digital colour correction. A specific colour patch, in this case orange, was used as a reference based on the known colour properties under the specific and controlled lighting conditions.

The experimental process developed could gather the required data to evaluate browning kinetics for cooking cheese under high heat conditions. The method for gathering this data was relatively straight forward, however there were hurdles regarding processing the data. The main hurdle was being able to directly relate the distributions of surface temperature and colour with respect to time.

3.4 Conducting Trials

The aim of the experimental trials was to measure and record changes in surface temperature and colour of a slab of cheese when subjected to a high temperature air flow. A square aluminium ring, with internal dimensions of 94mm by 94mm, was used to hold a 5mm thick slab of cheese for each experiment. All variables other than the temperature of heat guns were controlled to simplify the system and minimise variation. Experiments were carried out in an air conditioned dark room and at ambient temperature of 20°C.

3.4.1 Preparing the cheese

When required a 10kg block of frozen traditional mozzarella was cut using a bandsaw into 94x94mm lengths to match the dimensions of the ring used to hold mozzarella samples for processing. Lengths of mozzarella were defrosted over a four-day period at 4°C to ensure they were completely thawed. Mozzarella is difficult to cut evenly so a rig was fabricated to create a consistent thickness of 5mm. This involved placing a length of defrosted mozzarella into the rig, at a depth of 5mm, and then a wire cutter was run through it to give an even slab of cheese with a flat top surface. Figure 3.6 shows a schematic of the cheese cutting rig. For each experiment the cheese slab was cut within 5 minutes of commencing the trial.

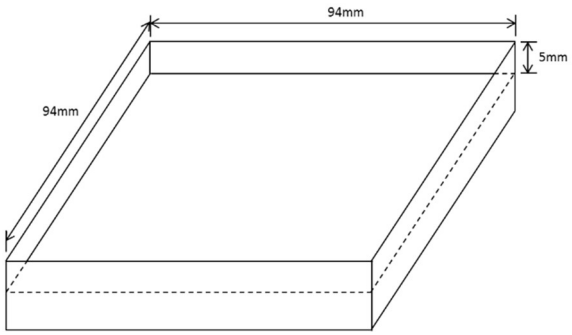

Figure 3.6 – Cheese cutting rig used to control thickness of cheese slabs for testing

3.4.2 Experimental Conditions

The equipment was set up for the cheese browning trials, as described in section 3.3. For each trial the only variable changed was the heat gun set point temperature. The experiments were carried out in a temperature controlled dark room to keep external heating and lighting conditions consistent, and the sample slabs were all prepared in the same manner as described in section 3.4.1. In addition, the settings and position of each camera were kept the same for all images taken.

Several experimental conditions were trialled to collect a range of data to be used for fitting a kinetic model. Table 3.1 shows the different experimental conditions used. Each experiment essentially included thousands of individual temperature and colour histories during heating, therefore replicates for all scenarios were not carried out. Scenario A was carried out twice, and scenarios B to D once each. Colour and IR images were recorded manually via a computer link every 10 seconds for total experiment times of between 20 to 40 minutes (longer total data collection times for experiments with lower temperatures and therefore slower reaction kinetics).

Table 3.2 – Experimental conditions for cheese slab browning trials

Scenario	Heat Gun Setting
A	550°C
B	600°C
C	550°C for 10min >> 600°C
D	550°C for 7min >> 600°C for 4 min >> 500°C

The output of the experimental process was many colour and IR images that required analysis to extract the data. The following section describes how the raw images were processed to extract and align the data within the images for each experiment.

3.5 Spatial Matching of Temperature and Colour Data

The temperature and colour both vary across the surface of the sample, even when heating is consistent and well controlled. Therefore, to produce a kinetic model for colour change based on temperature, the data need to be directly related in terms of position on a sample. Position based data differs from each image source due to relative image size and distortion, where the two cameras in different positions are trained on the same subject. Consequently, to investigate correlations directly, a method of remapping image data to match position and shape was required.

3.5.1 Raw Images

Infrared (IR) information was recorded as jpeg images, which gives a visual representation of surface temperature based on a defined temperature scale. The image file also contains a 320x240 matrix of temperature values within the metadata, which required conversion using proprietary FLIR software to obtain. The FLIR software was used to convert each image into a comma separated variable (.csv) file containing the temperature data. These images cannot be directly manipulated in any way, such as resizing or reshaping, as the background information, i.e. temperature data, would be lost. Therefore, in order align positional data the digital image space had to be manipulated to match the IR images. Figures 3.7 and 3.8 illustrate an example of the expected visual output of the same object using a digital camera and the IR camera. Here squares of aluminium were placed into the sample holder. Because the emissivity of the aluminium was substantially lower than the base material, differences in apparent temperature were observed in the IR image.

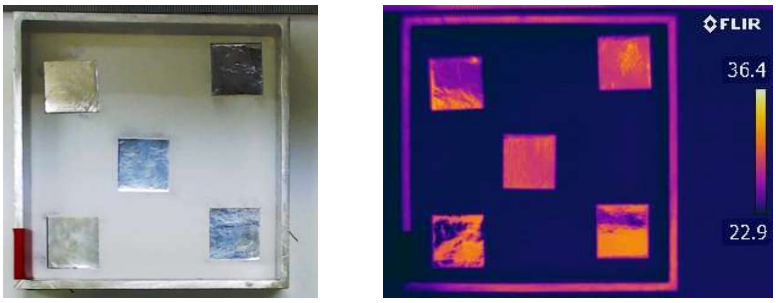

Figure 3.7 & 3.8 – An example of the same object imaged using a digital camera and an IR camera

3.5.2 Image Registration

To align temperature and colour data a method was required to identify positions in both IR and colour images and define how the colour image space could be manipulated to match the IR image space. Initially a direct relationship through triangulation based on known positions was considered,

however this did not account for optical distortion due to the camera positions differing and lens properties. Accurate matching of points was not possible without adjusting for image distortion.

Image registration is a well known technique used for image analysis and refers the process of aligning two or more images of the same scene. It is a computational method that determines the point-by-point correspondence between two images based on a reference coordinate system, which can then be used to fuse complimentary information in the images. Such a process can be applied to image data types, but also vector types, and is a useful tool in comparing data sets based on images (Goshtasby, 2012). The method developed for analysing IR data and colour data utilised image registration to remap the colour images to match positions denoted by coordinates in the IR image space.

The process first involved a calibration to determine the relationship between images produced from the IR and DSLR cameras. This was performed by imaging a reference object of known dimensions, thereby generating a grid defining how 'real world' parameters relate to both the IR and DSLR image spaces. The coordinate data from the calibration images was then used to relate the two image domains through a geometric transformation, where the IR image was designated as the fixed reference image. The DSLR camera produced colour images with 4608x3072 pixels compared to thermal images from the IR camera 320x240 pixels, and therefore the colour images were more suited to being transformed to match the IR image without losing useful data. Common practice for this process is to select many control points, and to use a least-squares regression to fit and characterise the geometric distortion.

The geometric transformation used to map the image data was based on a second-order polynomial approximation, where the equation parameters were fitted based on a least-squares regression. Equations 3.1 and 3.2 were used to define pixel positions of the control points in a colour image (v,w) equivalent to a specified position in the IR image (x,y) and c_1-c_{12} were the fitted coefficients. These equations could then be used to match the pixel position in the experimental colour images relative to the pixels in IR images. From this information, the colour at the position corresponding to each temperature measurement (as defined by the 320x240 matrix of data) from the IR images. Applying this process to each experimental image resulted in the history for both colour and temperature relative to time for up to 76800 individual points, covering the entire sample surface.

$$v = c_1 + c_2x + c_3y + c_4xy + c_5x + c_6y^2 \qquad \text{Eqn. 3.1}$$

$$w = c_7 + c_8x + c_9y + c_{10}xy + c_{11}x^2 + c_{12}y^2 \qquad \text{Eqn. 3.2}$$

3.5.3 Aligning Experimental Images

To determine a series of control points for the image registration process a calibration plate was fabricated from an aluminium plate using a CNC mill. The aluminium plate provided a significant difference in the thermal image, even at equilibrium, due to the emissivity difference between it and the background. Figure 3.9 shows the calibration plate and dimensions, which was sized to cover the sample region of 100x100mm square.

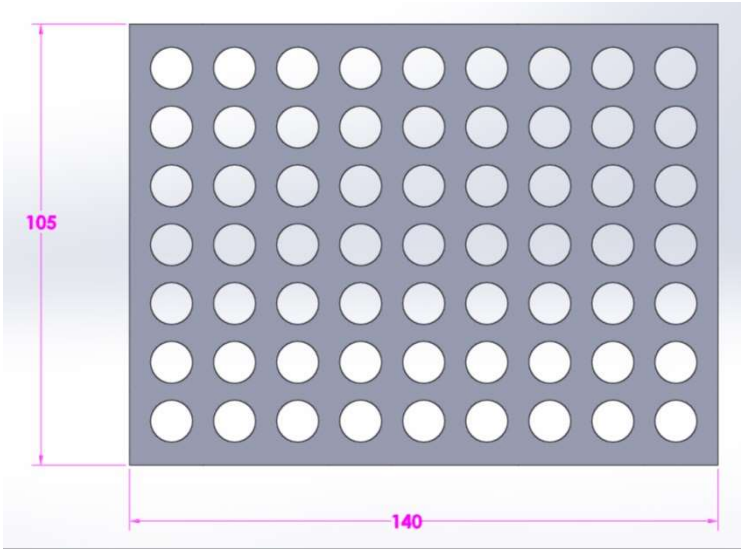

Figure 3.9 – Calibration plate, 140mm x 105 mm with 63 evenly distributed 10mm diameter holes

With the cameras in the appropriate positions, taking an image of this calibration plate resulted in a series of coordinates, based on the centre of each of the holes in the plate, defining a real world space as viewed by each image capturing device. As the camera positions remained fixed during experimentation, the pixel matching process could be applied to all images within an experimental run. Figure 3.10 shows an example of the calibration plate captured with the DSLR camera, and Figure 3.11 shows the calibration plate captured with the IR camera.

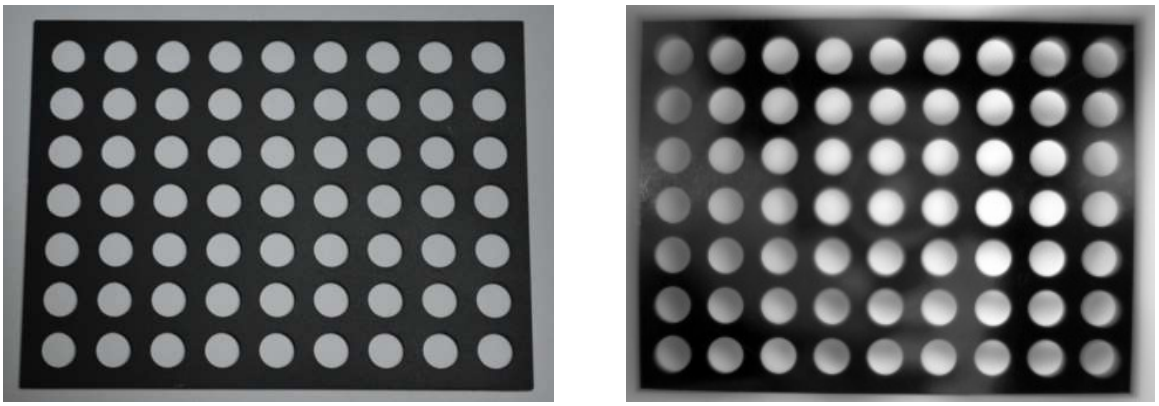

Figure 3.10 & 3.11– Images of the calibration plate captured with the DLSR camera and IR camera

MATLAB (Mathworks, Boston) was used to perform the image analysis and subsequent data analysis. The image registration and transformation process can be broken down into several key steps; determining the control points, fitting the transformation coefficients and remapping the colour image space. The output of this process is a 320x240xY matrix of IR data and a corresponding matrix of 320x240xY matrix of L* colour data, where Y is the number of experimental images.

The following method illustrates the process of calibrating and transforming images to align IR and colour data, and convert the colour data from sRGB to L* a* b* values.

Determine Control Points

1. The cameras were setup for the experiment and an image of the calibration plate resting in the sample region was taken on each camera.
2. The common 'Control Points' within the IR and colour calibration images were identified.

a. The images were converted to black and white.
b. The 'edge' MATLAB function was used to find edges in the calibration images to isolate the holes in the calibration plate.
c. The 'Region Props' MATLAB function was then used to determine the control points, based on the coordinates for the centre of each hole.
d. The IR coordinates were defined as (x,y), and colour coordinates were defined as (v,w), resulting in a total of 63 common Control Points for each calibration image.
e. Figures 3.12 and 3.13 illustrate the results of the control point identification process. The blue stars at the centre of each hole of the calibration plate were output as an array on coordinates, which were then used for the subsequent image transformation process.

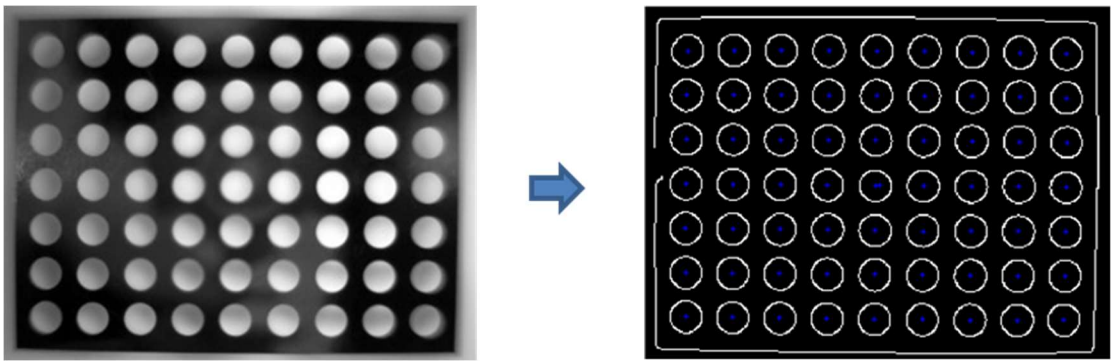

Figure 3.12 – Example of an original IR calibration image on the and resulting identification of Control Points, defined by the centre of each hole in the calibration plate

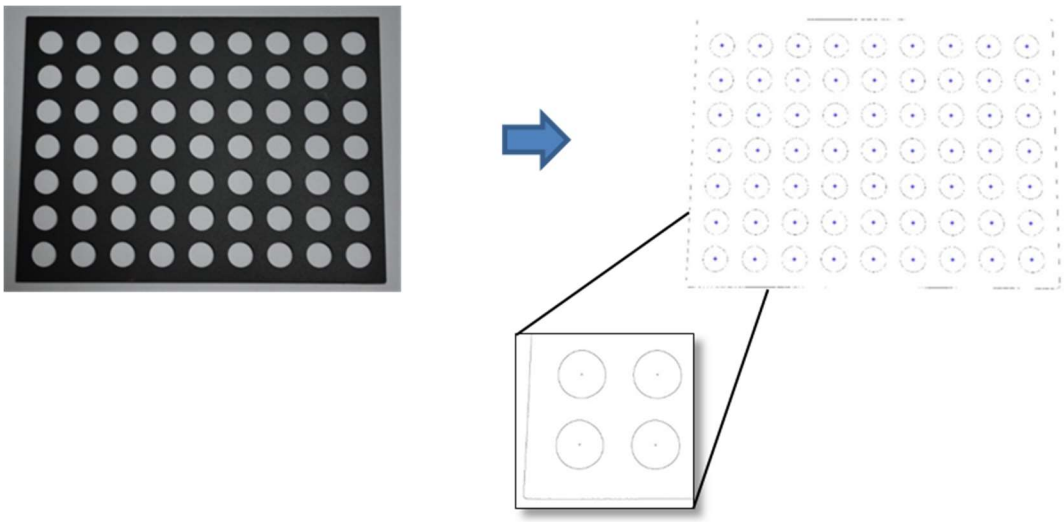

Figure 3.13 – Example of an original DSLR calibration image and resulting identification of Control Points, defined by the centre of each hole in the calibration plate

Transforming the Colour Image Space

3. The identified Control Points were used to calculate coefficients for the transformation equation.

a. The MATLAB function ‘fitgeotrans’ for a second-order polynomial was used to calculate the coefficients based on the ‘fixedPoints’ (IR image control point coordinates) and the ‘movingPoints’ (colour image control point coordinates).

4. The pixel coordinates in the colour image space corresponding to the reference IR image space were calculated, using the coefficients and Eqns. 3.1 and 3.2.
    a. For each pixel position based on a 320x240 matrix the matching pixel position in the colour image space was calculated.
    b. The resulting coordinates were written to a matrix to determine the corresponding colour value from the DSLR images.
5. A check step was included in the process to ensure that the transformation was accurate before remapping the experimental images.
    a. The remapped colour calibration image was overlaid on top of the IR calibration image to check that they matched
    b. Figure 3.14 illustrates the check process. The image on the left shows a successful calibration where the colour calibration image has been matched to the reference IR calibration image. The image on the right clearly shows an incorrect calibration, where the calibration images to not overlap.

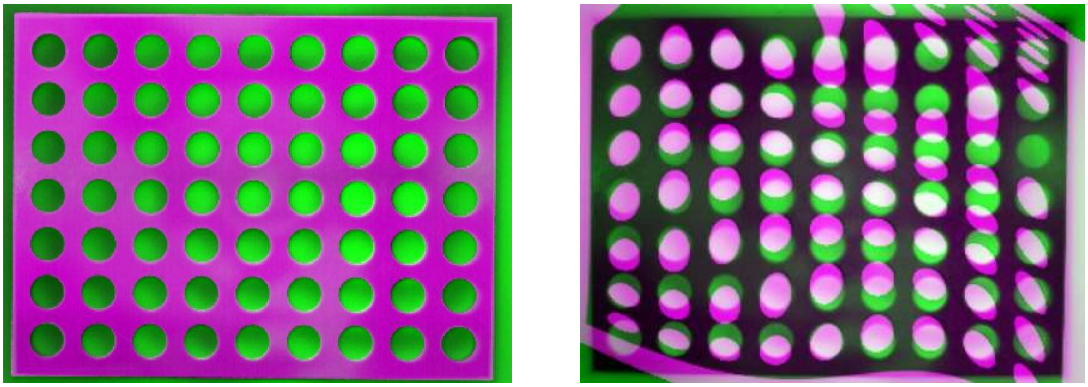

Figure 3.14 – Checking the calibration, on the left a correctly calibrated image, and on the right a deliberately warped calibration

c. Figure 3.15 illustrates the transformation and remapping process applied to a set of sample experimental images where the top right colour image was remapped based on the IR image (bottom left) space.

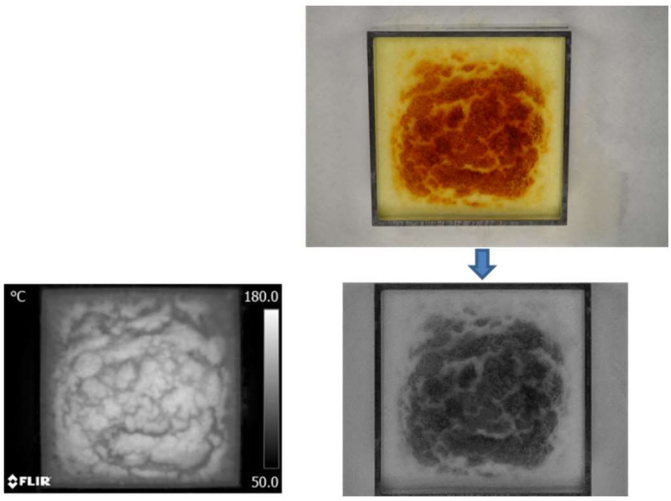

Figure 3.15 – Transformation and remapping process applied to a set of sample experimental images

Determine L a* b* Colour Matrix*

6. As the colour data was recorded as jpeg images with sRGB colour representation, the image data was converted into the L*a*b* colour space.
    a. The MATLAB function 'makecform', using the type 'srgb2lab' was used to convert the sRGB colour data into the L*a*b* colour space.
7. Starting with L* value, the colour value was calculated for each of the coordinates calculated in step 4.
    a. An average of 25 pixels, centred around each coordinate, was calculated to include the area relative to the IR pixel size.
    b. This process was repeated for each experimental image resulting in a 320 x 240 x n matrix, where 'n' represents the number of images for each experiment.
8. Step 6 was repeated to determine the a* and b* colour values.

The method developed allowed for the successful transformation of a colour image space to match an IR image space. As a result the colour values could be matched to temperature values for each position based on a 320x240 matrix, representing the history for both colour and temperature relative to time across the entire sample surface. The MATLAB files, A1_Define_CP.m, A2_Cal_Test.m and A3_Tform_LAB.m for this process can be found in the Appendix 1.

3.5.4 Extraction and Collation of Temperature Data

Temperature data was extracted from IR images using the proprietary FLIR software, FLIR Tools (FLIR Systems, Oregon). A script file was written in MATLAB (IR_Temps.m, Appendix 1) to collate each set of temperature data, where each file was opened and added to a matrix designated for each experimental run. The information was combined to create a 320x240xY matrix, where Y is the number of images defining experimental time points.

Having matched pixel positions, the temperature information and colour information for each position on a cheese surface during heating was determined. This data could then be used to develop a mathematical model representing the rate of browning with respect to time, and surface temperature.

3.6 Model Development and Fitting

A model was developed to describe the browning kinetics of a cheese surface during heating. The experimental information was collated and the process outlined in section 3.5 followed to determine the colour and temperature data with respect to time. These results were then used to fit the kinetic model.

3.6.1 Experimental Results

Figure 3.16 illustrates sample images from experimental runs under scenario B conditions, with a heat gun setting of 600°C, over a 20 minute period. Visual observations indicate that there is a correlation between temperature and browning based on the similar patterns that developed in both the IR and colour images. Closer analysis of the images show the potential to use the IR information as a predictor of browning, where localised temperature increases precede a colour change in that region. This can be seen when comparing the IR image at 10 minutes with the colour image at 15 minutes. The hotspots in the IR image, which are not brown in the colour image at 10 minutes, match reasonably well with the brown regions in the colour image at 15 minutes. The influence of temperature on the Maillard reaction has been well observed, where the reaction rate increases in relation to increased temperature. Increased temperature leads to an increase in the reactivity of the primary reactant compounds (Martins, et al., 2000). Hence, the localised regions of increased temperature would be expected to result in a corresponding colour change in those regions, as was observed.

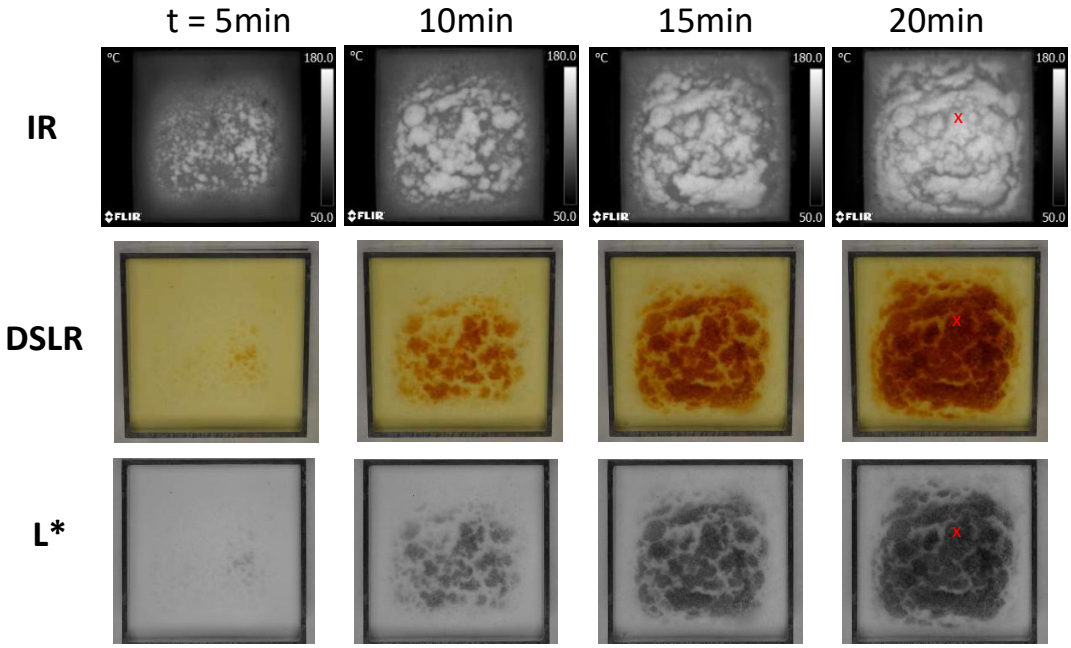

Figure 3.16 – Sample images showing surface temperature and colour change during baking (Heat gun setpoint 600°C) for 20min

For each set of experimental data, the IR images were converted to temperature values, and colour images are remapped and converted into L*a*b* colour values. An example of the resulting data is shown in Figures 3.17 and 3.18, illustrating the change in L* and temperature for a group of 5x5 pixels over a 20 minute heating process. The red 'x' in the final images of Figure 3.16 indicates the position for the plotted data. To better understand region size the equivalent real world dimensions were calculated. The length of 1 pixel is equivalent to 0.42mm, and therefore a 5x5 pixel region is

equivalent to 4.4mm^2. Figure 3.18 shows that temperature differences of up to 20°C occur within 200-500 seconds, however the relative L* values remain within a tight range. This indicates that temperature variation in the initial stages has a minimal effect on the rate and variation in colour change, most likely because the temperature is not high enough to result in significant browning within this time frame.

Using this data, a non-isothermal model could be developed to predict colour change in respect to L* based on the time/temperature history.

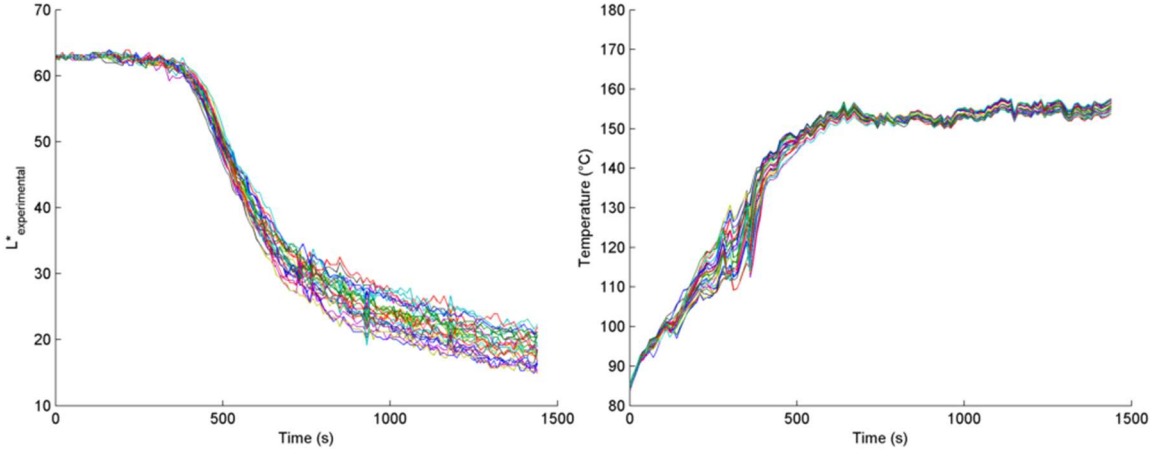

Figure 3.17 & 3.18 – L* value and temperature of cheese surface at position 'x' of Figure 3.15 (Heat gun set point 600°C)

3.6.2 Model Fitting

A first order kinetic model (Eqn 3.3) was developed to describe colour change on the surface of cheese during heating. The rate that L* value changes is relative to how far away the value is to an equilibrium colour, L^*_∞ (achieved when Maillard reactants have been exhausted), and the reaction rate constant k. This approach assumes that the concentration of reactants is proportional to $(L^* - L^*_\infty)$. When all reactants are consumed, the colour reaches L^*_∞, and so the driving force reduces towards zero.

$$\frac{dL^*}{dt} = -k\,(L^* - L^*_\infty) \qquad \text{Eqn. 3.3}$$

For many models of Maillard browning, the effect of temperature has been expressed by the Arrhenius relationship (Franzen, *et al.*, 1990). A modified form of the Arrhenius equation (Eqn 3.4) was used based on a reference temperature, T_{ref}, which is often preferable as then the rate constant at the reference temperature, k_{ref} has a meaningful value, where the traditional Arrhenius constant usually has a very high magnitude and creates sensitivity issues during model fitting (Trambouze, *et al.* 1988).

$$k = k_{ref}\, exp\left(-\frac{E_a}{R}\left(\frac{1}{T} - \frac{1}{T_{ref}}\right)\right) \qquad \text{Eqn. 3.4}$$

For this model a reference temperature of 120°C was chosen, which was between the minimum and maximum surface temperatures. Because the temperature varies with time and position, the non-isothermal kinetic equation (Eqn 3.3) was combined together with the Arrhenius equation (Eqn 3.4) to give Eqn 3.5 which was solved numerically for any given temperature, time history.

$$L(t) = \int_{L^*_0}^{L^*} k_{ref}\, exp\left(-\frac{E_a}{R}\left(\frac{1}{T}-\frac{1}{T_{ref}}\right)\right)(L^* - L^*_\infty)\, dt \qquad \text{Eqn. 3.5}$$

MATLAB was used to solve this kinetic model using the 'ode45' function. The kinetic parameters k_{120} and E_a were fitted to the relevant data, using a nonlinear regression function, 'lsqnonlin'. The 'lsqnonlin' function was used to assess and minimise the residual sum of squares between experimental L* and predicted L* values. During the initial stages of model fitting it was decided to set L^*_∞ at a constant value. The aim of this fitting process was to obtain a single set of parameters that fit the data well. To simplify the fitting process the average final L^* for the range of experiments was calculated and used as L^*_∞. This was calculated to be ~20. It is believed that this is an appropriate value for this process as where L^* below 20 were very dark visually and it is suggested that browning at this point is no longer driven by the Maillard mechanism. Hence data beyond this point was beyond the scope of this kinetic model.

The raw data indicates that some areas on the cheese surface during cooking did not heat up significantly and therefore did not brown. Figure 3.19 shows an example of the temperature profile at the end of an experimental run, illustrating the variation in surface temperature across the cheese surface. The temperature in the darker regions ranges between 100-115°C. As discussed in section 3.6.1, the data from these areas is not useful in developing a browning model, so as part of the analysis a method of defining and separating data, based on either temperature, L* or both, was developed to optimise the model fitting process. In addition, as there was such a large amount of data to be processed, isolating the relevant data gave the best chance of obtaining accurate and efficient model fitting.

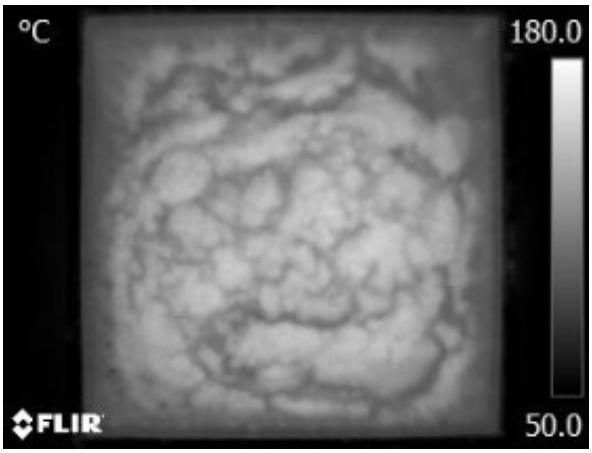

Figure 3.19 – IR temperature profile after 20 minutes with heat guns set at 600°C

It was noted that in some areas during the initial stages of heating a rise in L* occurred, indicating that the sample became lighter in colour. Literature has reported that the opaqueness of cheese increases when heated during the melting phase at temperatures below 100°C. The scattering of light increases due to changes in the microstructure of cheese when heated (Metzger *et al.*, 2000; Dave, *et al.*,2001; Pastorino, *et al.*, 2002). Due to this effect, data within this region is not useful for modelling so there was potential to omit this information to improve the model fitting process. In addition, browning rates are slow until temperatures above the range of 105-120°C (Shibukawa et al., 1989; Broyart *et al.*, 1998; Purlis & Salvadori, 2009 and Purlis, 2010). A temperature of 120°C was chosen as a minimum limit, where any point at a lower temperature could be considered not to have browned and the corresponding data could be disregarded for modelling purposes. To further

isolate relevant browning data the change in L* was considered to exclude positions where there was not a significant change in colour.

3.6.3 Model Fitting Results

Initial model fitting was carried out using average values for temperature and L* over a specified region of interest (ROI) for each trial. The ROI was defined as an area of 100 x 100 pixels around the centre of each sample image, as illustrated by Figure 3.20. For each experimental image the temperature and L* values within the ROI were averaged to build a matrix of time, temperature and colour for each experiment.

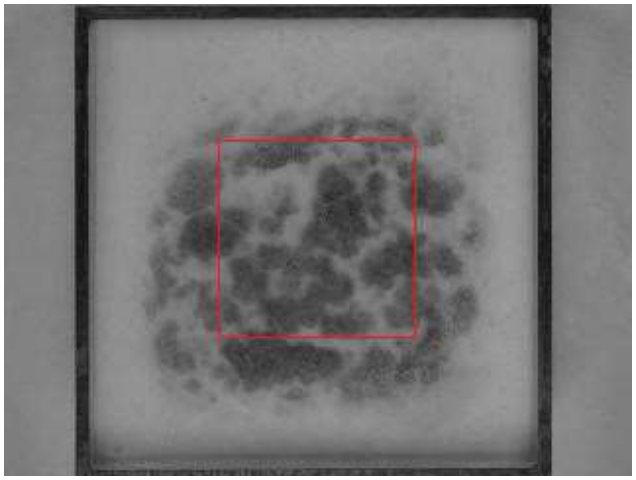

Figure 3.20 – Illustrating the 100x100 pixel region of interest of an experimental sample image

The model was solved for each trial individually and parameters optimised, which resulted in a good fit and similar E_a and k_{120} values. Figures 3.21 and 3.22 illustrate the experimental L* values, blue lines, compared to the relative L* values predicted from the model, red lines. The model predicted the lightness well for all trials, where the goodness of fit (R^2) for each trial was above 0.99. Table 3.2 outlines the fitted parameters for each scenario and the resulting R^2. E_a ranged from 114-131kJ/mol and k_{120} from 4.2 to 5.6E-4 s^{-1}. The values for E_a agree within the expected limits for the Maillard reaction (Rajchasom, 2014).

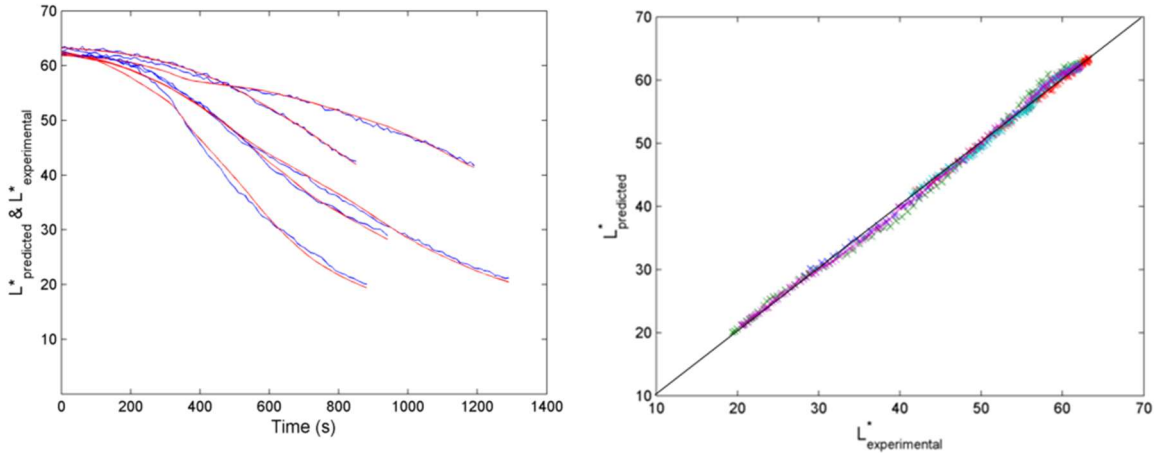

Figure 3.21 & 3.22 – Results based on the ROI averages; experimental L* compared to predicted L* with individual kinetic parameters fitted for each trial as outlined in Table 3.1. In Figure 3.21, blue represents experimental L* values, and red represents predicted L* value

Table 3.3 – Fitted parameters and resulting fit for each experimental scenario

Scenario	E_a (J.mol^{-1})	k_{120} (s^{-1})	R^2
A1	120470	4.20x10^{-4}	0.999
A2	114070	4.99x10^{-4}	0.996
B	126223	5.21x10^{-4}	0.999
C	130244	5.01x10^{-4}	0.996
D	130821	5.61x10^{-4}	0.999
Average	124366	5.00x10^{-4}	

As a simple method of defining one set of kinetic parameters, the results for E_a and k_{120} for each trial were averaged, giving values of 124kJ.mol^{-1} and 5.0x10^{-4}s^{-1} respectively. These values were used to solve for L* using the time/temperature histories for each trial run. Experimental L* data was plotted alongside the results for predicted L*, as illustrated in Figure 3.23. Figure 3.24 shows a direct comparison of experimental versus predicted lightness, indicating a good fit where R^2 was greater than 0.97 for each set of data.

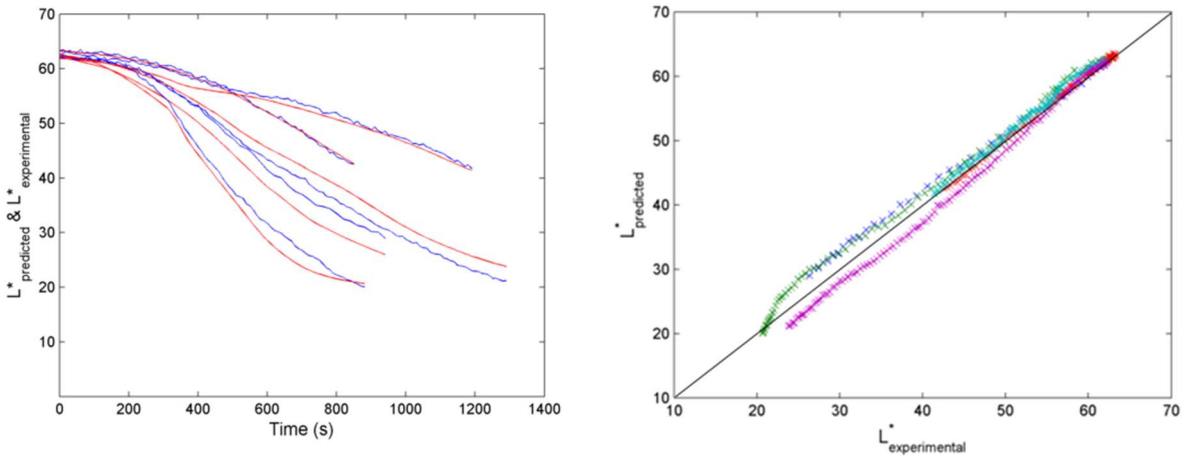

Figure 3.23 & 3.24– Results based on the ROI averages; experimental L* compared to predicted L* using average of the kinetic parameters (Ea 124kJ.mol^{-1} & k_{120} 5.0x10^{-4}s^{-1}) fitted for each trial as outlined in Table 3.1

This exercise showed that there is some variation in the ideal kinetic parameters between the experiments. To investigate the variation and suitability of one set of kinetic parameters, a series of five points for one experimental trial, scenario B, were selected and analysed. These five points are shown in Figure 3.25, and were defined based on the centres of blisters, discrete regions of browning.

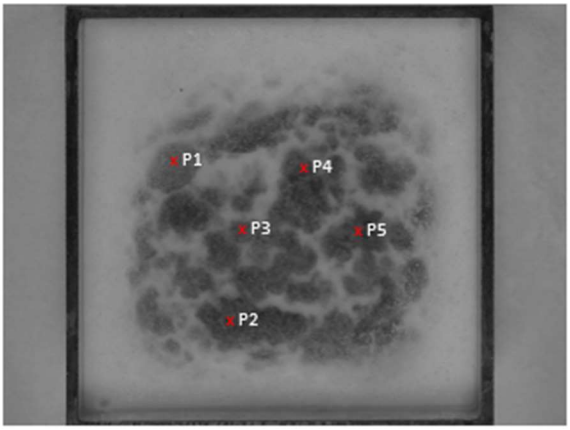

Figure 3.25 – Example experimental image from scenario B showing the five selected points for further analysis

When running the model, a total of 25 pixels surrounding each central point were used. The kinetics from the average ROI fitted above (E_a =124kJ.mol^{-1} & k_{120} =5.0x10^{-4}s^{-1}) were used to obtain an initial evaluation of fit for the five points. The median R^2 for the individual regions ranged from 0.79 to 0.95 as shown in Table 3.3, signifying a relatively poor fit when applied to a range of different points. The poor fit can be seen visually in Figures 3.26 A to E, where the change in L* value is over predicted at each point. Taking an average of temperature and L* captures a wide range of colour values, from those that did not change to those that browned significantly. These results show that for predicting L value, the use of kinetic parameters from average values is not ideal. To further investigate the kinetic parameters, data for the individual points were run through the model fitting process.

Table 3.4 – R^2 results from using the parameters fit from Average ROI data (Ea 124 kJ.mol^{-1} & k_{120} 5.0x10^{-4} s^{-1})

		P1	P2	P3	P4	P5
Resnorm		112596	65729	167185	72248	142611
R^2	Min	0.571	0.879	0.655	0.833	0.715
	Max	0.949	0.982	0.928	0.984	0.963
	Median	0.827	0.942	0.785	0.952	0.838

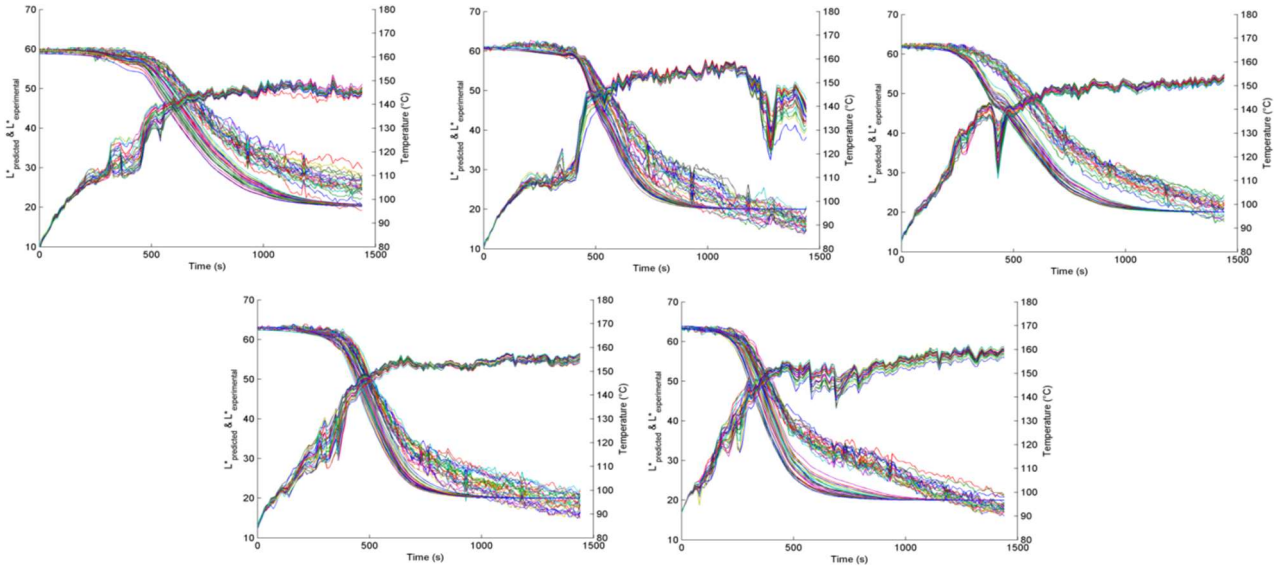

Figure 3.26 A to E – Predicting L* value for five specific points using the parameters fit from Average ROI data (Ea 124kJ.mol^{-1} & k_{120} 5.0x10^{-4}s^{-1})

During the optimisation process it was found that there was a range of combinations of E_a and k_{120} that resulted in a good fit, R^2 0.97 and above, making finding the 'optimum' parameters difficult. This was the case for each of the five points. Data for P1 was analysed more thoroughly to identify the parameters that resulted in the best fit possible. Figures 3.27 and 3.28 below illustrate the best fit with an R^2 of over 0.98, where the optimal kinetic parameters were E_a = 101.3 kJ.mol^{-1} and k_{120} = 3 .65x10^{-4} s^{-1}.

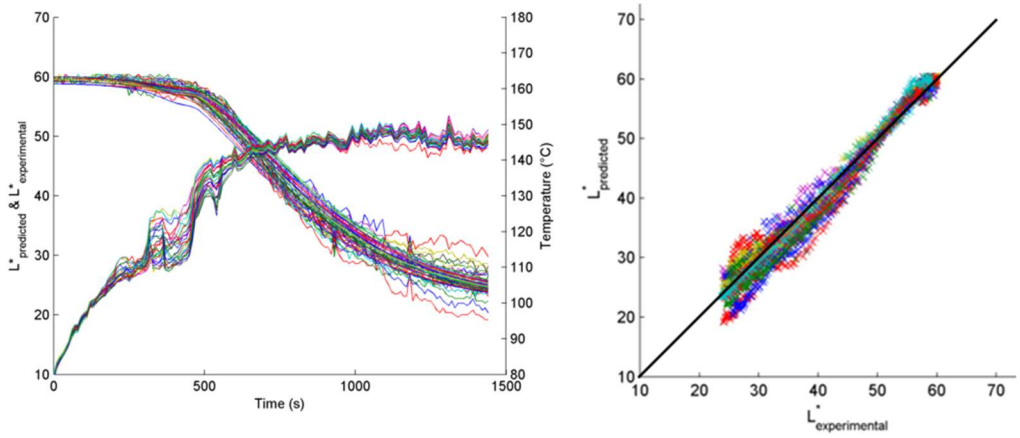

Figure 3.27 & 3.28 – Predicting L* using optimised parameters based on P1 data (Ea =101.3 kJ.mol^{-1} & k_{120} = 3.65x10^{-4}s^{-1})

These kinetic parameters were then applied to the remaining four points and the goodness of fit was quantified. The results are shown in Table 3.4 and Figures 3.29 A to D below, where the minimum median R^2 was 0.981 and minimum R^2 overall was 0.927. This indicates that although there is variation within the ideal kinetic parameters there is some consistency in performance.

Table 3.5 – R2 results from using the parameters fit from P1 data (Ea 101kJ.mol^{-1} & k_{120} 3.65x10^{-4}s^{-1})

		P1	P2	P3	P4	P5
Resnorm		10008	22802	15705	22209	20086
R^2	Min	0.949	0.956	0.951	0.950	0.927
	Max	0.998	0.996	0.994	0.997	0.996
	Median	0.987	0.981	0.982	0.985	0.985

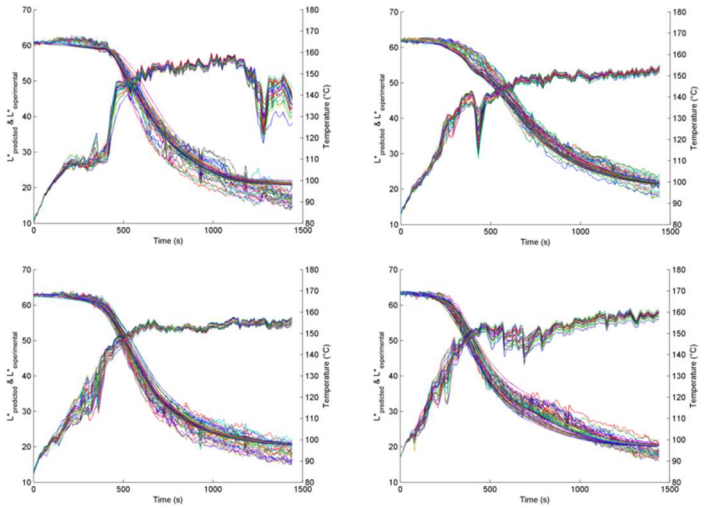

Figure 3.29 A to D – Predicting L* value for P2 to P5 using the parameters fit from P1 (Ea 101kJ.mol^{-1} & k_{120} 3.65x10^{-4}s^{-1}), where noisy lines are experimental data and smooth lines are model predictions

For each of these five points the rate of temperature increase was relatively smooth, and the range between the 25 pixels small. In comparison, the rate that actual L* decreased was also relatively smooth, but the range in values spread out towards the end of the trial. Cheese is not a perfectly uniform material, where concentrations of components will differ across the surface. These concentration differences will affect the rate of colour change during the application of relatively uniform heating. The Maillard reaction is mainly driven by reducing sugars and components containing a free amino group, hence the concentration of these components influences the degree of browning (Martins, *et al.*, 2001). In reality, there is variation in the extent of browning as the concentration of Maillard browning reactants differs, which results in a range of final L* given a similar heating profile. In addition to this there is not the same resolution when comparing L* to T, where there is better differentiation in colour than temperature. This leads to predicted results that are more generalised without the same degree of detail.

It was noted that for P1 to P5 that temperature did not fluctuate very much during the cooking process. To further investigate this, three points, P6 to P8, where temperature did fluctuate significantly were predicted using the kinetic parameters from the average ROI and P1 for comparison of performance. The positions of P6 to P8 are illustrated in Figure 3.30 below.

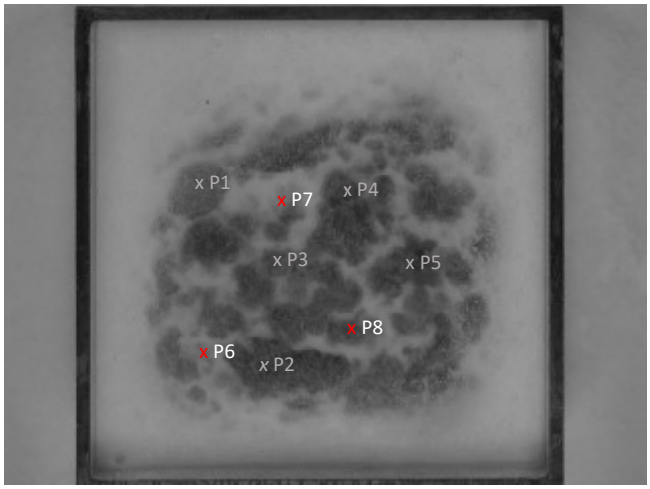

Figure 3.30 – Example experimental image from scenario B showing the additions points for analysis, P6 to P8

Figures 3.31 A to C show that the fit using the kinetics defined by P1 is poor where the change in L* is under predicted, resulting in R^2 ranging from 0.58 to 0.78. However, using the kinetic parameters from the average ROI resulted in a reasonable fit as illustrated in Figures 3.32 A to C, where R^2 ranged from 0.84-0.93.

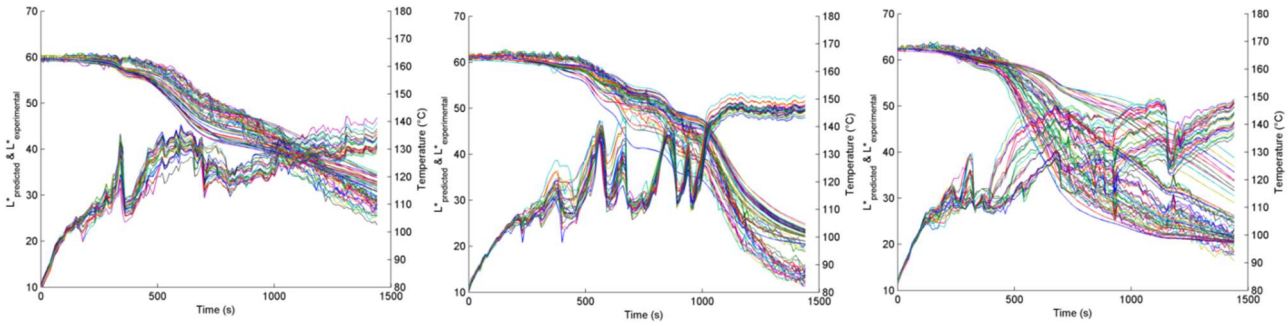

Figure 3.31 A to C – Predicting L* value for P6 to P8 using the parameters fit from Average ROI data (Ea 124kJ.mol^{-1} & k_{120} 5.0x10^{-4}s^{-1}), where noisy lines are experimental data and smooth lines are model predictions

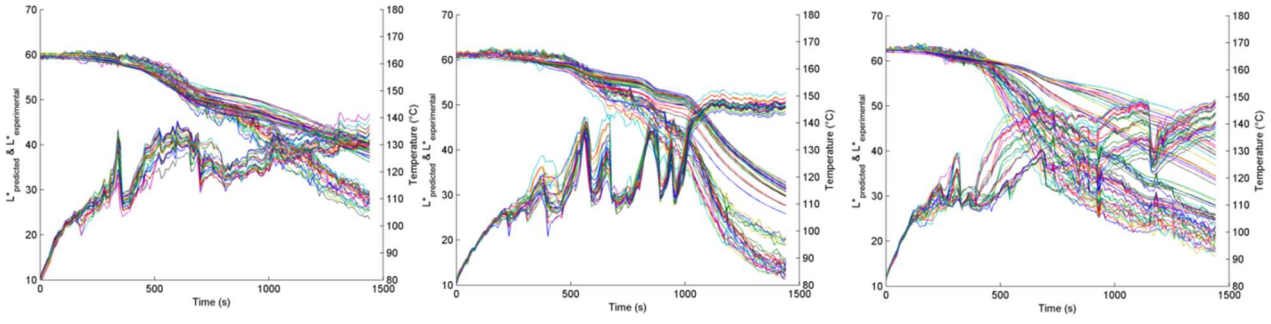

Figure 3.32 A to C – Predicting L* value for P2 to P5 using the parameters fit from P1 data (Ea 101 kJ.mol^{-1} & k_{120} 3.65x10^{-4} s^{-1}), where noisy lines are experimental data and smooth lines are model predictions

Processes occurring during baking of cheese are chaotic in terms of steam generation and bubble formation, which likely affect the rates of reaction and therefore the relative kinetic parameters. For example, with even heat applied to the cheese surface, steam formation with the cheese creates bubbles which affect the thickness of the top layer, with a likely flow on effect of varying heat flux

being applied at different positions. There is not fine enough detail in the data gathering process to be able to account for the wide variation in what occurs on the cheese surface during baking. The maximum rate of image capture was only one image every 10 seconds, and hence the temperature is only known at these times. Temperature changes more rapidly than colour change and can fluctuate up and down significantly, where browning is non-reversible.

Even though the specific conditions on the surface of the cheese cannot be accounted for, with the information available, the model produced gives a good representation of browning during baking. Because the model is relatively simple it is easy to adjust if necessary and it is straightforward to analyse further data. Directly comparing the predicted and experimental L*values may not be the most useful way of interpreting how well the model fits the data. Perhaps a visual representation of the cheese surface could give a better and more appropriate comparison.

3.6.4 Representative Images

Another method of representing and comparing the data is to view predicted L* as a recombined image, i.e. create an image of the cheese surface from predicted L* to compare to the experimental image. For a region of 201x201 pixels around the centre of the sample, L* was predicted at each pixel using both the kinetic parameters fitted from the average ROI and P1 data. The resulting predictions were recombined for experimental times of 8, 12, 16, and 20 minutes to create the representative images shown in Figure 3.33. A good correlation is evident when comparing the images visually, where the general shape of the browned areas match well for both sets of kinetic parameters. In terms of accuracy the overall brown area appears to be better predicted from the Average ROI kinetics, where the kinetics of P1 underestimate the overall colour change, appearing lighter than the experimental image. However, in terms of the distribution of L* in the dark regions the P1 kinetics show a better gradient over the dark region surface, where for Average ROI the dark regions appear flat in colour.

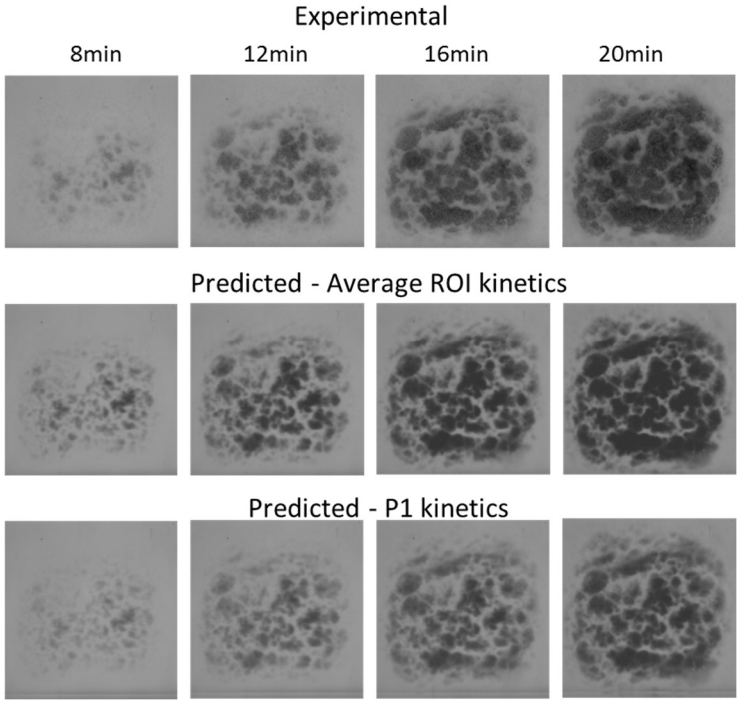

Figure 3.33 – Comparison of experimental L* images with recombined images using L* predicted using the kinetic parameters fit from Average ROI and P1 data

To quantify and compare the results objectively, the residuals between experimental and predicted L* were analysed. The results were evaluated and are shown in Table 3.5 below. A negative value indicates that a predicted element is darker than the experimental element and vice versa. This analysis indicates that predictions based on the Average ROI kinetics were more accurate, resulting in an overall lower difference from the experimental data with overall R^2 of 0.88 compared to 0.66 for the kinetics estimated from P1. In addition, the average residual using the Average ROI kinetics, both positive and negative, were evenly weighted where the degree of under and over prediction was similar. In contrast, the average residual for the P1 kinetics was heavily weighted in the positive, meaning that in general, predicted values were significantly lighter in colour than the experimental values.

Table 3.6 – Results from comparison of experimental L* images with recombined images using L* predicted using the kinetic parameters fit from Average ROI and P1 data

	Average ROI Kinetics – $R^2 = 0.88$		**P1 Kinetic – $R^2 = 0.66$**	
	-ve	**+ve**	**-ve**	**+ve**
Count	28156	12245	13450	26951
Average	-3.14	3.00	-1.33	5.17
Median	-2.24	1.93	-1.18	4.30
Maximum	-24.1	29.9	-23.8	29.8

It may be possible to improve the accuracy of the model to obtain better predictions for L*, however it must be questioned how useful a more accurate model would be. The ultimate application for this project is to be able to predict some measure of browning and blistering on the surface of cheese during baking. Knowing the exact colour value may not be the most appropriate or relevant process to make such predictions. It may be more relevant to assess the level of brown coverage on the surface of cheese. A sensory based measure for pizza assessment is the level of blister coverage (Fonterra Research and Development), which could be applied in this case. However, in order to do so, a blister with respect to cheese baking needs to be defined in a measurable way.

The results from this chapter suggest that browned regions can be accurately predicted, even when L* values are not perfect. Therefore, the predictions of L* could be used to determine a level of brown coverage, where the coverage could then be used as a measure to compare with the experimental results. Chapter 5 explores this idea through defining what a blister is and developing a process to quantifiably measure blister coverage.

3.7 Conclusions

An experimental process was developed to decouple and isolate browning kinetics of Mozzarella from the effects of blistering. The experiment allowed the simultaneous capture of both temperature and colour data for a relatively large area of cheese. First order kinetics were applied to the data to develop a model to predict colour change during baking, based on the surface temperature. During the model-fitting process, it was found there were a range of combinations of E_a and k_{120} that resulted in a good fit. Variation across the surface of cheese in terms of composition and heat rates are likely to contribute to variation in the rates of reaction resulting in a visual colour change. The overall analysis determined two sets of optimised kinetic parameters to describe the browning of cheese during heating, one based on an average temperature and colour over a defined region of interest, and the other based on a discrete region where browning occurred.

A visual representation of the cheese surface based on predicted L* value showed a good correlation compared to relative experimental browning pattern. Images created based on predicted L* values for both sets of kinetic parameters matched well with the shape and outlined of browned regions, however the ability to predict colour variation within discrete browned areas differed.

Browning is affected by temperature and heat flow and even in a small-scale setup there is significant variation in temperature and heat flow. This results in variation in browning. Knowing these properties and how they vary and can be controlled is important to be able to assess and analyse commercial applications of cheese baking.

Chapter 4
Commercial Oven Characterisation

A major application for this project is the commercial baking of pizzas in quick serve markets. The browning experiments in Chapter 3 showed that temperature and heat flow are significant process parameters affecting the appearance of pizza after baking. It is therefore important to understand how temperature and heat flow vary and are controlled in commercial applications. This will enable development of experimental techniques and models relevant to optimise such commercial applications for specific outcomes.

To enable this, a commercial pizza oven was modified to increase the data gathering capability during pizza baking. A series of experiments were carried out to characterise the modified pizza oven in terms of airflow, temperature distribution and heat transfer. Data from these experiments allowed for the development of experimental techniques for further browning and blistering analysis in subsequent chapters.

4.1 Commercial Pizza Oven

A commercial Lincoln Impinger II 1100 Series pizza oven was modified to investigate various aspects of the baking process. Heat is applied by six 1600 W elements, allowing the oven to be controlled in the temperature range from 93 to 288°C. Air is distributed around the oven through upper and lower diffuser plenums by an axial flow fan. Most of the air is recycled with some air losses and make up from the ends of the oven (pizza entry and exit points).

The oven was modified in several ways (see Figure 4.1 and 4.2). The conveyor was replaced with a trolley which was pulled through the oven on rails. Four load cells were used to support the rails, enabling continuous monitoring of pizza mass as a function of time during cooking. The cooking time could be controlled precisely by adjusting the speed of a winch used to pull the tray through the oven.

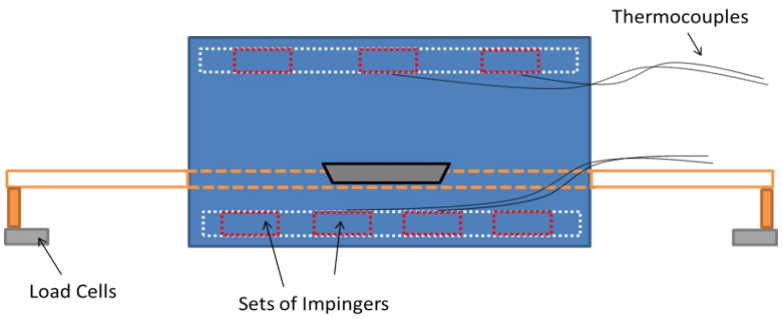

Figure 4.1 – Schematic diagram of commercial pizza oven modifications.

Twelve fixed and six removable thermocouples were used to record the temperature distribution across the oven and in the pizza during cooking. The fan speed was changed from fixed speed to variable control. This allowed investigation of the effect of air flowrate on temperature distributions and heat transfer coefficients at the surface of the pizza.

Figure 4.2 – Commercial pizza oven experimental setup and modifications.

An attachment point for a bore scope and a FLIR IR window were installed within the oven wall surface as shown in Figure 4.2. The borescope allowed in situ imaging of the cheese surface during baking. However, the image capture area was limited and in a fixed position, which made the use of such images not practical for this analysis (see Figure 4.3). The FLIR IR window was added to the front of the oven to facilitate surface temperature measurements using an infrared camera, without affecting the airflow inside the oven. Like the borescope however, this was limited in terms of being able to gather useful data for this analysis based on the fixed window and the angle of the image (see Figure 4.4).

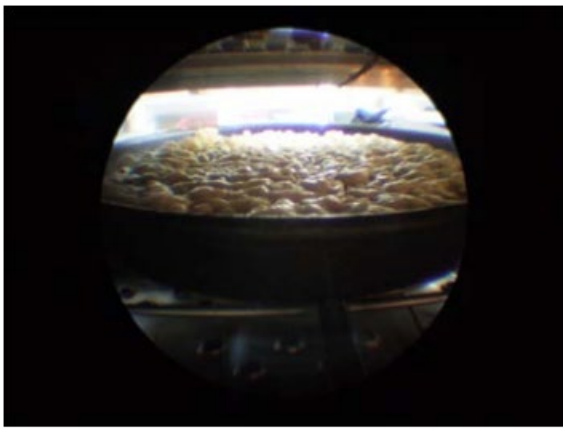

Figure 4.3 – Example image from borescope

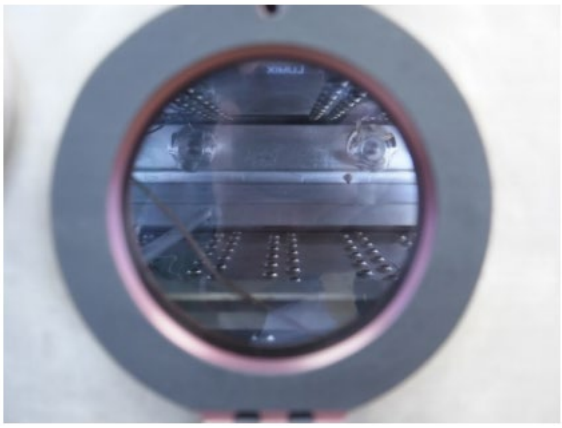

Figure 4.4 – View through IR window

All thermocouples, load cells and set points (fan speed, pizza residence time etc.) were recorded using an Omega data acquisition interface (OMB-DAQ-2416) connected to a PC running LabView. The modifications to this oven allowed control of a range of variables including bake time, oven temperature, and fan speed. Note that bake time in this case is based on the residence time for any and each part of a pizza. The main idea behind making it possible to manipulate these variables was that they affect firstly the rate of heat transfer and secondly the quantity of heat applied. As well as being able to control these variables, it was important to know how they affect the magnitude and rate of heat transfer.

4.2 Oven Air Flow

The Lincoln Impinger oven uses fan forced hot air to cook pizzas as they pass through at a constant speed. The flow of air within the oven is provided by a large fan at the rear of the oven, which forces air to be distributed into plenums at the top and bottom of the oven and then vertically through series of impingers (12mm holes in the plenum). The position and layout of the impingers is shown in Figures 4.5 and 4.6.

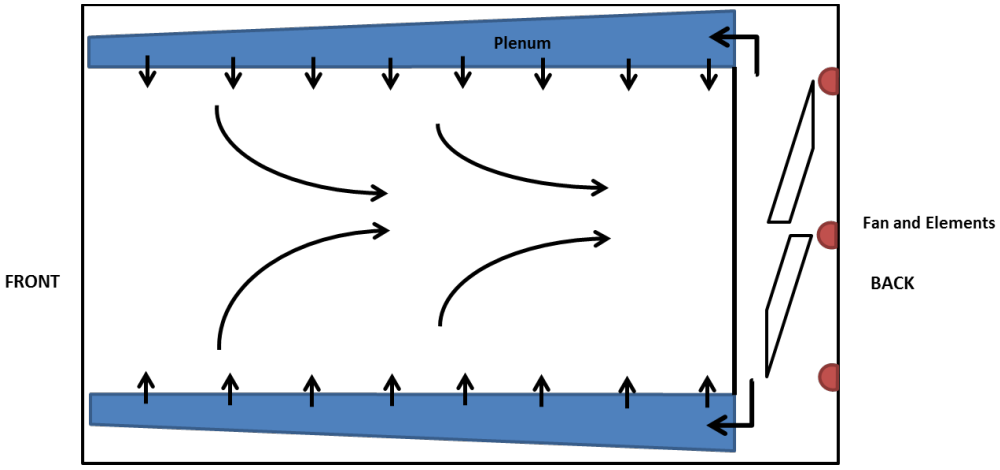

Figure 4.5 – Flow of air, pizza travels towards reader

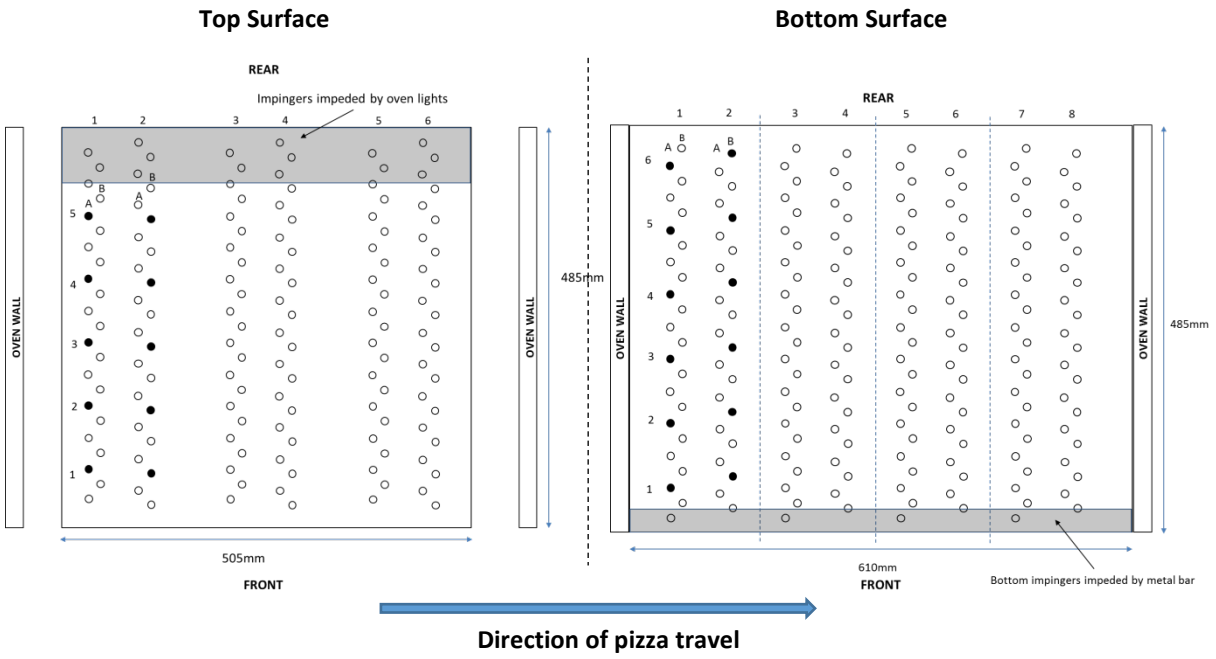

Figure 4.6 – Impinger layout from Top and Bottom plenums of the oven

To gain an insight into the dynamics of airflow within the oven, the variation in airflow was measured using a hot wire anemometer (Lutron, AM-4214SD) at a series of regular points. Air flow was measured from directly above/below individual impinger outlets, with the hot wire parallel to the impinger to measure vertical air velocity. Small bulldog clips were attached to the probe to ensure consistent and level measurements at each test point.

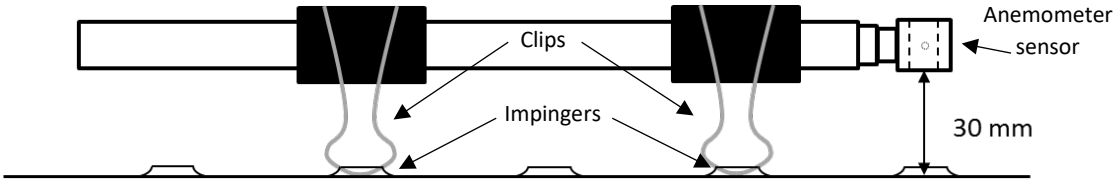

Figure 4.7 – Controlling airflow measurements from impingers

A total of 48 measurements were made from the bottom plate, and 30 from the top plate, at fan speed settings of 3, 5, 7 and 9. Results of these measurements showed significant variation in air speed depending on position, ranging from 0.6-9.3 $m.s^{-1}$. This variation is likely to be due to the design of the plenum and the impinger layout. Figure 4.7 shows an example of air speed measurements at a fan speed setting of 9, illustrating the pattern of air speed variation. The colour scale gives a visual representation of air speed from low (green) to high (red), and the relative positions for each air speed measurement are illustrated in Figure 4.8. A similar pattern of airflow variation was evident at each fan speed setting.

Fan Speed: 9

Entry → Exit

Position in y-axis	Position in x-axis: 1A	2B	3A	4B	5A	6B	7A	8B
6	3.4	0.8	0.7	0.9	3	1.5	1.2	3
5	7.1	5.6	3.3	1.6	2.1	6.1	4.6	7.5
4	7.4	7.4	6.9	6.8	3.9	7.9	8.1	7.5
3	7.9	6.3	7.7	7.7	6.3	8.2	8.5	8.2
2	7.2	8.3	7.9	8.1	7.8	8.3	8.9	8.4
1	8	8.4	7.6	8	7.8	7.7	8.8	9.3

Back → Front

Fan Speed: 9

Position in y-axis	Position in x-axis: 1A	2B	3A	4B	5A	6B
5	2.1	0.9	2.2	1.9	1.8	2.6
4	1.8	0.9	1.8	2.3	1.1	4.3
3	1.8	0.7	1.5	2.0	1.2	4.2
2	2.3	0.9	3.3	5.5	1.6	3.8
1	1.5	1.2	2.5	3.6	1.3	4.2

Figure 4.8 – Example of air flow measurements ($m.s^{-1}$) at a fan speed setting of 9. Green – Low air speed, Red – High air speed.

Overall, air speed from below was greater than from above. At a fan speed setting of 9, the average airspeed was 6.2 $m.s^{-1}$ from below, compared to 2.2 $m.s^{-1}$ from above. Therefore, the rate of heat transfer is higher from below. Air speed was lowest along the back of the oven and highest towards the front and exit of the oven. This variation is likely due to the design of the plenum, affecting how the air distributed. In terms of the oven layout, a pizza tray sits between positions 1 and 5. Within this zone there is less variation in air speed, and therefore heat transfer would be relatively even. In addition, a commercial pizza pan is made of heavy gauge steel which acts as a heat sink and promotes even heat transfer even across the pizza lower surface. As a result, the variation in air flow from below is unlikely to result in uneven heat flux, and therefore heat transfer to a pizza base from below would be consistent.

Air speed is highest towards the exit of the oven from both above and below, and the air flow profile from above appears more scattered than from below. However, in general the air flow from above is more consistent at each position, with overall a smaller range of air speeds promoting more even heat transfer. For industrial applications the layout of impingers can be customised to provide

optimised heat transfer and therefore baking conditions, depending on the desired application. In this case a pizza base likely requires more cooking than the cheese and top surface, which has dictated the layout and air distribution.

Additional trials were run to measure the variation in air flow at varying speed settings, where minimal change was observed from above and below at fan settings of 5,7 and 9. Figure 4.9 illustrates the overall average air speed from above and below at each fan speed setting. Air flow from below increased slightly with increasing fan speed, from 5.7 up to 6.2 $m.s^{-1}$. From above, airflow remained relatively consistent ranging from 2.0 to 2.2 $m.s^{-1}$. Note that for baking purposes a fan speed of 3 was lower than the minimum required to allow the heating elements to operate and therefore the corresponding airflow results were disregarded. As the air speed did not vary greatly, it can be assumed that the heat transfer would also not vary significantly, and therefore effect on baking would be minor. For further work it was assumed that air speed would not provide useful data for measuring and analysing the effect on baking within the operating parameters of the oven.

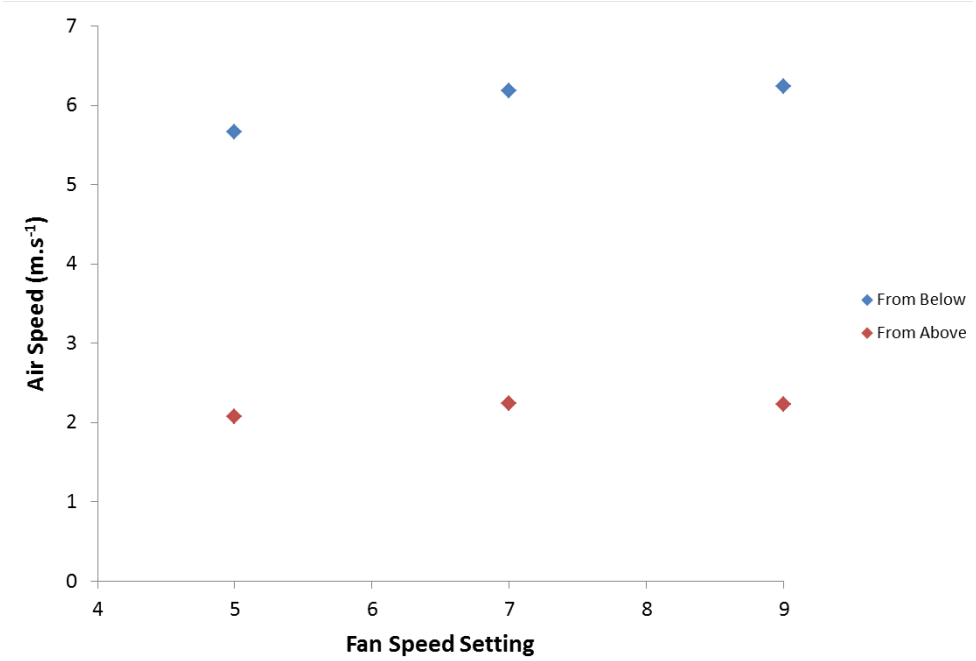

Figure 4.9 – Average air speed from above and below relative to fan speed setting

4.3 Oven temperature

The distribution in temperature across the oven was characterised. This information aids the analysis of pizzas baked within the oven in terms of baking variation that could be attributed to temperature variation.

The oven was heated to a range of setpoint temperatures and the resulting internal oven temperatures were recorded. Ten thermocouples were distributed within the oven at the outlet of impingers, and one thermocouple was placed at the rear of the oven next to the temperature sensor used for oven control. The position of the thermocouples within the oven is illustrated Figure 4.10, as viewed from above.

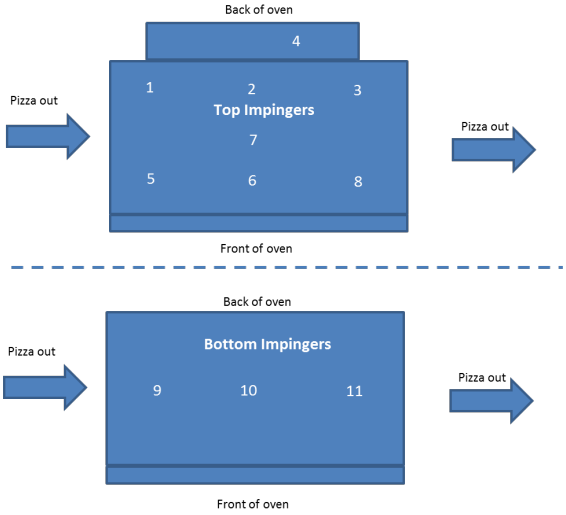

Figure 4.10 – Top down view of thermocouple positions for measuring temperature distribution

The operating temperature of the oven was from 93-288°C. From previous trials for cooking of pizzas in this oven, the practical range for pizza cooking was defined as 220-288°C. The oven temperature was calibrated manually as there was a significant difference between the oven display set point temperature and the actual temperature within the oven. To determine the correlation between set point and internal oven temperature, the temperature at the control probe (thermocouple 4) was measured at several oven display temperatures. Figure 4.11 below shows the resulting linear correlation. This correlation was used to determine the required oven display temperature to achieve the desired internal oven temperature. From this point onwards the oven set point temperatures are reported as the calibrated value of the internal oven temperature.

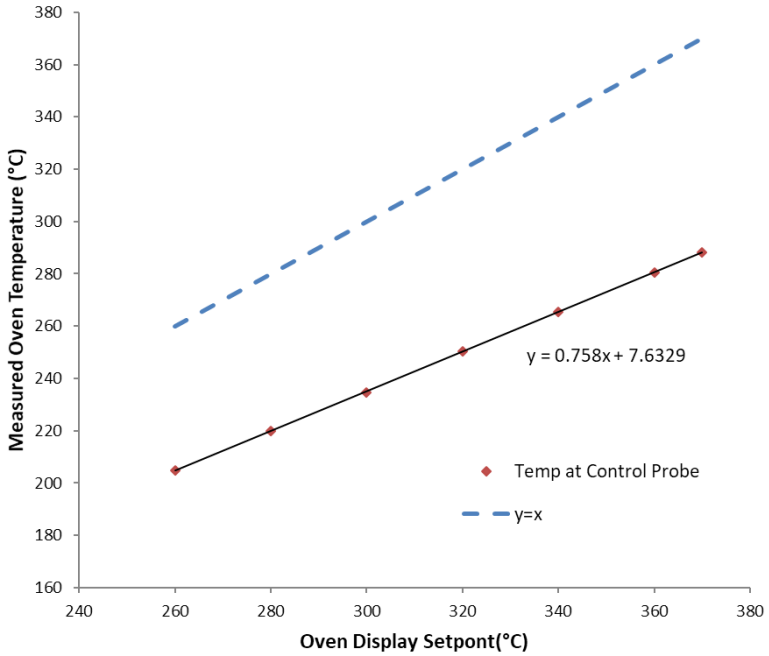

Figure 4.11 – Correlation between oven display and internal oven temperatures

To investigate the temperature distribution within the oven, measurements were taken at 15s intervals in set point from 220-280°C and the maximum temperature of 288°C. For each temperature measurement the oven was set to the desired temperature and allowed to reach steady state, approximately 8-10 minutes. During the analysis of the recorded data, it was identified that thermocouple 11 was reading erratically and significantly 10-20°C lower than the other

thermocouples. All the thermocouples where initially calibrated in an ice water slurry, however at baking temperatures, the data captured from thermocouple 11 was inconsistent and scattered, probably due to a short or damage during its installation into the oven. Hence, the data from thermocouple 11 was considered inaccurate and discounted for further analysis of temperature distribution.

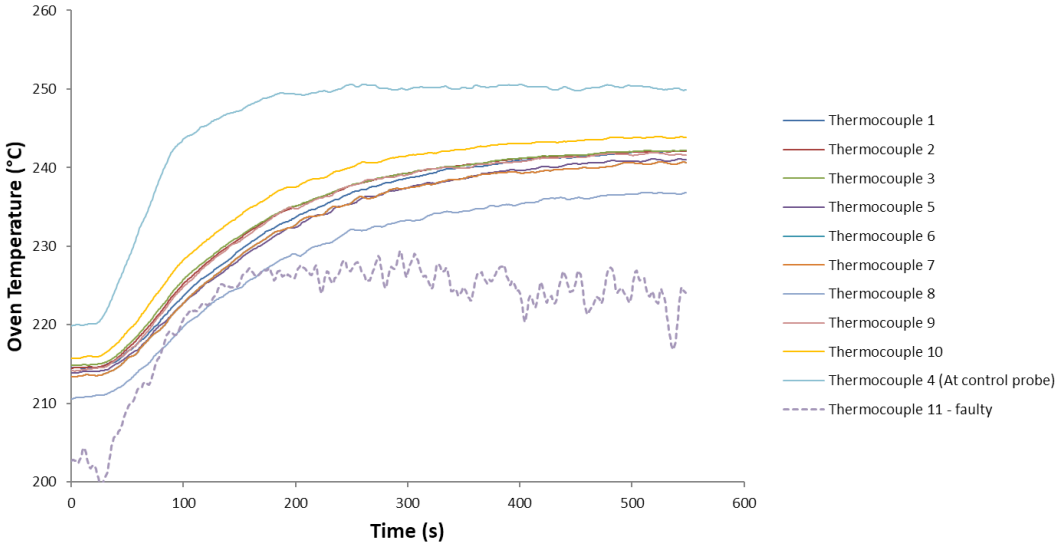

Figure 4.12 – Oven thermocouples readings at an oven temperature set point of 250°C

From the remaining results the temperature distribution was analysed. This analysis showed that the distribution pattern of temperature within the oven was similar at each temperature set point. An example of results at a set point of 250°C illustrates the resulting distribution as shown in Figures 4.12 and 4.13. The main observations from these results were that the temperature was higher at the back of the oven and there was a cooler spot in position 8. The rear of the oven would be expected to be hotter as the heat source is at the rear of the oven, where heat losses result in a gradient from front to back. The cooler temperature at position 8 indicates that there were greater heat losses at this point.

The air flow measurements in section 4.2 showed that air flow was greater towards the exit of the oven. Closer analysis shows that the highest air flow was at the front of the oven and nearest the exit, which is where thermocouple 8 was positioned. With air speed being higher towards the exit of the oven, the overall airflow is likely to be from the exit to towards the entry of the oven. Therefore, even though more hot air is being introduced at the exit, cool air from the environment was being drawn in, resulting in increased heat losses and a lower temperature.

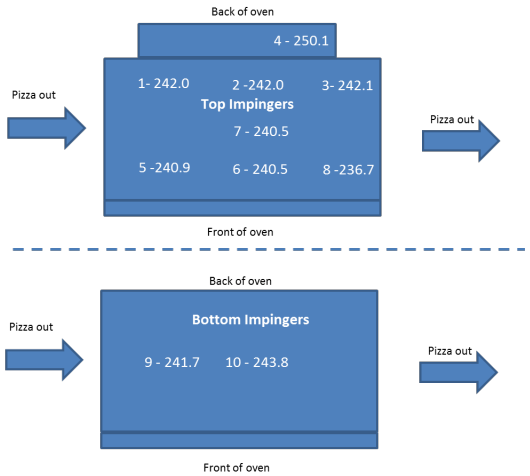

Figure 4.13 – Temperature distribution within the oven at a set point of 250°C

The average temperature within the oven was calculated and plotted against the set point temperature in Figure 4.14. This resulted in a linear correlation which could be used to calculate the average internal oven temperature if required for subsequent investigations. There was a notable difference between the temperature at the control probe and the internal oven temperature; from 5°C to 11°C across the operating range of the oven. This is to be expected as the control probe is in close proximity to the heating source and the internal oven is open partially to the atmosphere. The temperature within the oven takes longer to stabilise and is susceptible to fluctuation and variation due to heat losses. As previously discussed, the results indicated that the overall air flow within the oven flows from the pizza exit to the entry, contributing to heat losses within the system. The temperature difference could potentially increase under conditions where further heat transfer or losses occur. For example, the airflow would be disturbed as a tray moves through the oven during, as well as heat transfer effects due to evaporation during baking.

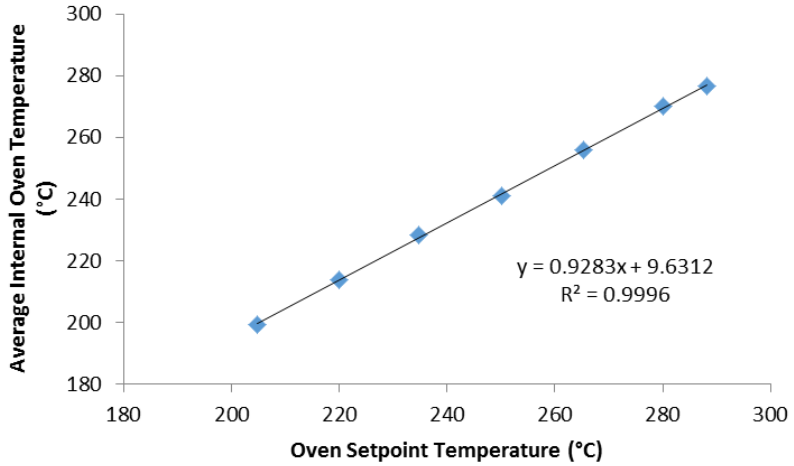

Figure 4.14 – Average internal oven temperature compared to temperature at the control probe

Overall, except for position 8, the temperature variation within the oven was small. The temperature range was within 3°C at all other positions in the oven. The linear correlation allows the internal oven temperature to be estimated based on the input parameters. The temperature difference between the set point and within the oven was attributed to heat losses and air flow and could be further affected when baking pizzas. These results were taken into consideration for subsequent experiments and analysis in order to control and minimise or eliminate the variation where possible.

4.4 Estimating heat transfer coefficient/heat flux

To further characterise the modified oven, the heat transfer co-efficient (HTC) was measured. The HTC is a critical parameter in understanding how the rate of heat transfer is affected by baking conditions. There are a range of methods possible for measuring HTC, where the main idea is to heat a material of known thermal properties and measure the change in temperature of the mass (Carson et al., 2006).

Two methods were used to measure the HTC of the commercial pizza oven for a range of baking conditions; heating an aluminium block, and water evaporation.

4.4.1 Method 1 - Aluminium block and iButton®

The method using the aluminium block was based on measuring the rate of temperature increase while the block passes through the pizza oven. For these experiments a constant 'Bake Time' time of 7 minutes was used, which was considered an average bake time based on previous baking trials in the commercial pizza oven. Bake time (t_{bake}) in this case was defined as the time that each point of

an object spends in the oven and was controlled by adjusting the speed of travel (v) through the oven. Figure 4.15 illustrates this and is the time taken for the front edge of the pizza tray to travel from point A to point B ($t_{bake} = \frac{\overline{AB}}{v}$).

Figure 4.15 – Illustration of points used to measure bake time from the entry to the oven (A) to the exit of the oven (B)

A pizza being baked is made up of a number of layers; baking pan, pizza base, tomato sauce, and cheese. When baking a pizza, the heat applied to the top cheese layer and bottom pan surface is by direct convection from the hot air flowing from above. This heat is then conducted through the pan, pizza base and sauce layers. To simulate pizza baking conditions for these experiments an insulator was used to simulate a pizza tray and base. The aluminium block sat on top of the insulator, which allowed for conduction from below and convection from air flow to the exposed surfaces. This resulted in a measurement representative of heat transfer to the cheese layer of a pizza. In regard to exploring the effect of baking conditions on browning and blistering of cheese on pizza the HTC to the top surface of a pizza is likely to be more relavant than the HTC on the bottom surface. This is because the heating rate for the cheese layer from below is limited due to evaporation, whereas the temperature in the air above reaches much higher temperatures resulting in higher heat transfer rates and the onset and development of browning and blistering.

To measure and log temperature for these experiments an iButton® was used. An iButton® is a device produced by Maxim Intergrated™ containing a computer chip enclosed in a 16mm stainless steel shell. These devices can be used for a range of applications including logging temperature and humidity. For these experiments a High-Temperature iButton®, model DS1922E, was used. The operating range of this model was 15°C to 140°C, with an accuracy of ±1.5°C between 110-140°C. Although the oven temperatures used were higher than the operating range of the iButton®, the maximum temperature the aluminium block reached under all experimental conditions was less than 120°C.

The aluminium block for HTC exeriments was made up of two pieces, a base and a lid, with a cavity made to fit an iButton® tightly. The block was produced to give an exact fit to minimise resistance to heat transfer between the block and the iButton®. Figure 4.16 shows the setup and dimensions of the aluminium block and the cavity for the iButton®. The insulator was 100mm x 100mm x 10mm dimensions and made of heat resistant polyamide.

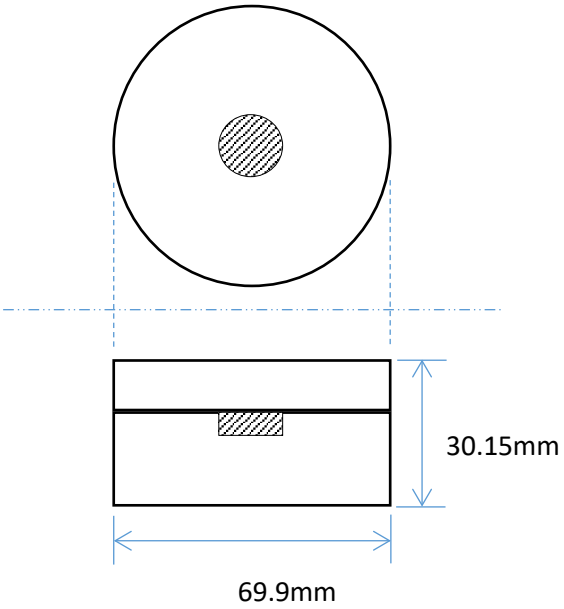

Figure 4.2 – Dimensions of aluminium block containing iButton temperature logger

For the HTC experiments there were two possible variables, oven temperature and fan speed. The trolley speed remained constant for all experiments, equivalent to a 7 minute bake time. Although HTC values vary with air velocity, as discussed in section 4.2, air velocity did not vary with fan speed setting in the oven. Therefore, the fan speed was set at 10 and remained constant for all experiments. The HTC was measured at oven temperatures of 220°C, 235°C, 250°C, and 280°C, with two replicates at 235°C and 250°C and three replicates at 220°C and 280°C.

The steps taken for each experiment were:

1. The oven was set at the desired temperature
    - The trolley speed was set for a 7 minute bake time and remained constant for all measurements
    - The fan speed was set at 10 and remained constant for all experiments
    - The oven was run for 20 minutes for the temperature to reach steady state before running an experiment
2. The iButton® was set to log temperature at 1 second intervals
3. The iButton® was placed inside the aluminium block cavity and the lid was put on
4. The aluminium block and insulator assembly was placed onto the oven trolley
    - A circular cooling rack was used on the trolley to hold the block and insulator
5. The pulley mechanism was started, to move the trolley through the oven
6. Once it exited the oven the iButton® was removed from the block.
    - The aluminium and insulating blocks were placed under cold running water for at least 3 minutes to cool before the next experimental run
7. The iButton® data was downloaded and reset
8. This process was then repeated for each set of experimental conditions

4.4.1.1 Calculating HTC

Using the known properties and dimensions of the aluminium block and the time/temperature history, the heat transfer coefficient can be calculated. Newton's law of cooling describes the theory of cooling or heating in highly conductive uniform slabs. Aluminium has a high thermal conductivity and it can be assumed that there was no internal resistance to heat transfer. Therefore, the temperature within the block could be assumed to be uniform. Equation 4.1 describes the

convective heat transfer under these conditions, which was used to derive Equation 4.2. M is the object mass(kg), c_p the specific heat capacity of the material (J $kg^{-1}.K^{-1}$), h the surface heat transfer coefficient on the exposed surface of the device ($W.m^{-2}.K^{-1}$), A is the exposed surface area (m^2), T_a is the equilibrium temperature (in this case the temperature of the air in the oven, K), T_t (K) is the temperature at time t (s).

$$Mc_p \frac{dT}{dt} = hA(T_a - T_t) \qquad \text{Eqn. 4.1}$$

$$ln\left(\frac{T_i - T_a}{T_t - T_a}\right) = \frac{hA}{Mc_p} t \ , \ Slope = \frac{hA}{Mc_p} \qquad \text{Eqn. 4.2}$$

Integrating equation 4.1 gives equation 4.2, which was used to obtain the HTC (h) from the experimental temperature data gathered. The logarithmic term was plotted against t to determine the slope, and along with the know properties of the aluminium block, allowed for the calculation of the HTC. A summary of the results is shown in figures 4.17 and 4.18 for all the experimental oven temperatures. Figure 4.17 shows the change in temperature with time as the aluminium block passed through the oven at a speed equivalent to a 7 minute bake time.

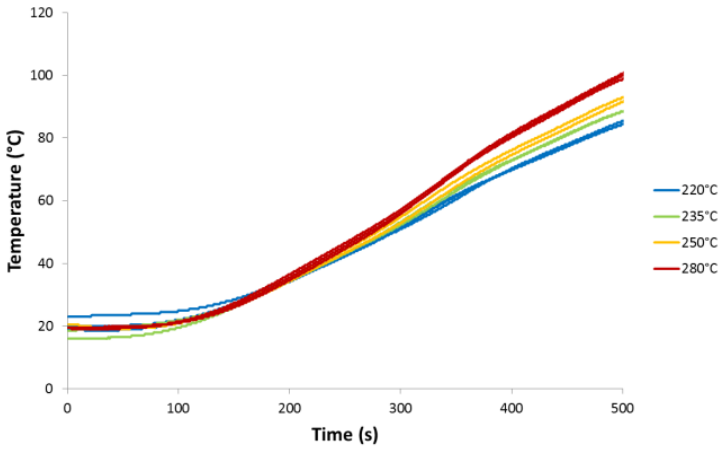

Figure 4.17 – Summary of iButton® temperature data at varying oven temperatures

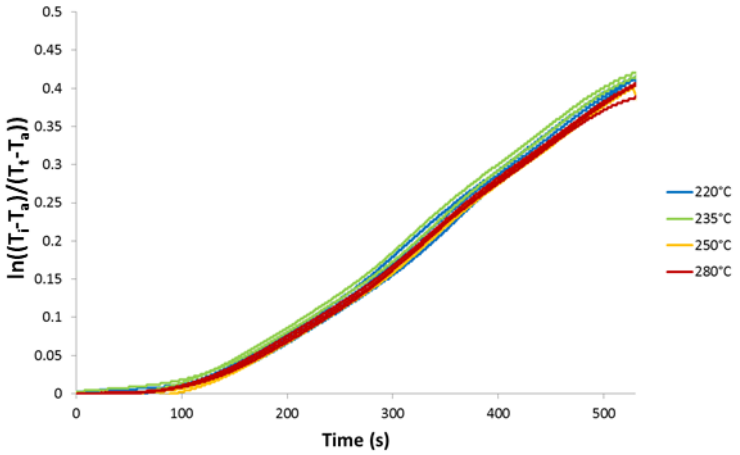

Figure 4.18 – Plot of the natural log term from Eqn. 3.2 against time at varying oven temperatures

The natural log term from Equation 3.2 was calculated and plotted against time to determine the slope. To measure the slope a constant heating phase was defined as the time between 250s and 450s for all experimental runs. Figure 4.18 indicates that the slope was similar and consisent at each

oven temperature setpoint, where the overall average slope over this time was 1.046E-03 (s^{-1}). From this slope and the known physical properties of the aluminium block (M = 0.31966kg, A = 0.010458m^2, c_p = 910 $J.kg^{-1}.K^{-1}$, Borgnakke & Sonntag 2013) the heat transfer coefficient was calcluated to be 29.1 $W.m^{-2}.K^{-1}$.

The HTC was calculated for each oven setpoint and the results are illustrated in Figure 4.19. The average HTC during the constant heating phase ranged from 29.1 – 31.0 $W.m^{-2}.K^{-1}$. This indicates a trend, however there is not a large change over operating temperature range of the oven.

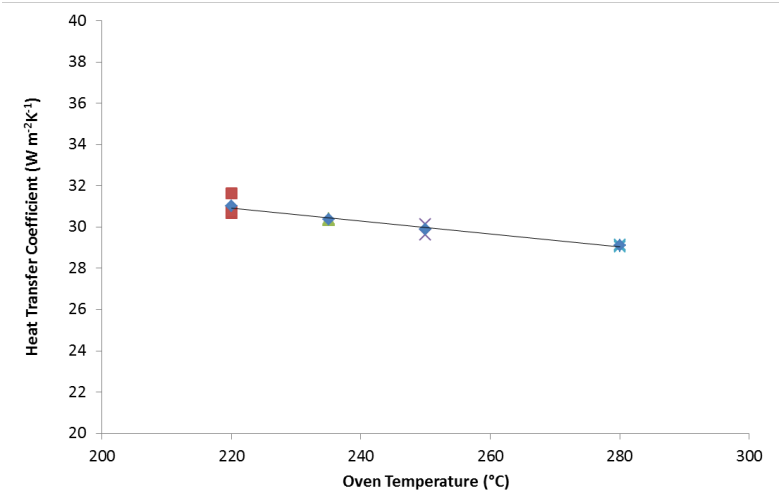

Figure 4.39 – Average calculated HTC from iButton® data

It can be seen from the Figures 4.17 and 4.18 that during the constant heating phase of baking the slope deviates slightly from a straight line. The likely cause of this is the variation in air flow within the oven due to impinger layout and position as indicated in section 4.2. As the block travelled through the oven, it experienced regions of higher and lower airflow, affecting the rate of heat transfer. The data was reanalysed to calculate the maximum slope over a moving 20 second period and the corresponding heat transfer coefficients were calculated. Figure 4.20 illustrates these results where the maximum HTC was similar across the temperature range with an average of 36.8 $W.m^{-}2.K^{-1}$. These results show the the HTC within the pizza oven is variable, ranging from 29.1 to 37.1 $W.m^{-2}.K^{-1}$.

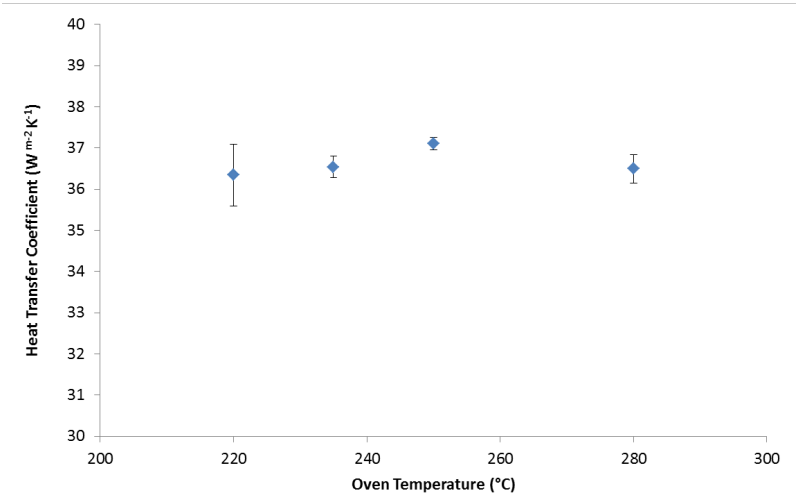

Figure 4.20 – HTC calculated from maximum slope over 20s interval at each oven temperature, error bars indicate the SD of replicate HTC values calculated for each oven temperature

As previously discussed, air flow varies depending on position within the oven due to the impinger layout, and therefore variability in the rate of heat transfer would be expected. To further investigate the heat transfer characteristics within the oven a second method measuring the rate of water evaporation was used to calculate the HTC .

4.4.2 Method 2 - Water Evaporation

This method involved estimating the HTC based on the rate of mass loss due to water evaporation under different oven conditions, and the properties of water/steam under known conditions. This set of experiments used the load cells installed on the commercial oven and pizza tray to measure the mass loss over time due to evaporation. As the airflow varies depending on position in the oven, and results in variations in load on the pan, this set of experiments was carried out from a static position in the centre of the oven. The fan speed was set at 10 for all trials, as for the iButton® measurements, leaving the oven temperature as the only variable. The oven was set to temperature set points at 220, 235, 250, 265, and 280°C to measure HTC over the operating range on the oven. The following experimental method was followed to gather the required data:

1. The oven was set at the desired temperature and fan speed
    - The fan speed was set at 10 and remained constant for all experiments
    - The oven was run for 20 minutes to allow the temperature to reach steady state before running an experiment
2. The pizza tray was place in the centre of the oven for 1min
3. Water was boiled and 500g was measured and poured into hot oven tray
4. A logging thermocouple was placed in the centre of the tray, secured with a bulldog clip
    - The thermocouple was fully submerged, but not touching the base of the tray
5. The tray was placed in the centre of the oven and the mass loss, water temperature and oven temperature were recorded using the datalogger.
6. After 8 minutes the data logger was stopped and the tray was removed
    - The data was saved, recording the relevant oven conditions, and replicate number
7. This process was repeated for each oven temperature
    - A minimum of 3 replicates at each oven temperature were carried out.

4.4.2.1 Calculating HTC

Based on the rate of evaporation of water at a specific temperature the HTC can be calculated. Equation 4.5 is derived from equating the rate of convective heat transfer to the water (Equation 4.3), and the latent heat of evaporation associated with the rate of mass loss observed (Equation 4.4). From the load cell data, the rate of mass loss could be determined, and the average water temperature could be calculated from the temperature logger. The pizza tray was static for the duration of each trial and therefore the effect of airflow from above and below remained constant, resulting in accurate mass loss data.

$$\emptyset = hA(T_{Air} - T_{Water}) \qquad \text{Equation 4.3}$$

$$\emptyset = m_L\, h_{fg} \qquad \text{Equation 4.4}$$

$$h = \frac{m_L\, h_{fg}}{A(T_{Air} - T_{Water})} \qquad \text{Equation 4.5}$$

The data gathered at each oven temperature was plotted, together with the average oven temperature, average water temperature and the rate of mass loss was determined. An example of these results is shown in Figure 4.21 for an oven temperature set point of 250°C. As the water was

heated prior to the start of each experiment there was minimal lag time and the rate of mass loss was consistent for the duration of the experiment, as indicated by the constant slope of the green line in Figure 4.21.

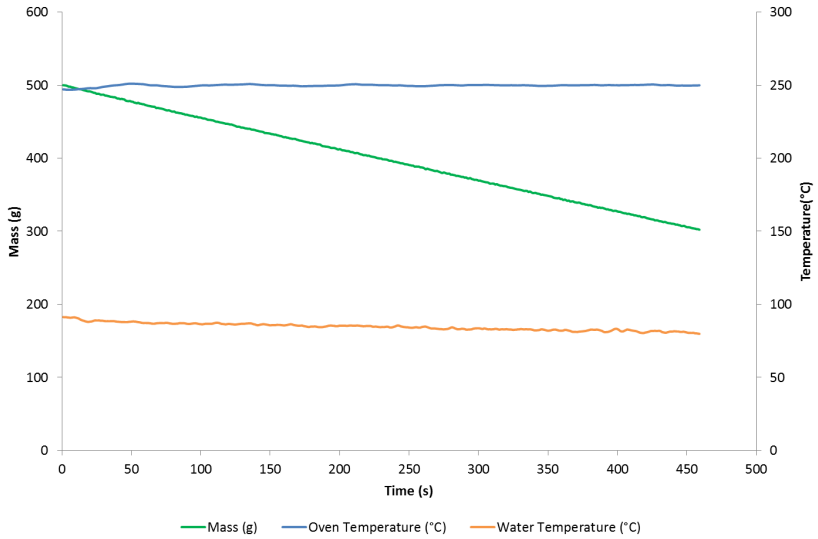

Figure 4.21 – Water evaporation results at oven set point of 250°C

Equation 4.5 was used to calculate the HTC coefficient at the range of set point temperatures based on rate of mass loss. The latent heat of evaporation (h_{fg}) was determined using steam tables (Wagner, & Kretzschmar, 2008) at the average water temperature. The heat transfer area used was 0.138 m^2, based on the total exposed surface area measured from dimensions of the pizza tray and the height of the water in the tray. Over the oven temperature range of 220°C to 280°C, the rate of mass loss ranged from $3.6x10^{-4}$ to $5.0x10^{-4}$ $kg.s^{-1}$.

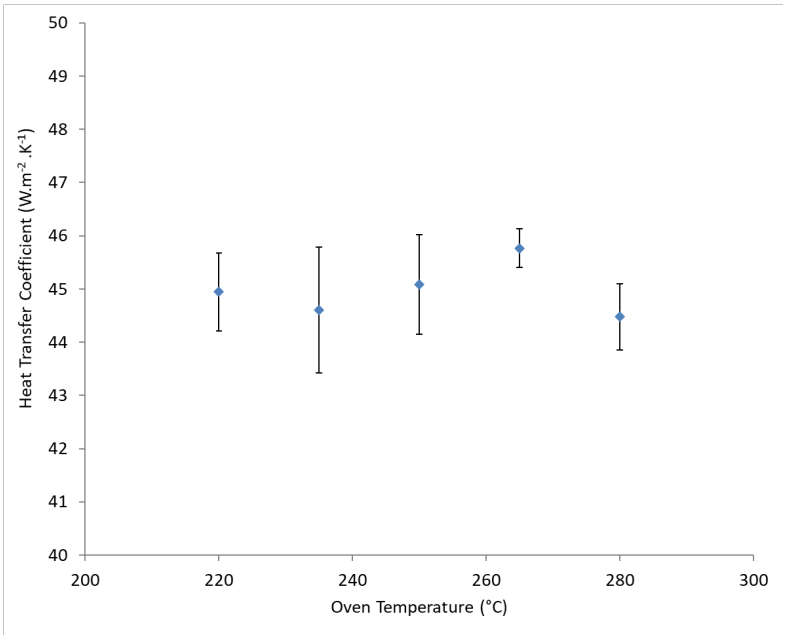

Figure 4.22 – Average HTC calculated from water evaporation over oven temperature setpoint range, error bars indicate the SD of replicate HTC values calculated for each oven temperature

Figure 4.22 illustrates the results of the HTC calculations for each baking condition. The results across the oven temperature range were relatively consistent, ranging from 43.4 to 45.7 $W.m^{-2}.K^{-1}$.

4.4.3 Overall Results

The results from the both Method 1 and Method 2 showed that the HTC does not change greatly over the range of baking conditions, and indicates that radiative heat transfer from internal oven surfaces does not play a signifcant role in heat transfer, within the ovens operating limits. At high temperatures, radiation heat transfer becomes the predominant mode of heat transfer (Incropera, 2011). If radiative heat transfer was significant the HTC would be expected to increase at higher temperatures. Therefore the heat flux applied for baking applications within the commercial pizza oven can be considered as directly proportional to the temperature difference between the oven and material surface, based on a known heat transfer coefficient.

The heat transfer coefficient calculated using each method differed by 10 - 15 $W.m^{-2}.K^{-1}$. However, they are in the same order of magnitude and do not vary largely over the range of baking conditions considered, hence the estimates give an accurate representation of heat transfer.

The difference in values can be accounted for based on the variance between measurement methods and experimental conditions. There are two main differences between methods, airflow and restriction of heat transfer. In terms of air flow, the aluminium block experienced fluctuating air speed and direction as it travels through the oven, however for water evaporation the tray remained static in the centre of the oven resulting in minimal variation and better heat transfer conditions.

In terms of restricting heat transfer, the aluminium block was placed on an insulator which reduced heat transfer from below to simulate pizza baking conditions. As a result, the estimated HTC using this method was more indicative of the top surface where lower air flows occur (see Section 4.2). These lower airflows would be expected to result in lower HTC values. The only constraint to heat flow for the water evaporation method was the metal tray, which is highly conductive resulting in minimal restriction to heat transfer. As air flows through the bottom plenum are higher, the bottom HTC would be expected to be higher. As the HTC estimated in Method 2 assumes heat flow over all surfaces, the value is an overall average. For these reasons, the results for Method 2 give the best representation of heat transfer conditions in regard to what a pizza experiences overall during the baking process, taking into account the total heat transfer from above and below. The HTC's calculated using Method 1, with the use of the insulator, are representative of heat transfer with respect to the cheese surface on the top of a pizza during the baking process. Both methods provide useful information for the further analysis of blister formation and browning during pizza baking, and the most appropriate figure to use depends on the analysis itself.

4.5 Conclusions

The modified commercial pizza was characterised in terms of airflow and temperature distribution, and heat transfer coefficients were measured via two methods.

From the airflow measurements it was found that most of the air comes from below, based on the impinger layout. The air flow distribution within the oven showed that pizzas should travel through positions 1-4 to give the most even airflow, based on Figure 4.8. The overall flow of air occurs from the exit to the entry points, causing some heat losses and variations. The temperature was shown to be lower at the exit of the oven due to cooler air being drawn in. Although the fan speed could be varied in the modified oven, there was minimal change to air flow over the control limits, and therefore heat transfer coefficient. For this reason, fan speed was discounted as a useful process parameter for further experimental analysis in the oven available for experiments.

The oven characterisation data gathered gives an understanding of the process parameters and information that could be used for further experimental analysis. The subsequent chapters further explore the cheese baking process, developing experimental techniques to investigate both blister formation and browning.

Chapter 5
Blister Characterisation

Chapter 3 explored the browning of mozzarella during baking, however that is only one attribute contributing to the appearance of baked pizza. The analysis of browning was simplified to focus solely on predicting brown colour formation as a function of a known time and surface temperature history, ignoring the processes that affect the surface temperature profile. It was identified that characterising and measuring blister formation may be a more useful approach to quantifiably measure baking performance. To explore this, the modified commercial oven, as characterised in Chapter 4, was used to bake a range of pizzas under various baking conditions. This chapter aims to investigate how baking process parameters affect blistering and to obtain a measure of baking performance based on blister formation.

5.1 What is a blister?

To be able to characterise and measure blistering, a definition of a blister is required. In the general literature, the term blister in regard to cooking cheese, has a fairly broad definition. For this reason, some clarification was required to be able to use this characteristic as a quantitative measure.

A blister is generally defined as a raised area on the surface of baked cheese (Clark & Bodyfelt, 2009). Another more specific definition given in literature is that blisters are trapped regions of heated air and steam that are potentially more likely to brown during baking (Ma, *et al.*, 2013a). These definitions are not very precise and do not lend well to a property that is easily measurable.

To assess the formation of blisters during cheese baking, the classification of what a blister is needs to be clearly and quantifiably defined. For the purpose of this project a blister was defined as a discrete brown region on the cheese surface. This is a simple and measurable definition which leads to a number of possible characterisation variables, including blister coverage, the number of blisters, and blister size. Using this approach means that enough browning must occur to differentiate a blister from the background.

A blister characterised in this way is likely to be permanent and will be present on the final baked pizza. It is possible/likely that some blisters will grow into each other forming a larger resultant blister. Regions of raised cheese (bubbles) formed from the entrapment of air and steam (as described by Ma *et al.*, 2013a) may be a precursor to blisters defined by browning. The gas inside these bubbles will slow heat transfer from the cheese surface, enhance evaporation and allow the surface temperature to reach high enough temperatures for browning. Some bubbles however, may pop before there is a measurable colour change, and therefore, these transient bubbles will not be identified in the proposed analysis. For these reasons, the approach used here focuses on the characterisation of cooked pizza and less so on the initial stages of blister formation.

5.2 Measurement of Blistering

Having defined what a blister is, the next step was to investigate the method of measuring blisters and blister formation. As blisters were defined as discrete regions of browning, the variation in surface colour of baked cheese could be used to differentiate brown areas from the background un-browned cheese.

The browning investigation in Chapter 3 used the change in L* with time as an indicator of browning, based on a series of images. However, to quantify blistering, a method to differentiate discrete brown regions from the background colour of a pizza within individual images was required. The principles and methodologies used in Chapter 3 to record and measure colour were extended to achieve this.

As part of the initial pizza baking trials and the browning investigation, a lightbox was used to record an accurate colour representation of baked cheese, as seen in Chapter 3.3. Images taken in the lightbox could be used to determine the colour of the surface of a pizza, based on L*a*b* values. The first part of the process involved correcting the colour of the desired images.

Following colour correction, each image was assessed to quantify surface colour and identify regions of browning. The method for assessing images of baked pizzas utilised threshold analysis, which is a common approach for computer vision and image analysis applications (Gonzalez & Woods, 2007).

The following sections demonstrate the colour calibration and image analysis processes followed to characterise and quantify blistering.

5.3 Colour Correction

To develop the image analysis process, a series of pizzas were baked in the commercial pizza oven (See Chapter 4) under varying operating conditions, providing a set of sample data. Varying the baking conditions gave a range in final appearances and these could be used to assess the performance of the analysis within the operating limits of the pizza oven. Three sets of baking conditions were used to produce these samples, as shown in Table 5.1. Images of cooked pizzas were taken under controlled lighting conditions in a lightbox, with a colour calibration chart.

Table 5.1– Baking conditions of sample pizzas to test the commercial pizza oven parameters

	Oven Temperature	Fan Speed	Bake Time	Overall Average L*
A	280°C	10	10min	52.4
B	280°C	10	7min	70.8
C	280°C	10	6min	80.6

To assess and compare images objectively, the colour was corrected to align each image to a known calibration standard. The software LensEye© (Balaban, 2013) was used to perform the image colour correction. The colour correction process involved evaluating a calibrated colour patch in the image relative to the known standard colour properties for the relative colour patch. Colour values were then adjusted based on this evaluation and the resulting corrected images were saved. LensEye required the input of L*a*b* values for the desired colour standard to perform the image correction process. An X-Rite ColorChecker (X-Rite, 2009) Classic chart was used when taking images in the lightbox to provide a reference colour. As was carried out in similar research (Kong 2014), the No.7 Orange colour patch was used as the colour reference throughout the project.

5.3.1 Determination of Colour Calibration values

Reference material was available for X-Rite ColorChecker Classic charts (X-Rite, 2009), giving standard sRGB and L*a*b values for each colour patch. These were based on specific lighting conditions; D50 illuminant for L*a*b* values and D65 illuminant for sRGB values. D50 and D65 illuminants are CIE standards used to represent the spectrum of natural daylight, which provides a basis for correcting and comparing images and colours captured under different lighting conditions (ISO 11664, 2007).

The reference material for X-Rite colour charts is based on an average of a large number of individual colour charts, and there can be slight variation between charts (X-Rite, 2009). In addition, colour patches can fade and change with time depending on storage conditions. Therefore, to check that the ColorChecker Classic reference values were accurate and appropriate, measurements were carried out using a spectrophotometer (Minolta CM-2600d) for comparison. As the values for D65 illuminant were recorded in terms of sRGB values, the L*a*b* conversion function in Matlab was used to calculate the relative L*a*b* values for comparison with the measured colour values.

The spectrophotometer was set up for a D50 illuminant and calibrated as per the operating manual. Measurements were then taken and recorded for the No. 7 Orange colour patch. For each individual measurement, the spectrophotometer took three readings and the results given were an average of these values. Three individual measurements were made, where the eye of the spectrophotometer was moved within the colour patch each time. This process was repeated with the spectrophotometer set up for a D65 illuminant. Table 5.2 shows the results, presented as an average of the three individual measurements recorded for each reference illuminant, in comparison to reference values. The results show that there was good agreement between reference and measured values.

Table 5.2 - X-rite ColorChecker Classic reference and measured values using a Minolta spectrophotometer for the No.7 Orange colour patch

	D50			D65		
	L*	**a***	**b***	**L***	**a***	**b***
Reference	62.66	36.08	57.10	61.57	31.00	57.00
Measured	62.77	35.02	58.36	61.52	31.66	56.55
Difference	*-0.11*	*1.06*	*-1.26*	*0.05*	*-0.66*	*0.45*

The calibration process using the Minolta Spectrophotometer showed that under both D50 and D65 lighting conditions the readings were relatively accurate. The values for L* were very similar with a difference of less than ±0.2, which is 0.2% of the scale. In addition as the colour correction process was the same for each image, the relative comparison resulted in objectively comparable information.

As long as images were processed in the same manner, the trends could be adequately assessed. This is because it is the change in colour, rather than the exact colour values that are important. However, aligning the images to a known colour standard gives an accurate representation of colour and means that the data could be used for future or similar investigations.

5.3.2 Colour Correcting Images

Having measured accurately the L*a*b* values for the No.7 orange patch, images could be corrected using the LensEye© software. The original light box images were converted into 24-bit bitmap files and resized to 1400x929px as required for the image correction process using LensEye©. To correct the colour of images, the software required two regions of interest, one containing the reference colour patch, and one containing the region of the pizza surface to be corrected. The LensEye© software allowed the size of the regions to be selected and saved individually so that the same size region of interest was used when correcting each image. In addition, pizza trays were placed in the same position in the lightbox for each image. This meant that each output image was of the same dimensions, allowing for direct comparisons and evaluation to be made.

The process was as follows:

1. Convert and resize images
    a. Convert images to 24-bit BMP files
    b. Resize images to 1400x929px
2. Open, correct, and save image
    a. Set analysis options for circular ROI's (region of interest)
    b. Under colour calibration enter measured values for the No.7 Orange colour standard
    c. Select region of pizza and region of Orange colour patch
    d. Analyse colour and save the resulting image

The outcome of this process was a series of images aligned to a known colour standard, which could be objectively compared and further analysed to investigate the effect of time and temperature of baking performance parameters.

5.4 Threshold Analysis

Visual observations are qualitative and only give a limited indication of possible trends. Quantitative measurements were required to be able to further investigate trends and work towards linking pizza outcomes to baking conditions.

The method chosen to assess images of baked pizzas utilised threshold analysis, a common approach for computer vision and image analysis applications (Gonzalez & Woods, 2007). The concept of basic threshold analysis involves comparing each pixel of an image to a set threshold value and is generally carried out using a grayscale image. Depending on the desired conditions, a pixel value becomes a 1 or 0 if its value is above or below the defined threshold, resulting in a binary representation of the overall image.

The first part of the threshold analysis process was to convert colour corrected pizza images (Section 5.3) from RGB to L*a*b* values. This process was similar to that carried out in Chapter 3 where a built-in MATLAB function 'makecform', using the type 'srgb2lab' was used for the conversion process, which resulted in a matrix of L*a*b* values for each individual image. For each image, there was an L* value for each pixel coordinate, based on the CIE L*a*b* scale for L*, where 0 is black and 100 is white (McLaren, 1976). Threshold analysis could be applied to this data based on a defined cut-off value, which separated the lighter coloured background from the darker coloured blisters. The L* value for each pixel within an image was compared to a set threshold value, where a value equal to or below this threshold was assigned as blistered (1) and a value above the threshold was assigned as not blistered (0). This process resulted in a binary representation of blistering, which was recorded in a matrix based on the original pixel coordinates of the relevant image. Figure 5.1 shows an example result of the thresholding process with an applied threshold of $L^* \leq 60$.

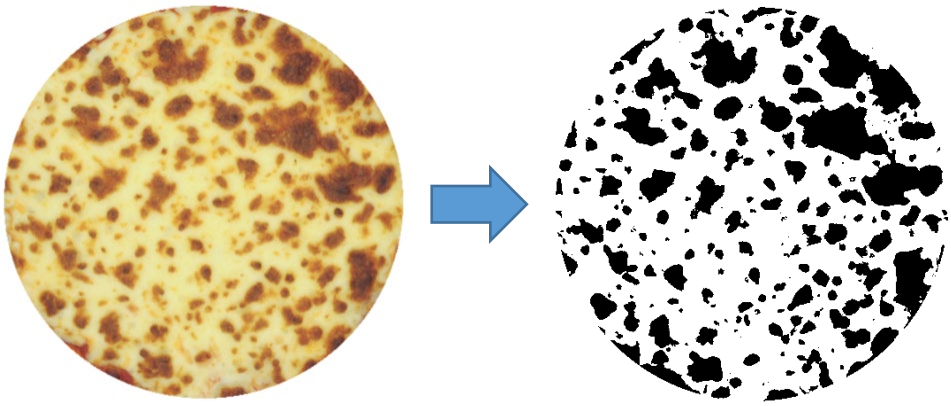

Figure 5.1 – Example result of threshold analysis process (L*≤ 60) for a pizza cooked at 280°C with a bake time of 7 minutes, Pizza B

The resulting binary data was assessed using the MATLAB function 'regionprops' to compute and quantify blister distribution. This function identified discrete regions of blistering based on the binary data, and output an array of individual blister sizes. At this point the size of blisters was recorded based on the number of pixels for each identified region. From this distribution of blisters the following parameters could be calculated:

- Number of blisters: the number of discrete regions within the distribution array
- Total blistered area: sum of the elements within each discrete region
- Average blister size: average number of elements per discrete region

Initially, an arbitrary threshold value of 60 was used to develop the MATLAB code to process the images. The methods below (coded as MATLAB .m files, Appendix 1) show firstly the image cropping and colour conversion from RGB to L*a*b*, and then the blister definition process.

1. Pizza_assessment.m – crop and convert images to L*a*b* values

To analyse images of cooked pizzas, the colour data was converted into L*a*b* values. Colour corrected raw images from LensEye© contain 2 sections as illustrated in Figure 5.2; the region of interest (ROI) for the pizza, and the ROI of the colour calibration square. Cropping the images removes the ROI of the calibration square, which would otherwise affect the results. The function can be summarised as the following steps;

a. Load relevant images
b. Crop images to isolate the pizza portion for each image
c. Convert images to L*a*b* and save the data as a 4D matrix - (L*, a*, b* , Image#)

Inputs:

- Colour corrected images of resolution 1400x929

Outputs:

- 2 x 4D matrices of L*a*b* colour values for each image
  - LAB double format (values defined between 0-100)
  - LAB uint format (values defined between 0-255)

Figure 5.2– Example of a colour corrected image using LensEye© showing the region of interest for both the pizza and the colour calibration patch (Pizza B)

2. Blister_assessment.m – assess pizza characteristics

To quantitatively assess cooked pizzas, threshold analysis was applied to each image, resulting in a binary representation of each image. The binary data was then assessed to determine a series of blister and baking characteristics. The function can be summarised in the following steps;

a. Load the relevant L*a*b* image data (from the 'Pizza_assessment.m' process)
b. Define the threshold to determine browned regions
c. Define the images to be assessed
d. Apply threshold to images to determine brown vs. not brown (this threshold is variable in order to investigate sensitivity)
    i. Results in a binary representation of pizza images
e. Use inbuilt Matlab function 'region props' to quantify browning and blistering
    i. # of blisters, % brown area, avg. blister size, blister size distribution etc.
f. Save B&W images showing 'blistered regions', based on the binary representation
g. Record 'Results' (blister characteristics) and 'Dstbn' (the size of each blister identified)

Inputs:

- L* threshold
- Image L*a*b* data

Outputs:

- Results.mat >> 3D matrix (LThreshold, Image#, Results)
    - Results recorded:
        1. L Threshold
        2. Number of blisters
        3. Total blistered area
        4. Average blister area
        5. Median blister size
        6. Maximum blister size
        7. Minimum blister size
        8. Average blister colour
        9. Average background colour
- Distrbn.mat >> 3D matrix (LThreshold, Image#, Blister Size)

Note that for this process, blister size was assessed based on numbers of pixels. This data was converted to metric units based on the known dimensions of a pizza baking tray. The pizza dishes used for all baking trails had a width of 285mm and the average pixel width of 5 trays was measured to be 665.7 pixels. This equates to pixel width of 0.43mm, which was used to convert units when assessing pizza images.

During the development of the image analysis process, it was found that depending on the threshold limit used to identify blisters, the results varied widely, even for analysis of the same image. Clustered blisters could be interpreted as a larger blister, or regions were included that were too small to be considered blisters based on visual interpretation. To minimise this effect and improve the accuracy of the analysis, the idea of placing a minimum limit on the number of pixels required to qualify as a blister was investigated.

5.4.1 Minimum Blister Size

Initial applications of the threshold analysis showed that a number of very small regions were identified as discrete blisters, potentially skewing results in terms of blister size and numbers. Figure 5.3 below illustrates this, comparing an original image with a binary image resulting from threshold analysis, where each discrete black region was recorded as a blister. The red circles in the binary image highlight some of the identified blisters that were less than 4 pixels in size. Blisters of this size were likely too small to be considered blisters in regard to visual analysis. This finding indicated a need to quantify a minimum blister size to obtain an accurate representation of blister characteristics.

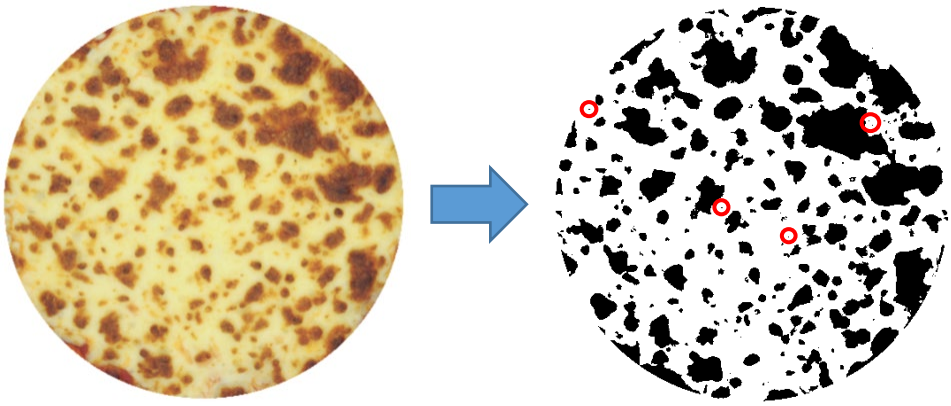

Figure 5.3 – Comparison of original image and binary image for Pizza B using threshold analysis, red circles show 'blisters' less than 4 pixels in size

To consider what was an appropriate minimum blister size, three sample images were analysed, applying different levels of minimum blister size. The three samples were spread relatively evenly in regard to average L* and gave a good representation of possible baking levels, as shown in Figure 5.4.

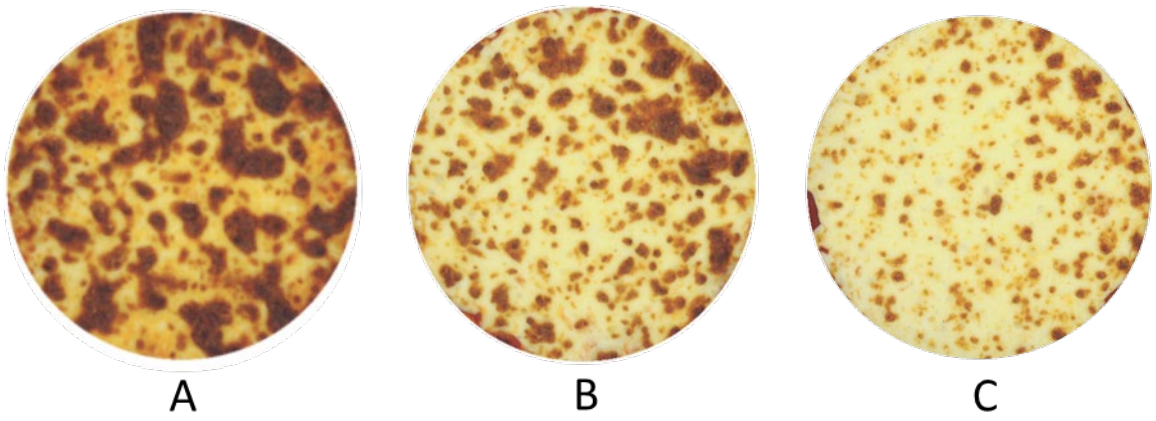

Figure 5.4– Images used to assess minimum blister size threshold, oven settings shown in Table 5.1

The image analysis process described previously for blister assessment was modified to exclude clusters of pixels less than 10, 20, and 30 pixels and calculate the resulting distribution. This process used the data from the pizza assessment process in the form of a matrix containing the L*a*b* colour data for each image. The Matlab .m files 'Blister_Assessment_MinSize.m' (Appendix 1) was used to carry out this analysis, which is outlined below.

1. Blister_assessment_MinSize.m – assess and record pizza characteristics for different minimum blister size values. Steps in the analysis include;
    a. Load the relevant L*a*b* image data (from the 'Pizza_assessment.m' process)
    b. Define the L* threshold to determine browned regions
        i. For minimum blister size assessment thresholds of 50 and 60 were used for each image
    c. Define the images to be assessed
    d. Define minimum blister size values to be measured
        i. Based on the total number of pixels that make up a blister
    e. Apply threshold to images to determine brown vs. not brown
        i. Results in a binary representation of pizza images
    f. Remove blisters below the defined minimum blister size
    g. Use inbuilt Matlab function 'regionprops' to quantify browning and blistering
    h. Save B&W images showing 'blistered regions', based on the binary representation
    i. Repeat for the remaining minimum blister size values
    j. Record 'Results' (blister characteristics) and 'Dstbn' (the size of each blister identified)

Inputs:

- L* threshold: 50, 60
- Minimum blister size: 0, 10, 20, 30 pixels
- Image L*a*b* data

Outputs:

- Results.mat (blister characteristics)
- Dstbn.mat (matrix of individual blister size)

Cumulative frequency distributions of the resulting blister information were prepared to obtain a visual representation of the distribution as shown in Figures 5.5 to 5.10. The plots illustrate the effect of defining different minimum blister sizes on the overall distribution. The MATLAB .m file

'cdfplots_Min_Blstr_Size.m' (Appendix 1) was used to create these plots, following the process outlined below.

2. 'cdfplots_Min_Blstr_Size.m' – Analyse effect of minimum blister size using the following steps;
    a. Define the L threshold* and images to be analysed
    b. Define the colour values for plot lines
    c. Load the relevant blister distribution data (from the 'Blister_assessment_MinSize.m' process)
    h. Use inbuilt Matlab function 'cfdplot' to create a cumulative frequency for blister size distribution at each level of minimum blister size
    d. Define axes, scale, legend and filename
    e. Export the resulting plot and repeat for each defined image

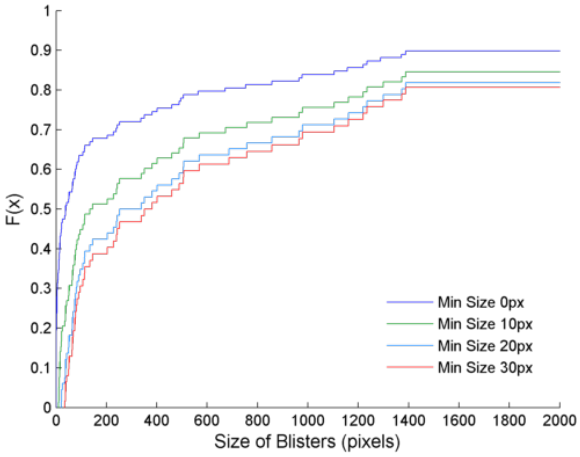

Figure 5.5 – Pizza A at a threshold of 50

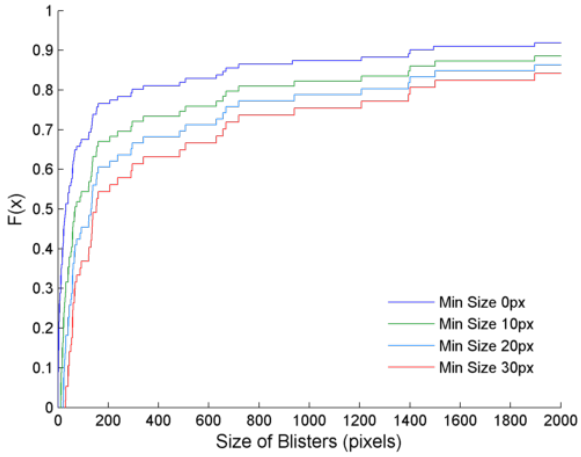

Figure 5.6– Pizza A at a threshold of 60

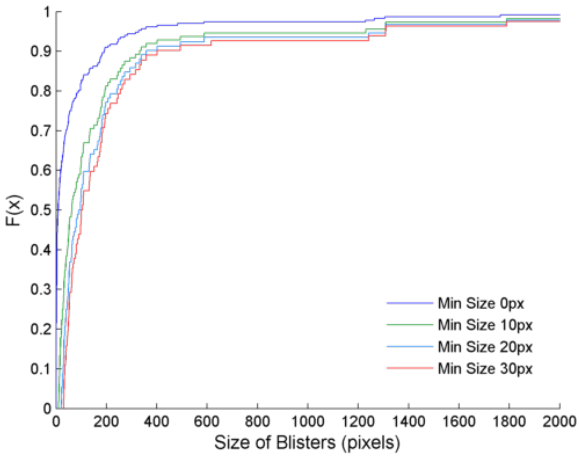

Figure 5.7 – Pizza B at a threshold of 50

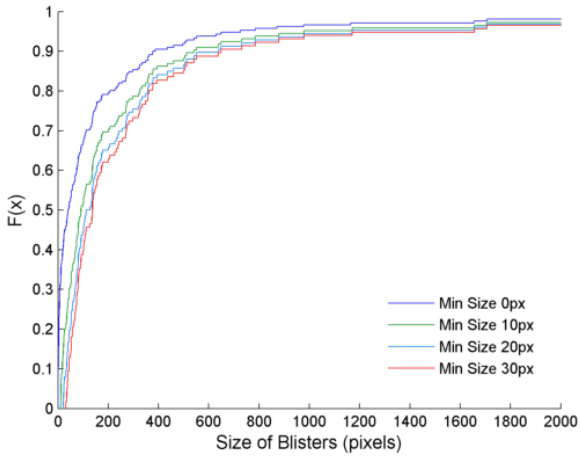

Figure 5.8 – Pizza B at a threshold of 60

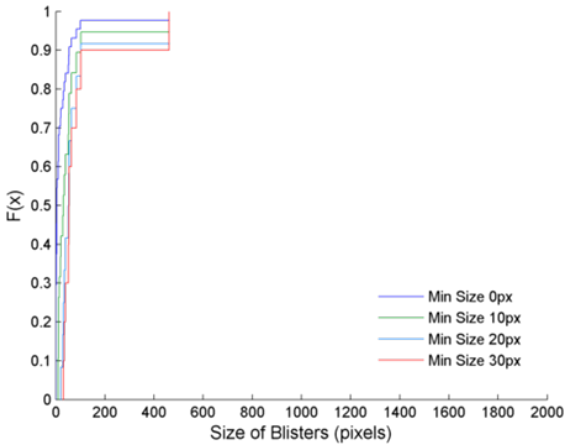

Figure 5.9 – Pizza C at a threshold of 50

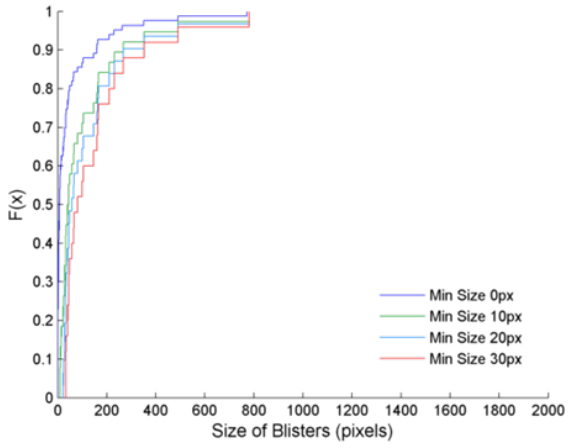

Figure 5.10 – Pizza C at a threshold of 60

The results indicated that removing blistered areas less than 10px in size removed a significant proportion of blisters. This was illustrated by the large gap between the curve for 0 and 10 pixels minimum blister size for each image. It can also be seen that based on the shape of the curves at 10px, 20px and 30px, that whichever minimum blister size was used, the resulting curves were of a similar shape, indicating that they follow the same trends. Therefore the specific level that was chosen was not vital as long it remained constant the same trends could be identified within the data.

To obtain an idea of the actual size of blisters their sizes were converted into mm. As described above, the width of a pixel was determined to be 0.43mm, resulting in the equivalent area of a pixel being 0.18mm^2. From this measurement a blister size of 10 pixels equates to 1.8mm^2, which would be small to the naked eye and outside of what would be considered a blister in regard to sensory analysis.

To select an appropriate limit for minimum blister size, experts in sensory analysis (Fonterra Research and Development) were consulted. A visual representation of blisters on a pizza with the equivalent size of 10, 20 and 30 pixels was prepared and considered with the experts in sensory analysis of baked pizzas. From this consultation, a minimum blister size of 20 pixels was selected as an appropriate limit for blister definition, based on the distribution results as well as a visual analysis of a 20 pixel blob on a pizza, illustrated in Figure 5.11. At 20 pixels the equivalent real world diameter is 2.2mm, which is small and a reasonable cut-off for the purpose of these analyses.

Figure 5.11 – Visual representation of a minimum blister size of 20 pixels (black dots represent 20 pixels, equivalent to 2.2mm diameter wide blister)

The addition of a limit for minimum blister size resulted in a better representation of actual blister number and distribution. To optimise the blister identification and analysis process, an L* threshold needed to be defined to obtain an accurate representation of blister size and distribution.

5.4.2 Determination of L* Threshold for blister definition

For the image analysis process, the L* threshold defines the cut-off point for blister classification. It was previously noted that depending on the L* threshold applied, significant variations in blister identification occurred. This leads to a poor representation of blisters when compared to visual observations in some cases. Figure 5.12 illustrates this by showing the difference in blister definition using three different L* thresholds for pizza images with a range of average L*. The average L* is a measure of the overall lightness of an image.

The blister characterisation process was completed for each image with the L* threshold set at 50, 60, and 70. The results are presented in Figure 5.12 and are based on the binary output from this process. These images indicate that the L* threshold significantly affects the blister outlines and number based on a general visual analysis.

For the darkest image (Figure 5.12A), an L* threshold of 50 appears to identify blisters well, showing good separation and outlines of blisters in comparison with the colour image. However, an L* threshold of 70 gives a poor result where the separation between blisters is lost. At the other extreme, for the lightest image (Figure 5.12C) an L* threshold of 50 appears to poorly define blisters showing weak outlines, whereas an L* threshold of 70 shows blisters with good outlines and separation. These results indicated that there is a correlation between the overall lightness of a pizza and the ideal L* threshold for blister identification.

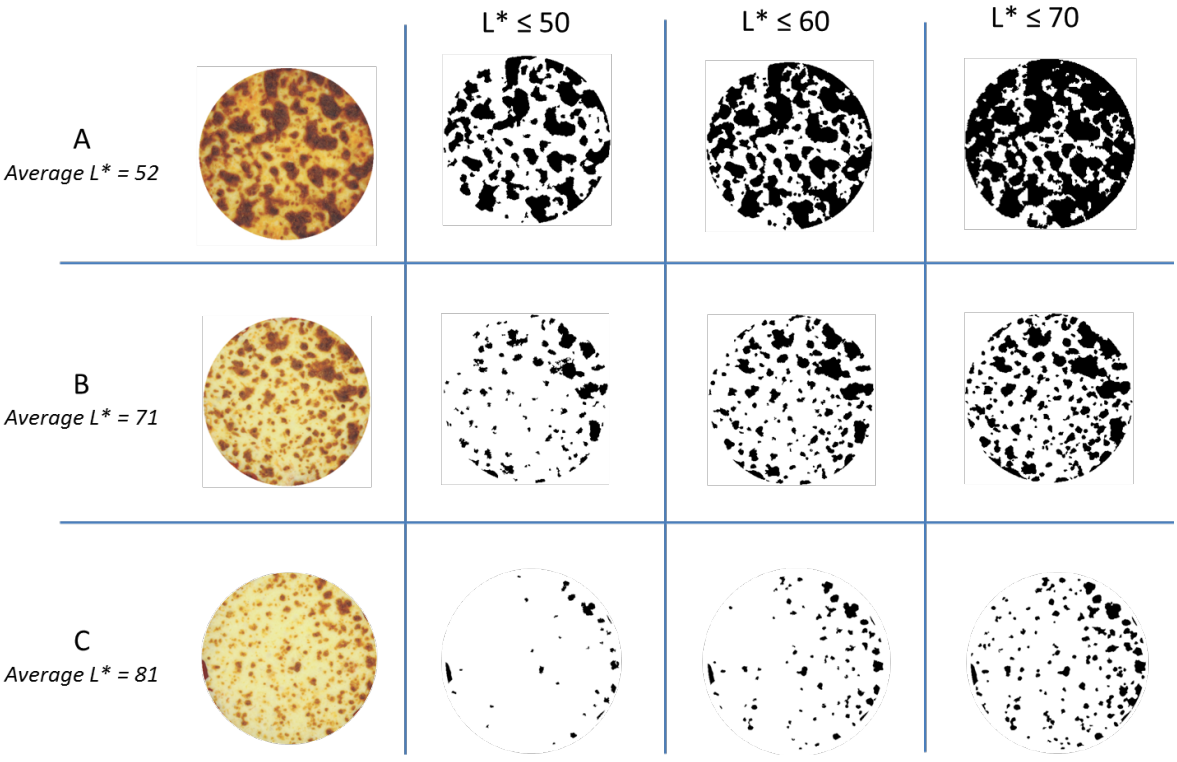

Figure 5.12 – Images illustrating the variability in blister identification depending on overall lightness and L* threshold

As would be expected, the greater the amount of heat applied to a pizza, the greater the extent of browning and the darker the overall colour. This means that depending on the level of baking, the colour of blisters varies and therefore affects the differentiation between blisters and the background colour. To demonstrate this difference, the average blister colour and background colour for the images in Figure 5.12 were calculated, based on an L* threshold of 60. The results in Table 5.3 show that the average blister and background colour was significantly darker for Pizza A than for Pizza C.

This confirmed that blister colour and background colour vary significantly depending on the extent of baking.

Table 5.3 – Average blister and background L* values for images A, B, and C at an L* threshold of 60

	Overall Average L*	Average Blister L*	Average Background L*
A	52.4	42.1	72.7
B	70.8	48.0	81.3
C	80.6	50.4	84.7

These findings show that the use of a single L*threshold was not suitable for comparable blister analysis of pizzas baked over the wide range of possible baking conditions. A method of scaling the L* threshold depending on the level of baking was required to obtain comparable blister information.

5.4.2.1 Dynamic Threshold

Pizza baking is a dynamic process and as baking progresses, the entire surface darkens. This results in a change in the difference between blistered areas and the background colour.

Kong (2014) investigated the assessment of pizza baking performance using both image analysis sensory analysis methods. The research involved evaluating browning and blistering characteristics for a range of baked pizza samples using threshold analysis and trained sensory panels. It was found that there was a correlation between the average L* and the perceived L* threshold for defining browning and blistering based on sensory evaluation. This correlation is illustrated in Figure 5.12. For a given average L* this relationship allows a relative L* threshold to be calculated, where the lower the average L*, the lower the L* threshold and vice versa. Using the derived equation, a dynamic L* threshold could be assigned to an individual image based on the average L*.

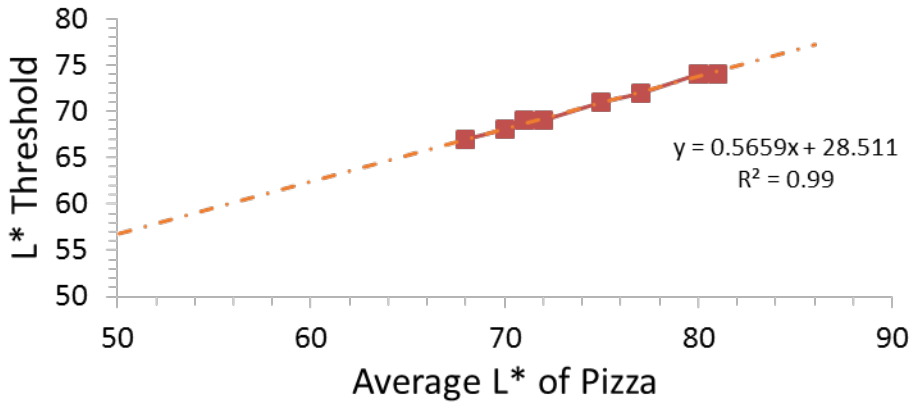

Figure 5.13 – Correlation between average L* of a pizza and relative L* threshold based on sensory evaluation, Courtesy Kong (2014)

The pizza images collected by Kong (2014) and used to develop the dynamic threshold correlation, were captured in a light box with the same specifications as the light box used for this project. To test the application of the dynamic model, images of Pizzas A, B and C were re-evaluated. Based on the average L* of these images, the relative L* threshold was calculated using the correlation shown in Figure 5.13. The dashed line on figure 5.13 represents the full range of average L* values found for Pizzas A, B and C, while the data points show the range of average L* that the correlation was

developed for. Figure 5.14 illustrates the results based on the binary output from the blister analysis process.

As previously identified, selecting a specific L* threshold to apply to all images results in poor blister identification in some cases. The use of the dynamic threshold calculated from the average L* identifies blisters well, where the blisters identified in the binary images visually match well with the original colour images. This is even though the correlation was applied in a much larger range of average L* than it was originally developed for. Based on the standard correlation the blister characteristics could be determined and are comparable across the range of possible baking conditions.

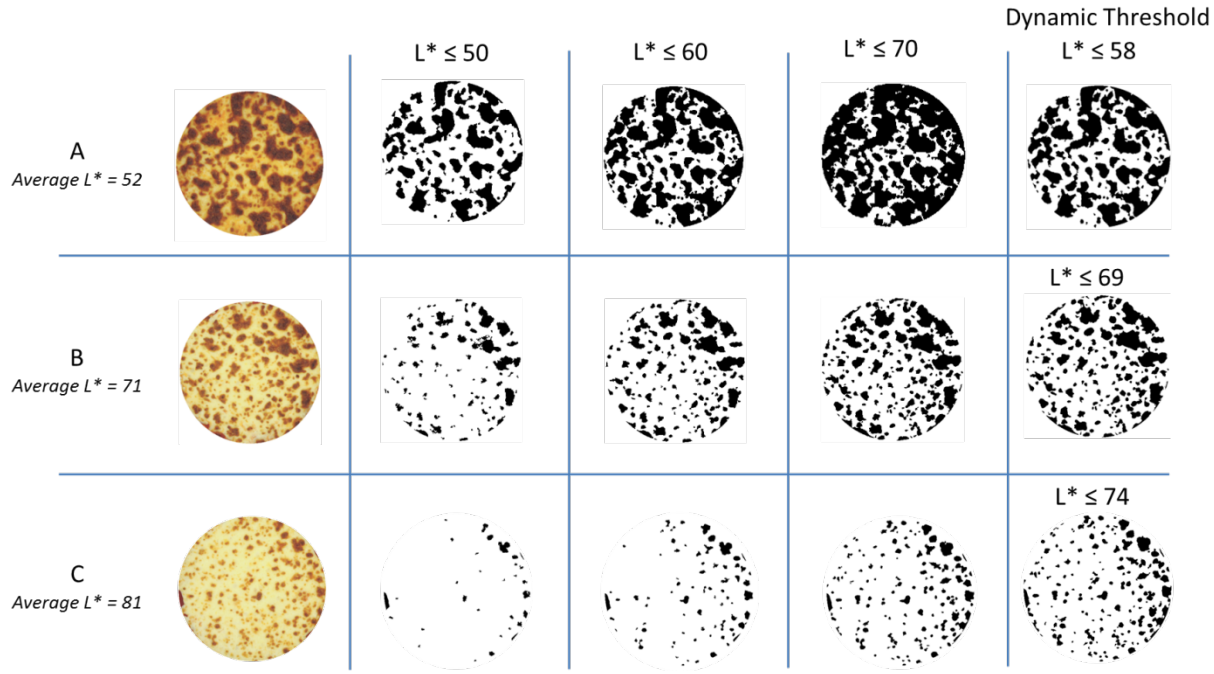

Figure 5.14 – Illustration of blister identification with the addition of a dynamic threshold calculated from the average L* for each pizza image

Colour perception varies between individuals (Matikas & Skusevich, 2010) and with this type of application there will always be a degree of subjectivity in terms of defining appropriate threshold limits. The overall purpose of this exercise was to investigate the effect of time and temperature on baking performance, which required a relative and consistent measure for comparison. The use of the dynamic threshold model gave a consistent platform to work from and produced data for the entire range of baking conditions that was directly comparable.

Based on this analysis method, pizzas were cooked over a large range of cooking times, fan speeds and temperatures. The data analysis method described above was applied to each image and the resulting data and images were compiled into a booklet. The booklet could be used by industry to link a cooking regime to pizza appearance outcome. This booklet is included as Appendix 2.

To develop the blister analysis process, images of pizzas baked in the modified commercial pizza oven were used. However, the process could be used in other applications such as the cheese baking experiment in Chapter 3. A sensory based measure of baking performance such as blister coverage could be applied to the kinetic model developed in Chapter 3.

5.5 Application of blister analysis to the browning model

With the ability to identify blisters developed in this chapter, it was then possible to predict blistering outcomes from the browning kinetics model from Chapter 3. Local temperature data could be used with the browning kinetics to predict colour distribution. Application of the blister identification methodology could then be used to estimate blister coverage. Blister coverage could also be calculated directly from the browning images for comparison.

Figure 3.33 (repeated here) shows the comparison between experimental and predicted L* for a cheese sample cooked using the heat gun set up described in Chapter 3.

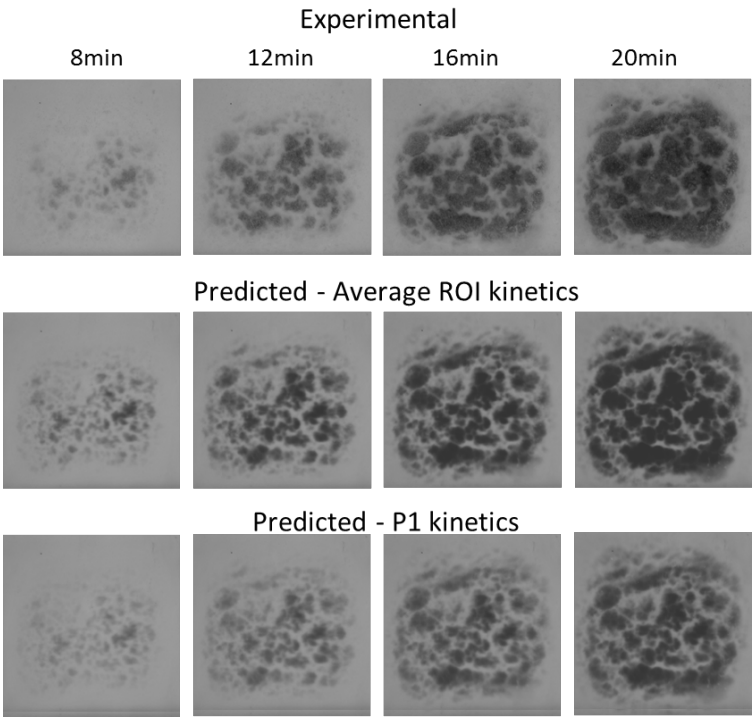

Figure 3.33 – Comparison of experimental L* images with recombined images using L* predicted using the kinetic parameters fit from Average ROI and P1 data

Figure 5.15 shows Figure 3.33 converted to binary images using the dynamic thresholding methods described above. Due to the different lighting conditions, the experimental colour images captured were significantly darker than those taken in the light box. When the dynamic thresholding was applied the results were not useful due to the darker images and lack of differentiation between browned and not browned regions. To compensate for this the dynamic thresholding equation was modified by reducing the y component from 28.511 to 25. The lighting conditions were consistent throughout the experiments in Chapter 3, therefore the changes made to the dynamic model did not affect the measurement or interpretation of results.

The results show that at the early stages of cheese baking, the kinetics based on a singular point (P1) gave more accurate representation of blister coverage, while kinetics derived from the average L* (Average ROI) data were better towards the end of the cooking period.

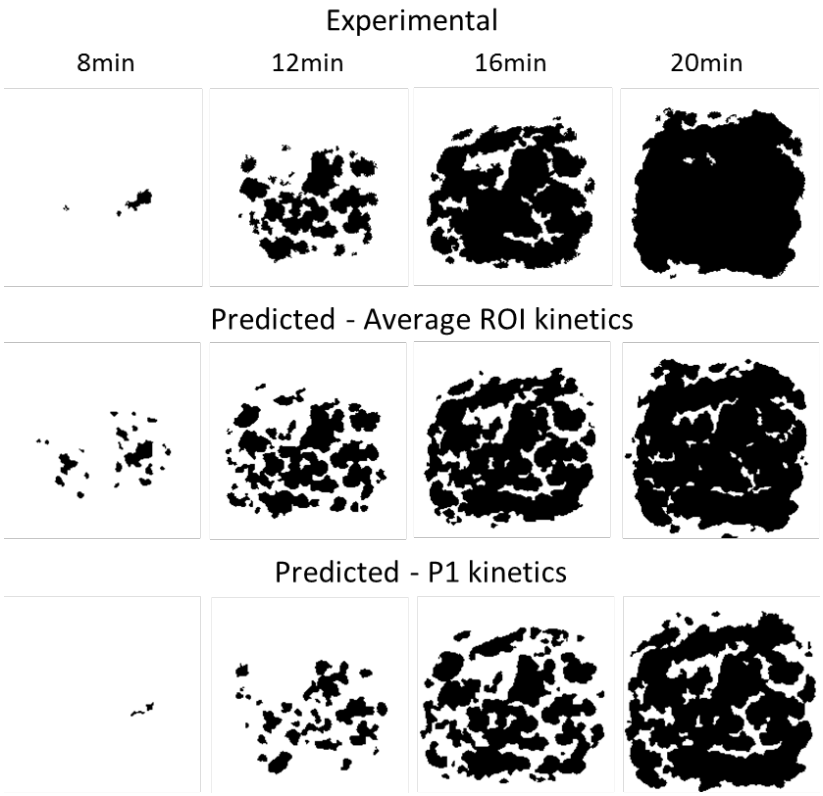

Figure 5.15 – Images from Figure 3.33 converted to binary images based on the dynamic thresholding method

This same analysis was applied to each of the cheese samples experimentally characterised in Chapter 3 (see Table 3.1 for details). Rather than compare binary images, Figures 5.16 to 5.18 were prepared, which show the blister numbers, average blister size and the increases in blister coverage (fraction of the cheese surface determined to be blistered), as a function of cooking time. For each attribute, the experimental results and predicted values using the Average ROI kinetics and P1 kinetics (as described in Chapter 3) were plotted, where the solid lines represent the experimental data and the dashed lines represent the predicted data.

Figure 5.16 shows the results for the number of apparent blisters as a function of time. A general trend is illustrated where blister numbers increase to a maximum and then reduce over time. This is likely to be due to the initial growth of individual blisters, which tend to combine and join together as they continue to grow. Both sets of parameters appear to over predict the number of blisters for the majority of the time. The P1 kinetics gave a more accurate representation of the initiation of blisters and number of blisters, following the trends of the experimental data more closely.

The results for experimental and predicted average blister size are shown in Figure 5.17. In general, blister size increases with respect to heating time, as exhibited by the overall average blister size data. Considering the number of blisters in relation to the average blister size, it is possible to determine a general pattern, where early on there are many small blisters and as blister numbers reduce, the average blister size tends to increase. The noisy nature of the data can be explained by this pattern, where the average blister size is significantly affected by a rapid change in the number of blisters. For example, the experimental data for Trial A1 (solid blue line) shows that the average blister size reduces from ~2000mm^2 down to ~500mm^2 towards the end of the experiment. At the same time the number of blisters increases from ~3 up to 12. Similar situations occurred for each data set, hence the erratic nature of the data.

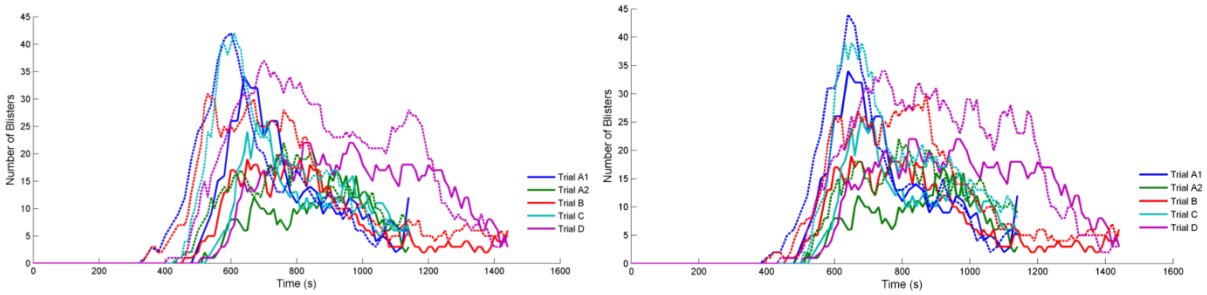

Figure 5.16 – Experimental and predicted blister numbers as a function of time, using the Average ROI (Left) and P1(Right) kinetic parameters (from Chapter 3)

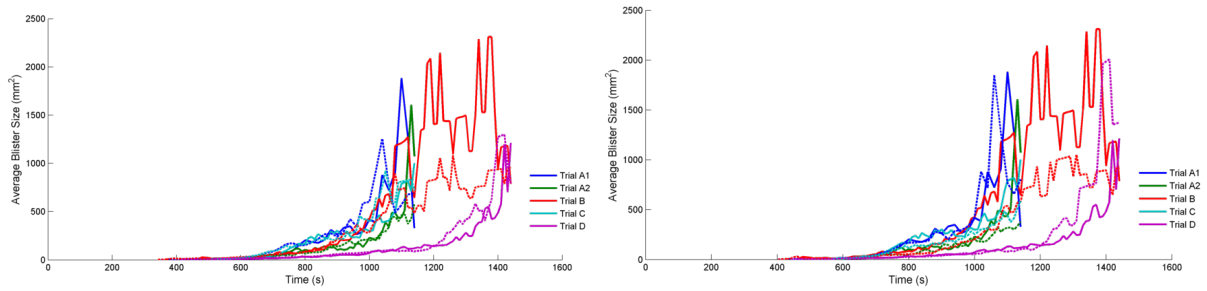

Figure 5.17 – Experimental and predicted average blister size as a function of time, using the Average ROI (Left) and P1(Right) kinetic parameters (from Chapter 3)

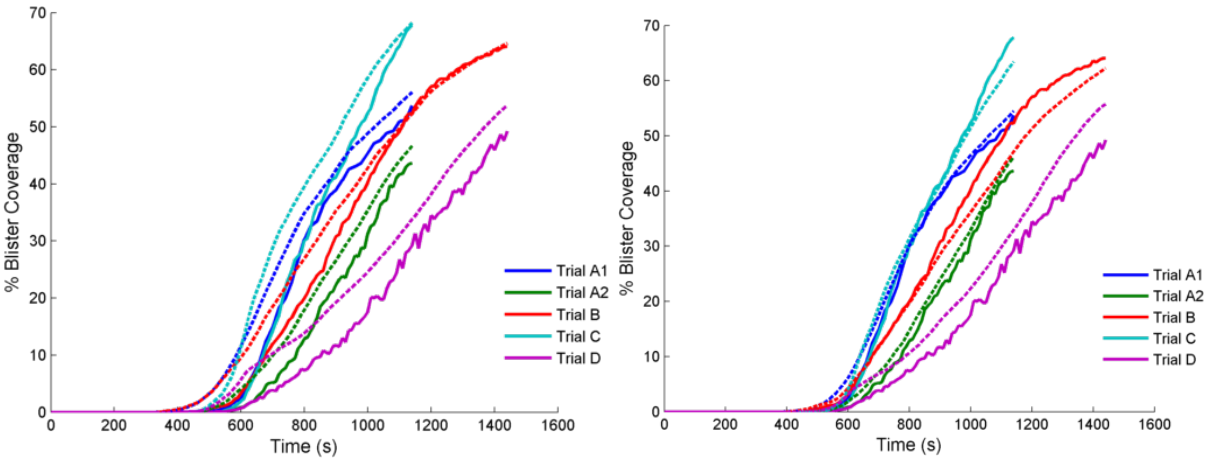

Figure 5.18 – Experimental and predicted blister coverage as a function of time, using the Average ROI (Left) and P1(Right) kinetic parameters (from Chapter 3)

Figure 5.18 illustrates the experimental and predicted % blister coverage for each experiment. These results give an overall indication of accuracy of the predictive kinetics. As suggested by the binary images in Figure 5.15 (showing Trial B), the P1 kinetics gave a more accurate fit in the early stages of heating, and the average ROI kinetics predicted better towards the end the heating process for Trial B. Both sets of kinetic parameters resulted in a good level of fit for blister coverage data across the board. Overall, the P1 kinetics gave a better fit across all the experimental trials with R^2 values ranging from 0.94 to 0.99, compared to the average kinetics which had R^2 values ranging from 0.90 to 0.98. This is in contrast with the results from Chapter 3 where the average ROI kinetics provided the best fit.

The use of blister coverage and the dynamic thresholding process resulted in a better fit than directly measuring and comparing L* values. The dynamic thresholding method could compensate for differences in the background and overall colour of a sample, which allowed for a better

representation of blistering and browning. In addition, a characteristic such as blister coverage is a more useful measure when considering a cheese baking process, as opposed to considering the specific colour of a cheese surface.

5.6 Conclusions

This chapter defined what a blister is to be able to characterise and measure blister formation and subsequent browning. A process was developed to analyse images of baked pizzas and determine a series of quantifiable characteristics. This process used thresholding to identify blisters with an image and took into account a defined minimum size of blisters. It was found that a dynamic thresholding method, derived from sensory data, resulted in the most accurate representation of blisters and browning for baked pizzas. Based on this analysis method, several pizzas were cooked over a large range of baking conditions to create a booklet outlining the resulting baking characteristics. The booklet could be used by industry to link a cooking regime to pizza appearance outcome.

The blister identification and analysis process was applied to the experimental and predicted data from Chapter 3. The results showed that a series of quantifiable characteristics can be extracted from the experimental and predicted data, which could be used to describe changes occurring during a cheese baking process and potentially linked to the properties of the cheese. Using blister coverage as a measure of baking, it was found that the kinetics based on a singular point (P1) gave the most accurate predictions. In addition, the predicted values using blister coverage were more accurate than directly comparing L* values. The next chapter further investigates the blister formation and browning of cheese in relation to pizza baking conditions and the resulting characteristics.

Chapter 6
Conceptual Modelling of Blistering

In the previous chapter a method of analysing blisters was developed with the use of a dynamic threshold to provide consistent comparison across a wide range of baking conditions. This process allowed for further investigation into blister analysis to gain an insight into formation of blisters and the effect of baking conditions on blister growth. This chapter explores the overall blister formation process to develop a conceptual model that could be used to predict pizza baking characteristics based on baking conditions.

6.1 How are blisters formed?

During the baking process of cheese, changes occur, affecting both internal and surface structure prior to the onset of browning and blistering. Figure 6.1 illustrates a conceptual model for the melt and flow of mozzarella, breaking the process down into a series of stages involving melt, flow, and steam formation (Brown & Bronlund, 2015), which in turn influence moisture content, surface temperature, and browning reactions.

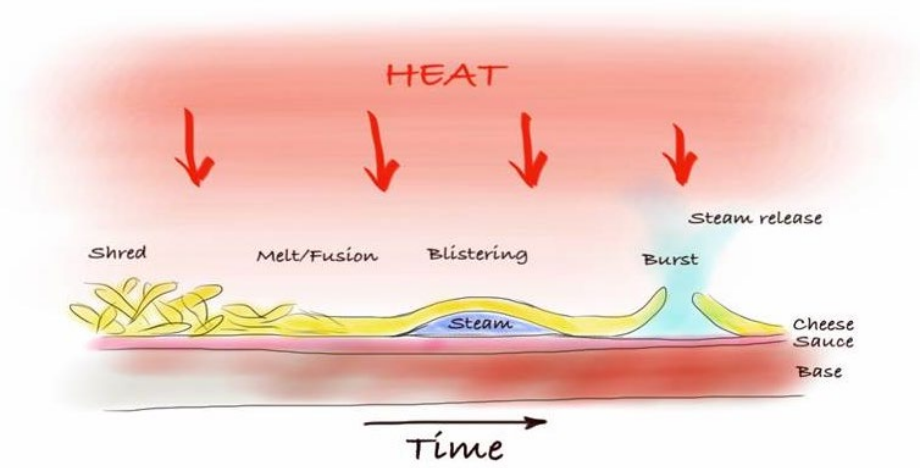

Figure 6.1 – Conceptualisation of blister formation (Brown & Bronlund, 2015)

Based on visual interpretations of cheese baking under various conditions, a hypothesis was formed for the general mechanism of blister formation and resulting blister size. Maillard browning is highly dependent on temperature and therefore changes that occur at the surface of mozzarella that result in an increase in temperature, play a significant role in blister formation.

The idea is that for browning and therefore blistering to occur, a cheese surface needs to dry out in order to reach Maillard browning temperatures (Rajchasom, 2014). Figure 6.2 illustrates the proposed simple breakdown of processes involved in cheese baking. During heating, cheese first melts and flows. When it reaches 100°C water begins to evaporate, creating a build-up of steam within the cheese. This steam accumulates in pockets that increase in volume by deforming the cheese surface to rise and form bubbles. This is analogous to blowing up a balloon, where the volume increases by deformation of the balloon walls and there is minimal pressure difference between the inside and

outside. Steam pockets create an insulating area below the cheese surface. As heat fluxes arriving at the surface cannot easily conduct into the bulk cheese/pizza, the resulting thin surface layer of cheese can dry rapidly. Once the surface dries out, temperatures can rise further and browning occurs. This overall process is driven by two main factors, steam formation and surface drying, both of which are dependent on heat transfer rates in the system.

There are a number of complex processes occurring that have been simplified to explore the overall understanding of cheese baking. The first point to consider is the nucleation of blisters and what may influence the blister initiation process. In Chapter 5, a blister was defined as a discrete brown region that forms on a cheese surface during baking. This is a quantifiable definition that allows for measurements and analysis; however it does not consider the process of how these discrete brown regions are formed. The proposed conceptual model suggests that bubble formation drives the onset of blistering, and therefore the nucleation of blisters can be considered to be driven by the nucleation of bubbles within the cheese layer. Blister nucleation may be influenced by a number of factors such as boiling nucleation, superheat, and the initial form factor and layout of cheese. For a bubble to nucleate and grow, it must displace the viscous molten material above it to form a void (Albalak, 1996).

Following nucleation, bubble/blisters grow as heat continues to be applied. Based on the aforementioned ideas, it is thought that the rate that the surface dries has a direct impact on blister propagation and growth. During the cheese baking process, moisture evaporates reducing the overall moisture content. Research has shown that there is an exponential relationship between mozzarella moisture content and relative viscosity. As moisture content decreases, viscosity increases exponentially (Zhu *et al.*, 2015). An increase in viscosity would limit flow and mixing, and increase bubble/blister lifetime, and therefore promotes surface drying.

As bubbles grow, molten cheese can flow due to gravity, effectively thinning the bubble wall. Similarly, if bubbles grow rapidly, the material being lifted can be stretched thinner, more quickly. If the walls thin to a critical level, they will burst, expelling the trapped steam and the blister will collapse. As the bulk cheese dries out, the viscosity of this material will be higher when new blisters initiate and thinning of the wall will be slower, allowing more time for the thin film to dry and become effectively stable.

The surface drying rate is driven by the rate that the system can apply heat to the surface, i.e. the heat flux. In general, the faster the surface dries, the faster the surface heats up, to a point where browning occurs, and vice versa. Accompanying Figure 6.2 is a hypothesis exploring how heat flux may affect the blister formation process.

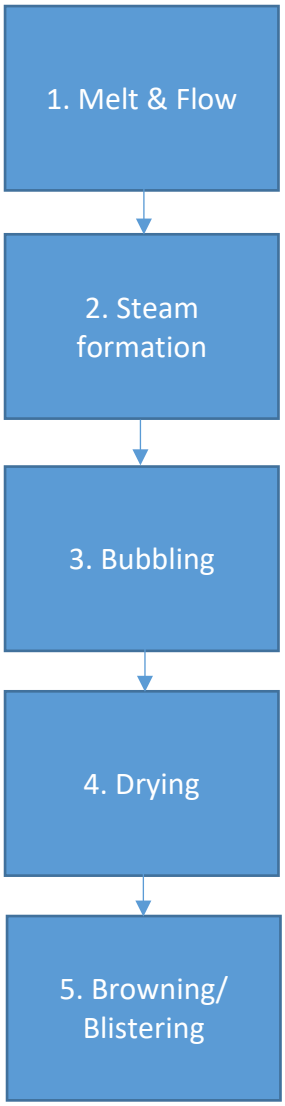

1. Melt & Flow – As cheese shreds melt and flow a uniform cheese layer is formed. This occurs at <60°C (Zhu, 2013)
2. Steam Formation – The cheese layer heats to 100°C liquid water beings to turn to steam
3. Bubble Growth – Bubbles nucleate and begin accumulating steam. As more steam accumulates, bubbles grow and the bubble surface stretches and flows, creating a thin layer
    a. Bubble growth may be limited by available superheat or incoming heat flux.
    b. The surface layer may reach a critical thickness during bubble growth and burst, releasing the entrapped steam and allowing the cheese layer to drop back into the bulk cheese. The integrity of this layer may vary as in some cases the moisture content of the cheese surface has not significantly changed whilst in other cases it may have dried out and form a skin on top of the molten cheese.
4. Surface Drying – As the surface layer loses moisture the viscosity of the layer increases, making the bubble more stable. As a result, the relative 'lifetime' of a bubble increases.
    a. Most of the heat flow goes into drying of the skin on the surface as steam acts an insulator
5. Browning/Blistering – When no water remains in the skin, temperatures increase above 100°C to promote browning

Figure 6.2 – Proposed process flow of cheese baking

Hypothesis under:

Low heat flux conditions (i.e. low cooking temperature and air velocity)**:**

- Cheese melts and flows slowly
- Cheese is more fluid as it dries slower and time allows moisture redistribution in the bulk,
- This promotes larger pockets of steam
- Larger pockets of steam accumulate before browning occurs forming larger raised areas and therefore fewer but larger blisters

High heat flux conditions (i.e. high cooking temperature and air velocity)**:**

- Cheese melts fast
- Cheese flow is limited due to drying, inhibiting the growth of steam pockets
- Smaller pockets of steam accumulate before browning occurs forming smaller raised areas and therefore more but smaller blisters

These ideas consider the cause of the initiation and propagation of blisters, which are the fundamental mechanisms affecting cheese baking performance. To investigate the nucleation of blisters through to blister growth and propagation a series of small experiments were carried out, as outlined in the following sections.

6.2 Blister Nucleation

Baking results, in terms of blister formation, are potentially affected by the initial form factor of the cheese. The most common form of mozzarella for pizza baking is shreds, small, evenly sized discrete particulates. Due to the nature of shredded cheese when spread onto a pizza, air gaps are present within the cheese. During melting, as the cheese layer begins to flow and fuse, the air gaps present may become trapped within the molten cheese. As steam forms, vapour could accumulate within any air gaps present, potentially providing nucleation points for blisters to form. In comparison, slices of mozzarella would not contain macroscale air pockets to provide possible nucleation points.

A small experiment was developed to assess this effect, comparing baking results with cheese in different form factors. The form factors used included shredded mozzarella, flat sheets of mozzarella, and a combination of both.

6.2.1 Small Scale Trials

To investigate the effect of cheese form factor on blister formation, a series of randomised replicate trials were carried out. Four combinations of factors were assessed for initial small scale trials:

A. 50g 5mm Sheet
B. 50g Shred
C. 2 x 25g 2.5mm sheets
D. 25g 2.5mm sheet (on bottom) + 25g shred (on top)

These trials were carried out in a commercial grade oven (Fisher and Paykel OB60 Built-in Oven), baking the samples in 0.01m^2 square rings for each trial. Baking conditions were kept constant, with the preheated oven temperature at 200°C, the tray placed in the same positions and a 10-minute baking time.

Visual observations of results indicated that there were not substantial observable differences in browning and blister formation based on the initial format of the cheese. Figures 6.3 and 6.4 show a set of example results, where the browning pattern and coverage are similar between all the images. However due to the small scale nature of the experiment, edge effects and other inconsistences, the results were not conclusive. A further experiment was carried out on a larger scale in order to improve control over the variables and minimise inconsistencies.

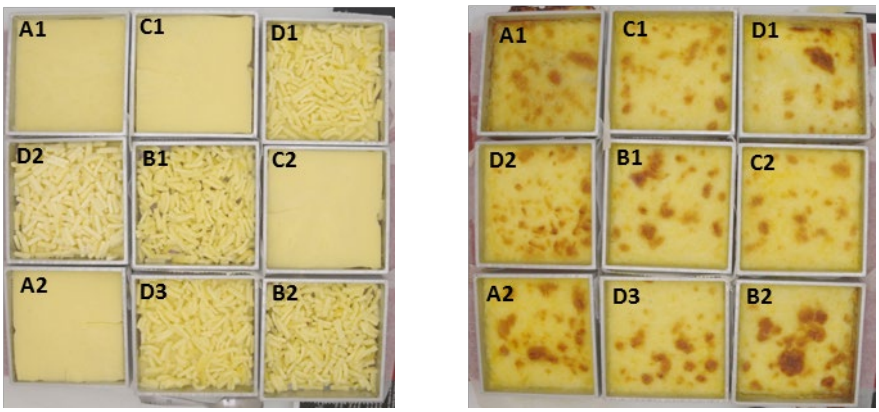

Figure 6.3 & 6.4 – Example images of various formats of cheese, before and after baking. Sample letters correspond to descriptions in 6.2.1 above, numbers refer to replicates

6.2.2 Scaled Up Trials

To minimise any inconsistencies due to the source and age of cheese, all samples were prepared from the same block of frozen mozzarella. A 3kg sample was cut from a 10kg frozen block of mozzarella. This was allowed to thaw at 4°C for three days before being sliced into ~4mm sheets. Note that cutting the sheets was a difficult process and resulted in some variation of sheet thickness. Half of these sheets were then cut further into shreds, approximately 4x4x30mm. The cheese samples were held at 4°C until they were required for cooking and all samples were cooked within a 48hr period to minimise any affects due to cheese ageing.

The experimental process involved preheating the oven to a set point of 230°C, giving an actual oven temperature of between 190-200°C. Once at temperature, samples were placed in the oven and IR and colour images were taken throughout the process. For shreds, 300g of mozzarella was spread evenly onto the tray. Sheets of mozzarella were cut to fit tightly into the baking tray, where sample weights varied between 270 to 320g. Four replicates for each form factor were carried out under the same baking conditions.

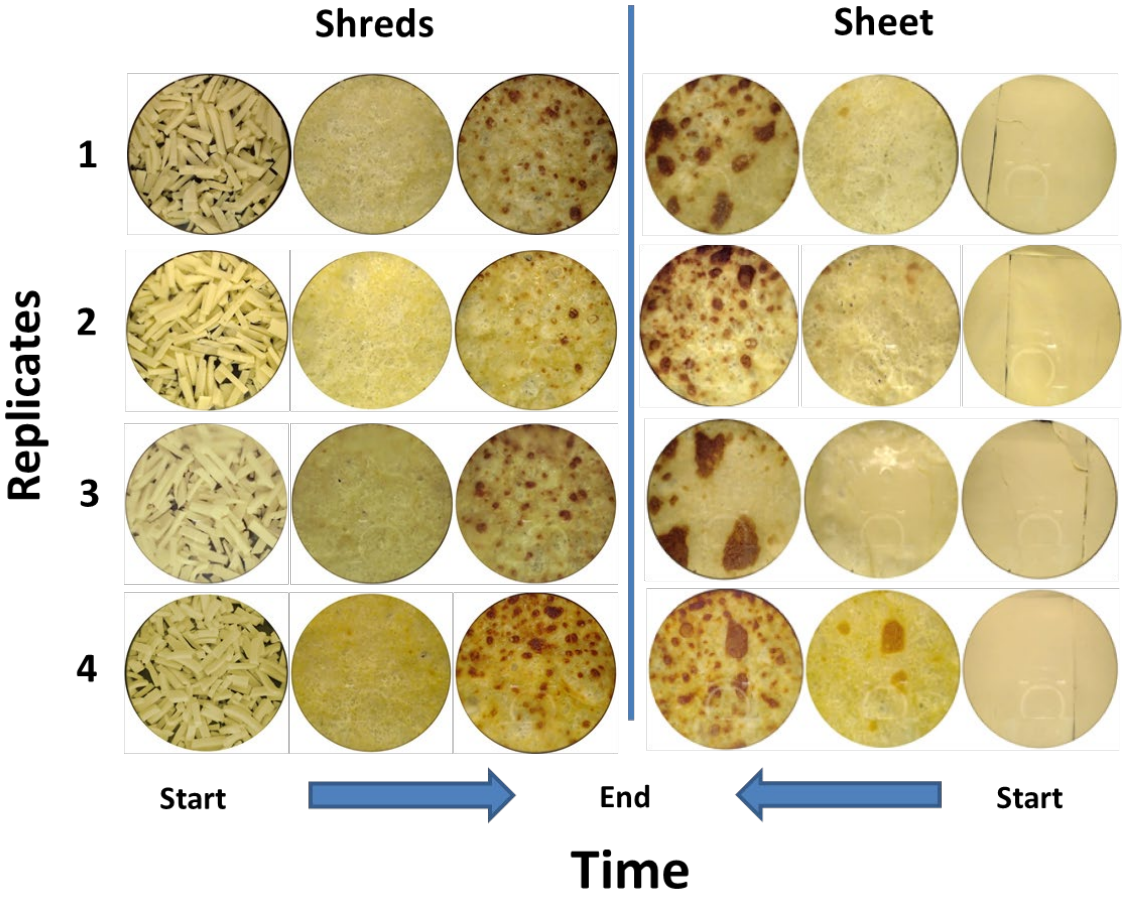

Figure 6.5 – Example of results from baking shreds and sheet of mozzarella under the same experimental conditions

Figure 6.5 illustrates the results of the replicates for each form factor. The three images for each sample represent pre-baking, mid-baking, and end of baking. The visual appearance of cooked shreds is similar across the samples; however variation can be seen within the sheet mozzarella samples even though all samples were baked under the same conditions. One possible reason for this is the production process of mozzarella. Looking at the surface of sheets of cheese cut from a large block, swirls and inconsistencies from the cheese formation process are visible. These variations potentially result in different concentrations of components across the cheese surface, leading to uneven baking performance. Note that this is an assumption based on the likelihood that there is surface variation, and the experimental design was not set up to study compositional differences. It is expected that shreds of cheese give a more uniform result as such variations would be distributed and spread among the sample.

The results of these experiments indicate that pockets of air due to the initial form factor of mozzarella do not affect the nucleation of blisters. It appears that blister formation is affected more by processing conditions, such as baking time and temperature, than the initial conditions. Further investigation into the effect of initial cheese format on blistering was unlikely to yield useful information in relation to the proposed conceptual model. Therefore, the focus of the following sections was to investigate how processing conditions affect baking performance for a commercial based pizza production setup, and how those results fit with the proposed hypothesis.

6.3 Blisters on Pizza

The proposed conceptual model suggests that heat flux has a significant impact on the blister formation process. The major application of this research is the commercial pizza baking industry, hence conditions for the further investigations were designed to emulate a commercial baking process.

To investigate the browning and blistering of mozzarella for commercial applications, a series of experiments were carried out under a range of processing conditions. The methods described in Chapter 5 were used to quantifiably assess baking results to determine how the different variables affect baking performance, and lead towards a method of defining baking conditions for a desired result.

6.3.1 Commercial Pizza Oven - Baking Pizzas

A modified pizza oven was used for this set of experiments, as described in Section 4.1. There were three main variables that could be controlled on the oven; Time, Temperature, and Fan speed. However, the results from air flow measurements (See Section 4.2) indicated that fan speed, within the controllable limits, did not change significantly and was not considered as a variable. An experimental design was set up to assess a range of suitable time and temperature combinations, informed by previous baking trials using the modified pizza oven. Table 6.1 illustrates the experimental design. Note that a temperature of 288°C was included as it was the maximum operating temperature of the oven. Only a portion of the overall table was assessed (marked x), as pizzas baked outside of this range would have been under or over cooked and outside of reasonable processing conditions.

Table 6.1 – Range of experimental baking conditions, indicating oven temperature and equivalent bake time

Oven Temperature (°C)	Equivalent Bake Time (min)						
	6	7.5	9	10.5	12	13.5	15
220					x	x	x
235	Under-cooked			x	x	x	
250			x	x	x		
265		x	x	x			
280		x	x	x	Over-cooked		
288	x	x	x				

6.3.2 Pizza baking method

Oven temperature was controlled via a PID controller, and bake time was controlled by the speed of the trolley travelling through the oven. The speed of the trolley was controlled to ± 1.0 $x10^{-4}$ $m.s^{-1}$. For each experiment, the oven was first preheated to the desired temperature for a minimum of 15 minutes for the oven and surfaces to reach equilibrium.

Baking pizzas:

1. The oven was set to the required temperature and trolley speed based on desired baking time
2. The pizza was prepared with components of base, sauce, and cheese.
    a. The pizza base and tray were weighed (Scale accuracy, 5000g ± 0.01g).
    b. 80g ± 2g of sauce was spread evenly onto the base (1:1 ratio Watties tomato paste and water).
    c. 240g ± 2g of cheese was spread evenly on the sauce.
    d. All initial weights of base & tray, sauce, and cheese were recorded.
3. Before baking, an image was taken in the light box under polarised lighting conditions with the colour chart visible, as described in Section 3.3.3.
4. The load cells were zeroed and the pizza was placed on the trolley at the entrance of the pizza oven. Baking time was based from when the front trolley wheels enter the oven to when the front wheels exit the oven. This determined the residence time that each point on the pizza spent in the oven.
5. The data logger was started and then the trolley mechanism was started.
6. Once the pizza exited the oven, the data logger was stopped and the final weight of the pizza and tray was measured and recorded.
7. Final images of the pizza were taken under both polarised and non-polarised lighting conditions.

6.3.3 Measuring mass loss

Mass loss due to baking was measured in two ways; the initial and final mass was measured using bench top scales, and from the load cells under the trolley during baking. Measuring the initial and final weight gave an overall mass loss, which was assumed to be the overall moisture loss. Based on this difference an average rate of moisture loss could be calculated. This did not account for the delay in moisture loss due to the initial heating phase to reach the boiling point. However, as the mass of pizzas and components were kept relatively consistent, the percentage mass loss was comparable for analysis.

Load cells at the four corners of the pizza trolley rails recorded the mass change during baking, however this data alone was not useful for analysis due to the airflow also applying load in the oven. Chapter 4.2 discussed the airflow within the modified oven, and showed that the airflow from both above and below varies depending on the position of the pizza within the oven. Airflow varies due to both air velocity differences, depending on impinger positions, as well as the overall impinger layout. During baking as a pizza moves through the oven, the balance of airflow from above and below affects the apparent mass of the pizza. If the balance results in a greater airflow from above the apparent mass of the pizza increases, and if the balance results in greater airflow from below the apparent mass of the pizza decreases.

To illustrate this effect, an empty pizza tray was passed through the oven and the mass logged. As the tray was empty, the actual mass of the tray remained constant as it passed through the oven. Figure 6.6 illustrates the results of the overall load cell data as the tray moved through the oven (orange line) compared to the actual mass of the empty tray (blue line). The apparent mass of the tray fluctuated by up to 30g below the actual mass as it moved through the oven and appeared to have three zones in terms of the overall balance. This effect meant that the raw load cell data was inaccurate and not useful for analysis. An attempt to improve the load cell data was made by using the empty tray data to account for the changing airflow, however the results were not consistent and hence not used for further analysis.

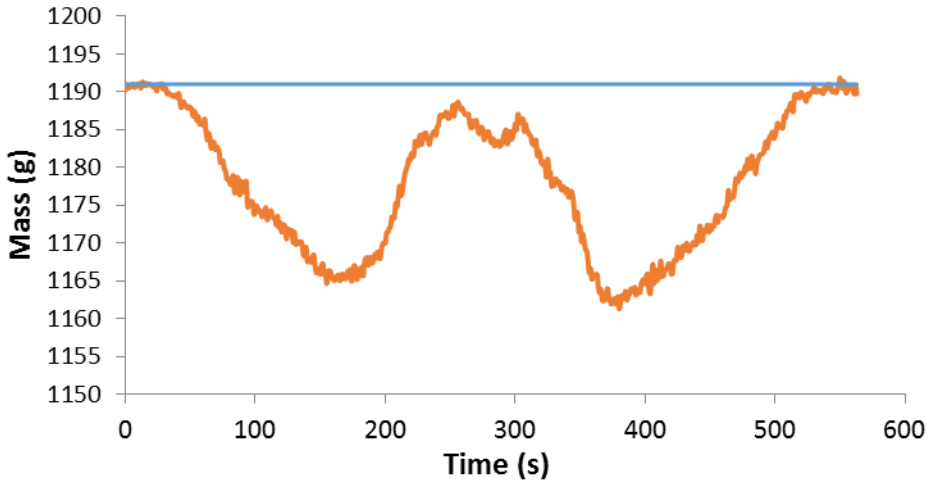

Figure 6.6 – Overall load cell data for an empty pizza tray passing through the modified pizza oven

6.3.4 Baking Repeatability

As there was a large range of experimental conditions, not all combinations could be feasibly replicated. To obtain a measure of repeatability, three different time and temperature combinations spread within the overall range were replicated a minimum of three times. Baking temperatures of 235°C, 265°C and 288°C were chosen, and for each temperature the central baking time was used to obtain a reasonable level of baking for each combination (i.e. time that resulted in a normal pizza appearance). The baking combinations used are shown in Table 6.2 below.

Table 6.2 – Baking time and temperature combinations for replicate trials

	Temperature (°C)	Time (min)
A	235	10.5
B	265	9
C	288	7.5

Pizzas were baked following the method outlined in 5.2.2 and the results were analysed following the methods outlined in section 5.4. Table 6.3 shows the results for the main performance parameters, including an average and standard error for each. Overall, the results showed good repeatability with relatively low standard errors in relation to the average for each performance parameter, especially % mass loss, % brown area, and average L*. This meant that even if replicates for each set operating conditions could not be performed, that the results gathered would be representative.

The results of percentage mass loss were very similar for each baking combination with a standard error of 0.2%, indicating that the heat flux in the oven remains consistent within each set of baking conditions. A consistent heat flux, relative to the operating conditions, would be expected to result in similar rates of moisture loss and therefore overall moisture, which is also reflected in these results. The level of browning, measured as percentage blister coverage, also had a low standard error of less than 3% for each set of operating conditions.

Table 6.3 – Overall results for replicate baking trials for combinations A, B and C (see Table 6.2)

Baking Combination	Average L* for Pizza Surface	% Mass Loss	% Blister Coverage	Number of Blisters (mm^2)	Average Blister Size (mm^2)	Median Blister Size (mm^2)
A						
Average	76.43	7.1%	21.6%	87	71.57	23.02
Standard error	1.10	0.2%	1.6%	9	12.18	5.76
B						
Average	66.84	7.3%	36.1%	94	109.42	28.33
Standard error	1.10	0.2%	2.1%	4	6.89	4.96
C						
Average	66.30	6.9%	36.7%	107	99.03	32.51
Standard error	0.60	0.2%	1.2%	14	14.50	3.62

Blister formation is driven by changes at the cheese surface and is affected by processing conditions rather than initial conditions as discussed in Section 6.1. Where the process conditions are the same, a similar result is expected. Figure 6.7 shows an example of the variation observed between replicates for baking combination B. They appear visually similar in terms of overall colour and extent of browning, which is reflected in the results.

Figure 6.7 – Colour corrected images of replicates for baking combination B, 9min at 265°C

These results demonstrate that the experimental process was well controlled, providing a reliable and reproducible system. In total, over 60 pizzas were baked for a range of time and temperature combinations. For each pizza, the mass loss, oven temperature, and initial and final images were recorded. The results from each baking trial were analysed to investigate the baking performance and identify any trends exhibited in the data.

6.4 Baking Results

Once baking trials were completed the resulting data was collated and analysed. Image analysis was the main form of assessment, where images were corrected so the extracted data could be directly compared for each experiment, as described in Section 5.3.

For the initial observations and comparison of baking results, sample images for each set of conditions were collated to create Table 6.4, giving a visual representation of the entire data set. The results illustrate that, based on visual observations, the size of blisters appears to decrease as oven temperature increases and baking time decreases. At the extremes, there a marked difference in blister size, where for 15 minutes at 220°C blisters are far larger than for 6 minutes at 288°C. As well

as blisters being larger at lower temperatures, they are also fewer in number. This is consistent with the conceptual model described at the beginning of this section, where a low heat flux leads to larger blisters, and higher heat flux leads to more, smaller blisters.

Further initial observations were that baking time had a greater impact on blister numbers and growth, than temperature, when the oven temperature was 250°C and above. For example, the images are similar for a 7.5min bake time, and do not change significantly at increased oven temperatures. To be able to confirm any of the observed trends, quantitative information was required.

Table 6.4 – Sample images of pizzas baked at different oven time and temperature combinations

Oven Temperature (°C)	Equivalent Bake Time (min)						
	6	7.5	9	10.5	12	13.5	15
220							
235							
250							
265							
280							
288							

To obtain quantitative data from the baking trials, the pizza images were processed using the dynamic threshold methodology to determine the relevant L* threshold for analysis. The blister analysis method described in section 5.4 was followed to determine the blister characteristics based on each set up condition.

The analysis resulted in a series of binary images, based on the dynamic threshold and blister identification. Table 6.5 illustrates the results based on the same sample images from Table 6.4. The

images appear to agree well in terms of blister identification, where the blister patterns match well with the original colour images.

Table 6.5 – Binary images based on analysis using a dynamic L* threshold for pizzas baked at different oven time and temperature combinations

Oven Temperature (°C)	Equivalent Bake Time (min)						
	6	7.5	9	10.5	12	13.5	15
220							
235							
250			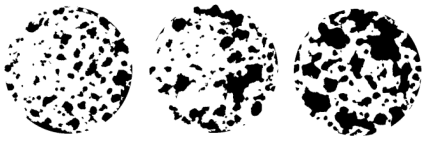				
265							
280							
288	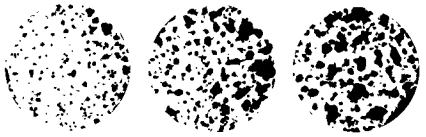						

6.5 Results from Pizza Baking Analysis

The main output of the threshold analysis process was a distribution of blister size. From this distribution, a range of performance measures for each image were calculated and recorded. This included blister coverage, number of blisters, average blister size and average L*.

All the results from baking and threshold analysis were collated to investigate the outcomes. There were many potential correlations and a significant amount of data to assess. To investigate the influence of baking time and temperature on the measured parameters, a method of plotting 3 variables in one plot was used, where the third variable was represented by a graduated colour bar.

For initial assessments, the two independent variables of Baking Time and Oven Temperature and the series of dependent variables were plotted to represent the set of data, shown in Figures 6.8 to 6.12.

The dependent variables explored were moisture loss, average L*, blister coverage, number of blisters, and average blister size. The blister characteristics were calculated from the results for L* across the surface for each pizza. For each plot, baking time was set as the x-axis, the desired dependant variable on the y-axis, and a colour bar was used to represent oven temperature. In this way, the general trends with respect to time, as well as those related to oven temperature, could be observed.

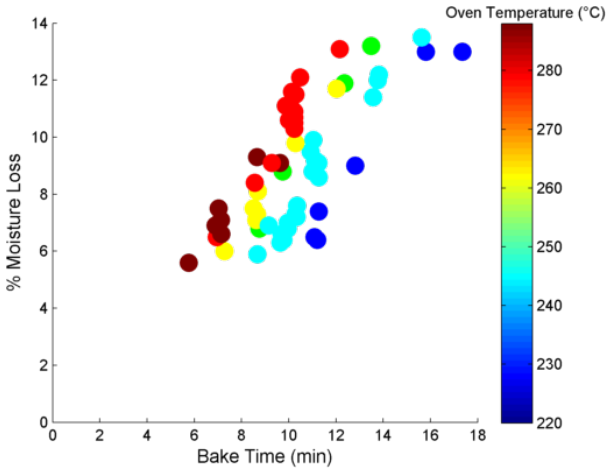

Figure 6.8 – Resulting % moisture loss based on baking time and oven temperature

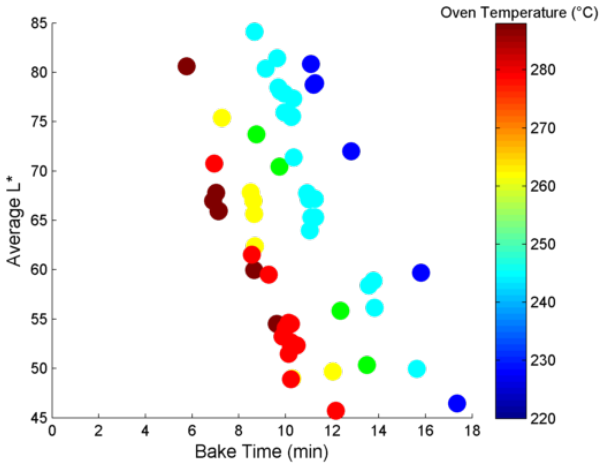

Figure 6.9 – Average L* based on baking time and oven temperature

The overall rate of moisture loss with respect to bake time and oven temperature is illustrated in Figure 6.8. The moisture loss results indicate that there is a linear relationship between moisture loss and bake time, relative to the oven temperature. Multiple regression for % moisture loss as a function of time and temperature shows strong correlation ($R^2 = 0.94$). This is an expected result, as all pizzas were baked within a time and temperature range where mass loss would be consistent and based on the rate of water evaporation under the given conditions.

Similarly, Figure 6.9 shows a linear trend where average L* decreases as baking time increases at each oven temperature. The average L* before baking ranged from 85-88, where variation is attributed to cheese shred layout and any sauce visible through gaps in the shred layer. The linear trend at each oven temperature is similar, however the baking time to achieve the same change in L* decreases as the oven set point temperature increases. Multiple regression for average L* as a function of time and temperature shows strong correlation ($R^2 = 0.93$). This indicates that the onset of colour change, and therefore browning, is highly dependent on temperature as would be expected for a Maillard reaction. Average L* only gives an overall representation of the surface of a pizza.

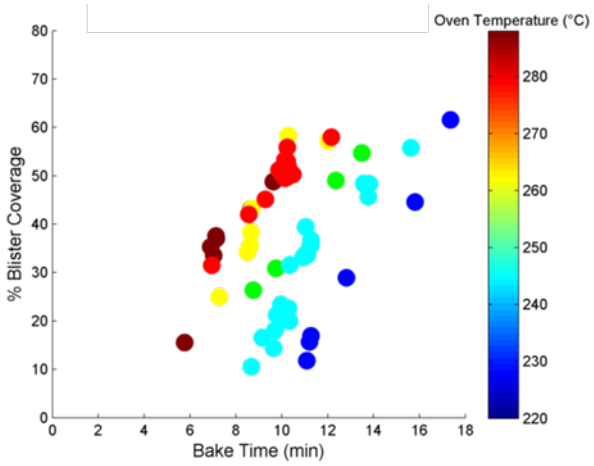

Figure 6.10 - Resulting % blister coverage based on baking time and oven temperature

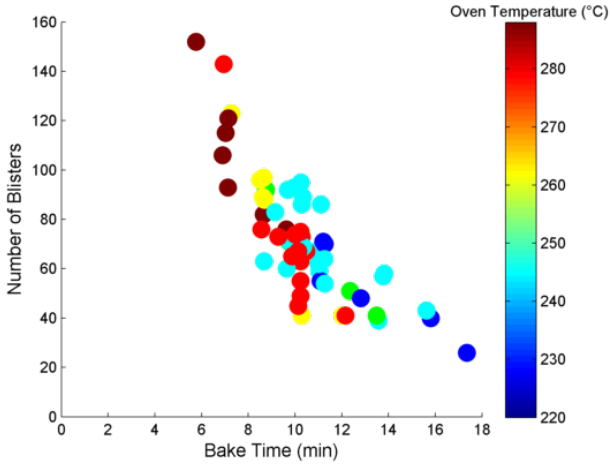

Figure 6.11 – Number of blisters based on baking time and oven temperature

Figure 6.10 illustrates the results of blister coverage relative to bake time and oven temperature. Multiple regression for blister coverage as a function of time and temperature shows strong correlation (R^2 = 0.90). As for Figures 6.8 and 6.9, there is a linear correlation in relation to bake time at each oven temperature set point. This shows that the longer a pizza is cooked, the browner and more blistered it becomes. This data also indicates that to achieve similar blister coverage, the required bake time varies depending on oven temperature; longer at lower temperatures and shorter at higher temperatures. For example, to achieve 10% blister coverage takes approximately 11 minutes at 220°C compared to approximately 6 minutes at 288°C.

At the extremes of possible baking conditions, it would be expected that the correlation would deviate away from linear moisture loss, average L* and blister coverage. However, the range of baking temperatures and times used were within the bounds where rate limiting factors did not come into effect.

Figure 6.11 illustrates the results of blister numbers relative to the bake time and oven temperature combinations. From the Figure, it is difficult to assess the trend within each oven temperature set point, however based on the entire data set there is a strong trend. In general, bake time has a significant effect on the number of blisters, where the longer the bake time, the fewer the number of blisters. It is likely that during longer baking times blisters may combine, effectively reducing the number of blisters. On considering the effect of temperature it can be seen that higher temperatures result in more blisters and lower temperatures result in fewer blisters.

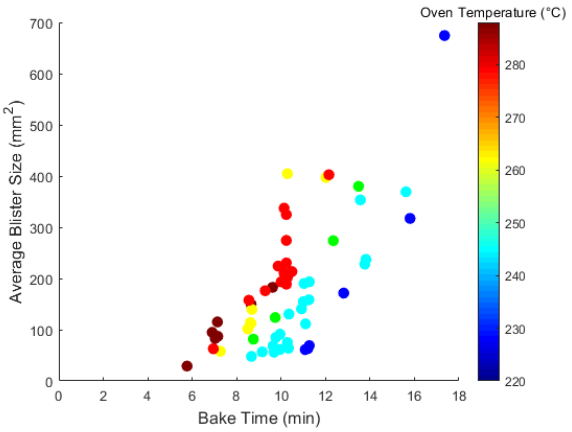

Figure 6.12 – Average blister size based on baking time and oven temperature

The change in average blister size is shown in Figure 6.12. This shows that as bake time increases, average blister size increases. In addition, the initiation and growth of blisters occurs in shorter times as the temperature increases. This illustrates the growth of blisters but does not take into account the number of blisters or overall blister coverage. Multiple regression for the number of blisters and average blister size as a function of time and temperature show a reasonable correlation, with R^2 0.78 and 0.81 respectively, which is significantly lower than for moisture, average L* and blister coverage. To further investigate the results, the interaction between key dependant variables was analysed.

Variables that may influence each other were plotted to assess the resulting trends. As an example, there is a likely interaction between blister coverage and the number of blisters. It can be assumed that the longer a pizza is cooked the greater the extent of blister coverage, which would continue to a point where the entire surface would be covered. Based on this assumption, as baking progresses the number of blisters would increase to a maximum before further growth causes individual blisters to combine. As blisters continue to grow and join together, blister numbers would then decrease.

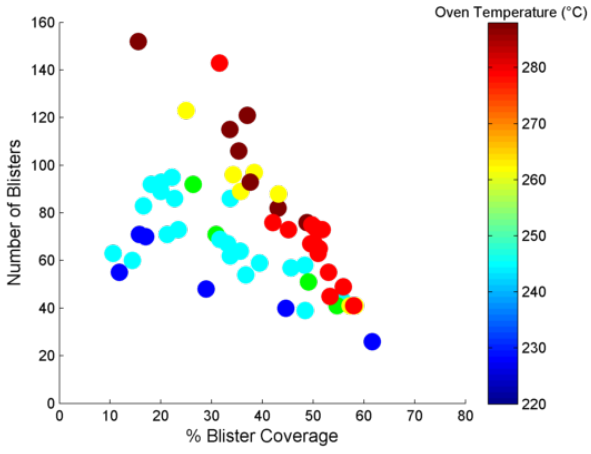

Figure 6.13 – Number of blisters vs. blister coverage and oven temperature

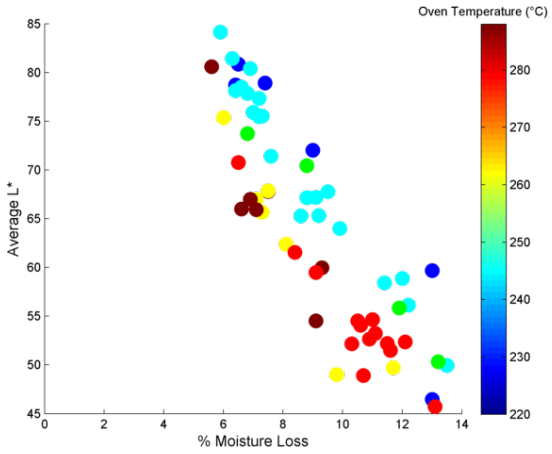

Figure 6.14 – Average L* vs. % moisture loss and oven temperature

Figure 6.13 illustrates the interaction between the number of blisters and blister coverage at each temperature setpoint for the data set. The overall results show that as blister coverage increases, the number of blisters decreases, indicating that blisters joined together as they grew. In addition, when blister coverage is less than 50%, higher oven temperatures resulted in greater blister numbers.

The data for 235°C (light blue) illustrates the variation in blister numbers in relation to blister coverage. It can be seen that as % blister coverage increases, blister numbers start off low at ~60, increase to a maximum (80-100), and then reduce to around 40 as adjacent blisters merge together. This pattern would likely occur at each temperature setpoint, however this data is not available as it is outside the bounds of the baking parameters assessed.

Figure 6.14 shows the relationship between average L* and moisture loss at each oven temperature set point. This illustrates that there is a general trend, where the greater the moisture loss, the lower the average L* and therefore the darker the pizza and more browning. However, of more significance is the relationship between moisture loss and oven temperature at a given average L*. Assuming the initial background colour is the same, the change in average L* is directly comparable between the different oven temperatures. Figure 6.14 indicates that at lower temperatures, more moisture is lost in achieving the same reduction in average L* compared to higher oven temperatures.

As part of the analysis, in addition to L* value, the change in a* and b* values were evaluated for each sample. Figure 6.15 illustrates the average L*, a* and b* values relative to % moisture loss and shows that L*, a* and b* all change with moisture content. This figure represents the results for the entire range of baking conditions and indicates that there is a direct relationship between average surface colour and moisture loss. This suggests that, irrespective of the baking time and temperature, the extent of moisture loss could be used to predict average surface colour.

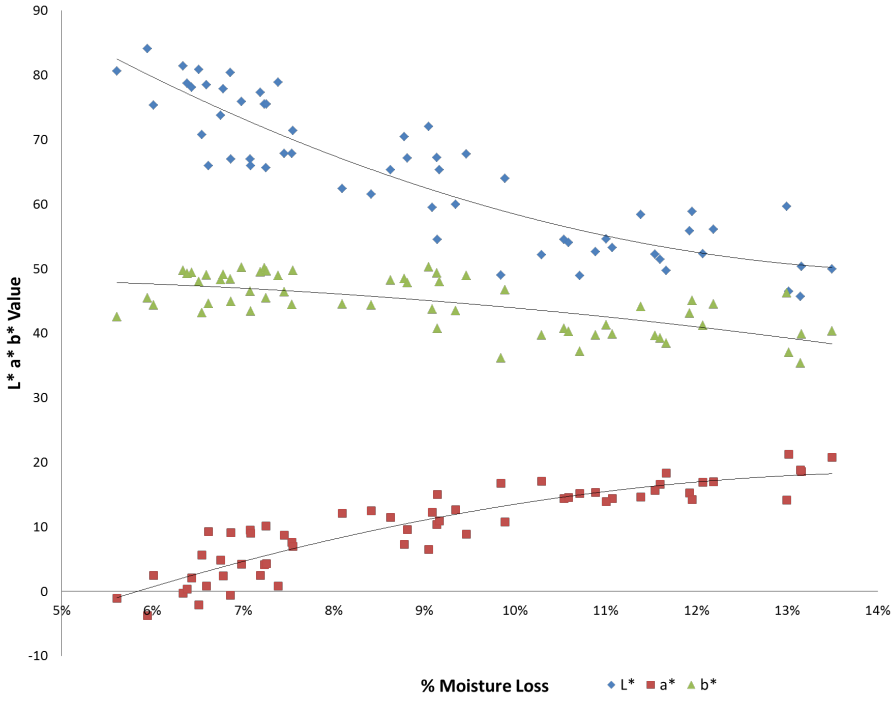

Figure 6.15 – Average L* a* b*results relative to % moisture loss for each set of baking conditions

Moisture loss, blister coverage and average L* can all be used to gauge and define an extent of baking, in addition just to bake time. However, what is important for analysis is what these parameters can tell us about the effect of bake time and temperature in relation to blister formation. Unlike blister numbers and blister coverage, average L* and moisture loss are not directly related, and further analysis is required to determine their impact on baking performance.

6.6 Analysis & Discussion

The following section further analyses the results and trends to explore the effects of bake time and temperature on blister formation.

6.6.1 Blister Count Vs Coverage

Comparing the number of blisters to % blister coverage, Figure 6.13 showed that higher oven temperatures generally result in greater blister numbers where blister coverage is less than 50%. Above 50%, the results indicate that blister numbers are similar relative to blister coverage at each oven temperature setting. This suggests for a blister coverage of 50% or greater, that oven temperature is irrelevant in regard to further blister growth and characteristics. Where blister coverage is less than 50% there is clear variation in blister growth and numbers relative to oven temperature.

The fact that higher oven temperatures result in greater blister numbers relative to blisters coverage means that blisters must be smaller. This is illustrated in Figure 6.13 where for any specific % blister coverage there are fewer blister numbers at 220°C than at 288°C. At a blister coverage of 35%, there were approximately 40 blisters at 220°C, compared to approximately 120 and 288°C. This difference is more prevalent at lower levels of blister coverage and converges as blister coverage increases beyond 50%. These results follow the hypothesis proposed in section 6.1, where higher temperatures trend towards smaller blisters, and low temperature trend towards larger blisters.

The heat transfer coefficient within the oven remains relatively constant over the operating temperature range, as determined in Chapter 4. As such, the change in heat flux under the different operating conditions is assumed to be solely due to the increase in temperature difference. To further investigate the effect of heat flux on blister characteristics, the time for initiation of moisture loss and blister formation was estimated, based on the linear relationships identified in Figures 6.8 and 6.10.

6.6.2 Blister Initiation

A linear relationship was applied to the data for Figures 6.8 and 6.10, which were used estimate to the initiation times for moisture loss and blister formation. This was done by extrapolating the slopes for % blister coverage and % moisture loss back to where they cross the x-axis at each oven temperature. The corresponding times gave an estimation for 0% moisture loss and 0% blister coverage. These results were combined, resulting in Figure 6.16, which illustrates the correlation between oven temperature and initiation times for moisture loss and blister formation.

The delay before the onset of moisture loss and browning occurs due to the pizza components heating up to evaporation and browning temperatures. The thermal mass of the system was kept consistent between trials by controlling the mass of the different pizza components and preparation method (Section 6.2.2). Therefore, there would be a constant quantity of sensible heating required, based on this thermal mass, to reach 100°C and the onset of moisture loss. It would be expected that the lag time for moisture loss decreases as oven temperature increases, due to a greater temperature gradient and therefore higher heat flux. This is reflected in the results shown in Figure 6.16, where the moisture loss initiation time reduces from approximately 5 minutes at 220°C down to approximately 2 minutes at 280°C.

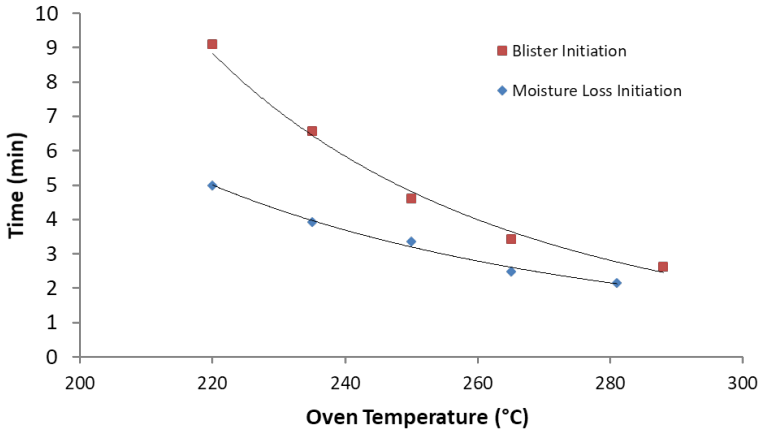

Figure 6.16 – Estimated times for moisture loss and blister initiation at different oven temperature set points (Note two data points were omitted due to difficulties estimating sensible intercepts for initiation of blisters ay 280°C, or moisture loss at 285°C)

The results for blister initiation time are also illustrated in Figure 6.16 and show a good relationship relative to the oven temperature, where blister initiation time decreases as oven temperature increases. Research has shown that for significant non-enzymatic browning to occur the surface temperatures need to be in excess of 105°C (Shibukawa et al., 1989; Broyart *et al.*, 1998; Purlis & Salvadori, 2009 and Purlis, 2010), and for this to happen the surface must be dry. There is a critical point where the surface layer dries out (stable skin formed) and temperatures begin to rise above 100°C. As the temperature continues to rise, the surface begins to brown and blister. Based on this, inferences can be made about surface moisture loss compared to overall moisture loss, where it can be assumed that the surface is dry when blisters begin to form.

A higher oven temperature gives a higher heat flux, which leads to a higher rate of moisture loss. The faster the surface dries, the shorter the time it takes for the surface to heat up to a temperature where browning occurs. The results for blister initiation time in Figure 6.16 show that the time decreases as oven temperature increases. This suggests that the cheese surface dries out faster as oven temperature increases, where blisters begin to form in less time.

Using the heat transfer data calculated from Chapter 4 and the time delay between the initiation of moisture loss and blister initiation, it is possible to estimate the mass of moisture lost before blister initiation for each oven temperature. Figure 6.17 shows the results of these calculations.

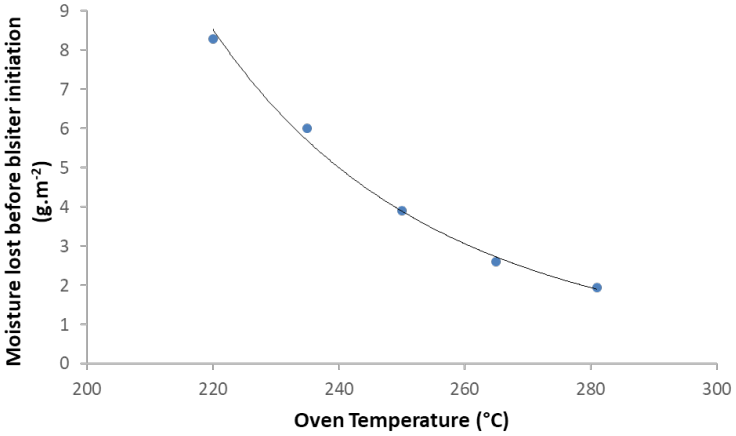

Figure 6.17 – Estimated moisture loss before blister initiation based on oven temperature

The trends in Figure 6.16 and 6.17 show that the time between initial moisture loss and subsequent blister initiation decreases as oven temperature increases. This indicates that heat flux has a greater effect on blister initiation than overall moisture loss. Considering that browning is correlated to surface moisture this idea can be taken further, where it can be assumed that heat flux has a greater effect on surface moisture loss in comparison to bulk moisture loss.

This interaction means that a pizza will brown faster with less overall moisture loss at higher baking temperatures. The next step is to consider what these results mean in relation to blister size and growth.

6.6.3 Blister Growth

To explore blistering and blister growth, further interactions between blister size, number of blisters, moisture loss, and blister coverage were analysed. The aim of this was to determine the impact of the control variables, oven temperature and bake time, on pizza characteristics during baking. Figures 6.18 to 6.21 illustrate several interactions, which were used to expand on the blister initiation concepts and the relationship between blistering and moisture loss.

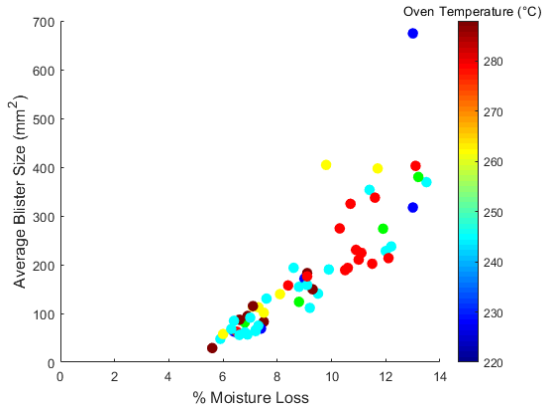

Figure 6.18 – Average blister size based on % moisture loss and oven temperature

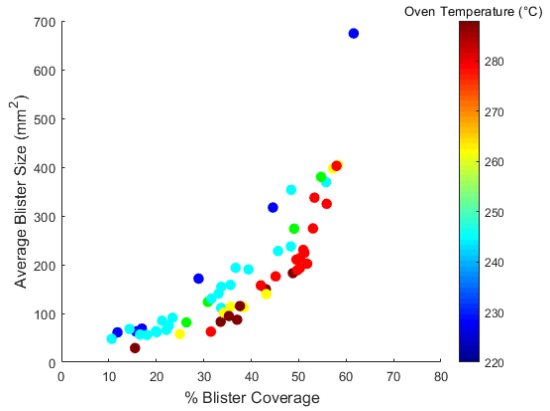

Figure 6.20 – Average blister size based on % blister coverage and oven temperature

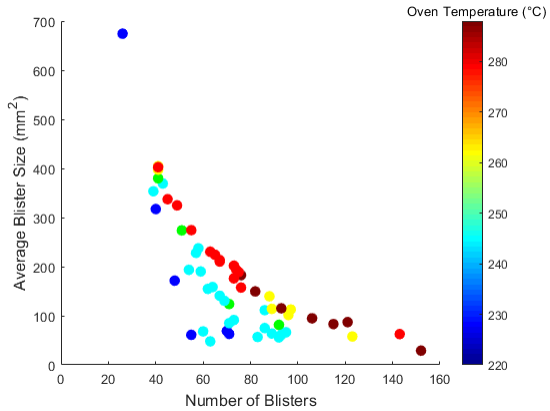

Figure 6.19 – Average blister size relative to the number of blisters and oven temperature

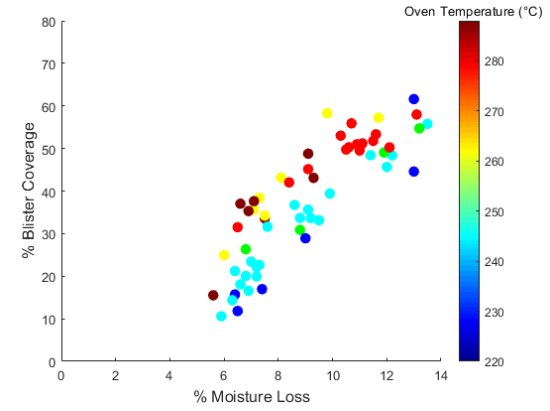

Figure 6.21 – Resulting % blister coverage based on % moisture loss and oven temperature

Figure 6.12 shows that average blister size increases as bake time increases and suggests that initiation and growth of blisters occurs in shorter times as oven temperature increases. Figure 6.18 shows the interaction between average blister size and % moisture loss, and indicates that as % moisture loss increases, the average blister sizes increases. This general trend is similar for all oven temperatures,

which suggests that average blister size is proportional to overall % moisture loss irrespective of baking temperature. However, this interaction does not consider the overall surface characteristics of a pizza.

The conceptual mechanism of blister formation and growth introduced in section 6.1 implies that blister size is relative to heat flux, with low heat flux resulting in larger blisters, and high heat flux resulting in smaller blisters. However, this idea does not take into account the extent of baking. It has been shown that blister size and numbers vary under the same heat flux conditions as measures of baking extent increase, such as bake time and % blister coverage. Using % blister coverage to define the extent of baking, Figure 6.19 illustrates that average blister size increases exponentially as blister coverage increases and that results appear to converge for all oven temperatures as blister coverage increases beyond 60%. This data also shows that average blister size can be similar irrespective of oven temperature, and therefore heat flux. Taking into account the extent of baking however, Figure 6.19 shows that for a given % blister coverage, the average blister size is dependent on heat flux. For example, at a blister coverage of 40% the average blister size was ~40mm^2 at the lowest heat flux, and ~20mm^2 at the highest heat flux. At a given % blister coverage, if the average blister size is smaller the number of blisters must be greater, and vice versa. This correlation is illustrated in Figure 6.20 and indicates that the rate an average blister size grows, relative to the decline in number of blisters, decreases greatly as heat flux increases. The trend at each oven temperature appears to be linear, where the gradient at 220°C was 2.3, more than seven times greater compared to 0.3 at 288°C.

Overall, these results demonstrate the effect of heat flux on blister size and number, building on the suggested hypothesis for blister formation and characteristics. Given a desired level of blister coverage, as heat flux increases, the average size of blisters reduces and the number of blisters rises. This describes the results based on baking conditions, however the mechanism of how this occurs can be explored further.

The % blister coverage results relative to % moisture loss are illustrated in Figure 6.21. This data indicates that blister coverage increases linearly as % moisture loss increases. Higher oven temperatures result in greater blister coverage relative to % moisture loss, where for a given % moisture loss, % blister coverage increases as oven temperature increases. This suggests that the pizza surface is drying out faster relative to overall moisture loss and therefore heating up faster at higher oven temperatures. This concurs with the earlier analysis from Figure 6.12. Based on these findings, moisture loss can be split into two categories: bulk moisture loss and surface moisture loss. Bulk moisture loss represents the steam formed within the cheese layer escaping and surface moisture loss represents direct moisture loss due to evaporation at the surface of the cheese layer.

The analysis of Figure 6.16 gave an insight into the relationship between surface moisture and bulk moisture. The initiation of moisture loss occurred in a shorter time and the delay between moisture loss initiation and blister initiation decreased as heat flux increased.

During baking, prior to the initiation of moisture loss, the cheese layer melts and flows. The time delay between the onset of moisture loss and blister initiation is the duration that steam is forming and flowing before the cheese surface dries out. As steam forms, some escapes to the atmosphere and brings the onset of moisture loss. As moisture is lost, the viscosity of the cheese increases. Molten cheese viscosity is affected primarily by moisture content, where viscosity increases exponentially as moisture content decreases (Zhu *et al.*, 2015). This moisture dependency on viscosity suggests a mechanism that can describe the role of heat flux and surface moisture in determining the resulting blistering characteristics.

The proposed conceptual model introduced in 6.1 suggested that the blister formation process begins with steam accumulation forming raised pockets with the cheese layer. At the cheese surface, as moisture content drops, viscosity increases. If this occurs rapidly, as would occur with a high heat flux, there is limited time for bubbles to form before a stable skin forms and the surface dries out. In addition, an increased viscosity means that there would be more resistance to growth. In this case, the resulting blisters would be smaller than for low heat flux conditions. If the cheese surface dries slower, there is more time for bubble growth before viscosity increases and a stable skin is formed. The longer time for steam to form and accumulate results in larger raised pockets and consequently larger blisters. This suggests that there is a critical moisture content where the cheese surface forms a stable skin where temperature can rise above 100°C. At this point steam would be trapped and would act as an insulator, where heat transfer to the skin would be greater than heat transfer away. Additional heat causes the temperature to increase above 100°C resulting in browning and blister initiation.

The findings from these experiments and analysis indicate that surface drying dynamics are fundamental to the onset of browning and blister development. Once the cheese layer has melted and steam generation begins, the bubble growth and surface drying periods define the eventual surface characteristics. Blister growth and size is driven by the moisture content and therefore viscosity, at the cheese surface. Oven temperature dictates how fast the surface will dry and therefore the general blister characteristics. Bake time determines the desired level of baking based on blister/browning coverage. Hence, heat flux and cheese surface dynamics, in regard to the rate of moisture loss and change in viscosity, are the critical factors in determining browning and blistering and characteristics.

These findings give an understanding of the effect of baking conditions and cheese (in terms of rheology and moisture content) to dynamics during baking and give the ability to predict baking characteristics. For a desired level of baking based on surface characteristics, it would be possible to predict the required baking conditions to achieve the desired results. This has useful applications in terms of being able to tailor cheese composition and baking conditions to achieve desired baking conditions at a commercial scale.

6.7 Conclusions

This chapter explored a proposed conceptual model of the blistering of cheese during baking, where a hypothesis was formed for the general mechanism of blister formation and resulting blister size. Initially the nucleation of blisters was considered and it was found that there was no discernible difference in browning and blistering based on the initial form factor and arrangement of cheese.

The pizza baking process using the modified commercial oven was found to be repeatable with a low standard error between replicate trials. Further experiments and analysis investigated the effect of bake time and oven temperature on pizza baking, resulting in key findings with regard to the blister formation process. Surface drying was found to be fundamental in terms of blister initiation and growth. The relationship between surface moisture and bulk moisture and their effect on viscosity, drive the process of blister growth. Drying rate is dependent on heat flux and is what dictates the general blister characteristics, relative to the extent of baking. Low heat flux trends towards fewer but larger blisters and high heat flux trends towards a greater number and smaller blisters.

In terms of the general impact of baking conditions, oven temperature determines blister size and number and bake time determines the desired level of baking. The overall findings agree and build on the initial conceptual model and give an understanding of the processes that define the final surface characteristics of a baked pizza. This understanding of cheese behaviour and influential factors during baking has potential benefits for commercial cheese manufacture and applications.

In this chapter the end results of pizza baking were analysed. Further exploration of the mechanisms of blister formation could be done by following the cooking process dynamically, measuring parameters in real time to assess changes throughout the baking process. This is the focus of the next chapter.

Chapter 7
Dynamics of Browning and Blistering

The results and analysis from Chapter 6 suggested that surface drying dynamics during baking are a fundamental factor that drives the onset of browning and blister development. To further investigate these findings a process to measure these characteristics in real time was required.

The investigations reported so far focussed on two separate parts, driven by different experimental designs: the kinetics of browning, and blister formation and characteristics. The blistering investigation required a large number of experiments as only the end points could be measured based on a single image. A method was developed to combine the elements of both experiments so that colour and temperature could be recorded in real time and therefore obtain a measure of blister growth and browning under oven baking conditions. This chapter outlines the methodology and further explores the relationship between moisture content, surface temperature and blister characteristics to better understand the impact on browning and blistering.

7.1 Development of Experimental Method to Measure Colour, Temperature and Mass Loss

The focus of this chapter is to further assess the characteristics of mozzarella cheese under oven baking conditions. A benchtop experiment was developed with aspects of the initial experiments from Chapter 3 to measure and record colour, temperature, and mass loss in real time. To do this a domestic benchtop oven was modified and measuring equipment applied as described below.

7.1.1 Recording Temperature Data

As for the experiments in Chapter 3 the FLIR E60 IR camera was used to measure and record surface temperature data. To capture images the camera was linked to a computer and triggered remotely at regular 20 second intervals using the FLIR Tools (FLIR Systems, Oregon) program.

In addition to measuring the surface temperature, it was necessary to accurately measure the internal oven temperature to ensure that conditions between experimental trials were controlled appropriately. A thermocouple was placed within the oven and linked with a temperature data logger (Measurement Computing USB-TC). The data logger was linked to a computer (Toshiba Tecra A10) using the software Tracer DAQ (Measurement Computing) and recorded data to a .csv file every second.

7.1.2 Recording Colour Data

Due to space limitations the DSLR camera used for the initial experiments was too large so a compact webcam (Logitech C920 HD Pro) was used for recording colour data. To record colour data the webcam was connected to a computer (Toshiba Tecra A10) and controlled using code written in MATLAB. The reason for using a DSLR camera in previous experiments was the ability to have full control over the image capture settings, allowing for consistent and comparable images. The proprietary Logitech software did not give the ability to specifically control all functions and settings, which could have resulted in potentially different image capture conditions throughout an experimental run. To overcome this MATLAB's Image Acquisition Toolbox was used to communicate

with the webcam and define a specific set of parameters for image capture. The setpoints for the image capture parameters are defined in the MATLAB file 'webcam_capture.m' (Appendix 1). This code was also used to initiate and save recordings for each experiment.

7.1.3 Measuring Mass Loss

The commercial oven baking experiments (reported in Chapter 6) only recorded initial and final mass accurately, limiting the amount of data and understanding that could be gained based on the process flowchart for cheese baking proposed in Figure 6.2. Recording mass loss continuously provided the ability to analyse and consider the different phases of cheese baking directly relative to temperature and colour parameters during the baking process. For this experiment a top pan balance (Mettler Toledo PB3002-S) was used and interfaced with a computer (Toshiba Tecra A10) using the software Labview 'Scales Logger.exe' (National Instruments, Austin, Texas). This software recorded information to a text file every second that was converted in an Excel file to extract the mass data.

7.1.4 Oven Modification and Experimental Setup

The goal of this chapter is to investigate the relationship and impact of moisture and temperature on the fundamental conditions resulting in surface colour change. To achieve the required data collection a benchtop oven was modified to accommodate the necessary equipment. A Breville Compact Smart Oven (BOV650XL) was physically modified to allow the relevant measurements to be made. The temperature range for this oven could be set from 50-230°C in 5°C increments. The internal surface was painted white with heat resistant paint to improve lighting conditions. Modifications were made to the top surface for capturing images and the bottom surface for recording mass.

7.1.4.1 Top surface

To capture colour and IR data a circular hole was cut into the top to view a tray inside the oven. Originally this hole was made to a fit an IR window (100mm FLIR IR inspection window IRW4C), a crystal lens that transmits short, mid, and longwave IR while also allowing illumination to shine through. However, initial calibration trials were unsuccessful in capturing accurate data. Comparing measurements with and without the window gave different results even with the IR window compensation settings using the procedure provided in the IR camera instructions.

As such, the hole (100mm diameter) remained uncovered to allow for clear colour and IR image capture. To protect the camera equipment from the rising heat, a heat gun was used on its lowest setting to blow horizontally across the oven surface to create an air curtain. A thermocouple was placed near the cameras during all experiments to monitor the local temperature and ensure the equipment was not affected or damaged. This thermocouple was linked to the same data logger as the thermocouple within the oven. Internal oven temperature was tested with this setup and it was found that stable temperature conditions could be achieved. Figure 7.1 shows the experimental setup for the IR camera, webcam, heat gun and thermocouple.

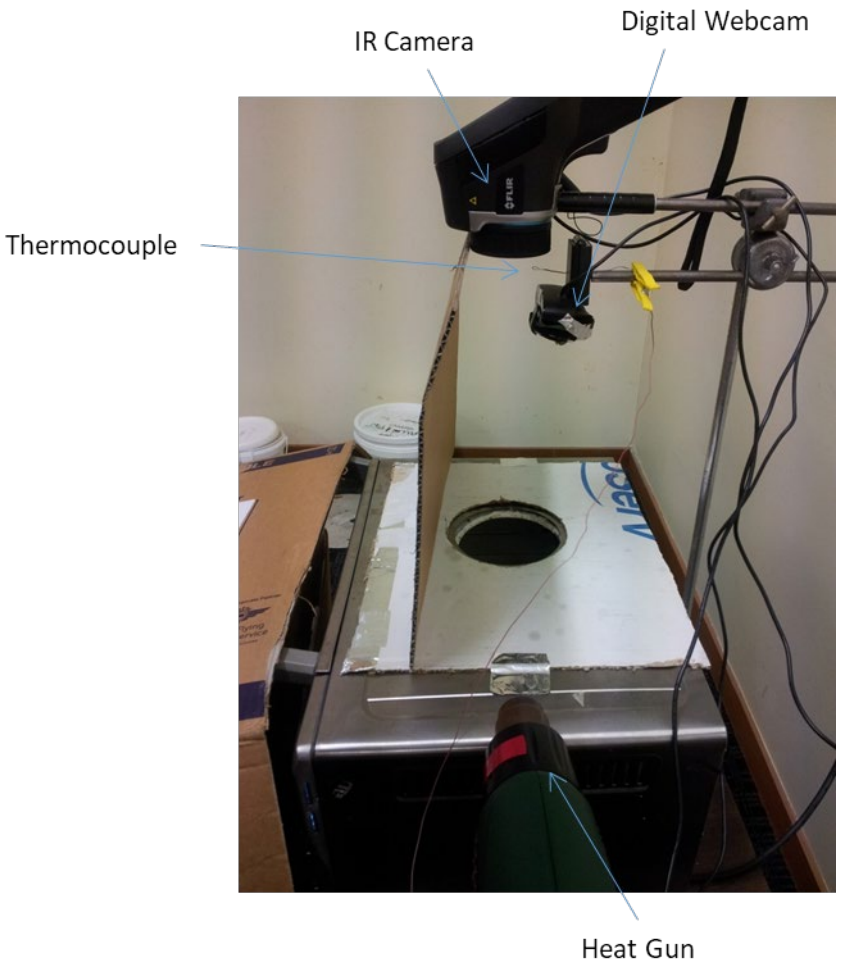

Figure 7.1 – Experimental setup for capturing colour and IR data

7.1.4.2 Bottom surface

A method of supporting a tray in the oven while using scales to record mass data was required. With the equipment available and resolution of the mass being measured it would have been impractical to place the entire oven on a set of scales (the initial sample mass was less than 250g). To isolate and measure just the baking tray, holes were cut through the bottom surface of the oven and the table the oven was sitting on. This allowed for a small tripod to be placed in the oven, with its legs resting on the scales below. Figure 7.2 illustrates the overall experimental setup including the tripod and scales below.

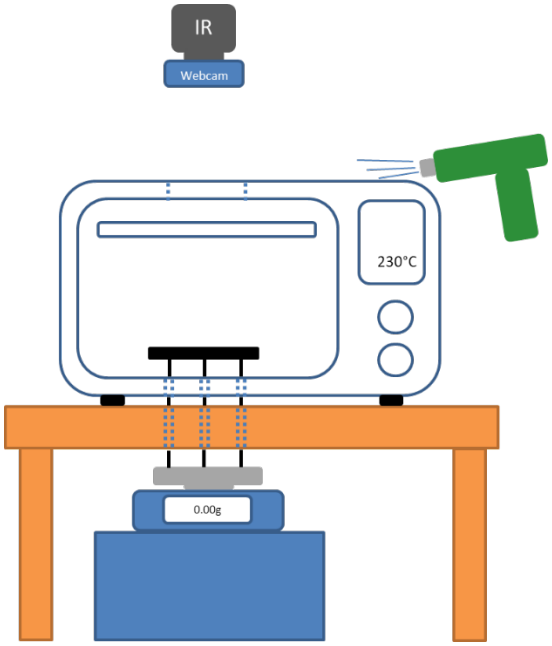

Figure 7.2 – Schematic of the overall experimental setup and oven modifications

7.1.4.3 Lighting

The lighting section of Chapter 3 outlines a method of controlling lighting conditions with the use of polarising filters. A similar approach was employed for these experiments to allow for consistent lighting conditions while minimising reflections on the cheese surface, with the use of a darkroom and only controlled illumination. Two light sources (Osram 100W with an 80° beam angle) were installed 5cm in front of the oven window and held in place with a clamp stand, as shown in Figure 7.3. An outline of each clamp stand was taped onto the floor to control the position of the lamps to ensure repeatability of lighting between experimental trials. A polarising filter film that covered the entire window was fixed to the handle of the oven approximately 3cm in front of the oven window. A polarising filter was adjusted to be in the same plane as the incoming light and fixed to the webcam in order to minimise any reflected light in the captured images. To help direct the light into the oven, a piece of cardboard was painted on one side and fixed ~10cm above the light sources. In addition, to prevent any external lighting interference with the cameras, a piece of cardboard was positioned between the light source and the cameras. The positions of these pieces of cardboard are shown in Figures 7.1 and 7.3.

Figure 7.3 Experimental setup and oven modifications showing lighting arrangement

7.1.5 Conducting Trials

The aim of these experiments was to cook cheese under various conditions and measure mass loss, surface temperature, and surface colour. Experimental trials were carried out at three different temperature setpoints, 205°C, 215°C and 230°C. From the internal mounted thermocouple this equated to 168°C, 175°C, and 185°C respectively. The aim was to have 10-15°C intervals from the maximum temperature and this was the closest achievable due on the oven temperature control settings. These temperature drops were due to the location of the oven temperature sensor used for control (in the oven wall) and the significant heat losses introduced by the exposed hole in the top of the oven. Even though these heat losses occurred, a stable internal oven temperature was achieved. The internal surfaces of the oven were made of low emissivity materials and the heating elements on both top and bottom of the oven were not directly exposed to the samples being cooked. For these reasons, negligible thermal radiation from the elements or oven surfaces to the cheese occurred. Four replicates were done at each temperature, but logging difficulties resulted in only one reliable data set and 168°C. Note that the specific temperature intervals and cooking times were not critical for analysis as the experiments were consistent and repeatable.

For each trial:

1. The oven was set to the required temperature
    a. Preheated for a minimum of 15 minutes for the oven and surfaces to reach equilibrium
2. The cheese and tray were prepared
    a. 240 ± 2g of cheese was spread evenly into the tray
3. The programs required were initialised on the computer (Toshiba Tecra A10)
    a. FLIR Tools (FLIR Systems, Oregon)
    b. Tracer DAQ (Measurement Computing)
    c. MATLAB's Image Acquisition Toolbox
    d. Labview (National Instruments, Austin, Texas)

4. The tray was placed in the oven and cooked for a minimum of 25 minutes
5. Once baking was completed, all the data recorded was saved and referenced relative to the oven temperature and replicate

7.2 Raw Data Conversion

Once the experimental trials were completed the resulting data was collated for analysis. The raw data output was made up of IR surface temperature, colour, and mass loss. In order to analyse the raw data, it first needed to be converted into a useable format. In general, the methods were similar to those discussed in Chapter 3, with some additional data extraction required for the webcam video.

The IR data had the lowest sample frequency with images taken at 20 second intervals, compared to all other parameter logging which were recorded at least once per second. Therefore, the IR data set defined the time step for direct comparison and further analysis. The data extracted for mass, colour images, and temperature images were aligned to match the time step dictated by the IR images.

7.2.1 Surface Temperature

Surface temperature data was extracted as in Chapter 3, where IR images were converted into .csv files using the FLIR Tools software and surface temperature data extracted using the IR_Temps.m MATLAB file (See Appendix 1). Each set of data was aligned with the relevant time steps for matching with the colour image data. The images in Figure 7.4 below show a visual example of the raw IR data with the temperature range set at 70-180°C, where the cheese melts and fuses over time and bright spots indicate higher temperatures where browning occurs.

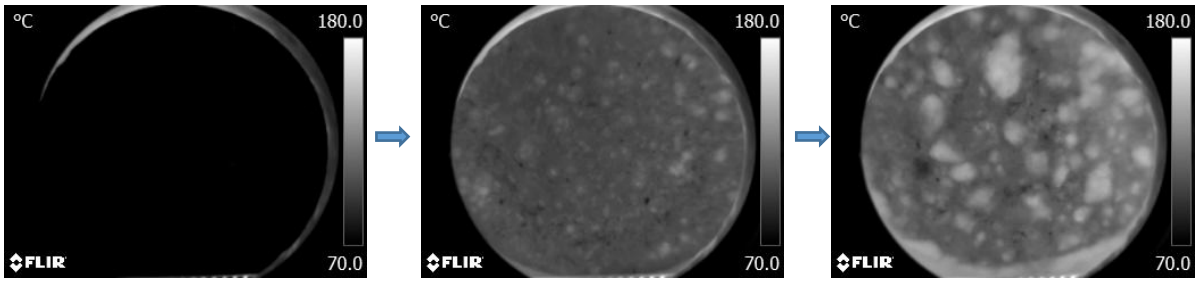

0min 12min 28min

Figure 7.4 – Example of raw IR images from cheese baking trial, oven temperature 168°C

7.2.2 Colour Data

Colour data was captured by the webcam using fixed camera properties and recorded as an .avi video file. Images were extracted from video files using the MATLAB script Split_vid.m (see Appendix 1), which allowed for still frames to be recorded based on a given time step basis. Figure 7.5 below shows the extracted images that align with the same times step as for the IR images from 7.4. Note that the hot spots from the IR images correspond with the brown areas from the colour image at 28 minutes.

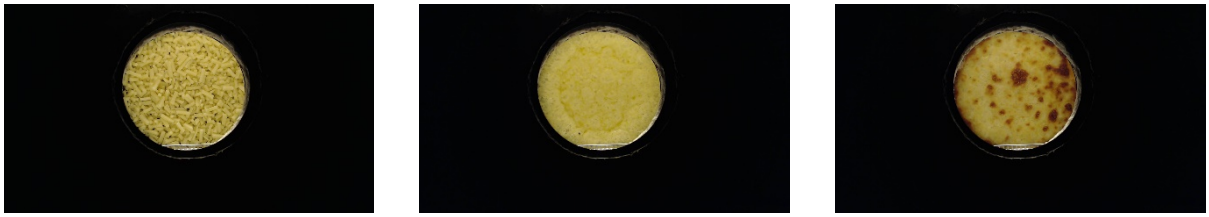

0min 12min 28min

Figure 7.5 – Example of raw colour images from cheese baking trial, oven temperature 168°C

The experimental setup from Chapter 6 only allowed the end point of each trial to be recorded for assessment, utilising standardised lightbox conditions. The idea behind this experiment was to explore cheese heating and browning dynamically in real time. As the lighting conditions were the same throughout each experimental run, and reproducible based on the experimental setup, results were comparable both within each trial and between trials. For this reason, colour correction was not required to analyse the dynamics of change during cheese baking.

Once the images were extracted, the process from Section 3.5 was followed to align the images with the temperature data, using images of the same calibration plate. Spatial matching of the temperature and colour data was carried out using image registration to transform and match the data. For further analysis the colour images were converted to the CIE L* a* b* colour scale. Figure 7.6 shows the transformed images from Figure 7.5 to match the IR image space, where a portion of the image is cropped based on the matching visible surface area. The process of transforming the original colour images reduces the amount of useful data available due to the size of the hole in the oven and how close it is possible to match the optics of the IR and colour cameras.

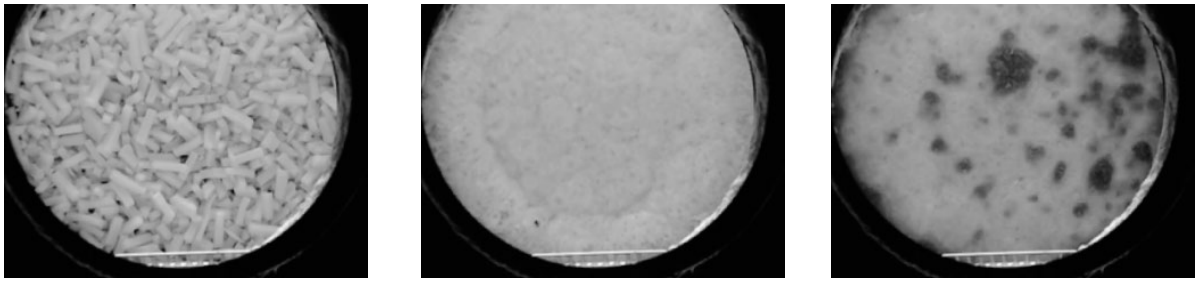

Figure 7.6 – Example of transformed colour images to match IR image space from cheese baking trial, oven temperature 168°C

7.2.3 Defining Region of Interest

Within both the IR and colour images the top surface of the oven and heating element shield are visible. The portion of the images outside of the cheese surface needed to be removed in order to carry out further analysis. To isolate the cheese surface and remove the unwanted area, the data was cropped to a region of interest. The region of interest was defined by cropping the cheese surface to a circle, maximising the useful information in a simple manner. This was achieved in MATLAB by defining the centre point of a circle and the radius which maximised the cheese surface data, while removing the unwanted data. A mask was created using the centre point and radius to isolate and modify the unwanted information. The unwanted data was converted to NaN so that did not affect the calculations for analysis.

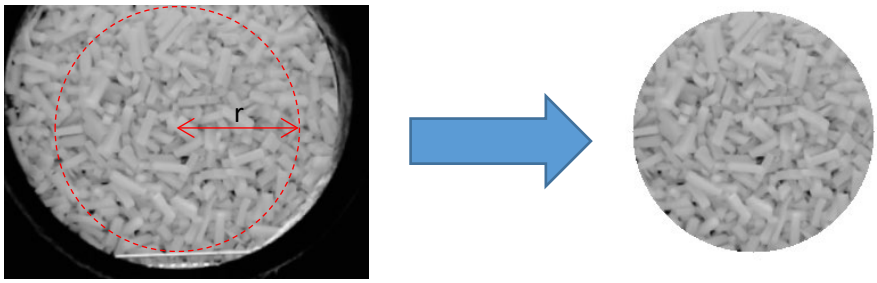

Figure 7.7 – Example illustrating the data cropping process

This process was applied to each data set for the IR and colour images. Figures 7.8 and 7.9 show example images for an oven temperature of 168°C. Observation of the 28min images indicate good alignment between the IR and colour data where the surface pattern appears to match.

0min 12min 28min

Figure 7.8 – Example of images cropped to ROI, oven temperature 168°C

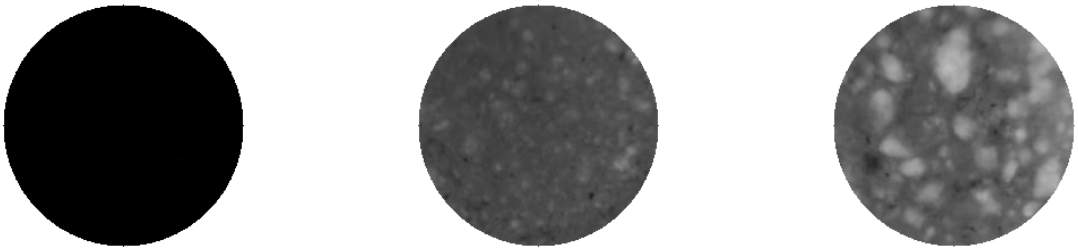

0min 12min 28min

Figure 7. 9 – Example of IR images cropped to ROI, oven temperature 168°C. IR grayscale 70-180°C

7.3 Initial Results

The raw data conversion process resulted in data sets including oven temperature, surface temperature, mass loss and colour. To perform an initial analysis of the data the average results for each parameter and data set were calculated and plotted. Note that data collection commenced from 1 minute for the temperature and colour data due to the data recording process. Mass loss data was collected for the entire duration a tray was placed in the oven as the recording process could be commenced prior to starting each experiment.

7.3.1 Surface Temperature

Figure 7.10 illustrates the average surface temperature for each data set. As expected, higher oven temperatures resulted in an earlier increase in surface temperature and higher overall surface temperatures. Differences in heating rates between trials at different oven temperatures can be observed based on visible increase in gradient between 0 and 15 minutes at higher setpoints. The temperature increases rapidly and then slows between 10 and 15 minutes baking time, depending on the oven temperature, as the average surface temperature increases beyond 100°C. The inflection point occurs earlier at higher temperatures, likely to be caused by the surface drying as heat is lost in evaporating water from the cheese.

A conceptual model of cheese baking was proposed in Chapter 6, breaking the process down into discrete phases, from the initial melting and fusing of cheese shreds, to steam formation and bubbling,

and through to drying, blistering and browning. This proposed model can be used to help describe and understand the observations based on the experimental data and can be illustrated by shading the phases with different colours, as shown in Figure 7.11. This shading was applied to Figure 7.10 to help visualise the phases of cheese baking relative to surface temperature. Note that these areas are estimates based on the surface temperature increasing from ambient up to 100°C and beyond as the surface dries out.

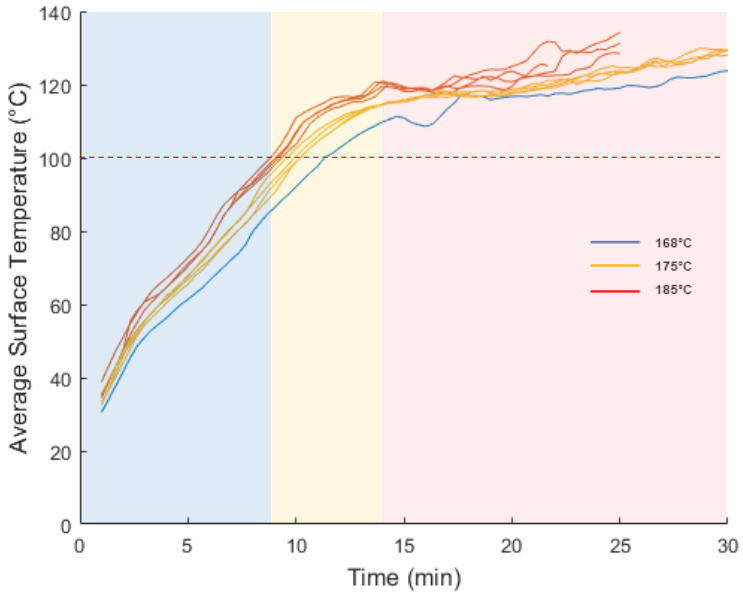

Figure 7.10 – Average experimental surface temperatures at different oven temperatures, based on defined ROI

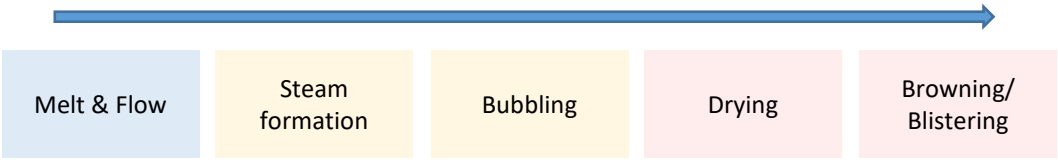

Figure 7.11 – Proposed process flow of cheese baking with colours attributed to baking phases

The data indicates repeatable results for replicate trials where the average temperatures are similar. However, for an oven temperature of 185°C there was some variation visible after 20 minutes. 185°C was the maximum oven temperature achieved with the experimental setup and the temperature was not as well controlled as for lower setpoints. These results are supported by the actual oven temperature data as illustrated in Figure 7.12. The actual oven temperature was consistent and stable for a setpoint of 175°C, and fluctuated by approximately ±8°C for a setpoint temperature of 185°C. This fluctuation is likely due to a combination of the modifications made to the oven and the temperature control mechanism.

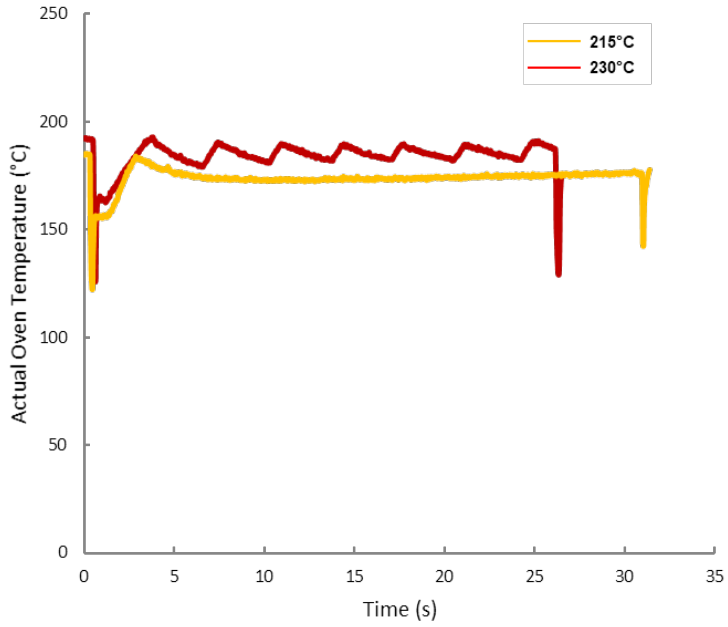

Figure 7.12 – Comparison of actual oven temperature relative to oven setpoint temperature of 215°C and 230°C

Note that Figure 7.10 is only for surface temperature and does not represent the bulk temperature of the cheese. At lower temperature the bulk temperature is likely to be similar to surface temperature, however as baking continues the surface temperature would have increased beyond the bulk temperature. It is also worth noting that these experiments were carried out with only a cheese layer, and the addition of a pizza base and sauce would also affect the bulk moisture and surface characteristics.

7.3.2 Colour

As for the surface temperature data, the average L* for each trial was calculated and plotted. The overall trends observed from Figure 7.13 were similar for each experiment, where the average L* initially increased to a point before steadily decreasing. This indicates that the colour initially became brighter, before the onset of browning and darkening of the surface. There are two possible reasons for this observation, the initial experimental conditions, and light scattering.

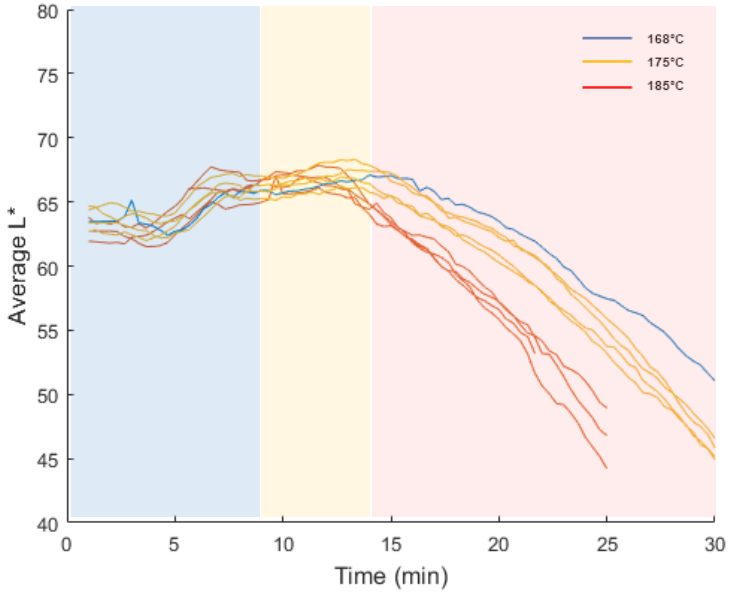

Figure 7.13 – Average experimental L* values at different oven temperatures, based on defined ROI

The initial colour data appears lower due to the appearance of cheese shreds in the oven tray. Figure 7.14x illustrates this where initially there is variation in surface colour due to the individual shreds and tray surface visible through the shreds. Colour increase can also be attributed to increased scattering of light during the melting phase at temperatures below 100°C (Dave, *et al.*,2001 and Pastorino, *et al.*, 2002). The cause of this observation may also affect surface temperatures based on differences in emissivity of substances such as the oven tray and free oil. The initial rapid increase between 0-5 minutes in L* is likely due the oven tray, and the further gradual increase between 5-14 minutes attributable to light scattering.

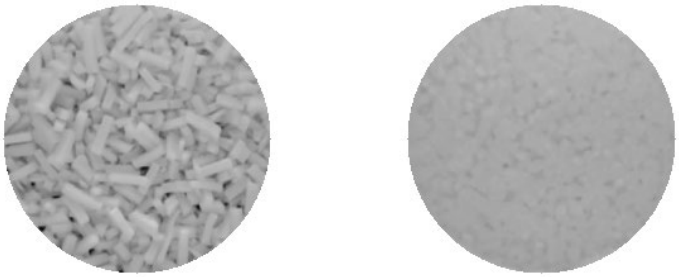

Figure 7.14 – Visual example of the comparison of cheese at 0 minutes and 10 minutes bake time

As with surface temperature, there is an observable difference in the rate of colour change at higher oven temperatures. There is a similar trend in inflection points that correspond between the two parameters. For example, at an oven temperature of 175°C the rate of temperature increase slows at approximately 14 minutes, which agrees with the same time that L* begins to decrease. Further analysis to explore and compare the surface variation may give an insight into the drivers behind these trends. As discussed in Chapter 6, there is a link between moisture content and browning. The addition of surface temperature data helps to further explore this link and understand the underlying dynamics.

For further analysis of the data the starting point was taken from the highest region of average L* for each data set. At a time of 10 minutes cheese was melted and fused for each experimental data set resulting in a realistic starting point for colour analysis. The average L* for each trial at 10 minutes ranged between 65.4 and 67.3 (Avg 66.3, SD 0.7, SE, 0.2). This time coincides with the steam formation and bubbling stages prior to the onset of surface drying and browning.

7.3.3 Mass Loss

The results for mass loss are shown in Figures 7.15 & 7.16, where 7.15 illustrates the absolute mass loss, and 7.16 shows the percentage mass loss. As with surface temperature and colour these results demonstrate the repeatability of the experiment where the rate of mass loss was similar between replicates. The rate of loss increased to a constant rate with a linear relationship relative to oven temperature.

This observation can be related to the to the initial stages if the conceptual model of blister formation introduced in Chapter 6. The cheese first melts and flows during initial temperature increase, and while the temperature remains below 100°C evaporation of water is slow and therefore mass loss is slow. As temperature increases to 100°C the rate of mass loss accelerated to a constant linear rate even at the end of baking showing moisture loss is always heat transfer and not mass transfer limited. As the bulk temperature of the cheese was not directly measured it can be estimated based on the evaporation rate, a similar approach to that discussed in Chapter 6.

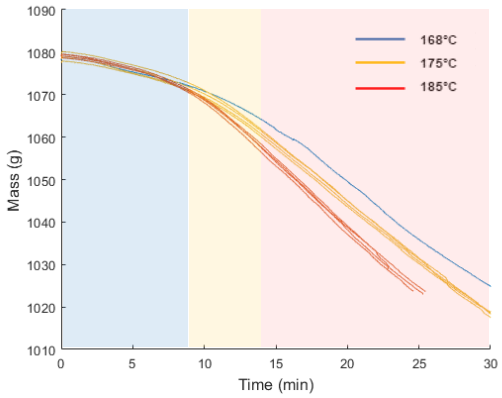

Figure 7.15 – Absolute mass loss at different oven temperatures

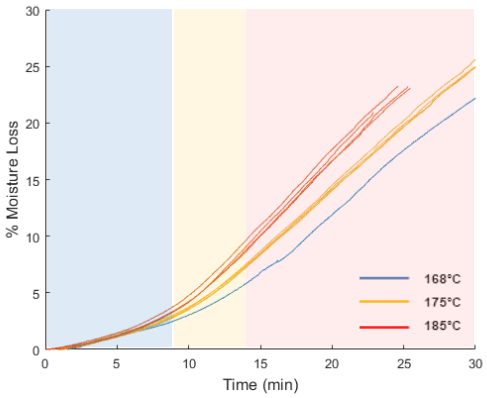

7.16 – Percentage mass loss at different oven temperatures

Mass loss during cheese baking is generally attributed to moisture loss through evaporation. The constant rate period can be used to estimate heat flux based on the latent heat of evaporation, similar to the heat transfer calculations carried out in Chapter 4. This is discussed later in the chapter.

7.3.4 Percentiles and Range

Average surface temperature and colour gave comparable results, however they do not consider the variation across the cheese surface during baking. To explore the variation in temperature and colour across the surface, the 10th percentile, 90th percentile, minimum and maximum values were determined. The resulting information is illustrated in Figures 7.17 to 7.24.

For surface temperature, illustrated in figures 7.17 to 7.20, a pattern emerged based on the spread of temperatures across the surface, particularly in relation to the 10th and 90th percentile data. Initially the overall range is wide but reduces as the average temperature approaches 100°C, and then increases beyond 110°C. This pattern was observed in all trials. These observations are explained by the initial heating up of the cheese to boiling point of water. Then a narrow band occurred as the bulk of the surface can't heat up further until free surface moisture is lost, as all the heat is lost as latent heat of evaporation. Further temperature increases indicate localised surface drying, where the difference between dry areas and cooler evaporating areas results in the range increasing. The initial heating is not uniform due to the cheese shreds and shred pattern in the tray, resulting in non-uniform temperature increase. As the shreds melt and fuse to become uniform the temperature range narrows and further heating leads to steam formation and surface drying. Surface variation increases as baking continues due to localised drying allowing for higher surface temperatures. For each trial the extremes of surface temperature approach to within ~10°C of the maximum air temperature in the oven. The thermocouple used to measure the internal oven temperature was taped to the side wall of the oven so as to not interfere with the images being taken. As a result, the actual air temperature above the surface of the tray would likely have been a few degrees cooler than at the walls of the oven.

In contrast, areas of lower surface temperatures as baking continues are relatively stable as indicated by the 10th percentile and minimum surface temperatures at all oven temperatures. These points are likely lower and in closer contact with the bulk of the cheese. Lower valleys in the cheese surface could also result in pooled oil which would prevent these areas from drying out and increasing further in temperature. Regarding overall comparison in trends between oven temperatures (Figure 7.20) the 10th percentile and minimum surface temperatures are similar throughout the duration of baking. In contrast, 90th percentile and maximum surface temperatures are higher at higher oven

temperatures. This indicates that when the surface dries out temperature increase is based on the relative heat flux, which would be higher as oven temperature increases. Whereas at the lower end, surface temperature is limited due to moisture evaporation, heat transfer to the bulk of the cheese, and the presence of oil.

The 10th percentile values are very similar between replicate trials at oven temperatures of 175°C and 185°C, whereas there was a noticeable increase and variation in the 90th percentile values during the course of baking.

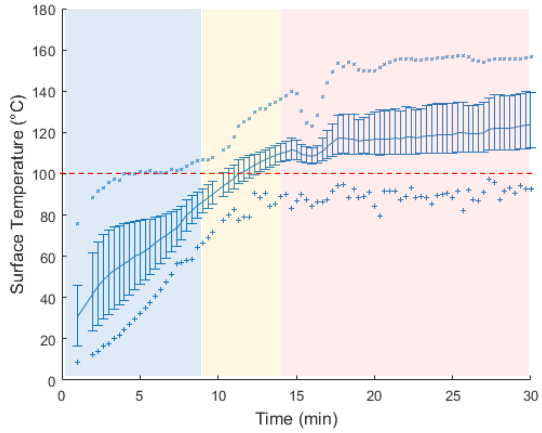

Figure 7.17 – Surface temperature distribution at 168°C as a function of time. Plotted as means with +/- 10th and 90th percentiles. +'s are minimums, and x's are maximums.

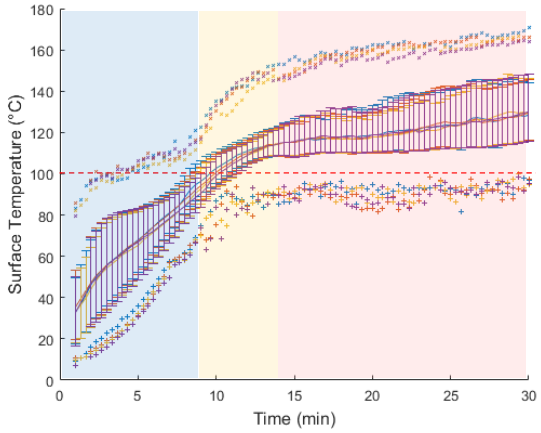

Figure 7.18 – Surface temperature distribution at 175°C as a function of time. Plotted as means with +/- 10th and 90th percentiles. +'s are minimums, and x's are maximums. Different colours represent replicate trials.

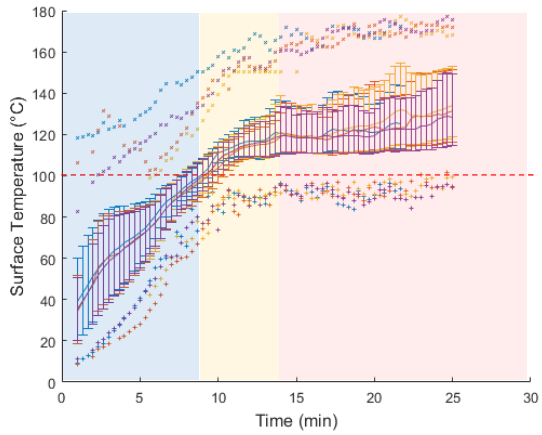

Figure 7.19 – Surface temperature distribution at 185°C as a function of time. Plotted as means with +/- 10th and 90th percentiles. +'s are minimums, and x's are maximums. Different colours represent replicate trials.

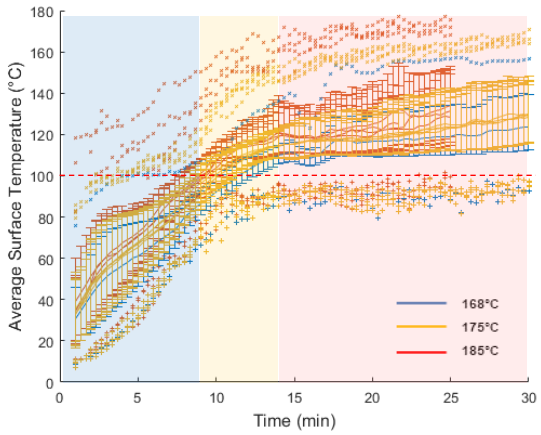

Figure 7.20 – Surface temperature distribution at all oven temperatures as a function of time. Plotted as means with +/- 10th and 90th percentiles. +'s are minimums, and x's are maximums.

For colour data, the range of values are illustrated in Figures 7.21 to7.24. When interpreting these figures it should be noted that the minimums and 10th percentile L* values (i.e. darker areas) correspond to locations where the surface temperatures are at the maximum and 90th percentile levels (i.e. hotter areas) and vice versa. The minimum L* values within the first 5 minutes indicate that the tray surface was visible at this time, as discussed previously.

There was a similar observation as for surface temperature where the range was initially wide, due to cheese shred pattern, and then narrowed as the cheese melts and fuses into a uniform layer. Some

of the variation prior to browning may be attributed to the lighting conditions within the oven and physical surface deformation causing light scattering. As baking continues, the range of L* distribution increases. This increase in spread is due to the onset of browning and blister formation and appears to coincide with the surface temperature increase beyond 105°C, where significant non-enzymatic browning occurs (Shibukawa et al., 1989; Broyart *et al.*, 1998; Purlis & Salvadori, 2009 and Purlis, 2010). In general, the results illustrate that L* decreases over time indicating that the overall surface continues to darken as baking continues. This occurs across range of L* values indicating that both browned and non-browned areas darken, however the browned areas to a greater extent.

Figure 7.24 illustrates that the decrease in L* initiates in less time and more rapidly as oven temperature increases. This indicates that the rate of surface drying increases, resulting in increased surface temperatures, as oven temperature rises. i.e. the faster the surface dries to a point where significant non-enzymatic browning occurs, the earlier the L* values begin to decrease. Across all oven temperatures the 90th percentile and maximum L* values are similar, which agrees with the observations of lower surface temperatures in the 10th percentile and minimums across all oven temperatures. This agrees as the occurrence and rate of browning would be lower at lower oven temperatures. In contrast, there is a significant decrease in 10th percentile and minimum L* values as oven temperature increases, which aligns with the observation of increased surface temperatures relative to oven temperature.

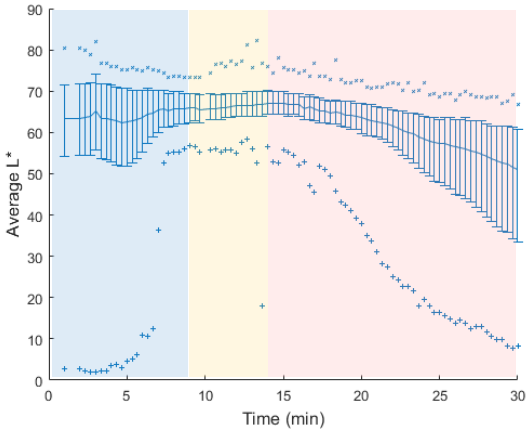

Figure 7.21 –L* distribution at 168°C as a function of time. Plotted as means with +/- 10th and 90th percentiles. +'s are minimums, and x's are maximums. Different colours represent replicate trials.

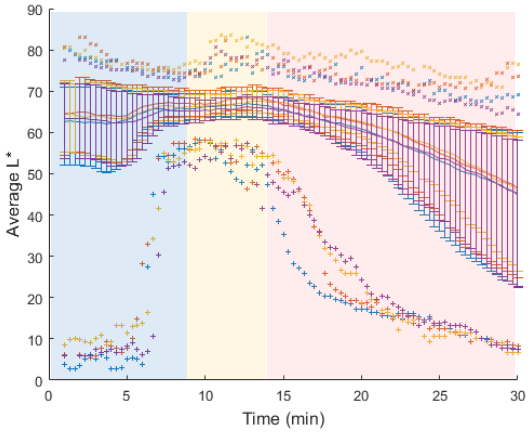

Figure 7.22 – L* distribution at 175°C as a function of time. Plotted as means with +/- 10th and 90th percentiles. +'s are minimums, and x's are maximums. Different colours represent replicate trials.

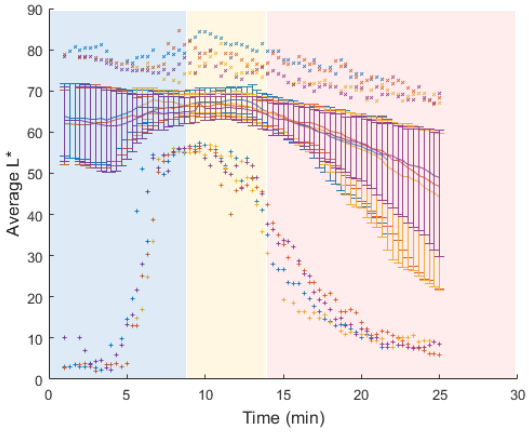

Figure 7.23 – L* distribution at 185°C as a function of time. Plotted as means with +/- 10th and 90th percentiles. +'s are minimums, and x's are maximums. Different colours represent replicate trials.

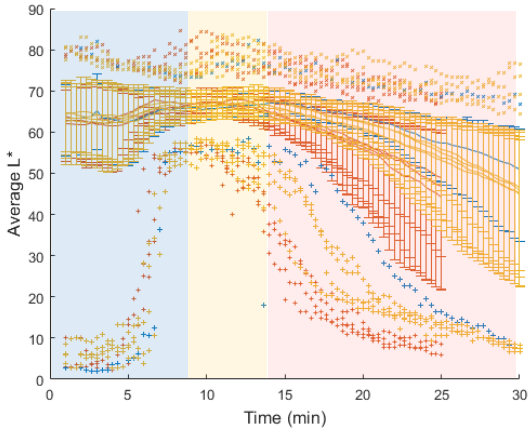

Figure 7.24 – L* distribution at all oven temperatures as a function of time. Plotted as means with +/- 10th and 90th percentiles. +'s are minimums, and x's are maximums.

As discussed previously, analysing L* value alone gives an indication of surface variation but does not give an insight into the impact on blister growth and size. Using the L* data to determine the onset on blister formation and size leads to a better interpretation of browning and blistering dynamics, relative to bake time, oven temperature, and moisture content.

7.4 Browning and Blistering Investigation

To investigate the browning and blistering dynamics for these experimental observations the results were analysed following the principles outlined in Chapter 5. The approach used a dynamic threshold based on sensory analysis which gave a consistent platform to perform quantitative analysis of baked pizzas. This method was applied to the data from the benchtop oven experiments and results assessed to allow for further analysis.

7.4.1 Initial Analysis

Initially the dynamic threshold model from section 5.4 was applied to evaluate the approach. The linear equation was applied to each image from sample data set. Previously there had been only one image per experiment to analyse representing the end point of the particular baking conditions. For the benchtop experiment there was a series of images throughout the process which the dynamic threshold was applied to individually accommodate for the variable nature of the process and that a single threshold would not be suitable across the entire time series.

Figure 7.25 illustrates the results for a sample data set and indicates that the original dynamic equation is not suitable for this experimental setup. The resulting binary images from the blister assessment process do not represent the blister formation and growth observed in the L* images. This makes sense when comparing the average L* to the L* threshold determined by the dynamic equation. For each time step the L* threshold was higher the than average L*, resulting in a large part of the surface to be identified as 'blistered'.

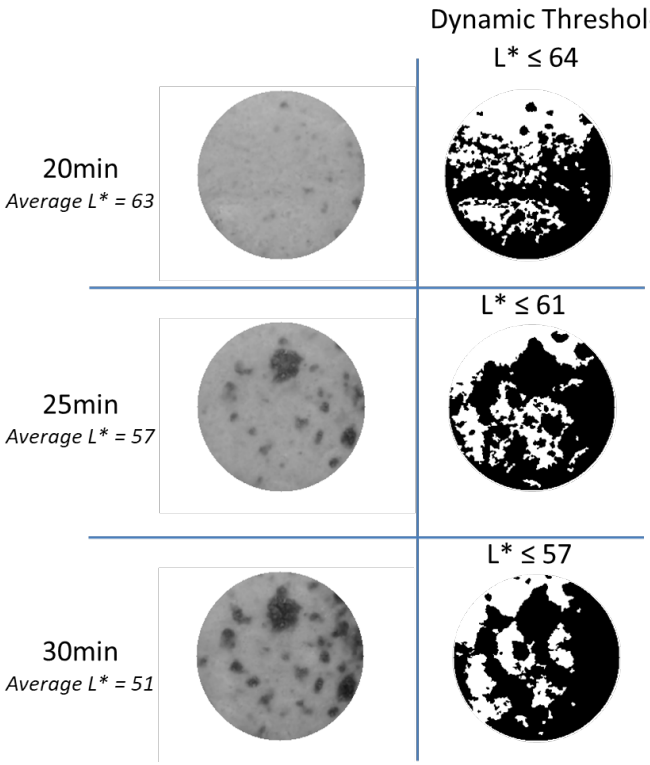

Figure 7.25 – Application of original dynamic threshold to experimental data at an oven temperature of 168°C

The reason that the original dynamic equation was not suitable is based on lighting conditions, which were different between the commercial oven and benchtop experiments. A lightbox was used to capture images for the commercial oven experiments, which allowed for optimal lighting conditions to capture surface characteristics. The conditions for the benchtop oven experiments were limited due to restrictions in the ability to light the material through the front panel of the oven and it was not possible to simulate the lightbox conditions. This resulted in an overall darker and different lighting conditions to those that were used in the development of the original dynamic model.

The principle of the dynamic threshold process remains valid for analysis of this data. Lighting for the benchtop experiment was controlled and consistent between trials allowing for comparative analysis between trials, but the results may not be directly comparable to previous experiments. However, the findings from the data may comparable based on analysis of the change in characteristics between trial setup conditions. Overall, the concept still held that a dynamic threshold gives a consistent platform to analyse data, but a modified model was required to account for the different lighting conditions.

The original dynamic correlation was based on sensory analysis where observers evaluated a range of baked pizza samples, resulting in a relationship between average L* and L* threshold. A similar approach was applied to develop a modified dynamic model for this set of experiments where a sample data set was evaluated by a selection of consumers. A series of original colour images, L* images, and the resulting binary images based on a range of L* thresholds were given to each consumer. These images ranged from 16 to 30 min, in two-minute intervals, and L* threshold from 46 to 60, in two step intervals. For each image the observers were asked to choose which binary image

gave the best representation of blistering relative to the colour images. Table 7.1 illustrates a sample of the images that were evaluated.

Table 7.1 – Sample of images with different L* threshold applied for data collected at an oven temperature of 168°C

Bake Time (min)	Original Images	L* Images	L* Threshold Lt = 48	Lt = 52	Lt = 56	Lt = 60
16						
20		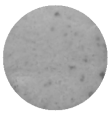				
24		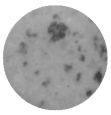				
28		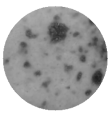				

The information from the consumer evaluation was collated and the resulting correlation between average L* and perceived L* threshold is illustrated in Figure 7.26. A similar trend to the original dynamic threshold from Figure 5.13 was evident where the lower the average L*, the lower the perceived L* threshold.

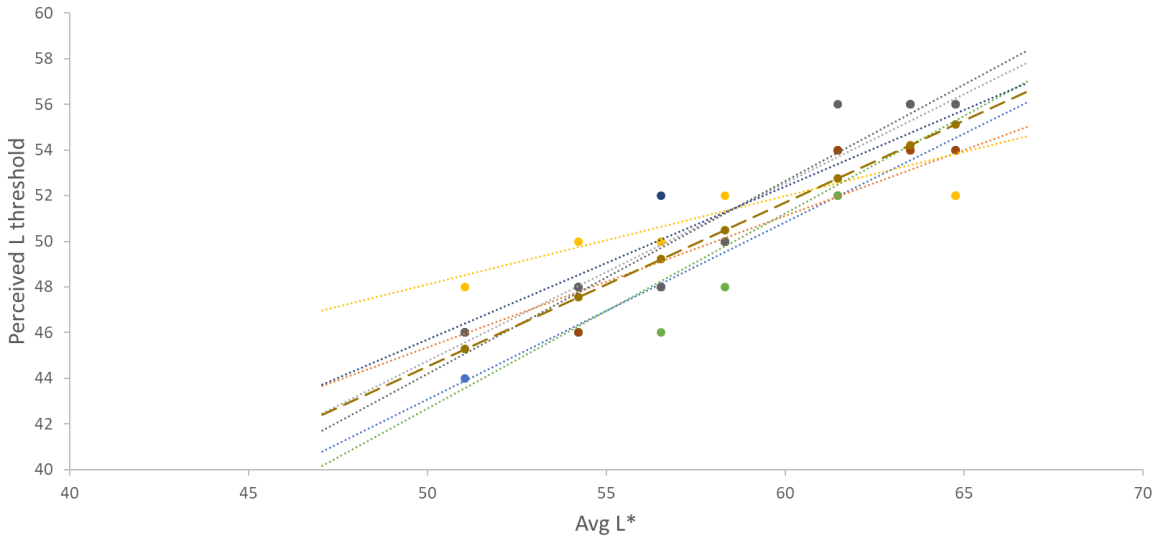

Figure 7.26 – Perceived L* Threshold compared to average based on consumer evaluation (n=6) of experimental data at an oven temperature of 168°C

evaluation does not help explain any lack of fit. The R^2 for this analysis was 0.83, indicating a reasonable fit.

Table 7.2 – Results of two-way ANOVA including average L* and the observers as factors

	Estimate	SE	tStat	pValue
Intercept	8.214	2.465	3.332	0.00148
Observer	0.0904	0.0745	1.214	0.229
Average L*	0.717	0.0414	17.29	5.58E-25

This resulted in a new dynamic threshold equation that could be applied to the data to analyse blister growth and characteristics. It is worth noting that the derived equation is only relevant for these particular trials, as future trials would have different lighting conditions. However, the outcomes from further analysis are relevant for comparison and discussion relative to previous findings as it is the changes with time and temperature that are important.

Table 7.3 – Application of the dynamic threshold for data at an oven temperature of 168°C

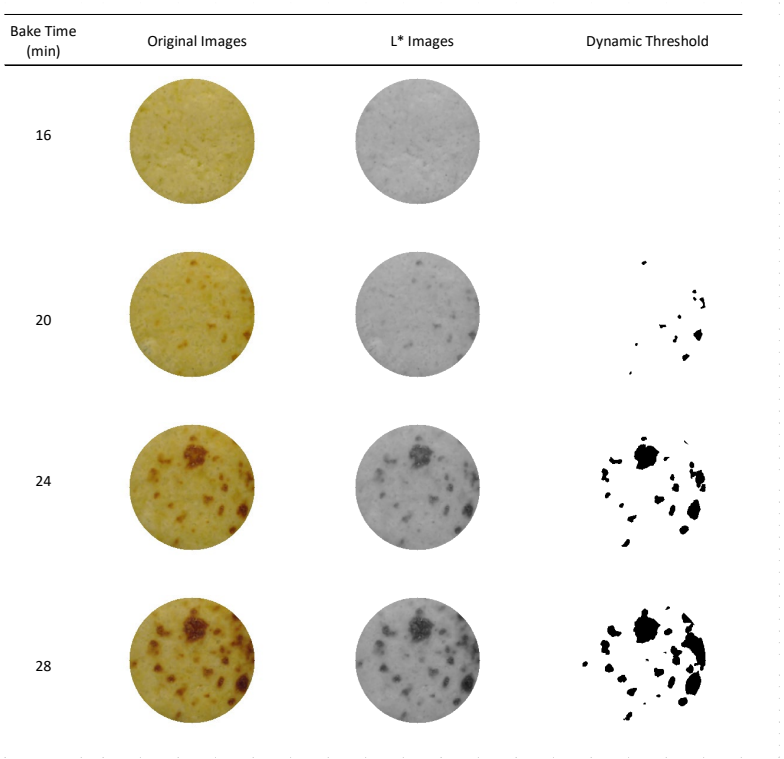

7.4.2 Results from Dynamic Threshold Analysis

Applying the dynamic threshold to the L* value data resulted in a distribution of apparent blister size, which was used to calculate a range of characteristics to be analysed in conjunction with the moisture and temperature data. The advantage of the results from this experiment is that the data was collected in real time and can be used to gain further insight into direct blister development and

growth, as opposed to the results from Chapter 6 which represented snapshots in time near the end of baking.

As in Chapter 6, the dependant variables relative to browning for analysis were blister coverage, number of blisters, and average blister size. Figure 7.27 illustrates the increase blister coverage relative to bake time and oven temperature. There is some variation between replicate trials, however the initiation of browning appears to occur at a similar time at each oven temperature. The onset of blistering at each oven temperature based on the initial increase in blister coverage shows that blisters form in less time at higher temperatures. As browning continues the increase in blister coverage appears to follow a generally linear trend relative to bake time.

This agrees with the results from Figure 6.10 in Chapter 6. In comparing the results from the two experiments it can be seen that the onset of browning starts later in the baking process for the benchtop setup. For example, to achieve 10% blister coverage in the benchtop experiments took approximately 17 to 18 minutes at 195°C, whereas it took approximately 11 minutes at 220°C in the commercial pizza oven. These results indicate that the heat flux was significantly lower in the benchtop oven.

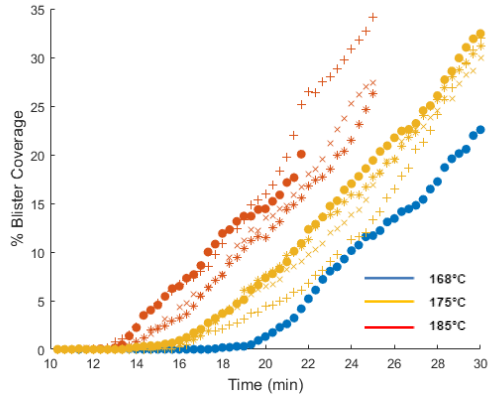

Figure 7.27 – % Blister coverage based on bake time and oven temperature

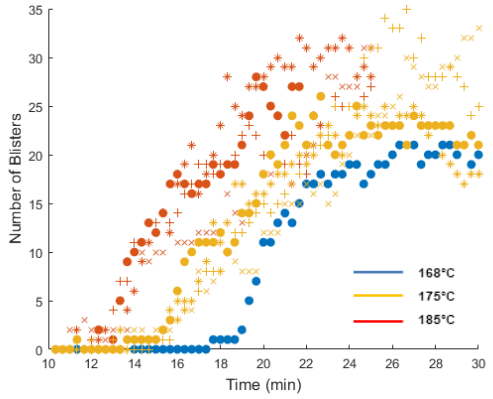

Figure 7.28 – Number of blisters based on bake time and oven temperature

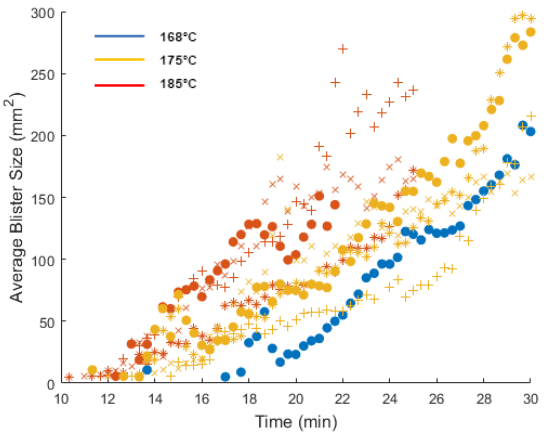

Figure 7.29 – Average blister size based on bake time and oven temperature

In terms of the number of blisters there does not appear to be considerable differences relative to time once they begin to form, as illustrated in Figure 7.28. Compared to the commercial oven results (and partially due to the differences in sample dimensions), blister numbers were relatively low and only near the end of the trials were the commercial oven trends seen, where blister numbers reduced over time. This is likely due to the lower heat flux conditions and the extent of baking within the experimental time frame. If bake time continued the number of blisters would eventually reduce as adjacent blisters join to form fewer but larger blisters. In the context of cheese baking applications, the extended time required for this would be outside of reasonable processing conditions.

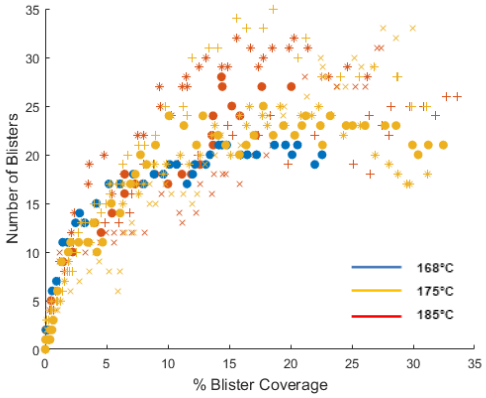

Figure 7.30 – Number of Blisters vs % Blister coverage. Colours represent oven temperature and symbols represent replicates

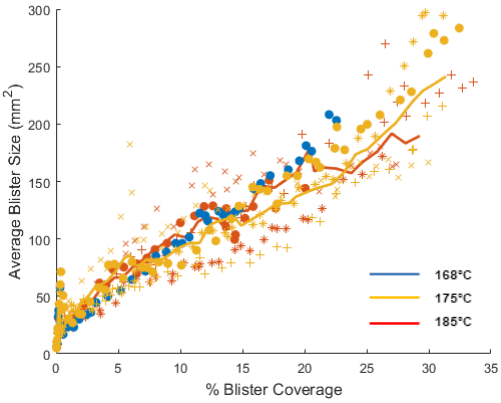

Figure 7.31 – Average Blister Size vs % Blister coverage. Colours represent oven temperature, symbols represent replicates, and lines represent averages relative to oven temperature

The interaction between characteristics helps further understand the dynamics and drivers of the observable outcomes during baking. Figure 7.30 and 7.31 illustrate the interactions between the size and number of blisters, and blister coverage, and indicate that there is only a minor difference based on oven temperature for these interactions. Analysis from the commercial pizza oven experimental data in Chapter 6 showed that heat flux impacted both the size and number of blisters relative to blister coverage, where a higher heat flux results in a greater number of smaller blisters for a given % blister coverage. The temperature range capable for the benchtop oven was much lower than the commercial oven, 168-185°C compared to 220-288°C, therefore working in a different range to previous data analysis and consequently the results are not directly comparable. In addition, the surface area analysed and resolution of images was significantly less for the benchtop experiments compared to the commercial oven. For the commercial oven the surface area was 0.286m^2 with a resolution of 0.18mm^2/pixel, compared 0.180m^2 at 0.51mm^2/pixel for the benchtop oven. This equates to ~60% more area analysed for the commercial oven experiments (see Figure 7.32). These factors contribute to the inability to directly compare these results to those from Chapter 6. To understand the scale of these differences relative to heat transfer, the heat flux and heat transfer coefficients (HTC) were calculated for the benchtop oven data.

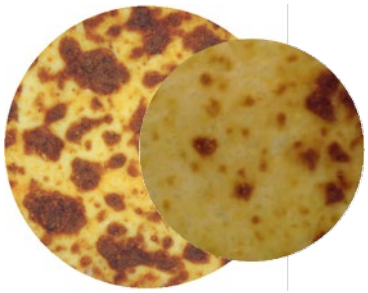

Figure 7.32 – Relative area assessed for commercial oven experiments (left image) compared to benchtop oven experiments (right image)

7.4.3 Effect of Heat Flux

In Chapter 4 the rate of heat transfer was calculated using the rate of mass loss of water through evaporation. The method from Section 4.4.2.1 was applied to the benchtop experimental data where the heat flux could be estimated from the constant rate period of moisture loss. The constant rate of mass loss is illustrated in Figure 7.15 between approximately 15 to 25 minutes bake time. A latent heat of 2256 $kJ.kg^{-1}$ was used for the calculations, assuming an evaporation temperature of 100°C. The surface area used was based on the top and bottom surface of the cheese, equal to $0.09m^2$. Over the temperature range from 168°C to 185°C the rate of mass loss ranged from 3.6×10^{-5} to 5.4×10^{-5} $kg.s^{-1}$, an order of magnitude less than that from the Commercial oven measurements. The results for heat transfer for the commercial oven were based on water evaporation alone and moisture evaporation from within the mozzarella for the benchtop oven. Although not directly equivalent, the results are comparable. In addition, it should be noted that the moisture loss data from pizza's in Chapter 6 is not comparable as in those experiments moisture was lost from a full pizza with base, sauce and cheese, and cheese alone for the Benchtop setup.

The resulting heat flux calculations relative to oven temperature are illustrated in Figure 7.33. Heat flux was significantly lower for the Benchtop setup, which can be expected as the oven temperature and air velocities were much lower. Air flow and heat distribution are much greater in the commercial impinger oven, which is reflected in the heat transfer coefficient (HTC) of 43-46 $W.m^{-2}.K^{-1}$ compared to 13-16 $W.m^{-2}.K^{-1}$ for the benchtop oven. These values agree with data from literature for for domestic low convection ovens and commercial impingement ovens. For home electric ovens HTC range from 14-17 $W.m^{-2}.K^{-1}$ for temperatures of 150-200°C, compared to 44 $W.m^{-2}.K^{-1}$ for commercial impingent ovens (Altomare, 1994).

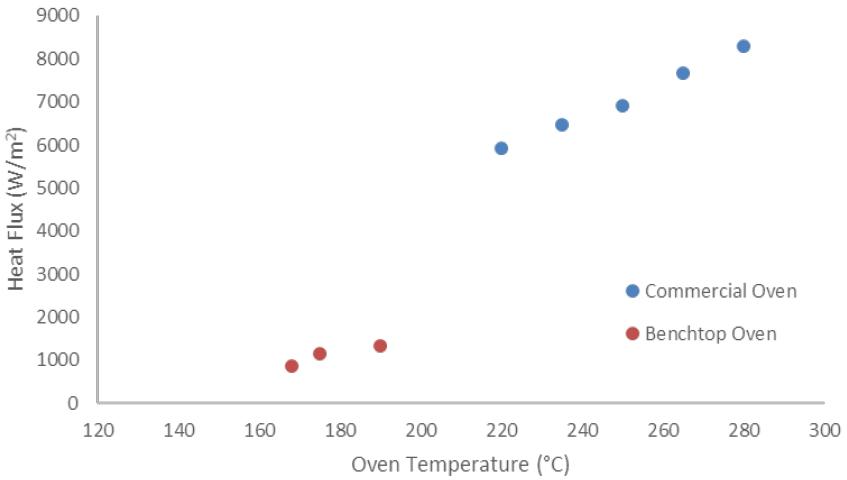

Figure 7.33 –Heat Flux vs Oven Temperature for the Commercial Oven and Benchtop Oven

The results from Chapter 6 illustrated that heat flux has a significant impact on the size and number of blisters. To further explore the relationship between heat flux and blister size a plot was produced based on the average blister size for a specific level of blister coverage. Figure 7.34 illustrates average blister size versus heat flux at a blister coverage of 30% for data from both the benchtop and commercial oven experiments. These observations confirm the correlation between heat flux and blister size where, as heat flux increases, average blister size reduces for the same level of blister coverage. Inherently, this means that the number of blisters will be greater for a higher heat flux.

There is a difference in this correlation between the benchtop oven data and the commercial oven data. This could be attributed to the difference in experimental setup but could also be attributed to the relative heat flux to the cheese layer. For the commercial oven experiments whole pizzas where baked, including base, sauce and cheese. Therefore, the heat flux to the cheese layer would be less than the overall heat flux as the heat from below must first flow through the base and sauce layers.

To compare the commercial oven data directly with the benchtop oven data, the effect on heat transfer to the cheese layer due to the pizza base and sauce need to be accounted for. In Chapter 4 the HTC of the commercial oven was calculated using two different methods, one of which utilised an insulator to simulate a pizza tray and base. The average HTC for the iButton method with an insulator was 30 $W.m^{-2}\ K^{-1}$ and 45 $W.m^{-2}K^{-1}$ for the water evaporation method. As the iButton method had an insulator below, the calculated heat transfer was relative to the top surface, whereas for the water evaporation method the heat transfer was from above and below. The heat transfer to the cheese layer from below the sauce layer would be at a maximum of 100°C, and would not be significant relative to the heat transfer at the top surface of the cheese. As such, the HTC from the iButton method gives the best estimate of the HTC to the cheese layer. This was applied to the temperature range for the commercial oven, assuming an average surface temperature of 100°C, resulting in adjusted values estimating the heat flux to the cheese layer.

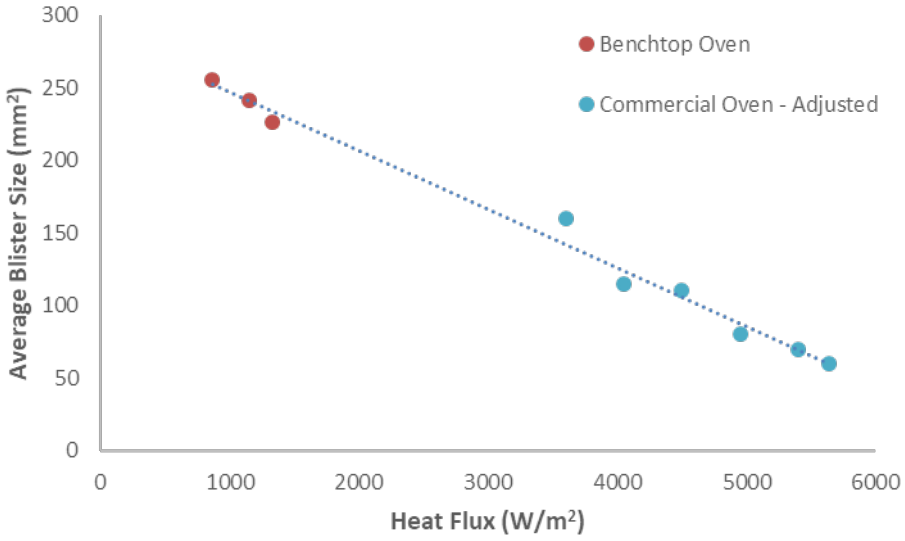

Figure 7.34 – Average blister size at 30% blister coverage compared to oven heat flux

The adjusted heat flux data for the commercial oven data are shown in Figure 7.34, illustrating the relative heat flux to the cheese layer for both experiments. The combined data indicates that there is a linear correlation between average blister size and heat flux, which could be used to predict average blister size. This finding suggests that the correlation may hold true irrespective of the differences in experimental setup and operating conditions.

To confirm this finding additional experimentation would be required to gather data over a wider range of heat flux conditions. However, the likely applications for these findings are in the 4000 $W.m^{-2}$ and greater range as the lowest oven temperature used in the commercial oven was likely to be already outside of the range for useful applications of mozzarella.

7.4.4 Blister Initiation

Chapter 6 introduced the idea that oven temperature and heat flux influence the interaction between the initiation of moisture loss and blister initiation, where the delay between moisture loss and blister initiation reduces as oven temperature increases. This relationship was analysed for the benchtop oven data as shown in Figure 7.35. A level of 0.5% moisture loss and 1% blister coverage was used to determine the data points for this plot. Non-zero levels were required as there had to be a measurable change in these parameters to indicate a significant change outside of measurement noise. The resulting relationship is similar to that identified from Figure 6.16 (Section 6.6.2) where as the temperature increases, the delay between the onset of moisture loss and browning reduces, from 17 minutes down to 11 minutes across the temperature range studied. The change in time for the initiation of moisture loss was very small at less than 30 seconds compared to the change in time for blister initiation at 6 minutes. This builds on the conclusions from Section 6.6.2 where heat flux has a greater effect on blister initiation and growth than overall moisture loss.

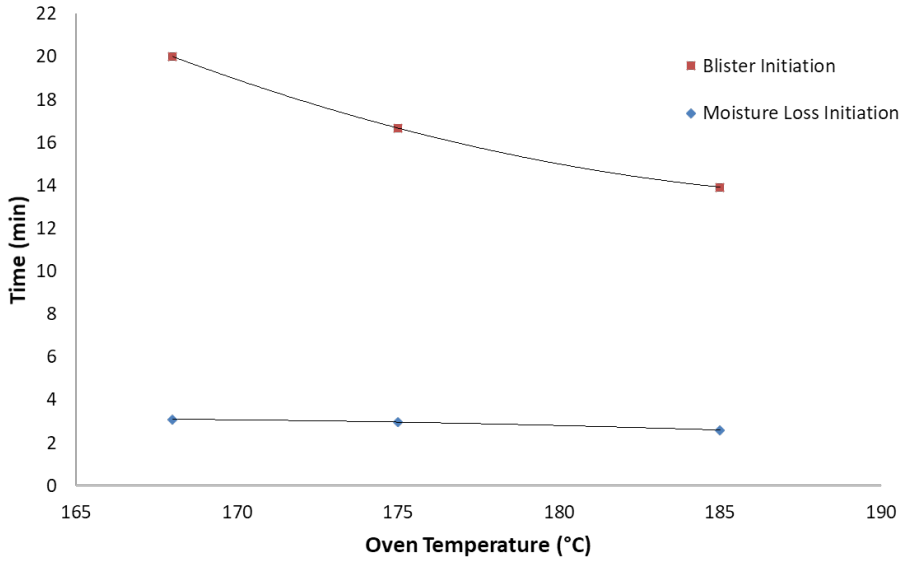

Figure 7.35 – Estimated average times for moisture loss and blister initiation at different oven temperatures

The results from Figure 6.16 are not directly comparable with Figure 7.35 as the data points for the commercial oven were based on estimates extrapolated from the linear relationships for moisture loss and blister coverage. To further investigate this relationship and directly compare the results from each oven, the same method was applied to the benchtop oven data. Figure 7.36 illustrates the combined results and shows that the relationship observed in Figure 6.16 continues with the addition of the benchtop oven data. This suggests that the onset of browning is highly correlated to oven temperature. As these results have been determined based on estimates, they are indicative of the underlying dynamics, though not definitive. To confirm these findings additional research would be required to obtain real time data across a wider range of heat flux and temperature conditions.

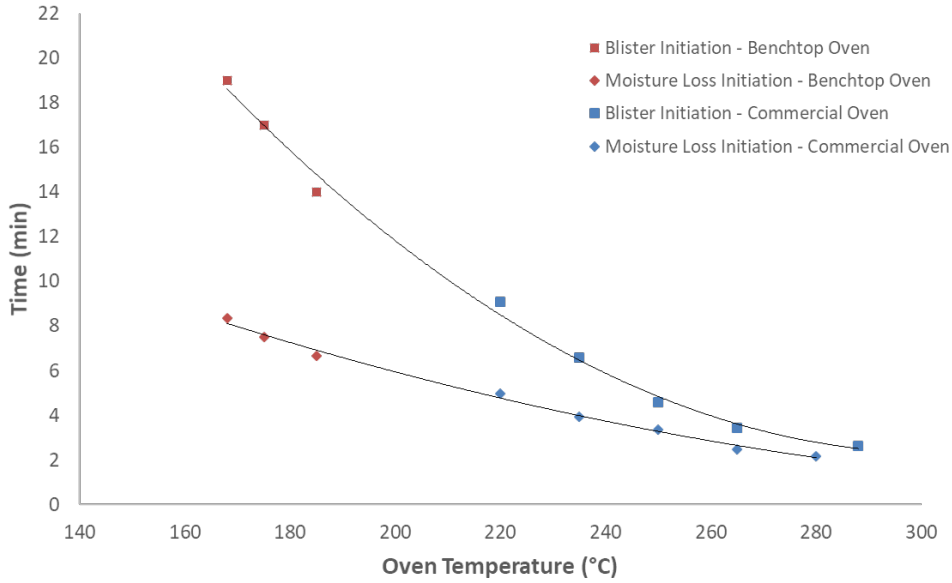

Figure 7.36 – Combined estimates for moisture loss and blister initiation for commercial and benchtop oven

The results shown in Figures 7.34 and 7.36 suggest that the rate of heat transfer has less influence on blister initiation and size than oven temperature once the surface is dry. Higher heat flux allows the surface to dry faster, however it is the surface temperature (which is relative to the oven temperature) that dictates the rate of browning. This agrees with research regarding the kinetics and reaction rates of Maillard browning. Maillard browning is highly temperature dependant, where higher temperatures result in increased rates of browning (Ames, 1990). The rate of reaction is dependent directly on temperature, irrespective of the rate of heat transfer. For these experiments the heat flux figures were averages based on the measurement methods. Once the cheese surface dries, heat flux at the surface would be lower as the temperature gradient is lower. From there it is the combination of time and surface temperature that drives the Maillard reaction and the resulting browning and blister growth.

7.5 Predicting Browning and Blistering

As established in Chapter 3, surface temperature can be used as a predictor for blister formation, where localised temperature increases precede a colour change in that region. The experimental data shows that surface temperature can fluctuate and vary significantly (Figure 7.20), therefore temperature alone has limited predictive capability. The kinetic model developed in Chapter 3 takes into account the temperature/time history and can be used to calculate L* values based on experimental surface temperature data resulting in a better prediction of blister formation.

The P1 kinetic parameters from Chapter 3.6.3 were applied to the integrated kinetic equation to predict L* based on the time temperature history for one data set, cheese baked at an oven temperature of 175°C. This was based on the analysis from Section 5.5, which identified the P1 kinetics to have the best fit relative to blister characteristics compared to the Average ROI kinetics. A general integrated form of the rate equation can be given as Equation 7.1.

$$L^* = L^*_\infty + (L^*_\infty - L^*_0) * \exp\left(-k_o \int_0^t \exp\left(\frac{-E}{RT}\right) dt\right) \qquad \text{Eqn. 7.1}$$

To do this, the Arrhenius exponential term was calculated at each pixel for each time point. These were then cumulatively summed and used to calculate L* at each time. The results are illustrated in

Table 7.4 comparing the original colour images, L*, predicted L*, and surface temperature. Note that the surface temperature data was inverted to match the colour gradient of the grayscale images, the darker the colour the higher the temperature.

Initial observations indicate a good correlation between the actual L* and predicted L* based on the extent of browning and visible blister pattern. The predicted L* appears slightly darker overall with more blisters. Differences in L* and apparent rate of blister formation and growth could be due to different experimental lighting conditions. The kinetic parameters were modelled based on the experimental setup in Chapter 3, where the rates and extent of colour change may have differed.

Table 7.4 – Comparison of original colour images, L*, predicted L*, and surface temperature (IR negatives) for cheese baked at 175°C

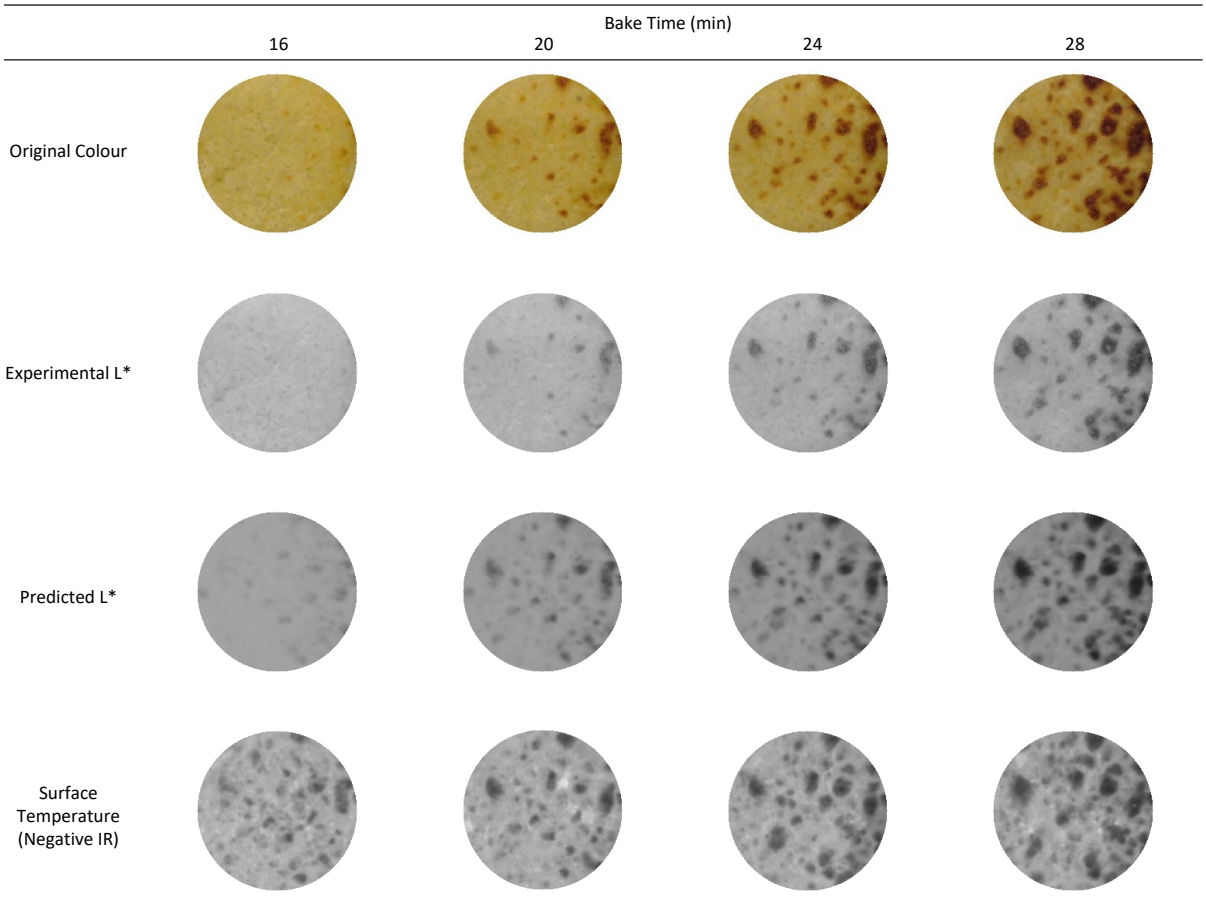

Following the analysis applied in Chapter 5, the predicted L* data was converted to binary images using the dynamic threshold process. Table 7.5 shows the resulting images from predicted L* compared to the experimental L* and relative binary images. The predicted binary images fit well and give an accurate representation of blister coverage based on the observable patterns. The number of blisters appears to differ slightly between experimental and predicted data, with more blisters observed in the predicted blister images. To further understand the predictive capability of the model, the blister characteristic data was plotted and analysed.

Table 7.5 – Comparison of original L* images and binary images based on dynamic threshold for experimental results and predicted data

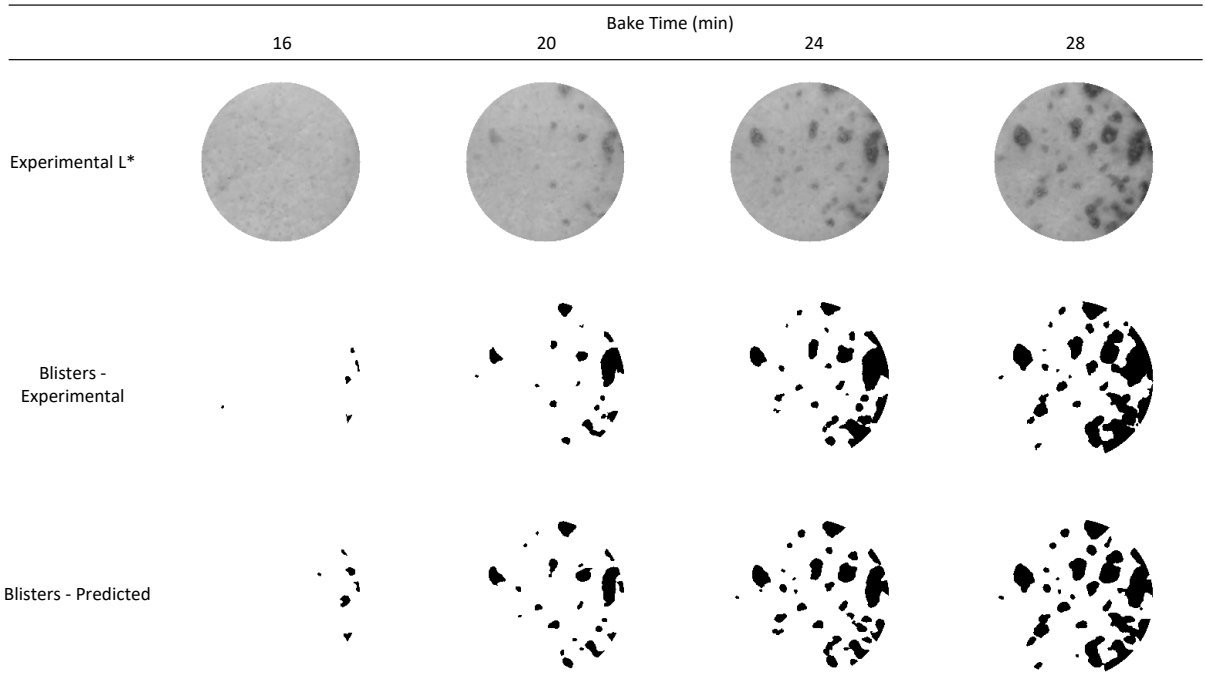

Figures 7.37 to 7.39 illustrate the experimental and predicted values for number of blisters, average blister size and blister coverage. The results for the number of blisters confirms the visual observations where the predicted values are higher, though they do follow the same general trend over time. The number of blisters initially increases rapidly before stabilising and then reducing as the blisters begin to coalesce. Figure 7.39 shows that the predicted average blister size matches the same trend as the experimental data and is within ~20mm^2 for most of the overall bake time. The % blister coverage gives an indication of the overall extent of browning given the time and temperature conditions. The results of the experimental and predicted % blister coverage illustrated in Figure 7.39 show that the kinetic model fits very well for this data set, with an R^2 of over 0.99. This shows that the overall predicted browning kinetics and resulting colour chang fit very well with the experimental data, adding to the analysis from Section 5.5.

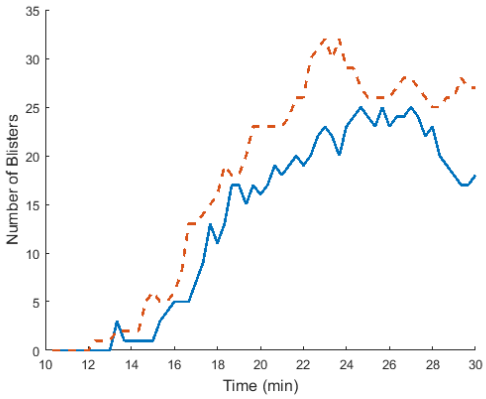

Figure 7.37 Experimental and predicted blister numbers as a function of time, blue represents experimental data and red dash represents predicted values

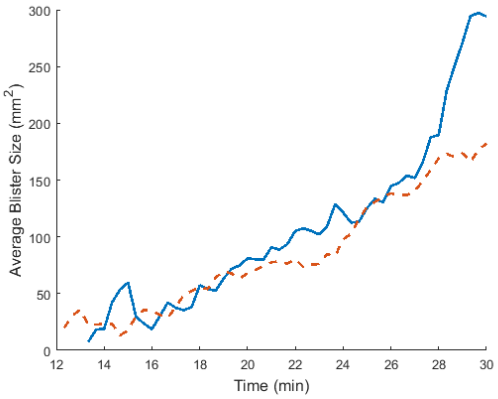

Figure 7.38 Experimental and average blister size as a function of time, blue represents experimental data and red dash represents predicted values

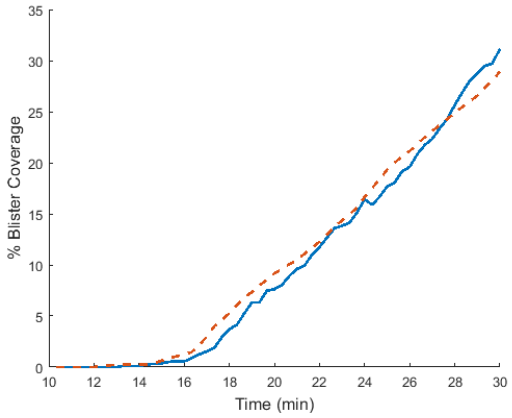

Figure 7.39 Experimental and predicted % blister coverage as a function of time, blue represents experimental data and red dash represents predicted values

Overall, this comparison shows that the kinetic model developed in Chapter 3 can predict browning based on a given time/temperature history and is repeatable for different experimental setups. There is some variation between the actual L* and predicted L*, however the addition of blister analysis utilising the dynamic threshold process takes into account much of this variation. The dynamic thresholding method allows for compensation based on the background and overall colour of the sample giving more accurate results relative to blister characteristics.

Further experiments could be carried out to better align the data with the use of more controlled lighting conditions, such as a lightbox, or through the use of colour correction with the experimental lighting conditions. The application of a lightbox would be limited as it would unable to be used for capturing data in real time.

7.6 Conclusions

This chapter combined the elements of the previous experiments to explore the relationship between moisture content, surface temperature and blister characteristics in real time to further understand the impact on browning and blistering. A process was developed to bake mozzarella and gather surface temperature, surface colour, and overall moisture loss data. The initial analysis simplified and consolidated the proposed conceptual model into three main phases; melt and flow, steam formation and bubbling, and drying and browning. The 10^{th} and 90^{th} percentile data for surface temperature and L* values showed a good correlation regarding the temperature dependence of Maillard browning.

The results of blister analysis showed that the data agreed with the findings from Chapter 6 where oven temperature determines blister size and number, and bake time determines the blister coverage. The relationship between heat flux and blister size was explored further and suggested that there is a linear correlation between heat flux and average blister size, irrespective of the experimental setup and operating conditions. Additional experimentation over a wider range of heat flux conditions would be required to confirm this finding.

The kinetic model developed in Chapter 3 was applied to the benchtop oven data to predict L* values for comparison with the experimental data. The results showed that the predicted blister characteristics matched well with the experimental data, especially for % blister coverage.

Overall, the findings in this chapter agree with the conclusions from previous chapters.

Chapter 8
Conclusions and Recommendations for Future Work

8.1 Conclusions

This study investigated Maillard browning reaction of Mozzarella during high temperature baking to develop an accurate kinetic model and gain an understanding of the blister formation and propagation process during pizza baking.

An experimental process was developed to isolate the browning kinetics of Mozzarella from blistering during heating. Data for the transient distributions of colour and temperature were captured simultaneously across a relatively large surface area. From this data, a first order kinetic model was developed to successfully predict the colour of cheese based on the localised temperature and time histories. It was found that a range of kinetic parameters resulted in a good fit. The reaction rates and kinetic parameters across the cheese surface differed, most likely due to variations across the surface and differing heating rates. The kinetic model was applied to temperature and time history data to create a predicted visual representation of the cheese surface during heating. Of the overall optimised kinetics, those based on average L* across the cheese surface were found to give the best fit with the experimental data (R^2 = 0.88).

A modified commercial pizza oven was used to bake several pizzas and gather data to determine the effect of baking conditions on the blistering and browning process of Mozzarella. An oven characterisation process found that baking temperature and bake time could be adjusted over a useful range and could be well controlled. A process was developed to analyse and assess blister formation and browning of pizzas baked under a range of operating conditions. This process used a lightbox to capture images in a controlled and consistent way and a series of MATLAB files were written to determine blistering and browning characteristics. It was found that a dynamic threshold gave the most accurate representation across the range of baking conditions for the blister identification process. The use of a dynamic threshold considers the contrast between blistered areas and the background colour of a pizza surface for the identification of blisters. This method was adapted from an approach used in approximate sensory evaluations. This method was applied to the data from Chapter 3 and it was found that measuring blister coverage resulted in more accurate predictions overall using the kinetic model, in comparison to directly measuring and comparing L* values. The kinetics based on a singular point (P1) gave the best fit across all of the experimental trials with a R^2 values for different samples ranging from 0.94 to 0.99.

The blister formation and browning of cheese during baking was further investigated to develop a conceptual model of blistering. The conceptual model broke the overall process into several stages, from melt and flow to blistering and browning and considered the role of heat flux during a pizza baking process. Several experiments were carried out to investigate blister nucleation and it was found that the initial form factor of the cheese did not affect the nucleation of blisters. It was identified that blister formation is likely to be more affected by processing conditions, such as baking time and temperature, than the initial conditions.

A series of pizza baking trials were carried out for a range of baking conditions that resulted in key findings with regard to the blister formation process. Surface drying was identified to be fundamental in terms of blister initiation and growth. The relationship between surface moisture and bulk moisture and their effect on viscosity, drive the process of blister growth. It was found that the drying rate is dependent on heat flux and this dictates the general blister characteristics relative to the extent of baking. In general, the oven temperature determines the number and size of blisters and bake time determines the extent of browning.

A benchtop oven was modified to combine the capture of surface temperature, colour, and mass loss during cheese baking in real time. The results for surface temperature and L* values displayed good correlations showing the temperature dependence of Maillard browning. Findings of the relationship between heat flux and blister size suggested that there is a linear correlation between heat flux and average blister size, irrespective of experimental setup and operating conditions. Finally, the first order model initially developed was applied to the benchtop oven data, which showed that the predicted blister characteristics matched well with the experimental data.

The overall findings from this analysis agreed with the conceptual model and gave an understanding of the processes that define the surface characteristics of a baked pizza.

8.2 Recommendations for Future Work

The understanding of cheese behaviour and influential factors during baking has potential benefits for commercial cheese manufacture and applications. There is additional work that could be done to further advance this understanding relative to commercial pizza baking and potentially develop innovative solutions to improve the control of desirable characteristics and reduce bake time.

This study was limited in terms of blister growth analysis, where only the average blister size was considered. To further understand the development and growth of blisters it is recommended that the growth rate of individual blisters be investigated. This would result in an additional measure for defining blister characteristics based on given baking conditions and provide additional predictive capabilities.

It is recommended that the process from Chapter 7, combining surface temperature, colour, and mass loss, be further developed to allow for experiments under higher and more relevant heat flux conditions. To better understand this relationship, the surface temperature data could also be used to estimate surface moisture and when different regions dry out relative to the subsequent browning. This would provide more applicable data to confirm the findings from this research and provide further insight into the relationship between bulk and surface moisture and their effect on the defining surface characteristics of a baked pizza. To further investigate the surface dynamics and characteristics there have been recent developments in imaging technology that collect and processing information from across the electromagnetic spectrum (including ultraviolet and IR), which could be explored. Hyperspectral imaging has become a useful scientific tool for rapid, non-destructive, assessment of a wide variety of food and agricultural products (Amigo et al., 2013). This technology would allow for the simultaneous capture of data over the electromagnetic spectrum, resulting in a wealth of additional data for analysis and potentially negating the need for spatial matching of images.

In general, the relationship between surface moisture and cheese viscosity influences the development and growth of blisters. It is recommended that further work could be done to improve the control of baking characteristics to reduce bake time. Given the developed understanding of the fundamentals that drive blister formation and browning it would be possible to manipulate

parameters that affect the surface drying dynamics. This could be through external baking conditions or adjusting the cheese composition itself to achieve a desired result.

With additional experimental data it would be possible to expand on the capability to apply the findings to practical cheese baking applications. Repeating the analysis for a range of % blister coverage would give the ability to determine the required input conditions for heat flux and bake time to achieve a desired finished product. An additional external method of controlling the browning could be a multi-stage baking process. Developing a multi-stage baking process would look to exploit the effect of surface moisture and viscosity, which directly influence blister size and growth. Stage 1 could be set up to melt and dry the cheese surface, to provide the conditions relative to the desired blister characteristics, such as large steam pockets (unbrowned blisters). The heat flux during this stage would determine the blister size and numbers. Stage 1 under low heat flux conditions would extend the time for surface drying, resulting in a thicker more viscous dry surface layer to support large pockets of steam. Stage 1 under higher heat flux conditions would reduce the surface drying time, resulting in a thinner dry surface layer and smaller steam pockets. Note that there would be a limit to how fast this initial process could occur, as the cheese needs to have time to melt and fuse to avoid scorching. Stage 2 could then be set up with a high heat flux to rapidly heat the surface, resulting in rapid browning where surface drying has occurred. If successful, this could have significant benefits for commercial applications by giving better control over the desired baking characteristics, resulting in a more consistent product and reducing overall processing time and cost.

Another possible application of a multi-stage process would be to initially heat the cheese enough to melt and fuse cheese shreds, then rapidly dry a desired area on the surface with the application of a hot stamp or high velocity/temperature impinger pattern, and then finish baking conventionally. This would preferentially dry a specific area and therefore brown that specific area. In this way it would be possible to manipulate the process to achieve a desired blister pattern or image, which could improve product uniformity or support branding.

These ideas look to manipulate the drying rate through external mechanical means. The cheese itself could also be modified to change how it reacts during baking to exploit the link between moisture content and viscosity. It may be possible to manipulate blister size for a given bake time and oven temperature by adjusting the cheese moisture content. A higher moisture content cheese would have a lower initial viscosity, which would result in smaller blisters due to a similar surface drying rate and therefore thinner dry surface. This would have benefits in terms of achieving a desired finished product, but also added value for a material that is cheaper to produce.

Maillard browning is an important factor in many high temperature food processing applications. The experiments and methods developed in this study could be applied to monitor and predict the browning of cheese, but could also be extended to other food systems where browning is pertinent. The ability to record colour, temperature and mass loss simultaneously in real time has potential applications for any baking system. The image analysis process could be applied to commercial manufacture to remove the subjectivity of human sensory analysis, resulting in a more robust, repeatable and consistent means of assessment.

The findings from this study provide a good insight into the fundamentals that affect cheese baking, adding to the current research field to better understand the browning reaction and its application in high temperature food processing.

References

Albalak, R. J. (1996). *Polymer devolatilization*. New York: M. Dekker.

Altomare R.E. (1994) Heat Transfer in Bakery Ovens. In: Yano T., Matsuno R., Nakamura K. (eds) Developments in Food Engineering. Springer, Boston, MA.

Ames, J. M. (1990). Control of the Maillard reaction in foods. *Trends In Food Science & Technology*, *1*, 150-154.

Amigo, J.M., Martí, I., Gowen, A., Marini, F., 2013. Chapter 9 – Hyperspectral imaging and chemometrics: a perfect combination for the analysis of food structure, composition and quality. In: Data Handling in Science and Technology. Elsevier, pp. 343–370

Baik, O., & Mittal, G. (2003). Kinetics of tofu color changes during deep-fat frying. *LWT-Food Science and Technology, 36*(1), 43-48.

Balaban, M.O. (2013). LensEye Program (Version 11.3.3) [software].

Boekel, M. v. (2009). *Kinetic modeling of reactions in foods. [electronic resource]*. Boca Raton : CRC Press, c2009.

Borgnakke, C., & Sonntag, R. E. (2013). *Fundamentals of thermodynamics*. Hoboken, NJ : Wiley, c2013.

Brosnan, T., & Sun, D.-W. (2004). Improving quality inspection of food products by computer vision: A review. *Journal of Food Engineering, 61*(1), 3-16.

Brown, C., Bronlund, J. E. (2015). *Mozzarella functionality in baking applications.* Report for Fonterra PGP Food Structures Platform, Massey University, Palmerston North.

Broyart, B., Trystram, G., & Duquenoy, A. (1998). Predicting colour kinetics during cracker baking. *Journal of Food Engineering, 35*(3), 351-368.

Carson, J.K., Willix, J., North, M. F. (2006). Measurements of heat transfer coefficients within convection oven. *Journal of Food Engineering*, *72*(3), 293-301.

Cho, J., Lee, H., Park, J., Sung, J., Choi, J., & Moon, K. (2016). Image analysis to evaluate the browning degree of banana (Musa spp.) peel. *Food Chemistry*, *194,* 1028-1033.

Clark, S., & Bodyfelt, F. W. (2009). *The sensory evaluation of dairy products*. New York : Springer, c2009.

Cunha, L. M. & Oliveira FAR. (2000). Optimal experimental design for estimating the kinetic parameters of processes described by the first-order Arrhenius model under linearly increasing temperature profiles. *Journal of Food Engineering, 46*(1), 53-60.

Dave, R. I., McMahon D. J., & Broadbent J.R. (2001). Reversibility of the temperature-dependant opacity of nonfat mozzarella cheese. *Journal of Dairy Science, 84*(11), 2364-2371.

Demir, A. D., Celayeta, J. M. F., Cronin, K., & Abodayeh, K. (2002). Modelling of the kinetics of colour change in hazelnuts during air roasting. *Journal of Food Engineering,* 55(4), 283-292.

Desai, N. & Nolting, J. (1994). Microstructure studies of reduced fat cheeses containing fat substitute, in E.L. Malin & M.H. Tunick, (Eds.) *Chemistry of Structure–Function Relationships in Cheese*, New York: Plenum Press.

Dufossé, L., & Galaup, P. (2010).Color. In Nollet, L. L., & Toldrá, F. (Eds.), *Sensory analysis of foods of animal origin*. 319-339. Boca Raton : Taylor & Francis.

Earle, R.L. (1983). *Unit Operations in Food Processing.* Oxford : Pergamon Press.

Emmons, D. B.,Kalab, M., Larmond, E., & Lowrie, R. J. (1980). Milk gel structure, x. Texture and microstructure in cheddar cheese made from whole milk and from homogenised low fat milk. *Journal of Texture Studies*, *11*(1), 15-34

Eskin, N. A. M., Ho, C.H., & Shahidi, F. (2005). Browning Reactions in Foods. In N. A. M. Eskin, & F. Shahidi (Eds.), *Biochemistry of foods [electronic resource]* (3rd ed., pp. 245-280). San Diego, CA: Academic Press [Imprint] of Elsevier Science & Technology Books. Retrieved from http://www.sciencedirect.com/science/book/9780122423529

Everett, D. W., & Auty, M. A. (2008). Cheese structure and current methods of analysis. *International Dairy Journal*, *18*(7), 759-773.

Everett, D., & Olson, N. (2003). Free oil and rheology of cheddar cheese containing fat globules stabilized with different proteins. *Journal Of Dairy Science*, *86*(3), 755-763.

Fan, Y., Li, J., Guo, Y., Xie, L., & Zhang, G. (2020). Digital Image Colorimetry on Smartphone for Chemical Analysis: A Review. *Measurement*, 108829.

Fennema, O. R. (1996) *Food Chemistry* (3rd ed.). New York : Marcel Dekker, 1996.

Franzen, K., Singh, R. K., Okos, O. (1990). Kinetics of Nonenzymatic Browning in Dried Skim Milk. *Journal of Food Engineering, 11*(3), 225-239.

Fox, P. F., Guinee, T.P., Cogan, T. M., & McSweeny, P. L. H. (2000). *Fundamentals of cheese science*. Gaithersburg, MD : Aspen Pub.

Giannakourou, M. C. & Taoukis, P. S. (2007). Reaction kinetics. In S. S. Sablani, M. S. Rahman, A. K. Datta, & A. S. Mujumdar (Eds.), *Handbook of food and bioprocess modeling techniques* (pp. 235-259). Boca Raton, FL: CRC Press.

Gilchrist, A., Nobbs, J., & John, L. (2010). Colorimetry, Theory. *Encyclopedia of Spectroscopy and Spectrometry* (pp. 380-385). Oxford, UK: Academic Press.

Gonzalez, R. C., & Woods, R. E. (2007). *Digital image processing*. Harlow : Prentice Hall, 2008.

Goshtasby, A. A. (2012). *Image Registration Principles, Tools and Methods* (1st ed.). London : Springer, 2012.

Guinee, T.P. & Fox, P.F. (2004). Salt in cheese: physical, chemical and biological aspects. In Fox P.F. (Ed.) *Cheese: Chemistry, Physics and Microbiology*. (pp. 207-259), Elsevier Academic: Oxford.

Gunasekaran, S. (2001). Non-destructive food evaluation techniques to analyse properties and quality. *Food Science and Technology (vol. 105).* New York, NY: Marcel Decker.

Gunasekaran, S., and Ak, M. M. (2003). *Cheese rheology and texture*. Boca Raton, FL : CRC Press.

Heldman, D. R., & Lund, D. B. (1992). *Handbook of food engineering*. New York : Marcel Dekker, Inc

Hong, Y.H., Yun, J. J., Barbano, D. M., Larose, K. L., & Kindstedt P. S. (1998) Mozzarella cheese: impact of three commercial culture strains on composition, proteolysis and functional properties. *Australian Journal of Dairy Technology, 53*(3), 163-169.

Ilo, S., & Berfhofer E. (1999) Kinetics of colour changes during extrusion cooking of maize grits. *Journal of Food Engineering, 39*(1), 73-80.

Incropera, F. P. (2011). *Fundamentals of heat and mass transfer*. Hoboken, NJ : John Wiley, c2011.

ISO/CIE, (2007). ISO 11664-2:2007(E)/CIE S 014-2/E:2006: CIE Colorimetry - Part 2: Standard Illuminants for Colorimetry. Vienna, Austria: ISO/CIE.

Jana, A. H., & Tagalpallewar, G. P. (2017). Functional properties of Mozzarella cheese for its end use application. *Journal of Food Science and Technology-Mysore*, 54(12), 3766-3778. 10.1007/s13197-017-2886-z

Johnson, M. E., & Olson, N. (1985) Nonenzymatic browning of Mozzarella cheese. *Journal of Dairy Science, 68*(12), 3143-3147.

Kindstedt, P.S. (1993). Mozzarella and pizza cheese. In Fox, P.F. (Ed.), *Cheese: Chemistry, Physics and Microbiology, Vol 2, Major Cheese groups,* (2nd ed., pp.337–362). Chapman and Hall: London.

Kindstedt, P.S. (2019). Symposium review: the Mozzarella/pasta filata years: a tribute to David M. Barbano. *Journal of Dairy Science, 102*(11), 10670-10676.

Kindstedt, P.S., L.J. Kiely & J.A. Gilmore. (1992). Variation in composition and functional properties with brine-salted mozzarella cheese. *Journal of Dairy Science, 75*(11), 2913-2921.

Kong, K. (2014). *Pizza image analysis and quantification using machine vision* (Master's report). University of Auckland, Auckland, New Zealand.

Kosikowski, F.V., & Mistry. V. (1997). *Cheese and Fermented Milk Foods* (3rd ed.). Westport, CT: F.V. Kosikowski & Associates.

Kuo, M. I.; Wang, Y. C. & Gunasekaran, S. (2000). A viscoelasticity index for cheese meltability evaluation. *Journal of Dairy Science, 83*(3), 412-417.

Kuo, M., Wang, Y., Gunasekaran, S., & Olson, N. (2001). Article: Effect of Heat Treatments on the Meltability of Cheeses. *Journal of Dairy Science*, *84*(9), 1937-1943.

Labuza, T. P. (1994). *Maillard reactions in chemistry, food, and health*. Cambridge, U.K. : Royal Society of Chemistry, 1994.

León, K., Mery, D., Pedreschi, F., & León, J. (2006). Color measurement in L∗a∗b∗ units from RGB digital images. *Food Research International*, *39*(10), 1084-1091.

Liu, S., Yang, D., Jin, S., Hsu, C., & Chen, S. (2008). Kinetics of color development, pH decreasing, and anti-oxidative activity reduction of Maillard reaction in galactose/glycine model systems. *Food Chemistry*, *108*(2), 533-541.

Lopez, A., Pique, M. T., Boatella, J., Parcerisa, J., Romero, A., Ferrá, A., et al. (1997). Influence of drying conditions on the hazelnut quality. III. Browning. *Drying Technology, 15*(3), 989-1002.

Lucey, J. (2008). Some perspectives on the use of cheese as a food ingredient. *Dairy Science & Technology*, *88*(4-5), 573-594.

Lucey, J. A., Johnson, M. E., & Horne, D. S. (2003). Invited review: perspectives on the basis of the rheology and texture properties of cheese. *Journal of Dairy Science, 86*(9), 2725-2743.

Lukac, H., Amrein, T. M., Perren, R., Conde Petit, B., Amadò, R., & Escher, F. (2007). Influence of roasting conditions on the acrylamide content and the color of roasted almonds. *Journal of Food Science, 72*(1), C033-C038.

Ma, J., Sun, D., Qu, J., Liu, D., Pu, H., Gao, W., & Zeng, X. (2016). Applications of Computer Vision for Assessing Quality of Agri-food Products: A Review of Recent Research Advances. *Critical Reviews In Food Science & Nutrition*, *56*(1), 113-127.

Ma, X., James, B., Balaban, M. O., Zhang, L., & Emanuelsson-Patterson, E. A. (2013a). Quantifying blistering and browning properties of Mozzarella cheese. Part I: Cheese made with different starter cultures. *Food Research International*, 54(1), 912-916. doi:10.1016/j.foodres.2013.06.007

Ma, X., James, B., Balaban, M. O., Zhang, L., & Emanuelsson-Patterson, E. A. (2013b). Quantifying blistering and browning properties of Mozzarella cheese. Part II: Cheese with different salt and moisture contents. *Food Research International*, *54*(1), 917-921. doi:10.1016/j.foodres.2013.05.029

Ma, X., Balaban, M.O., Zhang, L., Emanuelsson-Patterson, E. A. C., James, B. (2014). Quantification of pizza baking properties of different cheeses, and their correlation with cheese functionality. *Journal of Food Science, 79*(8), 1528-1534.

Martins, S., Jongen, W., & van Boekel, M. (2001). A review of Maillard reaction in food and implications to kinetic modelling. *Trends In Food Science & Technology*, *11*(9-10), 364-373.

Matikas, P., & Skusevich, D. (2010). Color Perception : Physiology, Processes and Analysis. New York: Nova Science Publishers, Inc.

Matsuda, H., Llave, Y., Fukuoka, M., & Sakai, N. (2013). Color changes in fish during grilling-Influences of heat transfer and heating medium on browning color. *Journal of Food Engineering, 116*(1), 130-137.

Matzdorf, B., Cuppett, S., Keeler, L., & Hutkins, R. (1994). Browning of Mozzarella cheese during high temperature pizza baking. *Journal of Dairy Science, 77*(10), 2850-2853.

McLaren, K. (1976). XIII—The development of the CIE 1976 (L* a* b*) uniform colour space and colour difference formula. *Journal of the Society of Dyers and Colourists, 92*(9), 338-341.

McSweeney, P. H. (2007). *Cheese problems solved. [electronic resource].* Boca Raton : CRC Press ; Cambridge, England : Woodhead Pub., 2007.

Mendoza, F., Dejmek, P., & Aguilera, J. M. (2007). Colour and image texture analysis in classification of commercial potato chips. *Food Research International, 40*(9), 1146-1154

Metzger, L., Barbano, D., Rudan, M., Kindstedt, P., & Guo, M. (2000). Article: Whiteness Change During Heating and Cooling of Mozzarella Cheese. *Journal of Dairy Science*, 83(1), 1-10. doi:10.3168/jds.S0022-0302(00)74847-8

Nourian, F., & Ramaswamy, H. S. (2003). Kinetics of quality change during cooking and frying of potatoes: Part II. colour. *Journal of Food Process Engineering, 26*(4), 395-411.

Nursten, H. E. (2005). *The Maillard Reaction : Chemistry, Biochemistry, and Implications*. Cambridge, UK: Royal Society of Chemistry.

Pastorano, A. J., Dave, R. I., Oberg, C. J., & McMahon D. J. (2002). Temperature effect on structure-opacity relationships of nonfat mozzarella cheese. *Journal of Dairy Science, 85*(9), 2106-2113.

Półtorak, A., Wyrwisz, J., Moczkowska, M., Marcinkowska-Lesiak, M., Stelmasiak, A., Ulanicka, U., & Sun, D. (2015). Correlation between instrumental texture and colour quality attributes with sensory analysis of selected cheeses as affected by fat contents. *International Journal of Food Science & Technology*, *50*(4), 999-1008.

Purlis, E. (2010). Browning development in bakery products: A review. *Journal of Food Engineering, 99*(3), 239-249.

Purlis, E., & Salvadori, V. O. (2007). Bread browning kinetics during baking. *Journal of Food Engineering, 80*(4), 1107-1115

Purlis, E., & Salvadori, V. O. (2009). Modelling the browning of bread during baking. *Food Research International, 42*(7), 865-870.

Rajchasom, S. (2014). *Characterising the kinetics of high temperature browning in foods : a thesis presented in partial fulfilment of the requirements for the degree of Doctor of Philosophy in Food and Bioprocess Engineering at Massey University, Manawatu, New Zealand.*

Rankin, S. A., Chen, C. M., Sommer, D., Esposito, A. (2005). Mozzarella and Scamorza Cheese. In Hui, Y. H. (ed.), *Handbook of food science, technology, and engineering. [electronic resource]* (150). Boca Raton: Taylor & Francis.

Rapusas, R. S., & Driscoll, R. H. (1995). Kinetics of non-enzymatic browning in onion slices during isothermal heating. *Journal of Food Engineering, 24*(3), 417-429.

Rudan, M. A., & Barbano, D. M. (1998). A model of Mozzarella cheese melting and browning during pizza baking. *Journal of Dairy Science, 81*(8), 2312-2319.

Rudan, M. A., Barbano, D. M., Joseph Yun, J., & Kindstedt, P. S. (1999). Article: Effect of Fat Reduction on Chemical Composition, Proteolysis, Functionality, and Yield of Mozzarella Cheese1. *Journal of Dairy Science*, *82*(4), 661-672.

Shibukawa, S., Sugiyama, K., & Yano, T. (1989). Effects of heat transfer by radiation and convection on browning of cookies at baking. *Journal of Food Science, 54*(3), 621-624.

Sonka, M., Hlavac, V., & Boyle, R. (2008). *Image processing, analysis, and machine vision* (3rd ed.). Toronto: Thompson Learning.

Sun, D.-W. (2000). Inspecting pizza topping percentage and distribution by a computer vision method. *Journal of Food Engineering, 44*(4), 245-249.

Trambouze, P., Landeghem, H. v., & Wauquier, J. (1988). *Chemical reactors : design, engineering, operation*. Houston, Tex. : Gulf Publishing ; Paris : Editions Technip.

Van Boekel, M. A. (2008). Kinetic Modeling of Food Quality: A Critical Review. *Comprehensive Reviews In Food Science And Food Safety*, *7*(1), 144-158.

Villota, R., & Hawkes, J. (2007). Reaction kinetics in food systems. In R. D. Heldman, D. B. Lund (Eds), *Handbook of food engineering* (pp. 39-144). Boca Raton, FL CRC Press.

Wadhwani, R., McManus, W., & McMahon, D. (2011). Improvement in melting and baking properties of low-fat Mozzarella cheese. *Journal of Dairy Science*, 94(1), 1713-1723. doi:10.3168/jds.2010-3952

Wagner, W., & Kretzschmar, H. (2008). *International steam tables : properties of water and steam, based on the industrial formulation IAPWS-IF97*. Berlin : Springer, c2008

Walstra, P. (2003). *Physical chemistry of foods. [electronic resource]*. New York : Marcel Dekker, c2003.

Wang, H.-H. & Sun, D. (2002a). Melting characteristics of cheese: analysis of effect of cheese dimensions using computer vision techniques. *Journal of Food Engineering, 52*(3), 279-284.

Wang, H.-H. & Sun, D. (2002b). Melting characteristics of cheese: analysis of effects of cooking conditions using computer vision technology. *Journal of Food Engineering, 51*(4), 305-310.

Wang, H., & Sun, D. (2003). Assessment of cheese browning affected by baking conditions using computer vision. *Journal of Food Engineering*, 56(4), 339-345.

Wu, D., & Sun, D. (2013). Review: Colour measurements by computer vision for food quality control – A review. *Trends In Food Science & Technology*, *29*(1), 5-20.

X-Rite. (2009). *ColorChecker Classic*. Retrieved from http://xritephoto.com

Yam, K. L., & Papadakis, S. E. (2004). A simple digital imaging method for measuring and analysing color of food surfaces*. Journal of Food Engineering, 61*(1), 137-142.

Zhu C. (2013) Characterisation of the rheological properties of mozzarella cheese : Masters in Engineering Thesis, Massey University, Manawatu, New Zealand

Zhu, C., Brown, C., Gillies, G., Watkinson, P., & Bronlund, J. (2015). Characterizing the rheological properties of mozzarella cheese at shear rate and temperature conditions relevant to pizza baking. *LWT - Food Science and Technology*, *64*(1), 82-87. doi:10.1016/j.lwt.2015.05.037

Zude, M. (2009). *Optical monitoring of fresh and processed agricultural crops*. Boca Raton, Fla. ; London : CRC, c2009.

Appendix 1

Appendix 1 – As soft copy

Chapter 3

- Colour and Temperature Data
  - MATLAB files to extract and align colour and temperature data
- Model Fitting and Optimisation
  - MATLAB files to fit and optimise the kinetic model

Chapter 5

- Blister Assessment
  - MATLAB files to determine and analyse blister characteristics
- Minimum Blister Size
  - MATLAB files to determine a minimum blister size
- Model Fitting and Optimisation
  - MATLAB file to apply the kinetic model using blister coverage

Chapter 7

- Colour Data
  - MATLAB files to capture video file and split file into still frames

Appendix 2

Booklet of Pizzas Baked in Various Conditions

- Presented in hard copy

This booklet contains information on Pizzas cooked under various baking conditions.

Images are arranged from darkest to lightest average L* value.

This booklet was developed to give an indication of baking performance based on baking time and oven temperature and provide summary data on surface appearance such as blister coverage, size and number.

What is a blister and its implications for the optical assessment of baked pizza pies?

Introduction

A blister is generally defined as a raised area on the surface of baked cheese (Chen et al., 2009). Another more specific definition given is that blisters result from trapped regions of heated air and steam that are potentially more likely to brown during baking (Ma, *et al*., 2013). These definitions are subjective and are currently not directly measurable. In order to assess the formation of blisters during cheese baking, the classification of what is a blister needs to be clearly and quantifiably defined. In this work, a blister was defined as a discrete brown region on the cheese surface able to be characterised by its colour relative to its surroundings. This is a simple and measurable definition which leads further to a number of useful characterisation variables, including blister coverage, number of blisters, and blister size distribution and average blister size.

Methods

The method used to characterise blisters began with the preparation of pizza pies using a standard recipe for the construction of the pie (see Brown and Bronlund 2015) and baking them in a Lincoln Impinger oven using a variety of baking times and air temperatures. After baking the pies, images of their surfaces were obtained using standardised lighting conditions (Balaban M, Personal Communication) and standard digital camera settings. The resulting JPEG files were then analysed using the image analysis tools (L, a, b values for each pixel) in MATLAB (2014b). The approach taken was to convert the image into a black and white (B/W) image using a preselected threshold criterion to identify blisters.

In order to avoid noise artefacts in the statistical interpretation of the images, a minimum region of interest was defined as being >20 adjacent pixels (out of a nominal sensor array of 1400x929 pixels). This corresponds to neglecting potential blisters smaller than 2.2mm in diameter.

Three potential threshold methods were examined:

1. Current Fonterra standard ($L^* < 80$ & $a^*>10$)
2. Best single value for entire range ($L^*<55$).
   This value was selected through visual inspection of all the pizza's analysed and judged to best represent blister coverage.
3. Dynamic threshold i.e. compensation of the blister threshold colour value according to the colour of its background. ($L^* < 28.5 + 0.57\overline{L^*}$).
   Using this method, as the average L* (i.e. $\overline{L^*}$) decreases (darkens), the threshold also reduces.

Analysis of all images found that using threshold method 1 ($L^* < 80$ & $a^*>10$), all pixels with $a^*>10$, also met the $L^* < 80$ requirement. For this reason this method could be simplified to $a^*>10$.

In determining a single L^* threshold it was noted that there was significant variation in what was visually observed to be a good representation of blisters and the relative results from image analysis. A L^* threshold that gave good results for a higher average L^*, gave poor results for images with a low averageL^*. Figure 1 illustrates this showing the difference in blister definition for a pizza with a low average L^* compared to that for a high averageL^*. This meant that the use of a single L^* threshold was unlikely to be useful over the wide range of pizza baking conditions. Of the single L^* thresholds evaluated, $L^* < 55$ was selected as being the most suitable through visual evaluation.

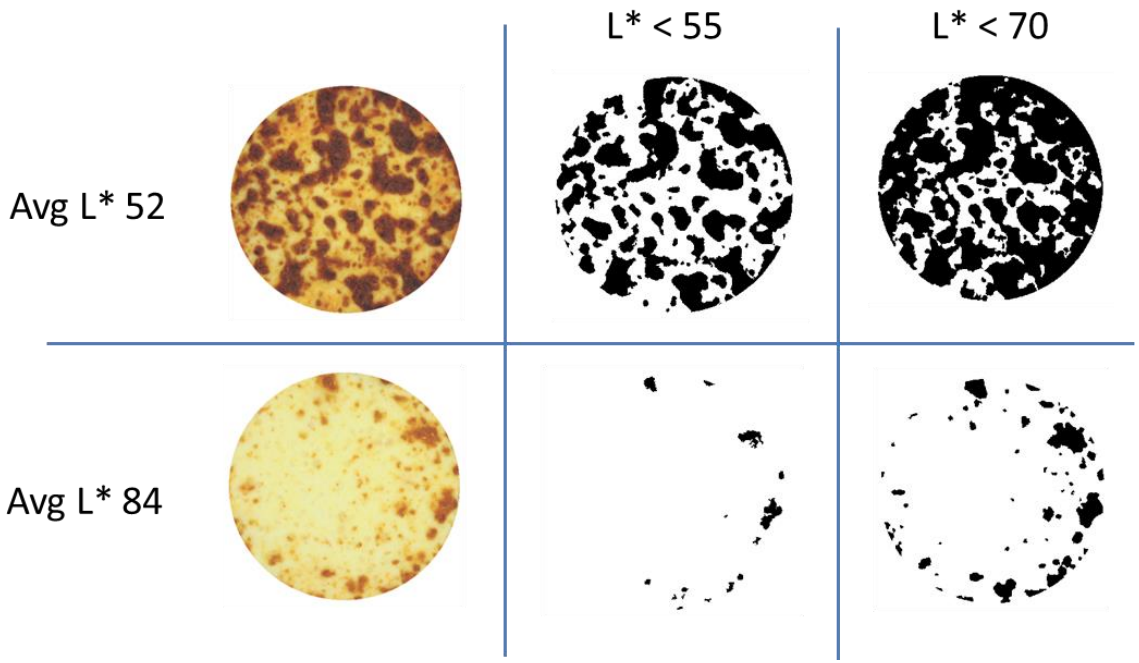

Figure 1 – Variability in ideal L^* threshold depending on overall lightness

Another potential issue is that an L* threshold that resulted in good separation of blisters, cut out a significant portion of browned area, and therefore did not give a good representation of browning coverage.

Pizza baking is a dynamic process and as baking progresses the entire surface darkens which results in a change in the difference between blistered areas and the background colour. Other pizza baking research has been carried out at Auckland University using threshold analysis to measure baking performance. Kelvin Kong investigated sensory attributes regarding the level of browning and blistering for a range of cooked cheese samples. This research found that there was a correlation between the average L* ($\bar{L}^*$) for a cooked pizza and the perceived L* threshold for defining browning and blistering based on sensory evaluation, illustrated in Figure 2. For a given average L* this relationship allows a dynamic L* threshold to be calculated, where the lower the average L*, the lower the L* threshold and vice versa. Using the derived equation a dynamic L* threshold can be assigned to each individual image based on the overall colour.

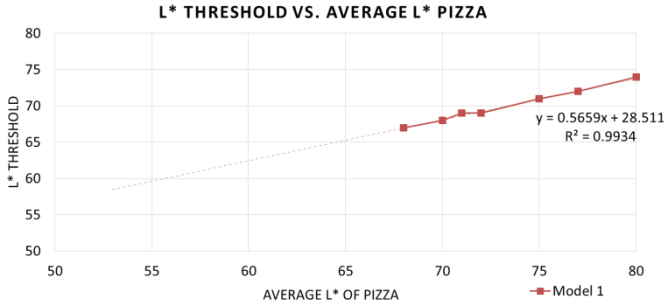

Figure 2 – Dynamic L^* threshold evaluation. Courtesy of Kelvin Kong

To test this approach the dynamic model was applied to the same sample images used in Figure 1. Figure 3 illustrates an example of the results at each end of the average L* spectrum. It can be seen that selecting a specific L* threshold to apply to all images would result in poor blister identification is some cases. An L* threshold of 55 appears to identify blisters well for the colour image for with an average L* of 52, but gives a poor result for an average L* of 84. The reverse is true for an L* threshold of 70. The use of a dynamic threshold calculated from the average L* fits well, where the blisters identified in the binary images appear to match well with the original colour images.

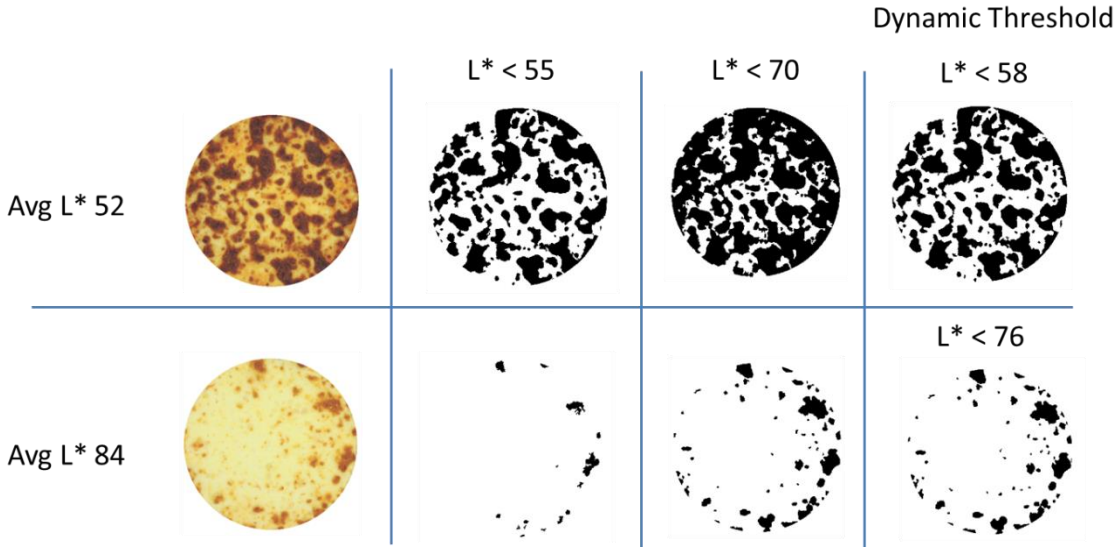

Figure 3 – Illustration of results using the dynamic threshold

Colour perception varies between individuals and with this type of application there will always some subjectivity in terms of defining appropriate threshold limits. The purpose of this exercise is to investigate the effect of time and temperature on baking performance, which requires a relative and consistent measure for comparison. The use of the dynamic threshold model gives a consistent platform to work from and produces data for the entire range of baking conditions that is directly comparable.

Data presented in this booklet

A series of pies (250 mm pans) were baked using selected oven settings to give a wide range of baked outcomes that encompassed most of the outcomes that pizza consumers might be expected to experience. The data in the following slides record the pie recipe and the oven settings and physical outcomes i.e. weight loss. The data also include the image analysis details –

a. The full colour image without correction captured using the standard light-box and camera settings
b. A Black and White image using the preferred L* threshold of <55 and the associated statistics of blister number, mean size, total blister area etc.
c. A Black and White image using the threshold of a*>10 and the same statistics as above.
d. A Black and White image using the dynamic threshold of $L^* < 28.5 + 0.57\overline{L^*}$ and the same statistics as above.

Conclusions

The images and summary data analysis presented in this document could be used to identify desired appearance for different applications and relate this back to the conditions required to cook the pizza. Three different blister threshold methods are presented in each case to allow comparison. The proposed definition of a blister when based on an image taken under standardised image capture conditions was given by the relationship:

$$L^* < 28.5 + 0.57\overline{L^*}$$

Further libraries of pizza images under controlled lighting conditions, together with blister analysis and a summary of baking conditions, would provide a valuable resource to trouble shooting customer issues and in developing pizza baking scenarios tailored to customer requirements.

References

Brown C. & Bronlund J.E. (2015) Mozzarella functionality in baking applications. Technical Report to Fonterra PGP – Food Structures Platform. Project: 800564 Model Baking Systems for Mozzarella Cheese.

Chen, C., Wolle, D., & Sommer, D. (2009). Mozzarella. In The sensory evaluation of dairy products (pp. 459-487). Springer US.

Ma, X., James, B., Zhang, L., & Emanuelsson-Patterson, E. A. (2013). Correlating mozzarella cheese properties to its production processes and microstructure quantification. Journal of Food engineering, 115(2), 154-163.

Pizza 1 - Cooking Results

Conditions:	
Oven Set Point Temperature	360°C
Actual Oven Temperature	281°C
Cooking Time	16 minutes
Fan Speed	10
Heat Transfer Coefficient	29.8W/m^2
Pizza Characteristics:	
Pizza Base	349.4g
Sauce	80.57g
Cheese	240.0g
Mass Loss	88.07g
Percentage Mass Loss	13.1%
Colour Analysis:	
Lab L*	45.71
StdDev L*	18.06
Lab a*	18.84
StdDev a*	9.95
Lab b*	35.4
StdDev b*	17.4

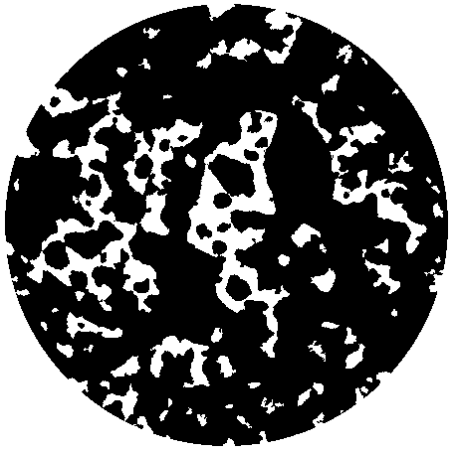

Blister Analysis - based on a*>10	
Total Blisters	14
Total Area	22864.75mm^2
%Brown	80.3%
Size of Blisters	
Average	1633.20mm^2
Max	22314.11mm^2
Median	19.12mm^2
Min	4.94mm^2

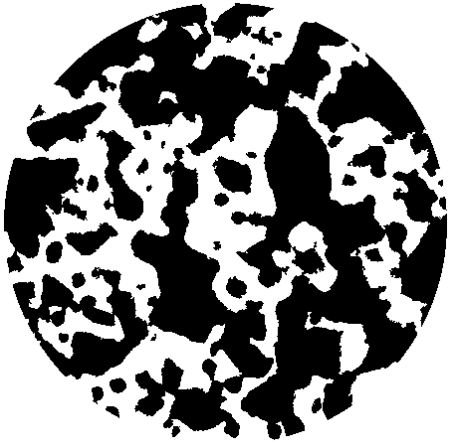

Blister Analysis - based on L*<55	
Total Blisters	39
Total Area	16967.58mm^2
%Brown	59.6%
Size of Blisters	
Average	435.07mm^2
Max	8862.69mm^2
Median	23.06mm^2
Min	4.21mm^2

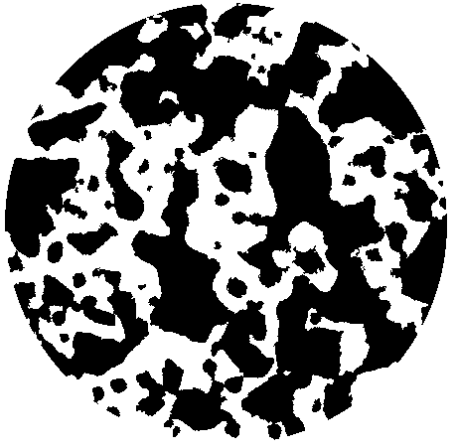

Blister Analysis - based on Dynamic L*<54	
Total Blisters	41
Total Area	16505.87mm^2
%Brown	58.0%
Size of Blisters	
Average	402.58mm^2
Max	8550.86mm^2
Median	26.17mm^2
Min	3.66mm^2

Pizza 2 - Cooking Results

Conditions:	
Oven Set Point Temperature	280°C
Actual Oven Temperature	220°C
Cooking Time	22 minutes
Fan Speed	10
Heat Transfer Coefficient	29.8W/m^2
Pizza Characteristics:	
Pizza Base	347.3g
Sauce	80.08g
Cheese	240.80g
Mass Loss	86.98g
Percentage Mass Loss	13.0%
Colour Analysis:	
Lab L*	46.48
StdDev L*	15.65
Lab a*	21.24
StdDev a*	9.04
Lab b*	37
StdDev b*	15.45

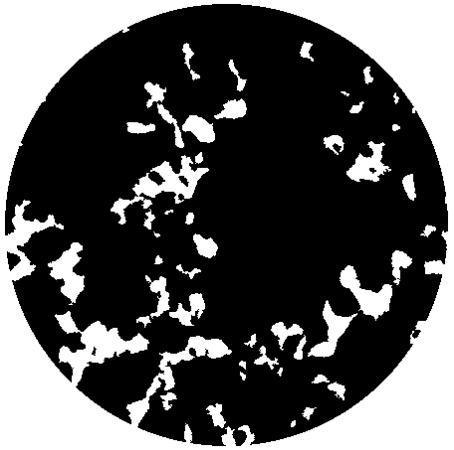

Blister Analysis - based on a*>10	
Total Blisters	5
Total Area	24816.63mm^2
%Brown	87.2%
Size of Blisters	
Average	4963.33mm^2
Max	24767.04mm^2
Median	11.16mm^2
Min	4.21mm^2

Blister Analysis - based on L*<55	
Total Blisters	26
Total Area	17532.32mm^2
%Brown	61.6%
Size of Blisters	
Average	674.32mm^2
Max	14401.00mm^2
Median	19.58mm^2
Min	3.66mm^2

Blister Analysis - based on Dynamic L*<55	
Total Blisters	26
Total Area	17532.32mm^2
%Brown	61.6%
Size of Blisters	
Average	674.32mm^2
Max	14401.00mm^2
Median	19.58mm^2
Min	3.66mm^2

Pizza 3 - Cooking Results

Conditions:	
Oven Set Point Temperature	340°C
Actual Oven Temperature	265°C
Cooking Time	14 minutes
Fan Speed	10
Heat Transfer Coefficient	29.8W/m^2
Pizza Characteristics:	
Pizza Base	338.9g
Sauce	80.62g
Cheese	240.77g
Mass Loss	64.99g
Percentage Mass Loss	9.8%
Colour Analysis:	
Lab L*	49
StdDev L*	20.29
Lab a*	16.72
StdDev a*	11.31
Lab b*	36.16
StdDev b*	16.55

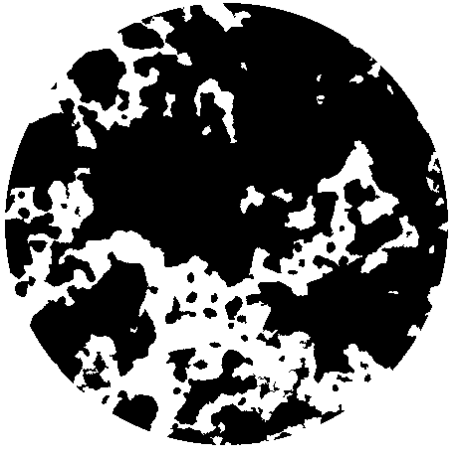

Blister Analysis - based on a*>10	
Total Blisters	41
Total Area	20377.78mm^2
%Brown	71.6%
Size of Blisters	
Average	497.02mm^2
Max	15815.04mm^2
Median	10.80mm^2
Min	3.84mm^2

Blister Analysis - based on L*<55	
Total Blisters	39
Total Area	16342.27mm^2
%Brown	57.4%
Size of Blisters	
Average	419.03mm^2
Max	13010.02mm^2
Median	14.46mm^2
Min	3.84mm^2

Blister Analysis - based on Dynamic L*<56	
Total Blisters	41
Total Area	16589.87mm^2
%Brown	58.3%
Size of Blisters	
Average	404.63mm^2
Max	13145.07mm^2
Median	12.81mm^2
Min	3.66mm^2

Pizza 4 - Cooking Results

Conditions:	
Oven Set Point Temperature	340°C
Actual Oven Temperature	265°C
Cooking Time	16 minutes
Fan Speed	10
Heat Transfer Coefficient	29.8W/m^2
Pizza Characteristics:	
Pizza Base	355.5g
Sauce	80.47g
Cheese	240.45g
Mass Loss	78.92g
Percentage Mass Loss	11.7%
Colour Analysis:	
Lab L*	49.71
StdDev L*	18.33
Lab a*	18.3
StdDev a*	11.14
Lab b*	38.41
StdDev b*	16.09

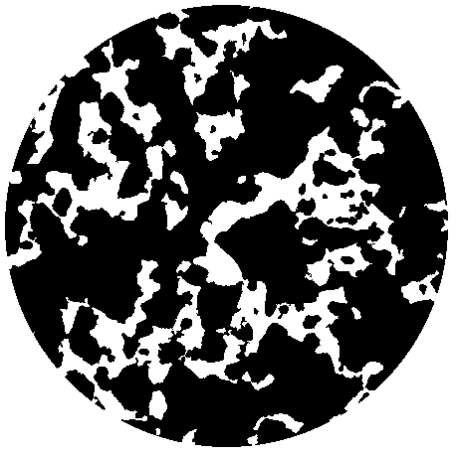

Blister Analysis - based on a*>10	
Total Blisters	22
Total Area	20975.64mm^2
%Brown	73.7%
Size of Blisters	
Average	953.44mm^2
Max	20417.13mm^2
Median	10.71mm^2
Min	3.84mm^2

Blister Analysis - based on L*<55	
Total Blisters	43
Total Area	15596.72mm^2
%Brown	54.8%
Size of Blisters	
Average	362.71mm^2
Max	6381.39mm^2
Median	50.33mm^2
Min	3.84mm^2

Blister Analysis - based on Dynamic L*<57	
Total Blisters	41
Total Area	16291.58mm^2
%Brown	57.2%
Size of Blisters	
Average	397.36mm^2
Max	6842.00mm^2
Median	52.34mm^2
Min	3.66mm^2

Pizza 5 - Cooking Results

Conditions:	
Oven Set Point Temperature	300°C
Actual Oven Temperature	235°C
Cooking Time	20 minutes
Fan Speed	10
Heat Transfer Coefficient	29.8W/m^2
Pizza Characteristics:	
Pizza Base	348.8g
Sauce	80.79g
Cheese	240.65g
Mass Loss	90.44g
Percentage Mass Loss	13.5%
Colour Analysis:	
Lab L*	49.95
StdDev L*	16.78
Lab a*	20.8
StdDev a*	10.43
Lab b*	40.32
StdDev b*	15.8

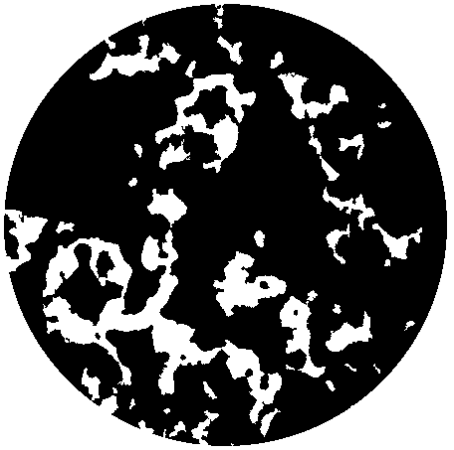

Blister Analysis - based on a*>10	
Total Blisters	6
Total Area	23262.59mm^2
%Brown	81.7%
Size of Blisters	
Average	3877.10mm^2
Max	23155.54mm^2
Median	7.78mm^2
Min	3.66mm^2

Blister Analysis - based on L*<55	
Total Blisters	41
Total Area	15079.57mm^2
%Brown	53.0%
Size of Blisters	
Average	367.79mm^2
Max	4206.44mm^2
Median	46.67mm^2
Min	3.66mm^2

Blister Analysis - based on Dynamic L*<57	
Total Blisters	43
Total Area	15879.28mm^2
%Brown	55.8%
Size of Blisters	
Average	369.29mm^2
Max	4365.65mm^2
Median	26.90mm^2
Min	3.84mm^2

Pizza 6 - Cooking Results

Conditions:	
Oven Set Point Temperature	320°C
Actual Oven Temperature	250°C
Cooking Time	18 minutes
Fan Speed	10
Heat Transfer Coefficient	29.8W/m^2
Pizza Characteristics:	
Pizza Base	335.8g
Sauce	80.10g
Cheese	240.9g
Mass Loss	86.4g
Percentage Mass Loss	13.2%
Colour Analysis:	
Lab L*	50.35
StdDev L*	17.73
Lab a*	18.57
StdDev a*	10.66
Lab b*	39.83
StdDev b*	16.36

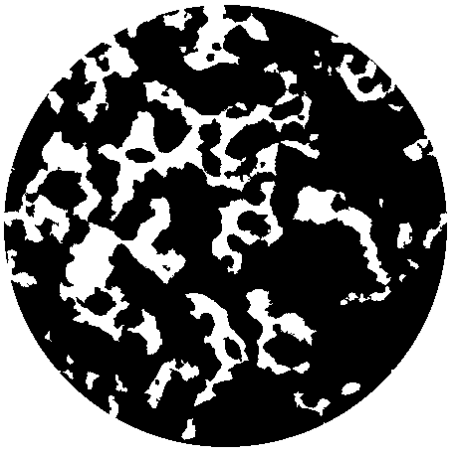

Blister Analysis - based on a*>10	
Total Blisters	12
Total Area	21729.60mm^2
%Brown	76.3%
Size of Blisters	
Average	1810.80mm^2
Max	21223.24mm^2
Median	32.57mm^2
Min	3.66mm^2

Blister Analysis - based on L*<55	
Total Blisters	43
Total Area	14775.05mm^2
%Brown	51.9%
Size of Blisters	
Average	343.61mm^2
Max	9847.41mm^2
Median	25.80mm^2
Min	3.66mm^2

Blister Analysis - based on Dynamic L*<57	
Total Blisters	41
Total Area	15575.86mm^2
%Brown	54.7%
Size of Blisters	
Average	379.90mm^2
Max	11552.42mm^2
Median	24.52mm^2
Min	3.66mm^2

Pizza 7 - Cooking Results

Conditions:	
Oven Set Point Temperature	360°C
Actual Oven Temperature	281°C
Cooking Time	14 minutes
Fan Speed	5
Heat Transfer Coefficient	29.8W/m^2
Pizza Characteristics:	
Pizza Base	331.1g
Sauce	80.0g
Cheese	240.57g
Mass Loss	75.57g
Percentage Mass Loss	11.6%
Colour Analysis:	
Lab L*	51.48
StdDev L*	18.62
Lab a*	16.61
StdDev a*	11.42
Lab b*	39.22
StdDev b*	15.58

Blister Analysis - based on a*>10	
Total Blisters	41
Total Area	19433.32mm^2
%Brown	68.3%
Size of Blisters	
Average	473.98mm^2
Max	16282.24mm^2
Median	12.26mm^2
Min	3.84mm^2

Blister Analysis - based on L*<55	
Total Blisters	44
Total Area	14175.18mm^2
%Brown	49.8%
Size of Blisters	
Average	322.16mm^2
Max	4504.00mm^2
Median	38.16mm^2
Min	4.39mm^2

Blister Analysis - based on Dynamic L*<58	
Total Blisters	45
Total Area	15181.31mm^2
%Brown	53.3%
Size of Blisters	
Average	337.36mm^2
Max	11663.87mm^2
Median	23.24mm^2
Min	3.66mm^2

Pizza 8 - Cooking Results

Conditions:	
Oven Set Point Temperature	360°C
Actual Oven Temperature	281°C
Cooking Time	14 minutes
Fan Speed	10
Heat Transfer Coefficient	29.8W/m^2
Pizza Characteristics:	
Pizza Base	330.70g
Sauce	80.30g
Cheese	241.30g
Mass Loss	78.72g
Percentage Mass Loss	12.1%
Colour Analysis:	
Lab L*	52.36
StdDev L*	18.68
Lab a*	16.93
StdDev a*	11.33
Lab b*	41.22
StdDev b*	16.42

Blister Analysis - based on a*>10	
Total Blisters	25
Total Area	19858.98mm^2
%Brown	69.8%
Size of Blisters	
Average	794.36mm^2
Max	16721.99mm^2
Median	16.84mm^2
Min	4.21mm^2

Blister Analysis - based on L*<55	
Total Blisters	67
Total Area	13239.87mm^2
%Brown	46.5%
Size of Blisters	
Average	197.61mm^2
Max	1873.74mm^2
Median	31.29mm^2
Min	3.66mm^2

Blister Analysis - based on Dynamic L*<58	
Total Blisters	67
Total Area	14304.01mm^2
%Brown	50.2%
Size of Blisters	
Average	213.49mm^2
Max	2288.05mm^2
Median	22.33mm^2
Min	3.66mm^2

Pizza 9 - Cooking Results

Conditions:	
Oven Set Point Temperature	360°C
Actual Oven Temperature	281°C
Cooking Time	14 minutes
Fan Speed	7.5
Heat Transfer Coefficient	29.8W/m^2
Pizza Characteristics:	
Pizza Base	331.5g
Sauce	80.06g
Cheese	240.17g
Mass Loss	72.15g
Percentage Mass Loss	11.1%
Colour Analysis:	
Lab L*	53.23
StdDev L*	20.1
Lab a*	14.4
StdDev a*	11.74
Lab b*	39.88
StdDev b*	16.33

Blister Analysis - based on a*>10	
Total Blisters	57
Total Area	17487.30mm^2
%Brown	61.4%
Size of Blisters	
Average	306.79mm^2
Max	9948.98mm^2
Median	19.40mm^2
Min	3.66mm^2

Blister Analysis - based on L*<55	
Total Blisters	63
Total Area	13343.26mm^2
%Brown	46.9%
Size of Blisters	
Average	211.80mm^2
Max	2499.23mm^2
Median	41.54mm^2
Min	3.84mm^2

Blister Analysis - based on Dynamic L*<59	
Total Blisters	65
Total Area	14579.06mm^2
%Brown	51.2%
Size of Blisters	
Average	224.29mm^2
Max	3424.11mm^2
Median	21.23mm^2
Min	3.66mm^2

Pizza 10 - Cooking Results

Conditions:	
Oven Set Point Temperature	370°C
Actual Oven Temperature	288°C
Cooking Time	14 minutes
Fan Speed	10
Heat Transfer Coefficient	29.8W/m^2
Pizza Characteristics:	
Pizza Base	339.4g
Sauce	80.32g
Cheese	240.89g
Mass Loss	60.41g
Percentage Mass Loss	9.1%
Colour Analysis:	
Lab L*	54.54
StdDev L*	20.11
Lab a*	15.03
StdDev a*	12.02
Lab b*	40.76
StdDev b*	16.09

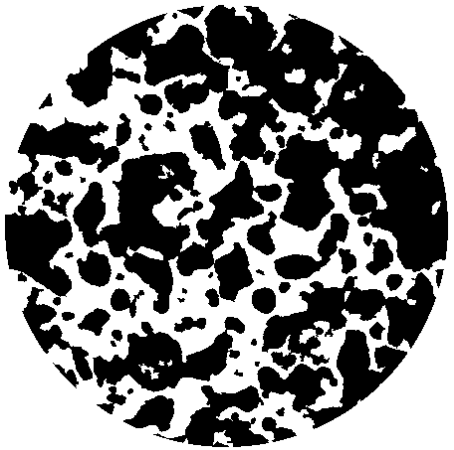

Blister Analysis - based on a*>10	
Total Blisters	58
Total Area	17644.13mm^2
%Brown	62.0%
Size of Blisters	
Average	304.21mm^2
Max	9678.87mm^2
Median	32.30mm^2
Min	3.84mm^2

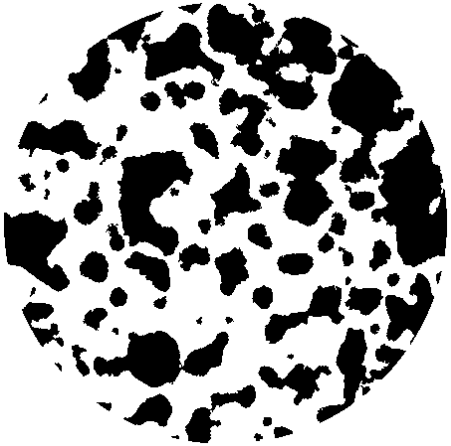

Blister Analysis - based on L*<55	
Total Blisters	70
Total Area	12656.83mm^2
%Brown	44.5%
Size of Blisters	
Average	180.81mm^2
Max	2351.00mm^2
Median	49.96mm^2
Min	3.66mm^2

Blister Analysis - based on Dynamic L*<59	
Total Blisters	76
Total Area	13886.22mm^2
%Brown	48.8%
Size of Blisters	
Average	182.71mm^2
Max	4819.49mm^2
Median	28.91mm^2
Min	3.66mm^2

Pizza 11 - Cooking Results

Conditions:	
Oven Set Point Temperature	320°C
Actual Oven Temperature	250°C
Cooking Time	16 minutes
Fan Speed	10
Heat Transfer Coefficient	29.8W/m^2
Pizza Characteristics:	
Pizza Base	335.7g
Sauce	80.71g
Cheese	240.65g
Mass Loss	78.36g
Percentage Mass Loss	11.9%
Colour Analysis:	
Lab L*	55.86
StdDev L*	18.59
Lab a*	15.28
StdDev a*	12.27
Lab b*	43.06
StdDev b*	14.95

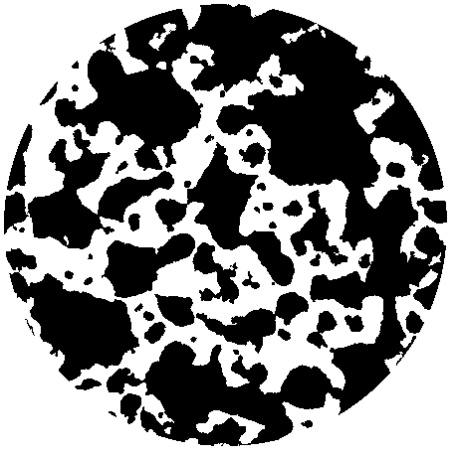

Blister Analysis - based on a*>10	
Total Blisters	49
Total Area	17773.33mm^2
%Brown	62.4%
Size of Blisters	
Average	362.72mm^2
Max	11108.83mm^2
Median	22.88mm^2
Min	3.84mm^2

Blister Analysis - based on L*<55	
Total Blisters	57
Total Area	12384.53mm^2
%Brown	43.5%
Size of Blisters	
Average	217.27mm^2
Max	4300.50mm^2
Median	34.59mm^2
Min	3.84mm^2

Blister Analysis - based on Dynamic L*<60	
Total Blisters	51
Total Area	13963.63mm^2
%Brown	49.1%
Size of Blisters	
Average	273.80mm^2
Max	4976.50mm^2
Median	45.20mm^2
Min	3.66mm^2

Pizza 12 - Cooking Results

Conditions:	
Oven Set Point Temperature	300°C
Actual Oven Temperature	235°C
Cooking Time	18 minutes
Fan Speed	10
Heat Transfer Coefficient	29.8W/m^2
Pizza Characteristics:	
Pizza Base	335.0g
Sauce	80.5g
Cheese	240.9g
Mass Loss	80g
Percentage Mass Loss	12.2%
Colour Analysis:	
Lab L*	56.14
StdDev L*	17.02
Lab a*	16.97
StdDev a*	12.55
Lab b*	44.5
StdDev b*	13.77

Blister Analysis - based on a*>10	
Total Blisters	37
Total Area	18353.25mm^2
%Brown	64.5%
Size of Blisters	
Average	496.03mm^2
Max	13649.97mm^2
Median	10.43mm^2
Min	3.66mm^2

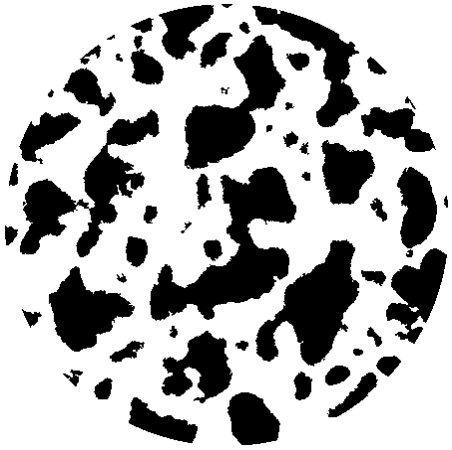

Blister Analysis - based on L*<55	
Total Blisters	59
Total Area	11744.03mm^2
%Brown	41.3%
Size of Blisters	
Average	199.05mm^2
Max	1671.34mm^2
Median	35.69mm^2
Min	3.84mm^2

Blister Analysis - based on Dynamic L*<60	
Total Blisters	58
Total Area	13767.64mm^2
%Brown	48.4%
Size of Blisters	
Average	237.37mm^2
Max	3257.22mm^2
Median	39.89mm^2
Min	3.66mm^2

Pizza 13 - Cooking Results

Conditions:	
Oven Set Point Temperature	300°C
Actual Oven Temperature	235°C
Cooking Time	18 minutes
Fan Speed	10
Heat Transfer Coefficient	29.8W/m^2
Pizza Characteristics:	
Pizza Base	337.4g
Sauce	80.25g
Cheese	240.14g
Mass Loss	74.89g
Percentage Mass Loss	11.4%
Colour Analysis:	
Lab L*	58.43
StdDev L*	18.77
Lab a*	14.62
StdDev a*	13.81
Lab b*	44.1
StdDev b*	13.46

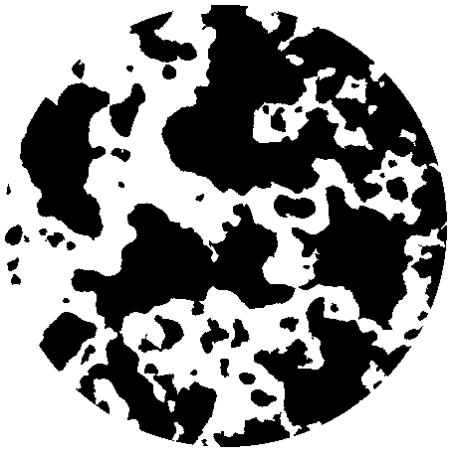

Blister Analysis - based on a*>10	
Total Blisters	46
Total Area	16637.99mm^2
%Brown	58.4%
Size of Blisters	
Average	361.70mm^2
Max	7480.67mm^2
Median	24.25mm^2
Min	3.66mm^2

Blister Analysis - based on L*<55	
Total Blisters	39
Total Area	11586.83mm^2
%Brown	40.7%
Size of Blisters	
Average	297.10mm^2
Max	3016.02mm^2
Median	34.59mm^2
Min	4.03mm^2

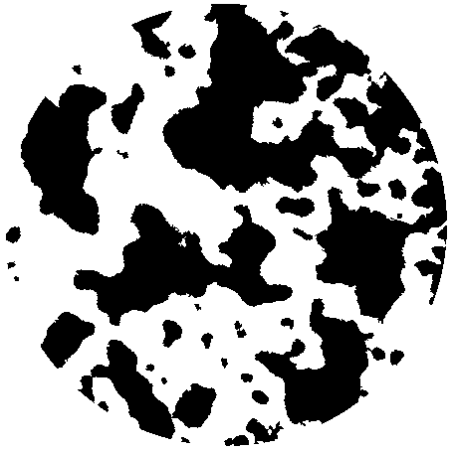

Blister Analysis - based on Dynamic L*<62	
Total Blisters	39
Total Area	13783.74mm^2
%Brown	48.4%
Size of Blisters	
Average	353.43mm^2
Max	4724.88mm^2
Median	21.96mm^2
Min	3.66mm^2

Pizza 14 - Cooking Results

Conditions:	
Oven Set Point Temperature	280°C
Actual Oven Temperature	220°C
Cooking Time	20 minutes
Fan Speed	10
Heat Transfer Coefficient	29.8W/m^2
Pizza Characteristics:	
Pizza Base	344.2g
Sauce	78.29g
Cheese	240.21g
Mass Loss	86.1g
Percentage Mass Loss	13.0%
Colour Analysis:	
Lab L*	59.69
StdDev L*	18.13
Lab a*	14.16
StdDev a*	13.2
Lab b*	46.26
StdDev b*	13.78

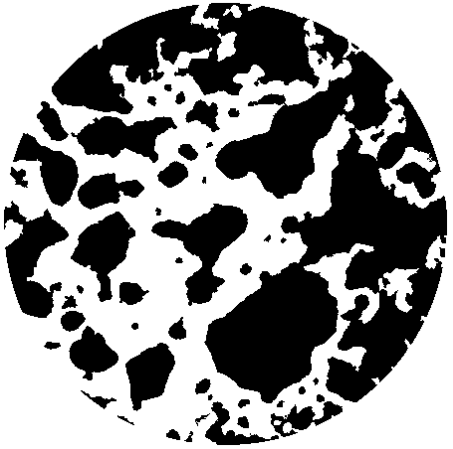

Blister Analysis - based on a*>10	
Total Blisters	51
Total Area	16186.17mm^2
%Brown	56.9%
Size of Blisters	
Average	317.38mm^2
Max	8170.77mm^2
Median	17.93mm^2
Min	4.03mm^2

Blister Analysis - based on L*<55	
Total Blisters	42
Total Area	10527.44mm^2
%Brown	37.0%
Size of Blisters	
Average	37.14mm^2
Max	1841.35mm^2
Median	47.03mm^2
Min	3.84mm^2

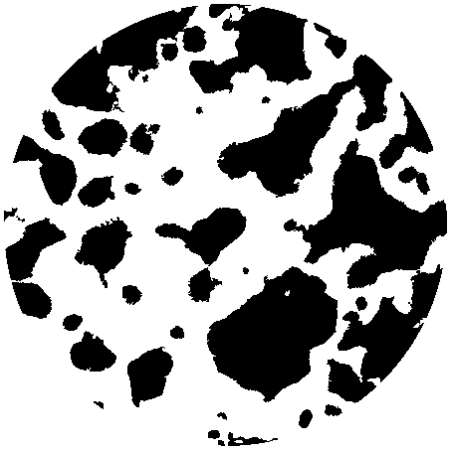

Blister Analysis - based on Dynamic L*<62	
Total Blisters	40
Total Area	12690.14mm^2
%Brown	44.6%
Size of Blisters	
Average	317.25mm^2
Max	3009.44mm^2
Median	64.78mm^2
Min	3.66mm^2

Pizza 15 - Cooking Results

Cooking Time	12 minutes
Fan Speed	10
Heat Transfer Coefficient	29.8W/m^2
Pizza Characteristics:	
Pizza Base	332.1g
Sauce	80.84g
Cheese	240.39g
Mass Loss	61.03g
Percentage Mass Loss	9.3%
Colour Analysis:	
Lab L*	59.98
StdDev L*	19.38
Lab a*	12.63
StdDev a*	13.06
Lab b*	43.48
StdDev b*	13.74

Blister Analysis - based on a*>10	
Total Blisters	87
Total Area	15154.23mm^2
%Brown	53.2%
Size of Blisters	
Average	174.19mm^2
Max	2573.16mm^2
Median	18.12mm^2
Min	3.66mm^2

Blister Analysis - based on L*<55	
Total Blisters	102
Total Area	6569.33mm^2
%Brown	23.1%
Size of Blisters	
Average	64.41mm^2
Max	531.07mm^2
Median	25.07mm^2
Min	3.66mm^2

Blister Analysis - based on Dynamic L*<62	
Total Blisters	82
Total Area	12265.94mm^2
%Brown	43.1%
Size of Blisters	
Average	149.58mm^2
Max	1445.33mm^2
Median	46.48mm^2
Min	3.66mm^2

Pizza 16 - Cooking Results

Conditions:	
Oven Set Point Temperature	360°C
Actual Oven Temperature	281°C
Cooking Time	12 minutes
Fan Speed	10
Heat Transfer Coefficient	29.8W/m^2
Pizza Characteristics:	
Pizza Base	338.6g
Sauce	80.42g
Cheese	240.20g
Mass Loss	55.45g
Percentage Mass Loss	8.4%
Colour Analysis:	
Lab L*	61.54
StdDev L*	18.74
Lab a*	12.53
StdDev a*	13.21
Lab b*	44.38
StdDev b*	12.96

Blister Analysis - based on a*>10	
Total Blisters	74
Total Area	14941.58mm^2
%Brown	52.5%
Size of Blisters	
Average	201.91mm^2
Max	2281.46mm^2
Median	30.65mm^2
Min	4.39mm^2

Blister Analysis - based on L*<55	
Total Blisters	77
Total Area	9410.41mm^2
%Brown	33.1%
Size of Blisters	
Average	122.21mm^2
Max	772.99mm^2
Median	52.34mm^2
Min	3.66mm^2

Blister Analysis - based on Dynamic L*<63	
Total Blisters	76
Total Area	11964.91mm^2
%Brown	42.0%
Size of Blisters	
Average	157.43mm^2
Max	1221.16mm^2
Median	42.36mm^2
Min	3.66mm^2

Pizza 17 - Cooking Results

Conditions:	
Oven Set Point Temperature	340°C
Actual Oven Temperature	265°C
Cooking Time	12 minutes
Fan Speed	10
Heat Transfer Coefficient	29.8W/m^2
Pizza Characteristics:	
Pizza Base	342.7g
Sauce	80.85g
Cheese	240.26g
Mass Loss	53.71g
Percentage Mass Loss	8.1%
Colour Analysis:	
Lab L*	62.38
StdDev L*	18.09
Lab a*	12.12
StdDev a*	13.5
Lab b*	44.49
StdDev b*	11.37

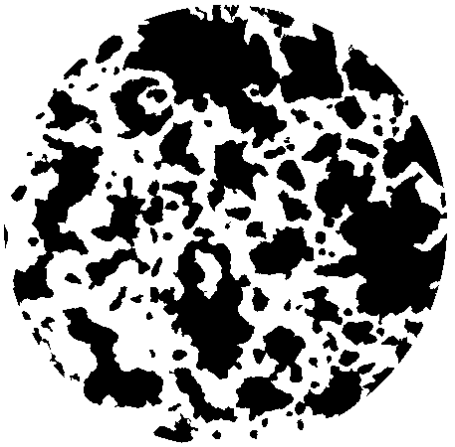

Blister Analysis - based on a*>10	
Total Blisters	92
Total Area	14873.87mm^2
%Brown	52.2%
Size of Blisters	
Average	161.67mm^2
Max	2835.04mm^2
Median	19.76mm^2
Min	3.66mm^2

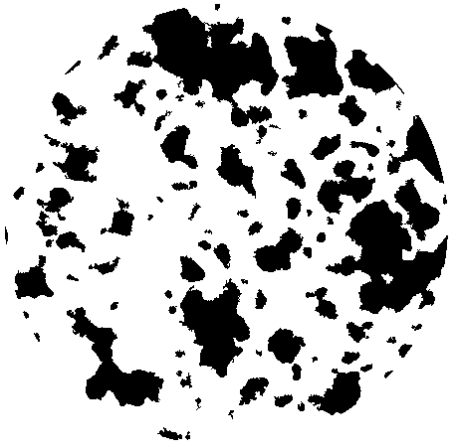

Blister Analysis - based on L*<55	
Total Blisters	93
Total Area	9033.61mm^2
%Brown	31.7%
Size of Blisters	
Average	97.14mm^2
Max	1547.45mm^2
Median	15.92mm^2
Min	3.66mm^2

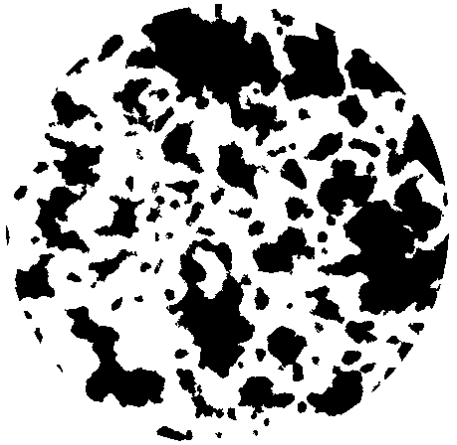

Blister Analysis - based on Dynamic L*<64	
Total Blisters	88
Total Area	12286.07mm^2
%Brown	43.2%
Size of Blisters	
Average	139.61mm^2
Max	2592.20mm^2
Median	19.95mm^2
Min	3.66mm^2

Pizza 18 - Cooking Results

Conditions:	
Oven Set Point Temperature	300°C
Actual Oven Temperature	235°C
Cooking Time	15 minutes
Fan Speed	10
Heat Transfer Coefficient	29.8W/m^2
Pizza Characteristics:	
Pizza Base	337.9g
Sauce	80.52g
Cheese	240.51g
Mass Loss	56.83g
Percentage Mass Loss	8.6%
Colour Analysis:	
Lab L*	65.3
StdDev L*	16.41
Lab a*	11.44
StdDev a*	13.83
Lab b*	48.21
StdDev b*	10.6

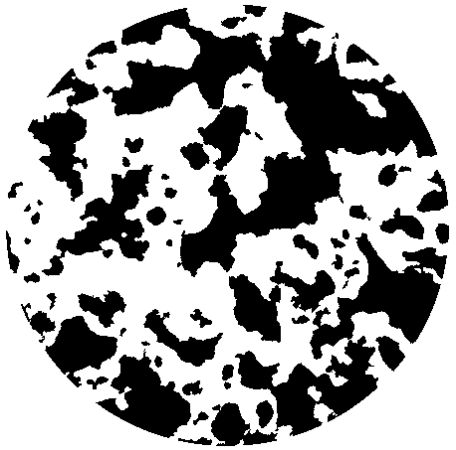

Blister Analysis - based on a*>10	
Total Blisters	62
Total Area	13677.03mm^2
%Brown	48%
Size of Blisters	
Average	220.60mm^2
Max	5287.97mm^2
Median	26.54mm^2
Min	3.84mm^2

Blister Analysis - based on L*<55	
Total Blisters	43
Total Area	6965.90mm^2
%Brown	24.5%
Size of Blisters	
Average	162.00mm^2
Max	1710.68mm^2
Median	45.57mm^2
Min	4.21mm^2

Blister Analysis - based on Dynamic L*<65	
Total Blisters	54
Total Area	10452.41mm^2
%Brown	36.7%
Size of Blisters	
Average	193.56mm^2
Max	3252.83mm^2
Median	42.46mm^2
Min	3.84mm^2

Pizza 19 - Cooking Results

Conditions:	
Oven Set Point Temperature	300°C
Actual Oven Temperature	235°C
Cooking Time	16 minutes
Fan Speed	10
Heat Transfer Coefficient	29.8W/m^2
Pizza Characteristics:	
Pizza Base	328.3g
Sauce	80.83g
Cheese	240.65g
Mass Loss	59.38g
Percentage Mass Loss	9.1%
Colour Analysis:	
Lab L*	67.19
StdDev L*	16.19
Lab a*	10.33
StdDev a*	13.74
Lab b*	49.35
StdDev b*	10.32

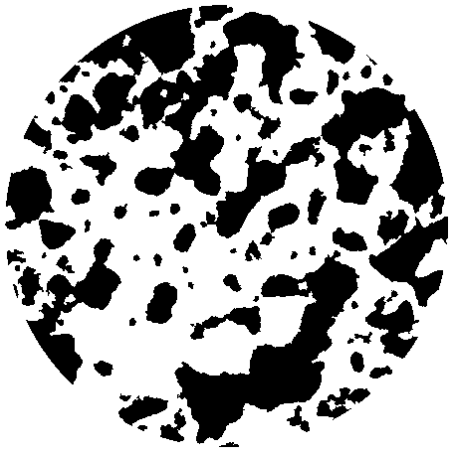

Blister Analysis - based on a*>10	
Total Blisters	74
Total Area	12660.86mm^2
%Brown	44.5%
Size of Blisters	
Average	171.09mm^2
Max	3296.93mm^2
Median	27.82mm^2
Min	3.66mm^2

Blister Analysis - based on L*<55	
Total Blisters	50
Total Area	6340.04mm^2
%Brown	22.3%
Size of Blisters	
Average	126.80mm^2
Max	1222.62mm^2
Median	56.55mm^2
Min	4.76mm^2

Blister Analysis - based on Dynamic L*<67	
Total Blisters	64
Total Area	10144.24mm^2
%Brown	35.6%
Size of Blisters	
Average	158.50mm^2
Max	1855.44mm^2
Median	37.33mm^2
Min	3.66mm^2

Pizza 20 - Cooking Results

Conditions:	
Oven Set Point Temperature	300°C
Actual Oven Temperature	235°C
Cooking Time	15 minutes
Fan Speed	10
Heat Transfer Coefficient	29.8W/m^2
Pizza Characteristics:	
Pizza Base	330.5g
Sauce	80.06g
Cheese	240.34g
Mass Loss	61.6g
Percentage Mass Loss	9.5%
Colour Analysis:	
Lab L*	67.77
StdDev L*	15.54
Lab a*	8.85
StdDev a*	13.69
Lab b*	48.94
StdDev b*	9.56

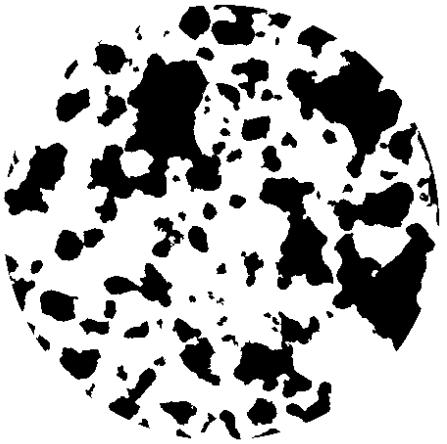

Blister Analysis - based on a*>10	
Total Blisters	82
Total Area	11077.36mm^2
%Brown	38.9%
Size of Blisters	
Average	135.09mm^2
Max	1940.53mm^2
Median	28.73mm^2
Min	3.66mm^2

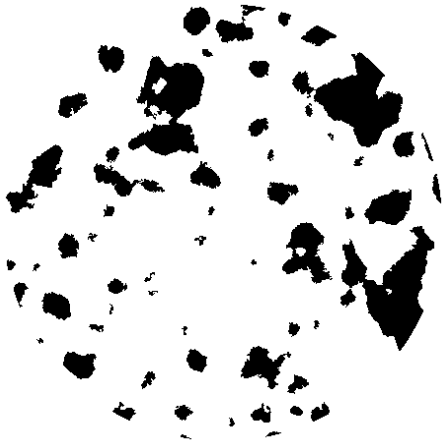

Blister Analysis - based on L*<55	
Total Blisters	61
Total Area	5565.03mm^2
%Brown	19.5%
Size of Blisters	
Average	91.23mm^2
Max	904.57mm^2
Median	27.45mm^2
Min	4.03mm^2

Blister Analysis - based on Dynamic L*<67	
Total Blisters	67
Total Area	9431.27mm^2
%Brown	33.1%
Size of Blisters	
Average	140.77mm^2
Max	1309.91mm^2
Median	47.40mm^2
Min	4.026mm^2

Pizza 21 - Cooking Results

Conditions:	
Oven Set Point Temperature	370°C
Actual Oven Temperature	288°C
Cooking Time	10 minutes
Fan Speed	10
Heat Transfer Coefficient	29.8W/m^2
Pizza Characteristics:	
Pizza Base	335.2g
Sauce	80.38g
Cheese	240.04g
Mass Loss	49.42g
Percentage Mass Loss	7.5%
Colour Analysis:	
Lab L*	67.82
StdDev L*	17.8
Lab a*	7.61
StdDev a*	13.5
Lab b*	44.43
StdDev b*	10.67

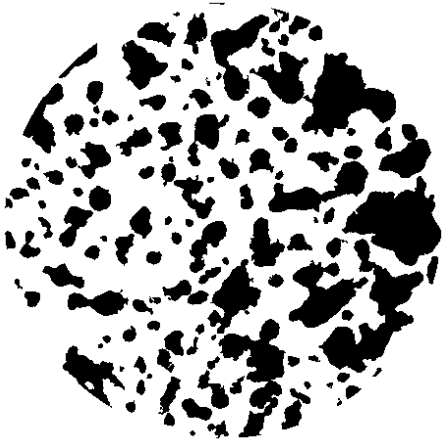

Blister Analysis - based on a*>10	
Total Blisters	126
Total Area	10774.49mm^2
%Brown	37.8%
Size of Blisters	
Average	85.51mm^2
Max	1074.03mm^2
Median	30.38mm^2
Min	3.66mm^2

Blister Analysis - based on L*<55	
Total Blisters	56
Total Area	1186.94mm^2
%Brown	4.2%
Size of Blisters	
Average	21.20mm^2
Max	176.41mm^2
Median	11.25mm^2
Min	3.84mm^2

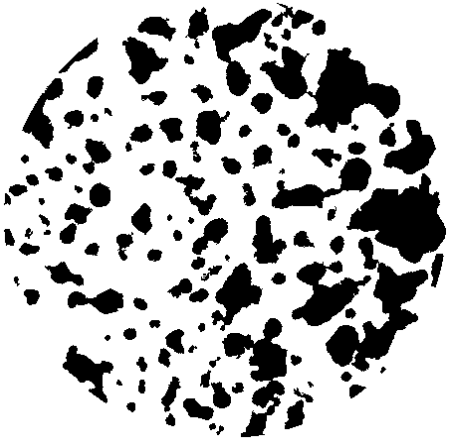

Blister Analysis - based on Dynamic L*<67	
Total Blisters	115
Total Area	9552.78mm^2
%Brown	33.6%
Size of Blisters	
Average	83.07mm^2
Max	1030.11mm^2
Median	29.28mm^2
Min	3.84mm^2

Pizza 22 - Cooking Results

Conditions:	
Oven Set Point Temperature	320°C
Actual Oven Temperature	250°C
Cooking Time	14 minutes
Fan Speed	10
Heat Transfer Coefficient	29.8W/m^2

Pizza Characteristics:	
Pizza Base	331.1g
Sauce	80.58g
Cheese	240.35g
Mass Loss	57.23g
Percentage Mass Loss	8.8%

Colour Analysis:	
Lab L*	70.45
StdDev L*	16.3
Lab a*	7.29
StdDev a*	13.87
Lab b*	48.46
StdDev b*	9.76

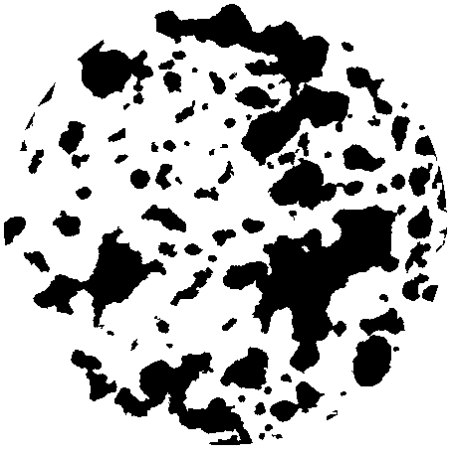

Blister Analysis - based on a*>10	
Total Blisters	91
Total Area	10281.12mm^2
%Brown	36.1%
Size of Blisters	
Average	112.98mm^2
Max	2202.41mm^2
Median	25.07mm^2
Min	3.84mm^2

Blister Analysis - based on L*<55	
Total Blisters	53
Total Area	5019.51mm^2
%Brown	17.6%
Size of Blisters	
Average	94.71mm^2
Max	1442.59mm^2
Median	32.94mm^2
Min	4.21mm^2

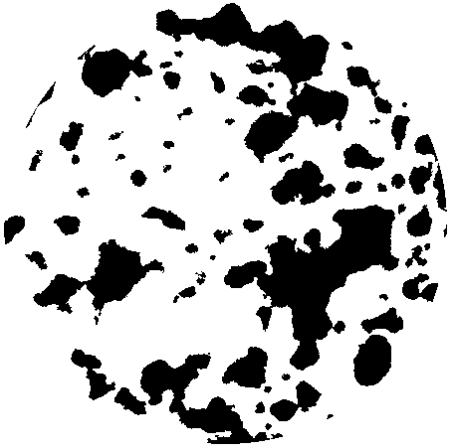

Blister Analysis - based on Dynamic L*<68	
Total Blisters	71
Total Area	8791.69mm^2
%Brown	30.9%
Size of Blisters	
Average	123.83mm^2
Max	2043.74mm^2
Median	24.34mm^2
Min	3.66mm^2

Pizza 23 - Cooking Results

Conditions:	
Oven Set Point Temperature	360°C
Actual Oven Temperature	281°C
Cooking Time	10 minutes
Fan Speed	10
Heat Transfer Coefficient	29.8W/m^2
Pizza Characteristics:	
Pizza Base	340.6g
Sauce	81.52g
Cheese	241.42g
Mass Loss	43.44g
Percentage Mass Loss	6.5%
Colour Analysis:	
Lab L*	70.76
StdDev L*	17.53
Lab a*	5.64
StdDev a*	13.28
Lab b*	43.18
StdDev b*	9.83

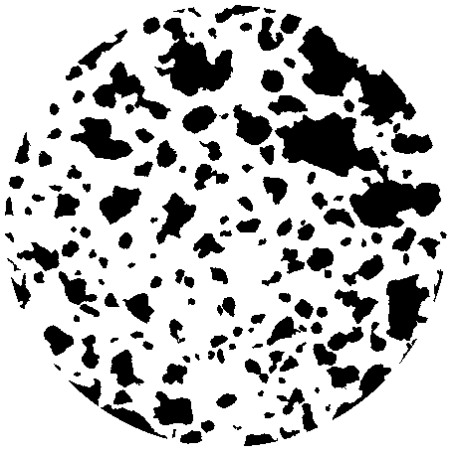

Blister Analysis - based on a*>10	
Total Blisters	161
Total Area	9527.71mm^2
%Brown	33.5%
Size of Blisters	
Average	59.18mm^2
Max	1315.59mm^2
Median	22.51mm^2
Min	3.66mm^2

Blister Analysis - based on L*<55	
Total Blisters	113
Total Area	5397.95mm^2
%Brown	19.0%
Size of Blisters	
Average	47.77mm^2
Max	562.73mm^2
Median	18.48mm^2
Min	3.66mm^2

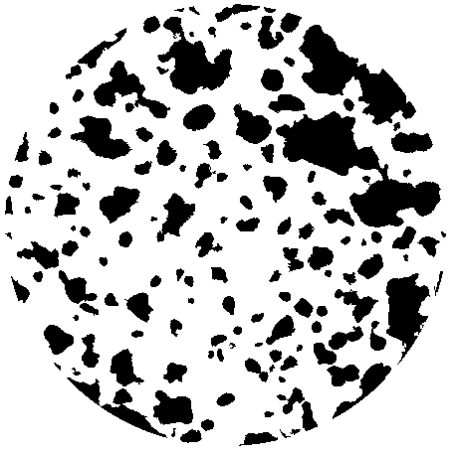

Blister Analysis - based on Dynamic L*<69	
Total Blisters	143
Total Area	8967.00mm^2
%Brown	31.5%
Size of Blisters	
Average	62.71mm^2
Max	1291.43mm^2
Median	23.42mm^2
Min	3.66mm^2

Pizza 24 - Cooking Results

Conditions:	
Oven Set Point Temperature	280°C
Actual Oven Temperature	220°C
Cooking Time	18 minutes
Fan Speed	10
Heat Transfer Coefficient	29.8W/m^2
Pizza Characteristics:	
Pizza Base	343.1g
Sauce	80.57g
Cheese	240.06g
Mass Loss	60.03g
Percentage Mass Loss	9.0%
Colour Analysis:	
Lab L*	72.03
StdDev L*	15.28
Lab a*	6.5
StdDev a*	14.15
Lab b*	50.24
StdDev b*	9.01

Blister Analysis - based on a*>10	
Total Blisters	67
Total Area	9546.74mm^2
%Brown	33.5%
Size of Blisters	
Average	142.49mm^2
Max	2461.53mm^2
Median	19.22mm^2
Min	3.66mm^2

Blister Analysis - based on L*<55	
Total Blisters	33
Total Area	4205.89mm^2
%Brown	14.8%
Size of Blisters	
Average	127.45mm^2
Max	1118.13mm^2
Median	37.70mm^2
Min	4.76mm^2

Blister Analysis - based on Dynamic L*<69	
Total Blisters	48
Total Area	8229.33mm^2
%Brown	28.9%
Size of Blisters	
Average	171.44mm^2
Max	1614.24mm^2
Median	24.06mm^2
Min	3.66mm^2

Pizza 25 - Cooking Results

Conditions:	
Oven Set Point Temperature	320°C
Actual Oven Temperature	250°C
Cooking Time	12 minutes
Fan Speed	10
Heat Transfer Coefficient	29.8W/m^2
Pizza Characteristics:	
Pizza Base	329.9g
Sauce	80.25g
Cheese	240.40g
Mass Loss	43.93g
Percentage Mass Loss	6.8%
Colour Analysis:	
Lab L*	73.74
StdDev L*	14.66
Lab a*	4.83
StdDev a*	12.95
Lab b*	48.3
StdDev b*	9.07

Blister Analysis - based on a*>10	
Total Blisters	110
Total Area	8455.70mm^2
%Brown	29.7%
Size of Blisters	
Average	76.87mm^2
Max	674.36mm^2
Median	29.10mm^2
Min	3.66mm^2

Blister Analysis - based on L*<55	
Total Blisters	66
Total Area	3192.80mm^2
%Brown	11.2%
Size of Blisters	
Average	48.38mm^2
Max	338.55mm^2
Median	29.10mm^2
Min	3.66mm^2

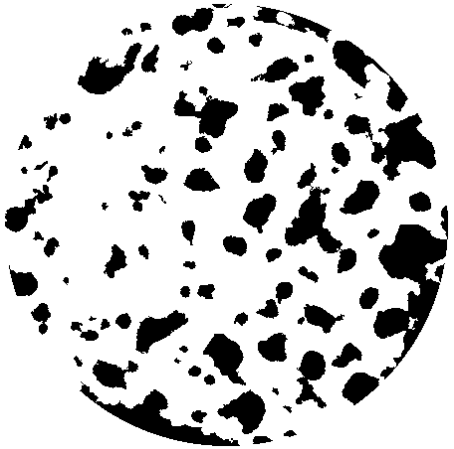

Blister Analysis - based on Dynamic L*<70	
Total Blisters	92
Total Area	7498.24mm^2
%Brown	26.3%
Size of Blisters	
Average	81.50mm^2
Max	919.758mm^2
Median	33.855mm^2
Min	3.66mm^2

Pizza 26 - Cooking Results

Conditions:	
Oven Set Point Temperature	340°C
Actual Oven Temperature	265°C
Cooking Time	10 minutes
Fan Speed	10
Heat Transfer Coefficient	29.8W/m^2

Pizza Characteristics:	
Pizza Base	345.8g
Sauce	80.11g
Cheese	240.34g
Mass Loss	40.05g
Percentage Mass Loss	6.0%

Colour Analysis:	
Lab L*	75.39
StdDev L*	15.37
Lab a*	2.51
StdDev a*	12.4
Lab b*	44.38
StdDev b*	8.94

Blister Analysis - based on a*>10	
Total Blisters	133
Total Area	7280.84mm^2
%Brown	25.6%
Size of Blisters	
Average	54.74mm^2
Max	1009.79mm^2
Median	17.39mm^2
Min	3.66mm^2

Blister Analysis - based on L*<55	
Total Blisters	86
Total Area	3214.58mm^2
%Brown	11.3%
Size of Blisters	
Average	37.38mm^2
Max	341.30mm^2
Median	16.93mm^2
Min	3.84mm^2

Blister Analysis - based on Dynamic L*<71	
Total Blisters	123
Total Area	7106.07mm^2
%Brown	25.0%
Size of Blisters	
Average	57.77mm^2
Max	952.52mm^2
Median	18.67mm^2
Min	3.66mm^2

Pizza 27 - Cooking Results

Conditions:	
Oven Set Point Temperature	300°C
Actual Oven Temperature	235°C
Cooking Time	14 minutes
Fan Speed	10
Heat Transfer Coefficient	29.8W/m^2
Pizza Characteristics:	
Pizza Base	338.8g
Sauce	80.08g
Cheese	240.21g
Mass Loss	47.69g
Percentage Mass Loss	7.2%
Colour Analysis:	
Lab L*	75.48
StdDev L*	12.52
Lab a*	4.11
StdDev a*	12.12
Lab b*	50.13
StdDev b*	8.77

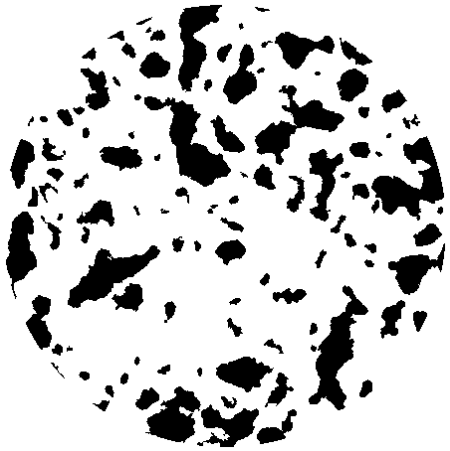

Blister Analysis - based on a*>10	
Total Blisters	107
Total Area	7692.04mm^2
%Brown	27.0%
Size of Blisters	
Average	71.89mm^2
Max	526.13mm^2
Median	19.76mm^2
Min	3.66mm^2

Blister Analysis - based on L*<55	
Total Blisters	51
Total Area	2000.56mm^2
%Brown	7.0%
Size of Blisters	
Average	39.23mm^2
Max	244.12mm^2
Median	17.57mm^2
Min	3.66mm^2

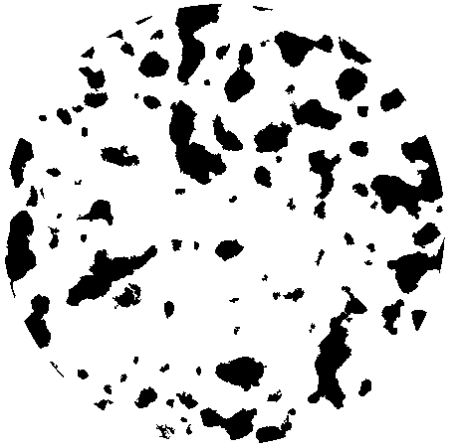

Blister Analysis - based on Dynamic L*<71	
Total Blisters	95
Total Area	6303.98mm^2
%Brown	22.1%
Size of Blisters	
Average	66.36mm^2
Max	504.90mm^2
Median	19.22mm^2
Min	3.66mm^2

Pizza 28 - Cooking Results

Conditions:	
Oven Set Point Temperature	300°C
Actual Oven Temperature	235°C
Cooking Time	14 minutes
Fan Speed	5
Heat Transfer Coefficient	29.8W/m^2
Pizza Characteristics:	
Pizza Base	341.2g
Sauce	80.8g
Cheese	240.92g
Mass Loss	48.12g
Percentage Mass Loss	7.3%
Colour Analysis:	
Lab L*	75.54
StdDev L*	13.66
Lab a*	4.33
StdDev a*	12.39
Lab b*	49.68
StdDev b*	9.01

Blister Analysis - based on a*>10	
Total Blisters	98
Total Area	7589.74mm^2
%Brown	26.7%
Size of Blisters	
Average	77.45mm^2
Max	921.04mm^2
Median	19.58mm^2
Min	3.66mm^2

Blister Analysis - based on L*<55	
Total Blisters	45
Total Area	2591.28mm^2
%Brown	9.1%
Size of Blisters	
Average	57.58mm^2
Max	419.62mm^2
Median	20.31mm^2
Min	3.66mm^2

Blister Analysis - based on Dynamic L*<71	
Total Blisters	86
Total Area	6449.10mm^2
%Brown	22.7%
Size of Blisters	
Average	74.99mm^2
Max	584.50mm^2
Median	19.76mm^2
Min	3.66mm^2

Pizza 29 - Cooking Results

Conditions:	
Oven Set Point Temperature	300°C
Actual Oven Temperature	235°C
Cooking Time	14 minutes
Fan Speed	7.5
Heat Transfer Coefficient	29.8W/m^2
Pizza Characteristics:	
Pizza Base	334.8g
Sauce	80.27g
Cheese	240.42g
Mass Loss	45.79g
Percentage Mass Loss	7.0%
Colour Analysis:	
Lab L*	75.94
StdDev L*	13.79
Lab a*	4.2
StdDev a*	12.6
Lab b*	50.19
StdDev b*	8.49

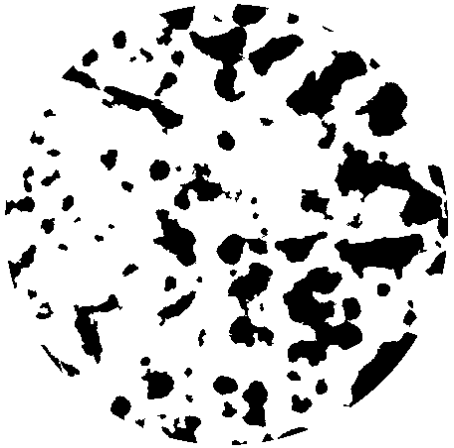

Blister Analysis - based on a*>10	
Total Blisters	86
Total Area	7573.09mm^2
%Brown	26.6%
Size of Blisters	
Average	88.06mm^2
Max	782.33mm^2
Median	26.44mm^2
Min	3.84mm^2

Blister Analysis - based on L*<55	
Total Blisters	54
Total Area	2507.65mm^2
%Brown	8.8%
Size of Blisters	
Average	46.44mm^2
Max	277.61mm^2
Median	20.13mm^2
Min	3.84mm^2

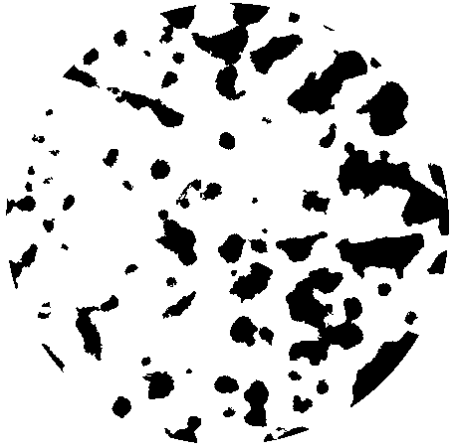

Blister Analysis - based on Dynamic L*<71	
Total Blisters	73
Total Area	6665.96mm^2
%Brown	23.4%
Size of Blisters	
Average	91.31mm^2
Max	786.53mm^2
Median	32.57mm^2
Min	3.66mm^2

Pizza 30 - Cooking Results

Conditions:	
Oven Set Point Temperature	280°C
Actual Oven Temperature	220°C
Cooking Time	15 minutes
Fan Speed	10
Heat Transfer Coefficient	29.8W/m^2
Pizza Characteristics:	
Pizza Base	340.2g
Sauce	80.66g
Cheese	240.34g
Mass Loss	42.2g
Percentage Mass Loss	6.4%
Colour Analysis:	
Lab L*	78.74
StdDev L*	10.04
Lab a*	0.38
StdDev a*	10.33
Lab b*	49.23
StdDev b*	8.45

Blister Analysis - based on a*>10	
Total Blisters	85
Total Area	4620.02mm^2
%Brown	16.2%
Size of Blisters	
Average	54.35mm^2
Max	660.81mm^2
Median	22.14mm^2
Min	3.84mm^2

Blister Analysis - based on L*<55	
Total Blisters	22
Total Area	848.21mm^2
%Brown	3.0%
Size of Blisters	
Average	38.55mm^2
Max	198.74mm^2
Median	26.17mm^2
Min	3.66mm^2

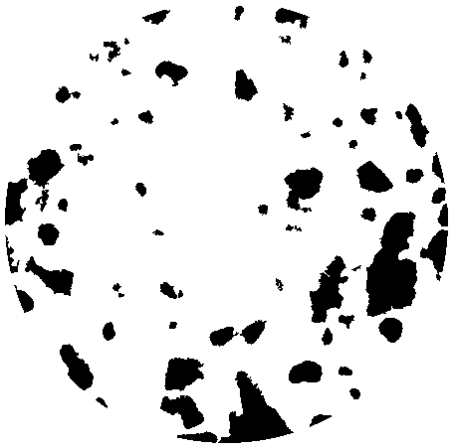

Blister Analysis - based on Dynamic L*<73	
Total Blisters	71
Total Area	4471.97mm^2
%Brown	15.7%
Size of Blisters	
Average	62.99mm^2
Max	673.99mm^2
Median	24.71mm^2
Min	3.84mm^2

Pizza 31 - Cooking Results

Conditions:	
Oven Set Point Temperature	280°C
Actual Oven Temperature	220°C
Cooking Time	16 minutes
Fan Speed	10
Heat Transfer Coefficient	29.8W/m^2
Pizza Characteristics:	
Pizza Base	336.1g
Sauce	80.63g
Cheese	240.09g
Mass Loss	48.52g
Percentage Mass Loss	7.4%
Colour Analysis:	
Lab L*	78.91
StdDev L*	11.76
Lab a*	0.86
StdDev a*	11.23
Lab b*	48.93
StdDev b*	8.68

Blister Analysis - based on a*>10	
Total Blisters	93
Total Area	5039.27mm^2
%Brown	17.7%
Size of Blisters	
Average	54.19mm^2
Max	1405.62mm^2
Median	17.57mm^2
Min	3.66mm^2

Blister Analysis - based on L*<55	
Total Blisters	20
Total Area	1504.63mm^2
%Brown	5.3%
Size of Blisters	
Average	75.23mm^2
Max	917.56mm^2
Median	12.90mm^2
Min	4.03mm^2

Blister Analysis - based on Dynamic L*<73	
Total Blisters	70
Total Area	4826.63mm^2
%Brown	17.0%
Size of Blisters	
Average	68.95mm^2
Max	1415.69mm^2
Median	17.84mm^2
Min	3.66mm^2

Pizza 32 - Cooking Results

Conditions:	
Oven Set Point Temperature	370°C
Actual Oven Temperature	288°C
Cooking Time	8 minutes
Fan Speed	10
Heat Transfer Coefficient	29.8W/m^2
Pizza Characteristics:	
Pizza Base	333.3g
Sauce	80.41g
Cheese	240.26g
Mass Loss	36.67g
Percentage Mass Loss	5.6%
Colour Analysis:	
Lab L*	80.61
StdDev L*	12.06
Lab a*	-1.07
StdDev a*	10.16
Lab b*	42.58
StdDev b*	9.36

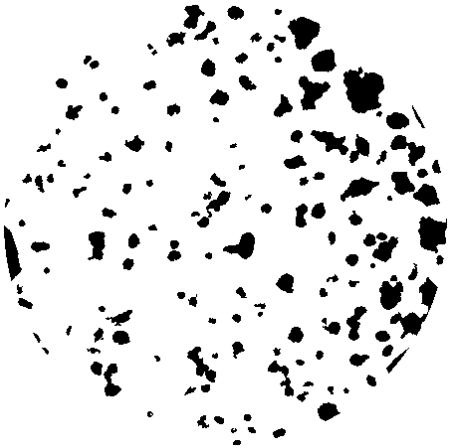

Blister Analysis - based on a*>10	
Total Blisters	152
Total Area	4006.05mm^2
%Brown	14.1%
Size of Blisters	
Average	26.36mm^2
Max	243.94mm^2
Median	13.73mm^2
Min	3.66mm^2

Blister Analysis - based on L*<55	
Total Blisters	106
Total Area	6262.99mm^2
%Brown	22.0%
Size of Blisters	
Average	59.08mm^2
Max	775.01mm^2
Median	25.53mm^2
Min	3.66mm^2

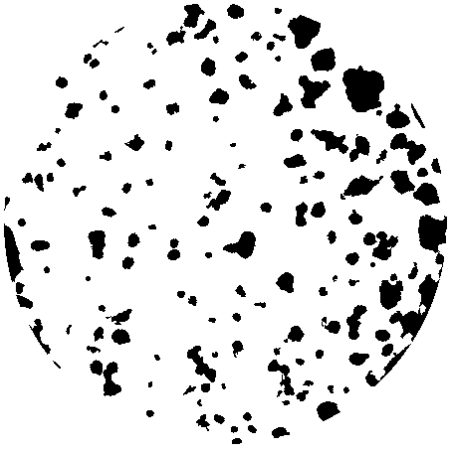

Blister Analysis - based on Dynamic L*<74	
Total Blisters	152
Total Area	4414.51mm^2
%Brown	15.5%
Size of Blisters	
Average	29.04mm^2
Max	262.06mm^2
Median	14.64mm^2
Min	3.66mm^2

Pizza 33 - Cooking Results

Conditions:	
Oven Set Point Temperature	300°C
Actual Oven Temperature	235°C
Cooking Time	12 minutes
Fan Speed	10
Heat Transfer Coefficient	29.8W/m^2
Pizza Characteristics:	
Pizza Base	336.3g
Sauce	80.18g
Cheese	240.49g
Mass Loss	39.07g
Percentage Mass Loss	5.9%
Colour Analysis:	
Lab L*	84.13
StdDev L*	9.68
Lab a*	-3.73
StdDev a*	9.54
Lab b*	45.44
StdDev b*	8.13

Blister Analysis - based on a*>10	
Total Blisters	59
Total Area	2713.71mm^2
%Brown	9.5%
Size of Blisters	
Average	46.00mm^2
Max	537.84mm^2
Median	12.08mm^2
Min	4.21mm^2

Blister Analysis - based on L*<55	
Total Blisters	15
Total Area	615.43mm^2
%Brown	2.2%
Size of Blisters	
Average	41.03mm^2
Max	202.95mm^2
Median	18.12mm^2
Min	4.39mm^2

Blister Analysis - based on Dynamic L*<76	
Total Blisters	63
Total Area	3015.29mm^2
%Brown	10.6%
Size of Blisters	
Average	47.86mm^2
Max	565.65mm^2
Median	14.46mm^2
Min	3.66mm^2